

©DELHI TECHNOLOGICAL UNIVERSITY-2016
ALL RIGHTS RESERVED

NANOMATERIALS MODIFIED PAPER BASED BIOSENSORS FOR CANCER DETECTION

by

SAURABH KUMAR

DEPARTMENT OF BIOTECHNOLOGY

Submitted

in fulfilment of the requirements of the degree of

DOCTOR OF PHILOSOPHY

to the



DELHI TECHNOLOGICAL UNIVERSITY

DELHI - 110042, INDIA

JULY 2016

DECLARATION

I, Saurabh Kumar, certify that the work embodied in this Ph. D. thesis is my own bonafide work carried out by me under the supervision of Prof. Bansi D. Malhotra and Dr. Jai G. Sharma (Department of Biotechnology, Delhi Technological University, Delhi) for a period of July 2012 to July 2016 at Department of Biotechnology, Delhi Technological University, Delhi. The matter embodied in this Ph. D. thesis has not been submitted for the award of any other degree/diploma.

I declare that I have devotedly acknowledged, given credit and refereed to the research workers wherever their works have been cited in the text and the body of thesis. I further certify that I have not wilfully lifted up some other's work, para, text, data, results etc. reported in the journals, books, reports, dissertations, thesis, etc., or available at websites and included them in Ph. D. thesis and cited as my own work.

Date:

Place:

Saurabh Kumar
(Reg. No.: 2K12/Ph.D.BT/03)



DELHI TECHNOLOGICAL UNIVERSITY

CERTIFICATE

This is to certify that the Ph. D. thesis entitled "**Nanomaterials modified paper based biosensors for cancer detection**" submitted by **Mr. Saurabh Kumar** (Registration No.: 2K12/Ph.D.BT/03) to the Delhi Technological University, Delhi for the award of Doctor of Philosophy is based on the original research work carried out under our supervision. It is further certified that the work embodied in this thesis has neither partially nor fully submitted to any other university or institution for the award of any degree or diploma.

Dr. Bansi D. Malhotra
(Supervisor)
Professor,
Department of Biotechnology
Delhi Technological University

Dr. Jai G. Sharma
(Supervisor)
Associate Professor,
Department of Biotechnology
Delhi Technological University

Prof. D. Kumar
Head,
Department of Biotechnology
Delhi Technological University

ACKNOWLEDGEMENTS

It is a pleasant aspect that I have the opportunity to express my gratitude to those incredible people who helped me to thrive in my doctoral work and shape my academic career.

It is with immense gratitude that I acknowledge the encouragement, guidance and support of my esteemed supervisor; Prof. Bansi D. Malhotra, Department of Biotechnology, Delhi Technological University (DTU), Delhi for rendering me to meet my professional goals. I am highly indebted to him for their scientific vision, enthusiasm, integral view on research and aspiration to achieve perfection that inspired me to perform quality work and good moral character. I am privileged for having them as my mentors. I owe my deepest appreciations to my supervisor Dr. Jai Gopal Sharma, Department of Biotechnology, DTU for his unconditional support and sound advice.

I express my kind regards and gratitude to Prof. Yogesh Singh, Vice chancellor, Delhi Technological University, Delhi for providing me the necessary research facilities to develop Nanobioelectronics Laboratory at Department of Biotechnology. I am very thankful to Prof. D. Kumar, Head, Department of Biotechnology, Delhi Technological University, Prof. P. B. Sharma and Prof. S. Maji for their support. I am also highly grateful to Dean (PG), DRC chairman, DRC members, SRC members and all the faculty members of the Department of Biotechnology, DTU for their comments, valuable suggestions and guidance during the entire tenure of my Ph.D. I express my gratitude to Dr. B. K. Yadav, Dr. D. C. Doval, and Dr. A. K. Dewan, Rajiv Gandhi Cancer Institute and Research Centre, Delhi, for providing me the clinical samples.

I am also thankful to the staff of the Department of Biotechnology specially Mr. Chhail Bihari, Mr. Jitendar singh and Mr. Mukesh Singh.

I would like to express my thankfulness to Dr. Gajjala Sumana, Dr. Ved Varun Aggarwal and Prof. Saleem Javed for interesting discussions. I would also thankful to my seniors Dr. Saurabh Srivastava, Dr. Chandra Mouli Pandey, Dr. Pinki Anand, Dr. Manish Srivastava, Dr. Jai Singh and Dr. Ajeet Kaushik for their unconditional support and valuable suggestions. I thank Mr. Sachidanand Tiwari, Ms. Anindita Sen, Ms. Niharika, Mr. Ashish, Ms. Shweta, Ms. Divya, Mr. Umar, Mr. Manish, Mr. Palu and Mr. Harry for providing the desired work atmosphere. I cannot explain how thankful I am to my friends Mr. Suveen Kumar, Ms. Shine Augustine and Mr. Dharendra Prabhakar. No matter where I go, they will always remain in my heart.

I have no word to express my indebtedness and gratefulness to all my family members, especially my grandfather, Shri Sidheswar Prasad; my father, Shri Jagdish Prasad; my mother, Smt. Laxmi Devi; and brother Mr. Suman Kumar for their continuous love, support, encouragement, and motivation to continue to study and understand the true value of education and the rewards of perseverance. The unconditional love and support of my wife, Hina was instrumental in helping me stay focused on the project. I am grateful to her for always being with me during the tiring moments of life. I extend my special thanks to my Mama ji Shri shailendra kumar, Mami ji, Gudu bhia, Minni Bhabhi, Happy and Sakshi for their love and support.

I sincerely acknowledge the Delhi Technological University (formerly Delhi College of Engineering), Government of NCT of Delhi, Delhi, for providing financial assistance in the form of Junior and Senior Research Fellowships which helped me to perform my work comfortably.

Last, but not the least, thanks to all my well-wishers who have not been mentioned by name but have given invaluable help in their own way.

Saurabh Kumar

ABSTRACT

Nanostructured materials have recently aroused much interest as immobilization matrices for biosensor applications. This is because these materials exhibit interesting properties such as a large surface-to-volume ratio, high surface reaction activity, high catalytic efficiency and strong adsorption ability that make them potential candidate materials to play a catalytic role for the fabrication of a biosensor. The nanomaterials based biosensors have been found to show improved sensitivity, detection limit and stability. Besides this, large surface area of a nanomaterial provides an improved loading of biomolecules with desired orientation. For biosensing applications, a wide range of conducting substrates such as glassy carbon, indium tin oxide (ITO), and gold coated glass substrate are currently being used. However, the rigidity, brittleness and cost limit their applications towards the development of a wearable, flexible, cost effective and disposable point-of-care device.

Conducting paper based biosensors have recently been attracting considerable attention because of their light weight, flexibility, portability, high sensitivity, fast response time and disposability. Moreover, coupling of a conducting paper based device (e.g. electrodes and transistors) with biological systems provides an efficient platform for the conduction of both electronic and ionic charge carriers that play a major role for communication with a desired biomolecule. Many methods including inkjet printing, screen printing, spin coating can be utilized to modify a paper to make it conducting. These methods, however, require skilled personal, costly conducting ink (gold, silver and graphite) paste, equipments, and are time-consuming.

Conducting polymers have been considered as a promising candidate to make paper conducting due to delocalization of π electrons since they are known to facilitate rapid electron transfer, mechanical flexibility and solution processability. Doping of a conducting polymer has been found to enhance its electronic, optical, physical, chemical and electrochemical properties. Among the various conducting polymers, poly(3,4-ethylenedioxythiophene): poly(styrenesulfonate) (PEDOT:PSS) has been considered to be a potential candidate for development of a conducting paper due to its homogeneous entrapment in/on a paper using simple dip coating method. Moreover, the conductivity of PEDOT:PSS modified paper can be significantly enhanced and tuned by treatment with a desired solvent. Further, incorporation of a nanomaterial may modulate the performance of a conducting paper in terms of electrochemical kinetics, signal stability and sensitivity. Recently, nanomaterials such as reduced graphene oxide (RGO), carbon nanotubes (CNTs), polymeric (PEDOT:PSS) electrospun nanofibers have recently aroused much interest in electrochemical sensors. This is due to their large surface area, enhanced biomolecule loading and excellent electrochemical properties. Therefore incorporation of nanomaterials in the PEDOT:PSS coated paper may further improve electrochemical performance of the desired paper sensor.

Cancer is currently a serious concern and a medical threat to the contemporary world. According to a recent report, there have been 8.2 million cancer deaths, 14.1 million new cancer cases and 32.6 million people are living with cancer necessitating its early detection. Carcinoembryonic antigen (CEA) has been found to be an important biomarker for the diagnosis and routine monitoring of cancer due to its association with colon, lung, ovarian and breast cancer that are responsible for more than half of all cancer deaths each year. The human CEA gene is clustered on

chromosome 19q and it comprises of 29 genes. CEA (a glycoprotein) comprises of ~60% carbohydrate having molecular mass of ~180-200 KDa, is one of the most widely used cancer biomarker. It plays an important role in early monitoring, screening and disease recurrence. In this context, determination of CEA in blood serum has been proposed for clinical diagnosis and monitoring of cancer.

The aim of this research is to develop a substitute for conventional electrode (ITO, gold and glassy carbon), that have been found to have limitations in applications for fabrication of smart point-of-care devices and their application in biosensing for CEA detection. We have fabricated PEDOT:PSS based conducting paper as electrode for CEA biomarker detection. Efforts have been made to improve the conductivity of PEDOT:PSS coated paper by using different solvents like ethylene glycol and formic acid. Further, incorporation of nanomaterials such as reduced graphene oxide, carbon nanotubes, PEDOT:PSS electrospun nanofibers modulate the paper electrode performance in terms of electrochemical kinetics and biosensing characteristics. The response of the paper electrode is validated using CEA concentration of serum samples of cancer patients obtained via immunoassay technique.

The thesis comprises of six **Chapters** as discussed below:

Chapter 1 on Introduction and Literature Survey highlights the detailed description of nanomaterials based conducting paper including their fabrication strategies, characteristics and potential applications. Beside this, a brief discussion on cancer, conventional techniques used for cancer biomarker detection and scope of biosensors in cancer detection. The attempts have been made to discuss limitations of conventional electrodes used in biosensing application and give a detailed literature review on paper based electrochemical biosensors.

Chapter 2 on Materials and characterization techniques describes the various materials used for the fabrication of paper based biosensors for CEA detection using electrochemical technique. Further, the analytical techniques such as four points probe conductivity measurement, X-Ray diffraction (XRD), Fourier transform infrared (FT-IR) spectroscopy, Raman spectroscopy, X-ray photoelectron spectroscopy (XPS), scanning electron microscopy (SEM), energy dispersive X-Ray spectroscopy (EDX), transmission electron microscopy (TEM), and electrochemical techniques used for characterization of the conducting paper, nanomaterial modified conducting paper and immuno-electrodes have been discussed in details. Attempts have also been made to describe the procedures and protocols used to immobilize antibodies and to estimate the various parameters related to the characteristics of paper based biosensors.

Chapter 3 on Reduced graphene oxide modified conducting paper sensor for cancer detection deals with results of the studies relating to the fabrication of a paper based sensor comprising of poly (3,4-ethylenedioxythiophene):poly(styrenesulfonate) (PEDOT:PSS) and reduced graphene oxide (RGO) nanocomposite. The effect of various solvents like methanol, ethylene glycol and H_2SO_4 on the electrical conductivity of PEDOT:PSS coated Whatman paper has been investigated. The conductivity of this solution processed conducting paper significantly is found to increase by 2 orders of magnitude on being treated with ethylene glycol. Further, incorporation of RGO into the solution processed conducting paper results in improved electrochemical performance and signal stability. The fabricated electrodes have been used for the detection of the cancer biomarker, CEA. This low cost, flexible and environment friendly conducting paper based biosensor has been utilized for cancer biomarker (CEA) detection, that reveals high sensitivity of $25.8 \mu\text{A ng}^{-1}\text{mLcm}^{-2}$ in the linear detection range of $2\text{--}8 \text{ ng mL}^{-1}$ with a good storage

stability (21 days). The response of paper electrode has been validated using CEA concentration of serum sample of cancer patient. This paper electrode can be decomposed by simple incineration and has immense potential as a smart medical diagnostic kit or a point-of-care biosensor. In order to further improve the performance of conducting paper, formic acid and CNT have been used as a suitable solvent and dopant, respectively. Compared to RGO, metallic impurities present in CNT have been found to improve the electrochemistry of CNT.

Chapter 4 on Carbon nanotube modified conducting paper sensor for cancer detection used nanocomposite of PEDOT:PSS and carbon nanotubes (CNT) to fabricate conducting paper (CNT/CP) via dip coating. It is found that conductivity of this paper increases by 2 orders of magnitude on being treated with formic acid (CNT/FA@CP) due to removal of the non-conducting molecule PSS from electrode surface. This fabricated paper is flexible, electrochemical active, and it can be easily disposed off by simple incineration. This smart conducting platform has been used for conjugation of the anti-carcinoembryonic antigen (anti-CEA) protein for quantitative estimation of CEA. The PEDOT:PSS-CNT based electrochemical paper immunosensor exhibits sensitivity of $7.8 \mu\text{A ng}^{-1} \text{mL cm}^{-2}$ with improved linear detection range of $2\text{--}15 \text{ ng mL}^{-1}$ and feasibility of paper electrode have been validated with CEA concentration in serum samples of cancer patient. It has been observed that incorporation of carbon nanotubes improved heterogeneous electron transfer rate constant (5 times) and linear detection range with respect to PEDOT:PSS-RGO based conducting paper. CEA biomarker released in serum of healthy person is $< 3 \text{ ng mL}^{-1}$ with a cut-off value 5 ng mL^{-1} and for cancer patient it is reported to be a maximal of 20 ng mL^{-1} .

Chapter 5 on PEDOT:PSS/PVA nanofiber decorated conducting paper sensor for cancer detection pertains to results of studies relating to the fabrication of a flexible, cost-effective, lightweight, label free and environment friendly electrochemical sensor. For this purpose, nanofibers of PEDOT:PSS/PVA have been grown on a conducting paper platform using electrospinning technique. The deposition of electrospun nanofibers (EsNf) is found to result in improved mechanical strength, large surface area, enhanced biomolecule loading and electrochemical characteristics. This platform provides improved charge transfer between electrode and solution resulting in higher sensitivity towards the electrochemical detection of cancer biomarker (CEA). The results of the amperometric response studies indicate that the paper electrode (BSA/anti-CEA/PEDO:PSS/PVA-EsNf/CP) can be used to estimate CEA in the range, 0.2 to 25 ngmL⁻¹, has high sensitivity of 14.2 $\mu\text{Ang}^{-1}\text{mLcm}^{-2}$ and shelf life of 22 days. This paper sensor covers the entire physiological range of CEA secreted in serum sample (< 3 to 20 ngmL⁻¹) with improved lower detection limit. This modified conducting paper electrode is a promising alternative over expensive conventional electrodes (ITO, gold and glassy carbon) for fabrication of smart point of care devices.

Chapter 6 on Summary and future prospects contains brief summary of the studies related to nanomaterial modified paper based biosensor for cancer detection. This Chapter also highlights the future prospects of nanomaterials modified conducting paper sensor for detection of other biomolecule including cancer biomarker.

The work described in this thesis is summarized in the form of following publications:

1. **S. Kumar**, P. Rai, J.G. Sharma, A. Sharma and B.D. Malhotra, PEDOT:PSS/PVA-nanofibers-decorated conducting paper for cancer diagnostics, **Advanced Materials Technologies**, 2016. (doi: 10.1002/admt.201600056).
2. **S. Kumar**, M. Willander, J.G. Sharma and B.D. Malhotra, A solution processed carbon nanotube modified conducting paper sensor for cancer detection, **Journal of Material Chemistry B**, 2015, 3, 9305–9314. (**Impact factor 4.9**)
3. **S. Kumar**, S. Kumar, S. Srivastava, B.K. Yadav, S.H. Lee, J.G. Sharma, D.C. Doval and B.D. Malhotra, Reduced graphene oxide modified smart conducting paper for Cancer biosensor, **Biosensors and Bioelectronics**, 2015, 73, 114-122. (**Impact factor 7.5**)

CONTENTS

	Page No.
Acknowledgements	i
Abstract	v
Abbreviations and Symbols	xiii
List of Figures	xvii
List of Tables	xxiii
Chapter 1: Introduction and Literature Review	1-46
1.1 Nanomaterials	3
1.2 Conducting polymers	8
1.3 Biosensors	10
1.3.1 Components of a biosensors	12
(a) Bimolecular recognition element	12
(b) Transducer	12
(c) Immobilization matrices	14
1.3.2 Nanomaterial based biosensor	15
1.4 Cancer	17
1.4.1 Biomarkers	19
1.4.2 Carcinoembryonic antigen (CEA)	21
1.4.3 Conventional methods for CEA detection	22
1.4.4 Biosensor for CEA detection	23
1.5 Paper	25
1.5.1 Conducting paper	26
1.5.2 Nanomaterials modified conducting paper	27
1.5.3 Applications of nanomaterials modified conducting paper	31
(a) Electronic applications	31
(b) Energy storage devices	33
(c) Biomedical applications	35
1.6 Objectives of the studies	44

Chapter 2: Materials and characterization techniques	47-84
2.1 Introduction	49
2.2 Materials	49
2.3 Characterization Techniques	50
2.3.1 Four point probe conductivity measurement	50
2.3.2 X-Ray diffraction (XRD) technique	53
2.3.3 Fourier transforms infrared (FT-IR) spectroscopy	55
2.3.4 Raman spectroscopy	58
2.3.5 X-ray photoelectron spectroscopy (XPS)	61
2.3.6 Scanning electron microscopy (SEM)	64
2.3.7 Transmission electron microscopy (TEM)	66
2.3.8 Tensile measurements	69
2.3.9 Contact angle (CA) measurement	71
2.3.10 Electrochemical techniques	73
(a) Chronoamperometry technique	74
(b) Electrochemical impedance spectroscopy (EIS)	76
2.4 Methods of immobilization of antibodies onto modified paper substrate	79
2.4.1 Physical adsorption	80
2.4.2 Covalent immobilization	80
2.4.3 Chemical cross-linking	81
2.4.4 Physical entrapment	81
2.5 Characteristics of a biosensor	81
2.5.1 Linear range, sensitivity and detection limit	81
2.5.2 Shelf life and reproducibility of the bioelectrode	82
2.6 Conclusions	82
Chapter 3: Reduced graphene oxide modified conducting paper sensor for cancer detection	85-108
3.1 Introduction	87
3.2 Experimental details	90
3.2.1 Fabrication of PEDOT:PSS based conducting paper	90

3.2.2 Preparation of reduced graphene oxide (RGO) and PEDOT: PSS/RGO composite	90
3.2.3 Fabrication of PEDOT:PSS/RGO based electroactive paper	91
3.3 Results and discussion	92
3.3.1 Electron microscopy studies	92
3.3.2 Electrical conductivity studies	93
3.3.3 FT-IR and XPS studies	96
3.3.4 Electrochemical studies	99
3.3.5 Electrochemical response studies	101
3.3.6 Stability, selectivity and reproducibility studies	103
3.3.7 Real sample analysis	104
3.4 Conclusions	107
Chapter 4: Carbon nanotube modified conducting paper sensor for cancer detection	109-132
4.1 Introduction	111
4.2 Experimental details	113
4.2.1 Fabrication of PEDOT:PSS based conducting paper	113
4.2.2 Fabrication of CNTs doped conducting paper	114
4.2.3 Fabrication of CNTs doped conducting paper sensor	114
4.3 Results and Discussion	115
4.3.1 Transmission electron microscopic studies	115
4.3.2 Raman and X-ray diffraction studies	116
4.3.3 Scanning electron microscopic studies	117
4.3.4 Electrical conductivity studies	118
4.3.5 X-ray photoelectron spectroscopic studies	120
4.3.6 Electrochemical studies	122
4.3.7 Electrochemical response studies	125
4.3.8 Real sample analysis	127
4.3.9 Stability and reproducibility studies	128
4.3.10 Disposability studies	129

4.4 Conclusions	131
Chapter 5: PEDOT:PSS/PVA nanofibers decorated conducting paper sensor for cancer detection	133-152
5.1 Introduction	135
5.2 Experimental details	136
5.2.1 Fabrication of conducting paper	136
5.2.2 Fabrication of PEDOT:PSS/PVA electrospun nanofiber decorated conducting paper	137
5.2.3 Biofunctionalization of PEDOT:PSS/PVA electrospun nanofiber decorated conducting paper	137
5.3 Results and discussion	138
5.3.1 Raman spectroscopic and zeta potential studies	138
5.3.2 X-ray photoelectron spectroscopic studies	139
5.3.3 Mechanical behavior	141
5.3.4 Contact angle studies	142
5.3.5 Electron microscopic studies	143
5.3.6 Electrochemical studies	144
5.3.7 Electrochemical response studies	146
5.3.8 Selectivity, stability and reproducibility studies	147
5.3.9 Real sample analysis	148
5.3.10 Disposability studies	149
5.4 Conclusions	151
Chapter 6: Summary and Future Prospects	153-160
6.1 Summary	155
6.2 Future prospects	159
References	161-178
Publications included in thesis	
Biodata	
Appendix: CD	

ABBREVIATIONS AND SYMBOLS

A	Ampere
Ab	Antibody
Ag	Silver
AgCl	Silver chloride
Anti-CEA	Carcinoembryonic antibody monoclonal
Au	Gold
AuNP	Gold nanoparticle
BSA	Bovine serum albumin
CEA	Carcinoembryonic antigen
cm	centimeter
CNT	Carbon nanotube
CP	Conducting paper
EDC	N-(3-Dimethylaminopropyl)-N'- ethylcarbodiimide
EG	Ethylene glycol
EIS	Electrochemical impedance spectroscopy
ELISA	Enzyme-linked-immuno-sorbant-assay
EsNf	Electrospun nanofiber
eV	Electron volt
FA	Formic acid
F _{ab}	Fragment antigen binding
F _c	Fragment crystallizable
FET	Field-effect-transistor

$[\text{Fe}(\text{CN})_6]^{4-}$	Ferrocyanide
$[\text{Fe}(\text{CN})_6]^{3-}$	Ferricyanide
fM	Femto Molar
FTIR	Fourier transform infrared spectroscopy
GO	Graphene oxide
h	Hour
H_2SO_4	Sulphuric acid
HRP	Horseradish peroxidase
IgG	Immunoglobulin G
ITO	Indium-tin-oxide
K_{ct}	Heterogeneous electron transfer rate constant
kDa	Kilo Dalton
$\text{K}\Omega$	Kilo-ohm
L	Liter
mL	Milliliter
MWCNTs	Multi-walled carbon nanotubes
M	Molar
ng	Nanogram
NHS	N-Hydroxysuccinimide
nm	Nanometer
PBS	Phosphate buffer saline
PEDOT:PSS	Poly(3,4-ethylenedioxythiophene: poly(4-styrenesulfonate)

PVA	Polyvinyl alcohol
R_{ct}	Charge transfer resistance (Nyquist diameter)
RGO	Reduced graphene oxide
RSD	Relative standard deviation
R_s	Solution resistance
s	Second
$S\text{cm}^{-1}$	Siemens per centimeter
$-\text{SO}_3^-$	Sulfonyl group
SEM	Scanning electron microscopy
SWCNT	Single-walled carbon nanotube
TEM	Transmission electron microscopy
V	Volt
WHO	World health organization
XPS	X-ray photoelectron spectroscopy
XRD	X-ray diffraction
μ	Micro
2D	Two dimensional
3D	Three dimensional

LIST OF FIGURES

		Page No.
Figure 1.1	Different types of nanomaterials	4
Figure 1.2	Structure of reduced graphene oxide	7
Figure 1.3	Structure of poly(3,4-ethylenedioxythiophene (PEDOT) and poly(4-styrenesulfonate) (PSS)	10
Figure 1.4	Schematic of a biosensor	11
Figure 1.5	Structure and binding sites of the antibody	13
Figure 1.6	Schematic of cell division in normal and cancer cell	19
Figure 1.7	Constituents of a paper	26
Figure 1.8	Fabrication of conducting paper via different techniques	29
Figure 1.9	Application of conducting paper in various fields	37
Figure 2.1	(a) Schematic of four probe that measure voltage (V) and supply current (A) to the surface of the sample and (b) assembly of four point probe technique	52
Figure 2.2	(a) The diffracted X-rays make angle 2θ with the incident X-rays, where θ is the angle between incident rays and scatter plane (incident angle) and (b) optical image of XRD Bruker model, D-8 advance.	54
Figure 2.3	XRD pattern of PEDOT:PSS	54
Figure 2.4	(a) Schematic of optical layout of Michelson Interferometer and (b) optical image of FT-IR spectrophotometer (Perkin Elmer, spectrum BX II).	57
Figure 2.5	FT-IR spectrum of polyaniline (PANI) modified paper electrode	57
Figure 2.6	(a) Energy level diagram for Raman scattering including Rayleigh, Stokes and anti-Stokes scattering and (b) optical image of Raman spectrophotometer (Varian 7000 FT-Raman)	60
Figure 2.7	Raman spectra of reduced graphene oxide (RGO)	61
Figure 2.8	(a) Schematic of the XPS process and (b) optical image of XPS instrument (Kratos, Axis-Nova).	63

Figure 2.9	XPS survey scan spectra for electrochemically deposited polyaniline.	63
Figure 2.10	Schematic representation of scanning electron microscope.	65
Figure 2.11	(a) Optical image of SEM Hitachi model S-3700N and (b) SEM image of Whatman filter paper 1.	65
Figure 2.12	A schematic showing various components of TEM.	68
Figure 2.13	(a) Optical image of JEOL JEM, TEM instrument and (b) TEM image of nanostructured zirconia (ZrO_2) grafted reduced graphene oxide (RGO).	68
Figure 2.14	A typical stress-strain curve.	69
Figure 2.15	(a) Optical image of universal testing machine (UTM, Instron 3369) and (b) Tensile strength versus strain curve of Whatman filter paper 1.	70
Figure 2.16	(a) Optical image of CA meter (Data Physics OCA15EC) and (b) CA image of ITO electrode.	72
Figure 2.17	Optical image of Autolab Potentostat/Galvanostat, EcoChemie, Netherland.	74
Figure 2.18	Chronoamperometry plot obtained for PEDOT:PSS/ITO electrode.	75
Figure 2.19	Nyquist plot with depressed arc where, the polarization is due to combination of kinetic and diffusion processes	77
Figure 2.20	The electrode-solution interface can be modeled by an equivalent circuit (Randles circuit) comprising of the solution resistance (R_s), charge transfer resistance (R_{ct}), Warburg impedance (Z_w) and double layer capacitance (C_{dl})	77
Figure 2.21	Electrochemical impedance spectra of PEDOT:PSS/ITO electrode recorded in PBS solution (pH 7, 50 mM, 0.9% NaCl) containing 5 mM $[\text{Fe}(\text{CN})_6]^{3-/4-}$ as redox probe .	78
Figure 2.22	Schematic presentation of developed immobilization methods.	79
Figure 3.1	Schematic of proposed electroactive paper sensor.	91
Figure 3.2	(A) TEM image of synthesized reduced graphene oxide (RGO) (B) SAED of RGO (C) TEM image of	93

	PEDOT:PSS/RGO (D) SAED pattern of PEDOT:PSS/RGO composite (E) SEM of PEDOT:PSS adsorbed onto Whatman paper (F) SEM of PEDOT:PSS/RGO Whatman coated paper.	
Figure 3.3	Optical image of electroactive paper (A) foldable nature of electroactive paper (B, C) demonstration of LED emission when current flow through electroactive paper. Flexibility studies of PEDOT:PSS/RGO based electroactive electrode (D) Schematic diagram of electrode folding at different deformation angle. (E) The ratio of measured conductivity (σ_{meas}) to initial conductivity (σ_0) of electroactive paper with respect to folding angle. (F) The ratio of measured conductivity (σ_{meas}) to initial conductivity (σ_0) of electroactive paper verses folding cycle (1 cycle = 360°).	95
Figure 3.4	(A) The schematic illustration of the mechanism of conductivity enhancement on conducting paper surface by EG treatment. (B) The FT-IR spectra of (i) PEDOT:PSS/Whatman paper (ii) conducting paper (iii) conducting paper treated with EG (C) X-ray photoelectron spectra (XPS) of (i) conducting paper (ii) conducting paper treated with ethylene glycol.	97
Figure 3.5	(A) FT-IR spectra of electroactive paper (B) XPS spectra of electroactive paper	98
Figure 3.6	Electrochemical studies conducted on paper electrode (A) Electrochemical impedance spectra (B) Chronoamperometry plot obtained for (i) conducting paper (ii) conducting paper treated with EG (iii) electroactive paper (C) Electrochemical response studies of anti-CEA immobilized electroactive paper at different concentration of CEA (D) Calibration plot between the magnitudes of current recorded and CEA concentration (curve i); control experiment in absence of antibody (curve ii).	101
Figure 3.7	(A) Electrochemical current response of anti-CEA immobilized electroactive paper electrode (immuno-electrode) measured as a function of time (day) (B) Electrochemical current response of	104

	immuno-electrode in the presence of other analytes (C) Electrochemical current response of different immuno-electrode fabricated via the same set of procedure in presence of CEA (2 ng mL^{-1}) and (D) CEA concentration values obtained by immunoassay and the electroactive paper method.	
Figure 4.1	Fabrication and characterization of CNTs/FA@CP modified paper electrode.	115
Figure 4.2	TEM image of (a) carbon nanotube (b) CNTs/PEDOT:PSS composite (c) Raman spectrum of (i) PEDOT:PSS and (ii) PEDOT:PSS/CNTs composite [Inset shows the Raman of CNTs] (d) XRD pattern of PEDOT:PSS/CNTs composite and inset showing XRD of CNTs.	116
Figure 4.3	SEM image of (a) PEDOT:PSS coated paper (b) CNTs/PEDOT:PSS coated paper (c) anti-CEA/CNTs/PEDOT:PSS paper sensor	117
Figure 4.4	(a) Optical image of conductive and electrochemically active paper (CNTs/FA@CP) showing (b) high flexibility (c-d) Lighting an LED lamp (e-f) easy to dispose off.	119
Figure 4.5	S (2p) XPS spectra of (a) modified papers, XPS curve fitting of (b) PEDOT:PSS coated Paper (c) Ethylene glycol doped PEDOT: PSS coated over paper <i>i.e.</i> conducting paper (d) conducting paper treated with formic acid (FA@CP) (e) CNTs doped conducting paper treated with formic acid.	121
Figure 4.6	Electrochemical characterization of modified paper electrode (a) chronoamperometric studies of modified paper electrode. Impedance spectra of (b) conducting paper (c) conducting paper treated with formic acid (FA@CP) (d) CNTs modified conducting paper treated with formic acid (CNTs/FA@CP) (e) anti-CEA/CNTs/FA@CP paper electrode and circuit were fitted with equivalent Randles circuit $R_s(R_{ct}C)$. (f) Bode plot of different modified electrode.	123
Figure 4.7	(a) Electrochemical response studies of the BSA/anti-CEA/CNTs/FA@CP paper electrode obtained as a	127

	function of CEA concentration (1-100 ngmL ⁻¹) using chronoamperometry and (b) calibration plot between the magnitudes of current recorded and CEA concentration (curve i); control experiment in absence of antibody (curve ii). (c) Current response time of BSA/anti-CEA/CNTs/FA@CP paper electrode as a function of time (day) (d) Current response time of five different BSA/anti-CEA/CNTs/FA@CP paper electrodes fabricated using the same set of procedure in presence of CEA concentration (2 ngmL ⁻¹).	
Figure 4.8	Energy dispersive X-ray (EDX) analysis.	129
Figure 5.1	(a) Schematic representation of the electrospinning setup for the synthesis of PEDOT:PSS/PVA nanofibers (Inset showing (i) optical image of electrospun modified paper with (ii) high degree of flexibility) and (b) bio functionalized electrospun PEDOT:PSS/PVA nanofiber for carcinoembryonic antigen detection.	138
Figure 5.2	Raman spectrum of (i) PEDOT:PSS and PEDOT:PSS/PVA composite.	139
Figure 5.3	S2p XPS spectra of (i) conducting paper (CP) (ii) PEDOT:PSS/PVA electrospun nanofiber coated CP	140
Figure 5.4	(a) (i) Optical image of conducting paper coated with PEDOT:PSS/PVA electrospun nanofiber showing (ii) high flexibility (b) Stress-strain curve of different modified paper	141
Figure 5.5	Contact angle measurement of (i) conducting Paper (CP) (ii) PEDOT:PSS electrospun nanofibers coated over conducting paper (PEDOT:PSS/PVA-EsNf/CP) (iii) anti-CEA immobilized PEDOTE:PSS/PVA-EsNf/CP.	142
Figure 5.6	SEM images of (a,b,c) PEDOT:PSS/PVA-EsNf/CP at different magnification (d) anti-CEA/PEDOT:PSS/PVA-EsNf/CP.	144
Figure 5.7	Electrochemical characterization of modified paper electrode (a) chronoamperometry plot obtained for (i) conducting paper, CP (ii) PEDOT:PSS/PVA-EsNf/CP (iii) anti-CEA/PEDOT:PSS/PVA-EsNf/CP (iv) BSA/	145

	anti-CEA/PEDOT:PSS/PVA-EsNf/CP. (b) Electrochemical response studies of BSA/anti-CEA/PEDOT:PSS/PVA-EsNf/CP electrode at different concentration ($0-100\text{ngmL}^{-1}$) of CEA (c) calibration plot between the magnitudes of current recorded and CEA concentration (d) linearity plot of paper sensor (BSA/anti-CEA/PEDOT:PSS/PVA-EsNf/CP)	
Figure 5.8	(a) Interferents studies conducted via measurement of electrochemical current response of BSA/anti-CEA/PEDOT:PSS/PVA-EsNf/CP bioelectrode (paper sensor) in the presence of other analytes (b) Electrochemical current response of different immunoelectrode fabricated under similar condition in presence of CEA (2 ngmL^{-1}). (c) Electrochemical current response of BSA/anti-CEA/PEDOT:PSS/PVA-EsNf/CP bioelectrode measured as a function of time (day) and (d) CEA concentration values obtained by immunoassay and the BSA/anti-CEA/PEDOT:PSS/PVA-EsNf/CP bioelectrode.	148
Figure 5.9	Energy dispersive X-ray (EDX) analysis of incinerated paper electrode (BSA/anti-CEA/PEDOT:PSS/PVA-EsNf/CP)	151

LIST OF TABLES

		Page No.
Table 1.1	Cancer biomarkers that are currently in clinical use.	20
Table 1.2	Comparison between conventional electrodes and paper electrodes.	38
Table 1.3	Paper based electrochemical biosensors: fabrication and characteristics.	39
Table 3.1	The sensing characteristics of electroactive paper have been summarized along with some of those reported in literature.	106
Table 4.1	Conductivity and electrochemical properties of modified paper electrode.	126
Table 4.2	Determination of carcinoembryonic antigen concentration in serum samples using BSA/anti-CEA/CNTs/ FA@CP paper electrode.	128
Table 4.3	Shows response characteristics of BSA/anti-CEA/CNTs/FA@CP electrode along with those reported in literature.	130
Table 5.1	Mechanical properties of modified paper.	142
Table 5.2	Shows response characteristics of the BSA/anti-CEA/PEDOT:PSS/PVA-EsNf/CP bioelectrode along with those reported in literature.	150
Table 6.1	Sensing characteristic of RGO, CNTs and PEDOT:PSS/PVA electrospun nanofibers integrated conducting paper electrode for CEA detection.	159

CHAPTER 1

Introduction and Literature Review

1.1 NANOMATERIALS

There is an increased interest in nanomaterials for application in healthcare. Nanoscale materials are defined as a set of substances where at least one of the dimensions is in the range of 1 to 100 nm, while a nanometer is defined as 10^{-9} meter. Nanomaterials have been found to have unique electrical, optical, thermal, mechanical, and chemical properties to their bulk counterparts. This is attributed to the nanometer size of the materials which results in: (i) large surface- to- volume ratio; (ii) high surface energy; (iii) spatial confinement; (iv) reduced imperfections, which do not exist in the corresponding bulk materials. These properties at the nanoscale are dependent on the size, shape, and the material behavior. The two main reasons why materials at the nanoscale can have different properties are: increased relative surface area and new quantum effects. The large surface area (large surface area to volume ratio) of nanoscale materials results in more “surface” dependent material properties. Next, spatial confinement effect of nanomaterials yields the quantum effects. Therefore, energy band structure and charge carrier density in the materials may be modified quite differently from their bulk that in turn may result in electronic and optical properties of the materials [1-2]. The nanomaterials are experiencing a rapid development due to their potential applications in the field of electronics, photovoltaic, catalysis, ceramics, drug delivery, imaging, biomaterials and biosensors [3].

Nanostructured materials are classified as zero dimensional (nanoparticles), one dimensional (nanowires and nanorods), two dimensional (thin films) nanostructures [4]. Depending upon the nature of the material and its unique properties, nanomaterials can be categorized as inorganic nanomaterials such as metal/metal oxide (gold, silver, iron oxide etc) and organic nanomaterials like carbon

nanomaterial (graphene, carbon nanotube etc) and polymeric nanomaterial [poly(3,4-ethylenedioxythiophene:poly(4-styrenesulfonate) (PEDOT:PSS) nanofibers, nanostructured polyaniline etc]. **Fig. 1.1** shows different types of nanomaterials.

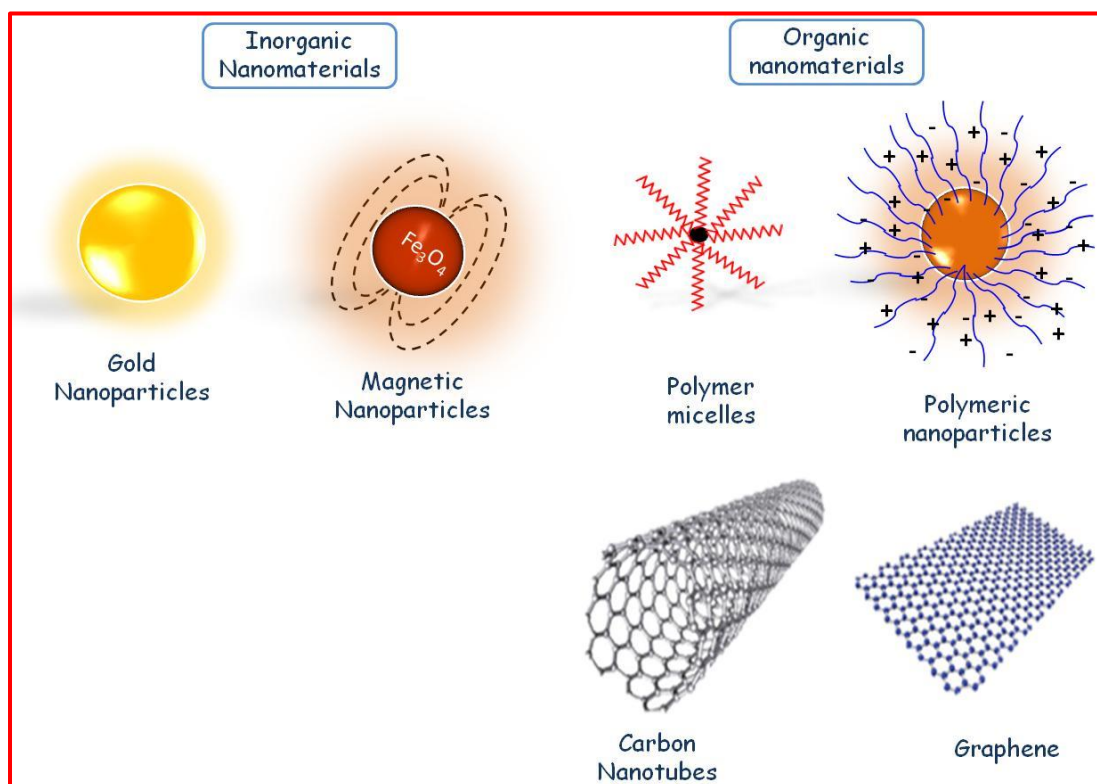


Fig. 1.1: Different types of nanomaterials.

1.1.1 Inorganic nanomaterials

Inorganic nanostructured materials such as metals [gold (Au), platinum (Pt), silver (Ag) etc.] /metal oxides [iron oxide (Fe₃O₄), zinc oxide (ZnO), titanium oxide (TiO₂), zirconium oxide (ZrO₂) etc] are known to be crystalline with precise chemical composition, surface termination, and dislocation-defect free. The interesting optical and electrical properties of these materials are due to electron and phonon confinement, high surface-to-volume ratio, modified surface work function, high surface reaction activity, high catalytic efficiency and strong adsorption ability. These nanomaterials have been predicted to have many applications such as catalysis, fuel

cell, heavy metal detection, photonics band-gap materials, single electron transistors, non-linear optical devices, and biological fields in areas such as targeted drug delivery, optical imaging and biosensors etc. [5-7].

1.1.2 Organic nanomaterials

Among the various organic nanomaterials, carbon nanomaterials [carbon nanotubes, graphene oxide, reduced graphene oxide etc.] exhibits unique combination of electrical, mechanical, thermal, and chemical properties which make them promising candidates for a wide range of electronics, optoelectronics, photovoltaic, biomedical and biosensing applications [7-8]. Carbon nanomaterials composed of entirely sp^2 bonded carbon, are found in all dimensionalities including zero-dimensional fullerenes, one-dimensional carbon nanotubes (CNTs), and two-dimensional graphene.

Carbon nanotubes (CNTs) are the one-dimensional form of graphitic carbon that was discovered in 1991 by Sumio Iijima [9]. Carbon nanotube consists of a long cylinder made of the hexagonal honeycomb lattice of carbon bound by two pieces of fullerenes at the ends. A single-walled carbon nanotube (SWCNT) is a seamless cylinder of high aspect ratio whose diameter is of the order of nanometer and length may be several hundred micrometers, making it effectively a one dimensional structure called a nanowire. Multi-walled carbon nanotube (MWCNT) comprise of nested, concentric shells of SWCNT with a spacing between individual walls of 3.4 Å. CNTs exhibit extraordinary strength, unique electrical properties and are efficient thermal conductors. Since chemical bonding of nanotubes is composed entirely of sp^2 nature, which are stronger than the sp^3 bonds found in diamonds and provide nanotubes with their unique strength. CNTs have been well investigated due to their superior properties and multifarious applications. End/sidewall-localized COOH and

NH₂ groups generated by oxidation of carbon nanotube have been exploited for covalent attachment of bimolecular probes, polymers and metallic particles. They have been widely explored for efficient electrochemical biosensing devices owing to its unique electrochemistry [10-12].

The recent synthetic carbon allotrope is two-dimensional graphene, representing a single graphite sheet. Graphene, the ultimate example of expanded aromatic carbon, had been considered for a very long time to be an exclusively theoretical material. The single graphene layers were recently prepared successfully by means of a simple mechanical exfoliation of graphite using scotch tape [13]. The carbon bonds are sp² hybridized where the in-plane σ_{C-C} bond is one of the strongest bonds in materials and the out-of-plane π bonds that give rise to a delocalized network of electrons. Being a standard 2D material, graphene chemistry has not yet attracted much interest. The main obstacle is the lack of functional groups for chemical and bimolecular functionalization. Progress in making graphene suspension rich in functional groups, has opened up a new way to liquid-phase chemistry of graphene through chemical reduction method [14]. Thus the derivatives of graphene like graphene oxide (GO), and reduced graphene oxides (RGO) have entered into the emerging field of graphene research. These suspended forms of graphene have further broadened the area of applications such as in composite materials, biomedical and biosensors. Graphene oxide (GO), an oxidized form of graphite, is a layered material obtained by exfoliation of the graphite oxide. In contrast to pristine graphite, the GO sheets are highly decorated by several oxygenated functional groups on its basal planes (hydroxyl and epoxies) and at its edges (carboxyl). This results in a hybrid structure comprising of a mixture of sp² and sp³ hybridized carbon atoms. However, GO has a highly disrupted sp² carbon lattice and exhibits a large number of defects

and functional groups make it insulator. Thus to improve the conductivity of GO, it is necessary to convert it into reduced graphene oxide (RGO). Moreover, RGO shows superior electrochemical behavior such as large voltammetric current and lower oxidation potential that make it a promising candidate for electrochemical biosensing. RGO has been widely explored for the development of electrochemical sensors and biosensors because (1) it has abundant defects and chemical groups facilitate charge transfer and thus ensure high electrochemical activity; (2) the abundant functional groups on the RGO surface offer the convenience and flexibility for functionalization to enhance the sensor performance; (3) the chemical and electrical properties of RGO are highly tunable; and (4) as compared to the non-conductive GO, RGO can efficiently transport charges. **Fig. 1.2** shows Schematic of reduced graphene oxide. RGO can be functionalized through covalent or noncovalent methods in order to further enhance its sensitivity, specificity, loading capacity, biocompatibility etc. [15-16].

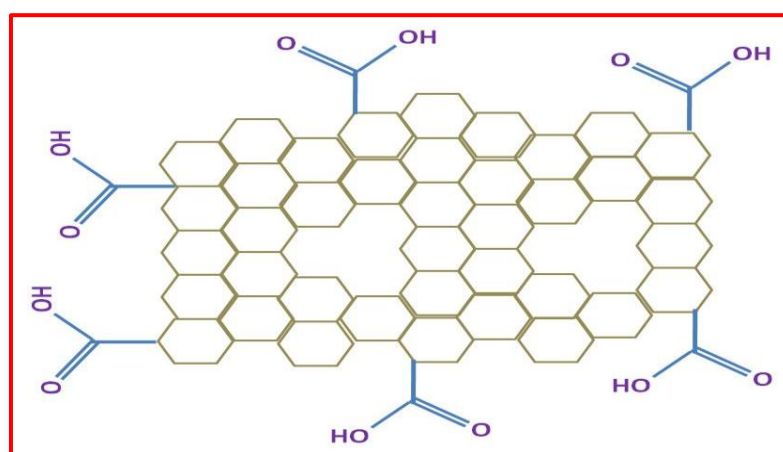


Fig. 1.2: Structure of reduced graphene oxide.

1.2 CONDUCTING POLYMERS

Conducting polymers are polyconjugated polymers that conduct electricity, as well as retain the properties of conventional organic polymers such as solution processability and mechanical flexibility. The alternate single and double bond arrangement in conducting polymer facilitates the delocalization of π (pi) electrons which assist the rapid electron transfer. For a polymer to become intrinsically electrically conducting there should be an overlap of molecular orbital to allow the formation of delocalized molecular wave function and presence of partially filled molecular orbital to allow free movement of electrons in a polymeric lattice [17]. Doping of a conducting polymer has been found to enhance electronic, optical, physical, chemical and electrochemical properties. The concept of solitons, polarons and bipolarons are used to explain electronic phenomena in conducting polymer [18]. The various factors such as polaron length, conjugation length, chain length and charge transfer to adjacent molecules influence the conductivity of conducting polymer [17]. Next, the surface functional groups of conducting polymer nanomaterials can be modified covalently using specific bioreceptors, allowing the immobilization of biomolecule on electrode substrates [19-20]. Therefore, conducting polymers have been predicted to have enough potential for the development of low cost and high performance sensor materials that offer high permeability, biocompatibility, and rapid electron transfer. Among the various conducting polymers (polyaniline, polypyrrole, polythiophene etc.), poly(3,4-ethylenedioxythiophene: poly(4-styrenesulfonate) (PEDOT:PSS) has emerged as an interesting candidate for fabrication of flexible sensor. It is a mixture of two ionomers *i.e.* poly(3,4-ethylenedioxythiophene) (PEDOT) and poly(styrene sulfonate) (PSS). **Fig. 1.3** shows the structure of PEDOT and PSS. The 3,4-ethylenedioxythiophene (EDOT) is a

monomer of PEDOT. EDOT is a positively charged conjugated polymer compound of thiophene ring. It has been found to have poor solubility. However it can be dispersed in water-dispersible negatively charge polymeric sulfonic acids such as poly(styrenesulfonic acid) (PSS). Hydrophobic and conducting PEDOT-rich grains are encapsulated by hydrophilic and insulating PSS-rich shells [21]. The electrical conductivity of PEDOT:PSS can be tuned by chemical modification that depends on nature and the degree of doping. Doping with solvent such as ethylene glycol, formic acid, methanol etc induces a conformational change in PEDOT:PSS polymer. These conformational changes have been found to result in increased electrical conductivity due to increase in the intrachain and interchain charge-carrier mobility [22]. PEDOT:PSS has been found to be optically transparent, conducting, high ductility, moderate band gap and low redox potential. The low oxidation potential and moderate band gap of PEDOT gives unique electrochemical and spectroscopic properties [23]. In the doped conducting state (oxidized state) PEDOT is sky blue and transparent. However, the change in redox state leads to the change in color from sky blue to dark blue, due to change in electronic structure. The low oxidation potential of PEDOT and the resulting ambient stability arises because of the high HOMO (highest occupied molecular orbital, analogous to valence band associated with inorganic semiconductor) level. The difference between the HOMO level and the LOMO (lowest occupied molecular orbital, analogous to conduction band) level is referred to as the band gap of the material. The film forming ability, thermal stability and homogenous adsorption of PEDOT:PSS on a flexible substrate make it suitable for use in optoelectronic devices, flexible electronics and electrochemical devices [24-25]. Additionally solution processability makes it convenient to use as an ink/paste during device fabrication. The nanostructured PEDOT polymer is gaining much

attention due to its application in optoelectronic, electronics and sensor devices [23, 26-27].

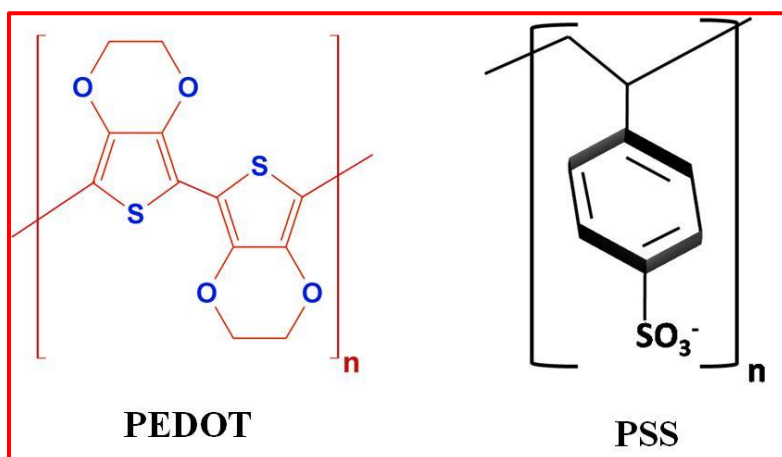


Fig. 1.3: Structure of poly(3,4-ethylenedioxythiophene (PEDOT) and poly(4-styrenesulfonate) (PSS).

1.3 BIOSENSORS

According to the International Union of Pure and Applied chemistry (IUPAC) “A biosensor is a self-contained integral device that is capable of providing specific quantitative or semi-quantitative analytical information using a biological recognition element which is in direct spatial contact with a transduction element” [28]. In a biosensor, physiochemical change occurs due to specific interaction between the target analyte and the biological element is detected and measured *via* a transducer. A biosensor consists of three major components such as a bio-recognition element for selective recognition of an analyte also known as bio-receptor, an immobilization matrix for the immobilization of a recognition biomolecule and a transducer for conversion of biochemical response into a measurable signal. Enzymes, DNA and antibodies are the most commonly used bio-sensing materials in the development of the biosensors because of their specific nature. These biomolecules are not stable in

the solutions. Thus it is necessary to immobilize them onto a matrix that can provide a bio-compatible environmental to the bio-molecule. The bioreceptor recognizes the target analyte and the corresponding biological response are then converted into equivalent electrical signals by the transducer. The amplifier in a biosensor responds to change in small input signal from the transducer and delivers a large output signal that contains the essential waveform features of an input signal. The amplified signal is then processed by the signal processor where it can later be stored, displayed and analyzed [17]. **Fig. 1.4** shows the Schematic of a biosensor. In the past decade biosensing devices have aroused much interest in health care and for environmental monitoring due to their high specificity, sensitivity, speed, portability and low cost [29-30].

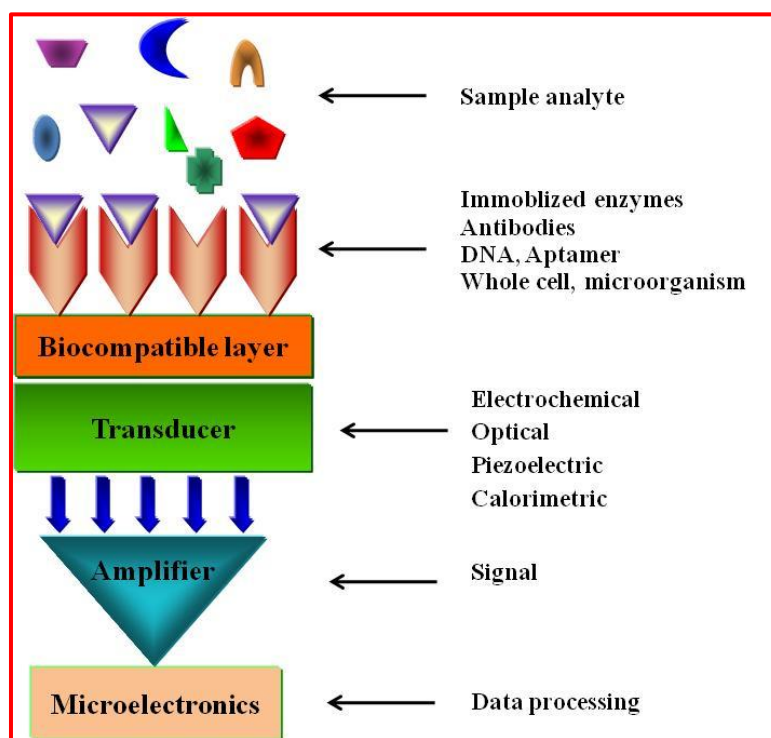


Fig. 1.4: Schematic of a biosensor.

1.3.1 Components of a biosensor

(a) Biomolecular recognition element

Bioreceptor is a molecular assembly that has the capability of recognizing a target analyte. This is considered as the key to specificity for biosensor technologies. The bioreceptors are as numerous as the analytes that have been monitored using biosensors. These are generally classified into four major categories that include: (i) antibodies, (ii) enzymes, (iii) nucleic acids, and (iv) cells [31]. The most common bioreceptors used in biosensors are antibodies (Ab) and on the basis of their elective properties and the synthesis protocol they are classified as polyclonal, monoclonal or recombinant. An interesting approach in which an antigen and an antigen-specific Ab interact is similar to a lock and key fit model. The interaction between a specific Ab and its unique antigen is highly stereo-selective, which results in the formation of three-dimensional (3D) structures. Due to its 3D configuration and the diversity inherent in individual Ab, it is possible to develop an Ab that can recognize and bind to any one of a large variety of molecular shapes. This unique property of antibodies and their ability to recognize molecular structures allows one to develop antibodies that specifically bind to chemicals, biomolecules, microorganisms etc. [32]. **Fig. 1.5** shows the structure of an antibody.

(b) Transducer

A transducer is a device that converts any type of signal into an electrical signal. The signal produced as a result of interaction of bioreceptors with the analyte may be in the form of electrochemical (change in potential or current), optical (color change, luminescence, absorption, surface plasmon resonance), calorimetric (heat measurement), piezoelectric (mass change) response that can be converted to an electric signal *via* suitable transducer. Transducer monitors the physiochemical

change produced by specific interactions between the target analyte and bioreceptor. It converts a biochemical signal into an electrical signal that is processed into an analogue or digital signal [34]. The concentration of an analyte is proportional to the amount of signal generated, allowing the transducer to perform both the qualitative and quantitative measurements.

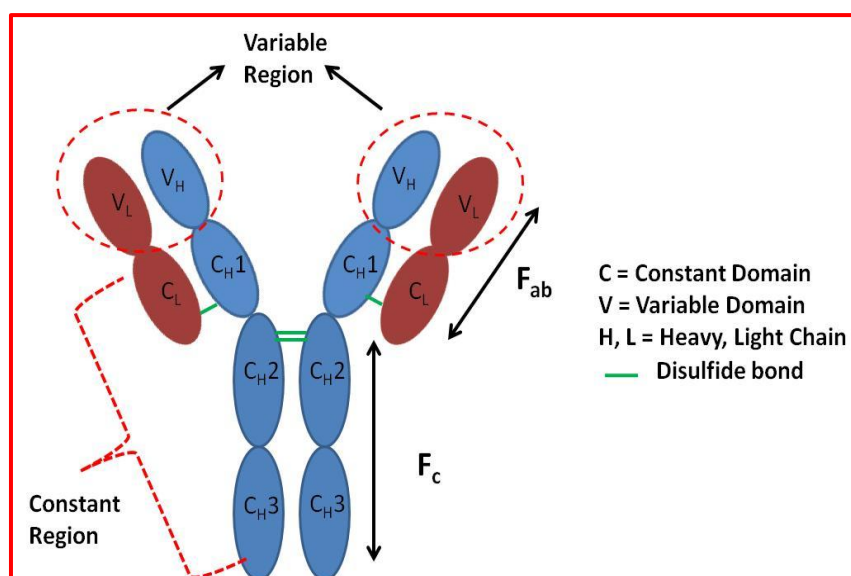


Fig. 1.5: Structure and binding sites of the antibody. Antibodies are glycoproteins belonging to the immunoglobulin super family. Each antibody consist of four polypeptides- two heavy (H) chains and two light (L) chains which are held together by disulfide bonds to form a flexible “Y” shaped molecule. Each chain (H and L) is composed of a variable (V) region and a constant (C) region. The two structural portions of the antibody, i.e. the variable (F_{ab}) and the constant (F_c) region, impart distinct biological functions. One of the major functions of the F_{ab} region is antigen recognition [33].

Among the various transducers, electrochemical biosensors have received special attention as they allow high sensitivity, high signal to noise ratio, portability and fast response time [35]. This biosensor combines the analytical power of electrochemical techniques and the specificity of biological recognition processes. The most commonly used transducers in electrochemical biosensors are either amperometric or potentiometric. The analytical information in potentiometric devices is obtained by converting the biological response or biochemical reaction into a

potential signal by the use of ion selective electrodes. Amperometric biosensors on the other hand monitor the current generated against applied constant potential by reduction or oxidation of the electroactive species involved in the biorecognition process. Due to the high sensitivity and wide linear range, amperometric biosensors have attracted much attention. The ongoing research on new sensing concepts, combined with numerous technological advancements, has expanded horizons for extensive clinical applications of amperometric devices [36]. The enhanced sensitivity, specificity, simplicity, low sample volume, and inherent miniaturization of modern electrochemical bioassays allow them to compete with the most advanced optical protocols [35]. Feng *et al.* reported an electrochemical biosensor for label free neoplastic cell detection using aptamer and functionalized graphene [37]. The high binding affinity of the aptamer to the over-expressed nucleolin on the neoplastic cell surface enabled the electrochemical aptasensor to detect as low as thousand cells. Chen *et al.* developed a simple, label free electrochemical biosensor for oral cancer detection based on nuclease-assisted target recycling and DNAzyme for the detection of DNA species related to oral cancer in saliva [38].

(c) Immobilization matrices

The immobilization of bioreceptor plays a key role in the development of a whole range of biosensors. The control of this step is very important to ensure high reactivity, orientation, accessibility and stability of the surface-confined probe and to avoid nonspecific binding [39]. Many methods like adsorption, entrapment, biotin-avidin coupling and covalent binding can be used for the biomolecular immobilization and the selection of these methods relies on the matrix [40]. To maintain the bioactivity of a given biomolecule, the optimization of the immobilization matrix on the sensing chip is a pre-requisite. The matrix must provide similar local aqueous

micro-environment to the bioreceptor as in biological media, so as to prevent self-aggregation, microbial attack and enhance accessibility towards the target analyte [41]. Mostly physical adsorption and covalent binding method are used for immobilization of bioreceptors. In the physical adsorption method a biomolecule can be directly adsorbed on the surface of matrix due to *Vander Waals forces*, ionic binding or hydrophobic forces etc. The main advantage associated with direct adsorption onto solid surfaces is that it is simple and can be used under mild conditions. It requires only a minimum of activation steps and causes little or no conformational change of the biomolecule or destruction of its active center. However, it has the disadvantage that the adsorbed biomolecule may leach from the matrix during operation due to changes in temperature, pH, ionic strength or even the mere presence of substrate. In a covalent binding, biomolecule and matrix bind with the help of functional group that are present on them. This method has been employed to improve uniformity, density and distribution of the bound proteins, as well as reproducibility on the surfaces. The two main precautions which should be taken during covalent attachment are, (i) the binding reaction must be performed under conditions that do not cause loss of bioreceptor activity, and (ii) the active site of an bioreceptor must be unaffected by the reagents used.

1.3.2 Nanomaterial based biosensor

For the fabrication of an efficient biosensing platform, immobilizing matrix plays a crucial role. A successful matrix should immobilize or integrate biomolecules at a transducer surface and efficiently maintain the functionality of the biomolecules, while providing accessibility towards the target analyte and an intimate contact with the transducer surface. In this context, nanomaterials have recently aroused much interest as an immobilization matrix for biosensor. This is because nanomaterials

exhibit interesting properties such as a large surface-to-volume ratio, high surface reaction activity, high catalytic efficiency and strong adsorption ability that make them potential candidate materials to play a catalytic role for the fabrication of a biosensor [42-43]. It enhances the performance of a biosensor in terms of sensitivity, detection limit and stability. Besides this, large surface area of the nanomaterials provides a better matrix for the immobilization of biomolecules leading to its increased loading with desired orientation. Currently nanomaterial based biosensor have drawn considerable interest for early detection of cancer. Rusling *et al.* developed nanostructured electrodes composed of carbon nanotubes for detection of prostate cancer biomarker (PSA) [44]. The high sensitivity (~ 800 times higher) was achieved by attaching HRP-tag secondary antibody to carbon nanotube with detection limit of 4 pgmL^{-1} . Kumar *et al.* fabricated electrochemical biosensor for oral cancer biomarker (CYFRA-21-1) detection using nanostructured zirconia platform [45]. The fabricated electrode shows linear detection range of $2\text{-}16 \text{ ngmL}^{-1}$ with stability up to 6 weeks. Further to improve the characteristics of biosensor zirconia decorate reduced graphene oxide was used. A linear detection range of $2\text{-}22 \text{ ngmL}^{-1}$ and stability of upto 8 weeks was achieved [46]. Emami *et al.* covalently bound HER2 antibody with iron oxide nanoparticle and resulting bioconjugate were immobilized over cysteamine modified gold electrode for detection of breast cancer biomarker, HER2 [47]. The fabricated nanostructure modified bioconjugate not only facilitate electron transfer in redox probe but also improve the sensitivity by increase loading of antibodies. Norouzi *et al.* used gold and ZnO nanoparticles as an immobilization matrix for detection of carcinoembryonic antigen, a cancer biomarker released in colon, rectal, breast, ovary and lung cancer [48]. The fabricated electrochemical biosensor shows wide detection range ($0.1\text{-}70 \text{ ngmL}^{-1}$ and $70\text{-}200 \text{ ngmL}^{-1}$) with detection limit of 0.01

ngmL⁻¹ and fast response time (less than 20 s). Ali *et al.* fabricated label free, high sensitive (7.76 kΩμM⁻¹) and wide detection range (1.0 fM–0.5 μM) impedometric biosensor to detect breast cancer biomarker (ErbB2) using zinoxide nanofibers as an immobilization matrix [49]. Veisi *et al.* reported an electrospun polyaniline nanofiber modified interdigitated microelectrode for detection of cancer biomarker (COX-2) [50]. The high surface area of electrospun nanofiber improved the characteristics of biosensor. It is clear from the above report that nanomaterial could enhance the biosensor characteristics such as sensitivity, linear detection range, detection limit, fast response time and stability.

1.4 CANCER

Cancer is currently a serious concern and is a medical threat to the contemporary world. An estimated 14.1 million new cases of cancer and 8.2 million deaths were reported in 2012 necessitating early diagnosis of this dreaded disease. It is expected that annual cancer cases will rise from 14 million in 2012 to 22 million within the next two decades [51]. Cancer occurs due to uncontrolled growth and spread of abnormal cells. The division of normal cells is precisely controlled and new cells are only formed for growth or to replace the dead ones. However, cancerous cells do not self destruct and continue to divide rapidly even though they are not needed; they crowd out other normal cells and function abnormally (**Fig. 1.6**). They can also destroy the correct functioning of major organs. The losses of cellular regulation that give rise to most or all cases of cancer are due to genetic damage [52].

Mutations in two broad classes of genes may results in the onset of cancer: proto-oncogenes and tumor suppressor genes. Proto-oncogenes are activated to become oncogenes by mutations that cause the gene to be excessively active in

growth promotion. Either increased gene expression or production of a hyperactive product can occur. Tumor suppressor genes normally restrain growth, so damage to them allows inappropriate growth. Many of the genes in both classes encode proteins that help regulate cell birth (*i.e.* entry into and progression through the cell cycle) or cell death by apoptosis; others encode proteins that participate in repairing a damaged DNA. Cancer commonly results from mutations that arise during a lifetime's exposure to carcinogens, which include certain chemicals and ultraviolet radiation. Thus the cancer-forming process, called oncogenesis or tumorigenesis, is an interplay between genetics and the environment. Most cancers arise after genes are altered by carcinogens or by errors in copying and the repair of genes [53]. Even if the genetic damage occurs only in one somatic cell, division of this cell will transmit the damage to the daughter cells, giving rise to a clone of altered cells. It is not yet clear if mutation in a single gene leads to the onset of cancer. More typically, a series of mutations in multiple genes creates a progressively more rapidly proliferating cell type that escapes normal growth restraints, creating an opportunity for additional mutations. Eventually the clone of cells grows into a tumor. In some cases cells from the primary tumor migrate to new sites (metastasis), forming secondary tumors that often have the greatest health impact [54]. Therefore technologies to recognize and understand the signatures of normal cells and how these become cancerous and provide important insights into the aetiology of cancer that can be useful for early detection, diagnosis, and treatment [55].

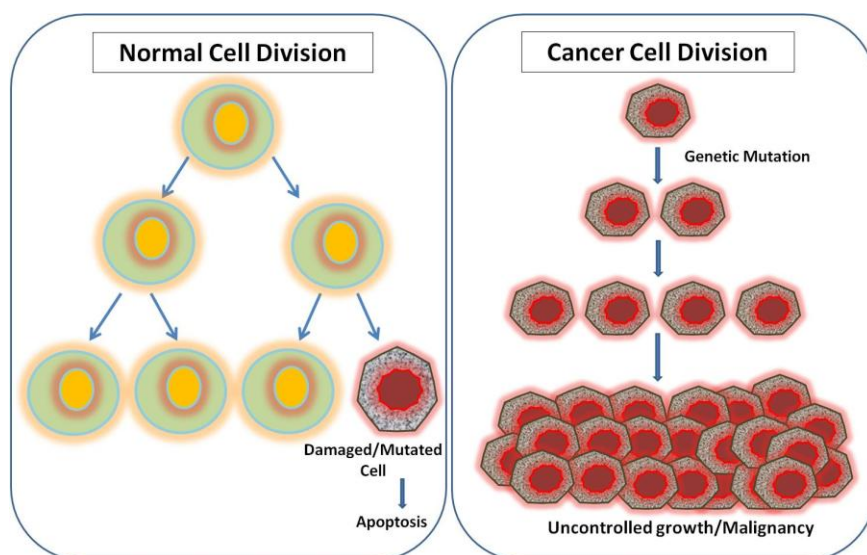


Fig. 1.6: Schematic of cell division in normal and cancer cell.

1.4.1 Biomarkers

The detection of clinical biomarkers is known to play a crucial role in the early detection of a cancer, design of individual therapies, and to identify underlying processes involved in the disease [56]. Biomarkers are chemical substances related with the elevation of malignant tumors which are found in blood, urine, or body tissues [57]. They are normally produced directly by the embryonic tissue or tumor tissue [58]. Biomarkers indicate changes in the expression of a protein that is correlated to risk or progression of a disease or its response to treatment, and that can be measured in tissues or in the blood [58]. As a result, a biomarker can be specific cell, molecule or gene, gene product, enzyme or hormone [58]. An ideal cancer biomarker should have high clinical sensitivity and specificity, quick release in the blood enabling early diagnosis, capability to remain elevated for longer time in the blood, and ability to be assayed quantitatively [59-61]. More than 160 types of biomarkers identified to date can be used to indicate the stage of a cancer. Although there are many techniques available for cancer diagnosis, expression of specific biomarkers, and their accurate estimation, can be helpful in the diagnosis, staging and

effective treatment of a cancer at an early stage [62]. **Table 1.1** summarizes some currently used biomarkers and their clinical utility in cancer diagnosis.

Table 1.1: Cancer biomarkers that are currently in clinical use [63].

Tumor Marker	Cancer Type	Year of discovery	Application based on ASCO and/or NACB recommendations
Alfa-fetoprotein	Germ-cell hepatoma	1963	Diagnosis Differential diagnosis of NSGCT Staging Detecting recurrence Monitoring therapy
Calcitonin	Medullary thyroid carcinoma	1970s	Diagnosis Monitoring therapy
CA125	Ovarian	1981	Prognosis Detecting recurrence Monitoring therapy
CA15-3	Breast	1984–5	Monitoring therapy
CA19-9	Pancreatic	1979	Monitoring therapy
Carcinoembryonic antigen	Colon	1965	Monitoring therapy Prognosis Detecting recurrence Screening for hepatic metastases
ER and PgR	Breast	1970s	Select patients for endocrine therapy
HER2	Breast	1985–6	Select patients for trastuzumab therapy
Human chorionic gonadotropin-β	Testicular	1938	Diagnosis Staging Detecting recurrence Monitoring therapy
Lactate dehydrogenase	Germ cell	1954	Diagnosis Prognosis Detecting recurrence Monitoring therapy
Prostate-specific antigen	Prostate	1979	Screening (with DRE) Diagnosis (with DRE)
Thyroglobulin	Thyroid	1956	Monitoring
Abbreviations: DRE, digital rectal examination; ER, estrogen receptor; NACB, National Academy of Clinical Biochemistry; NSGCT, nonseminomatous germ cell tumor; PgR, progesterone receptor.			

1.4.2 Carcinoembryonic antigen (CEA)

Carcinoembryonic antigen (CEA) is an important biomarker for the diagnosis and routine monitoring of cancer. It is a highly glycosylated cell surface glycoprotein, belonging to a group of substances known as the tumor-associated antigens and comprises of 60% carbohydrates having a molecular mass of 180-200 KDa. The gene encoding CEA is now classified as a member of the immunoglobulin supergene family. This family includes genes coding for adhesion proteins such as intercellular adhesion molecule 1 (ICAM-1) and lymphocyte function-associated antigen 1 as well as the major histocompatibility antigens. The human CEA gene family is clustered on chromosome 19q and comprises 29 genes [64].

Carcinoembryonic antigen stands out as being most widely used biomarker to detect cancer as its elevated levels are found in patients with colorectal, lung, ovarian, pancreatic and breast and liver cancer [65-68]. Post-operative normalization of serum CEA level has been reported to be a favourable prognostic indicator in lung cancer and the identification of abnormal pre- and post-operative serum CEA levels may be useful in the auxiliary cancer prognosis or post-operative surveillance of colorectal cancer patients [69]. According to WHO report [70] more than half of all cancer deaths each year are due to lung, stomach, liver, colorectal and female breast cancers. Therefore, monitoring of CEA level before and after cancer therapy facilitates early recognition of recurrences or detection of previously unremarked metastases. In the serum of healthy individual, CEA reaches concentration up to approximately 2.5 ngmL^{-1} , cut-off value 5 ngmL^{-1} and cancer patient are known to report maximal 20 ngmL^{-1} . In some cancer patients, concentrations more than 100 times higher (compared to normal value) have been recorded [71]. It has also been observed that smoking may results in increased concentration of CEA [64].

1.4.3 Conventional methods for CEA detection

Carcinoembryonic antigen (CEA) was reported almost five decades ago by Gold and Freedman and was hypothesized to be an oncofetal antigen that is expressed in normal adults tissue as well [72]. CEA has recently been favoured as a target antigen for primary and metastatic colorectal detection and other carcinomas of epithelial origin [73]. Owing to technological advancements various methods for CEA detection have been developed from the last many years. These include immunohistopathology [74-75], radio-immuno assays [76-77], enzyme linked immune sorbent assay (ELISA) [78-79], reverse transcriptase polymerase chain reaction (RT-PCR) [80-81] and radioactive tracer fluoro-2-deoxy-D-glucose-positron emission tomography (FDG-PET) [82-83]. Goldenberg *et al.* reported a 3-step unlabeled antibody immunocytochemical staining method for CEA detection where horseradish peroxidase stain was used. The immunocytochemical reaction could be used to detect CEA concentration above $0.7 \mu\text{g g}^{-1}$ in ethanol and $3.0\text{-}5.0 \mu\text{g g}^{-1}$ in formalin fixed specimens. The CEA concentration values detected by this method are considerably high indicating low sensitivity of the method [74]. Kleist *et al.* used continuous cell line (HT29) from human carcinoma of colon for synthesizing colon tumour antigen CEA which was detected by immunofluorescence technique. The weak fluorescence of CEA indicated low sensitivity of the detection method [75]. Goldenberg *et al.* reported a radioimmuno detection technique for CEA detection in which the prepared hyperimmune goat IgG against CEA was radio labeled with ^{133}I (iodine radioactive isotope) [76]. The detection limit of this method was 2 cm and any tumour below 2 cm was undetectable. This is a major drawback of this method. RT-PCR based detection of CEA/mRNA molecules in peripheral blood of 95 colorectal carcinoma (CRC) patients was carried out by Xu *et al.* [80]. The sensitivity of the

method achieved was 2 copies per tube that were high enough to determine very low levels of CEA in peripheral blood. Yonemura *et al.* employed RT-PCR coupled with conventional cytological assay for determination of CEA mRNA in peritoneal washes of 230 patients of gastric cancer [81]. This method coupled with RT-PCR with cytological assay indicated higher sensitivity over the conventional cytological assay alone.

Positron emission tomography (PET) can be employed to distinguish recurrent tumours from post therapeutic changes. PET is a functional imaging technique relying on physiological changes or metabolic functions for the detection of disease. Fluoro-2-deoxy-D-glucose (FDG) is a radioactive glucose analog used in medical imaging modality PET. The increased glucose metabolism of tumour cells is the base for using FDG-PET in oncology which makes it an important tool for quantitative analysis of malignant tumours. Flanagan *et al.* used FDG-PET for investigating unexplained elevation of plasma CEA levels in 22 colorectal cancer patients post colorectal surgery. PET was more sensitive than conventional imaging methods with a positive predictive value of 89% (15 out of 17) in CRC patients [82]. ELISA has been considered as gold standard technique for detection of proteinaceous molecules and has been traditionally employed for CEA detection [78]. Various modified ELISA techniques using gold nanoparticles have been used to further improve the sensitivity [79]. In spite of the reliable detection, ELISA is a time consuming, complex, requires large sample volume and is an expensive detection method.

1.4.4 Biosensor for CEA detection

Though conventional techniques provide low detection limits but are complex, time consuming, require large sample volume and expensive. The requirement of trained personnel and expensive equipments as in case of FDG-PET is another major

disadvantage of these techniques. They are not rapid and the diagnosis periods ranges from a few hours to a few days and hence are laborious and time consuming. The success of these techniques has been marred by low sensitivity and specificity. Although a number of groups have modified the fundamental techniques for obtaining better results, like modified fluorescence RT-PCR, combining conventional cytology with RT-PCR, radioimmuno assays, yet the achieved sensitivity and specificity of these techniques is low and calls for an urgent need for rapid, reliable, specific, and sensitive alternative technique for CEA detection. In the past decade, the use of simpler and faster analytical procedures based on biosensor particularly electrochemical biosensor has emerged as a promising alternative [84]. They are based on the high affinity interactions between antigen and specific antibodies. Electrochemical biosensors combine the high specificity and affinity of biochemical interactions with the inherent sensitivity of the electrochemical transduction. Other advantages include reduced assay time, portability, simplicity, miniaturization and flexibility. Lin *et al.* utilized gold nanoparticles entrapped chitosan matrix over ITO electrode for electrochemical detection of CEA [85]. A linear detection range of 2-20 ng/mL and stability of upto 14 days was achieved. Tang *et al.* covalently bound CEA antibody with glutathione modified gold nanoparticle and resulting bioconjugate were electropolymerized with o-aminophenol over gold electrode for detection of CEA [86]. The fabricated electrode shows linear detection range of 0.5 to 20 ngmL⁻¹. Huang *et al.* demonstrated electrochemical immunosensor via differential pulse voltammetry for detection of CEA using gold nanoparticle and carbon nanotube modified glassy carbon electrode [87]. The detection range of 0.3-2.5 and 2.5-20 ngmL⁻¹ was observed. Wu *et al.* fabricated electrochemical immunosensor for CEA detection using reduced graphene oxide tetraethylene pentamine (RGO-TEPA)

modified glass carbon electrode [88]. The fabricated electrode detection range was 0.05-20 ng/mL with stability up to 10 days.

It is clear from the above reports that there is a considerable scope to improve the sensing characteristic of CEA *via* nanomaterial integration. However, the rigidity, brittleness and cost of conventional electrode (ITO, gold and glassy carbon) limit their application towards development of wearable, flexible, cost effective and disposable point of care devices. The next section deals with the nanomaterial modified paper for electrochemical biosensor for cancer biomarker detection.

1.5 PAPER

The word paper is etymologically derived from Latin word ‘Papyrus’. The main constituent of paper is cellulose. It is an organic compound having chemical formula $(C_6H_{10}O_5)_n$. It is a natural polymer composed of a linear chain of $\beta(1\rightarrow4)$ linked D-glucose units and joined together by $\beta(1\rightarrow4)$ glycosidic bond. The intra–intermolecular hydrogen bond leads to formation of microfibrillar structure which provides excellent mechanical properties. Paper can be made by dewatering a dilute suspension of cellulose fibers, and the filtration process is followed by pressing and heating. The water suspension of fibers, which is called pulp, is mainly made from wood by separating the wood into its constituent fibers in a mechanical, thermo-mechanical, or chemical process [89]. The structure of the cellulose fibers is schematically shown in **Fig.1.7**.

Paper is a flexible, lightweight, low cost, recyclable and biodegradable material. It is initially used for the packaging, displaying and storing information but in due course of time, mankind has discovered broader applications in filtration (Whatman paper), transformer (as a dielectric material) and also used as actuator.

Recently filter paper has been utilized as the substrate material for low cost flexible electronics such as batteries, supercapacitors and in biosensing applications [90]. This is because paper has a large roughness, poor chemical and mechanical barrier that enable it to absorb conducting materials into its porous structure. Further, paper substrate can be modified chemically to incorporate a wide variety of favorable functional groups that can modulate the bulk and surface properties of paper [91-92].

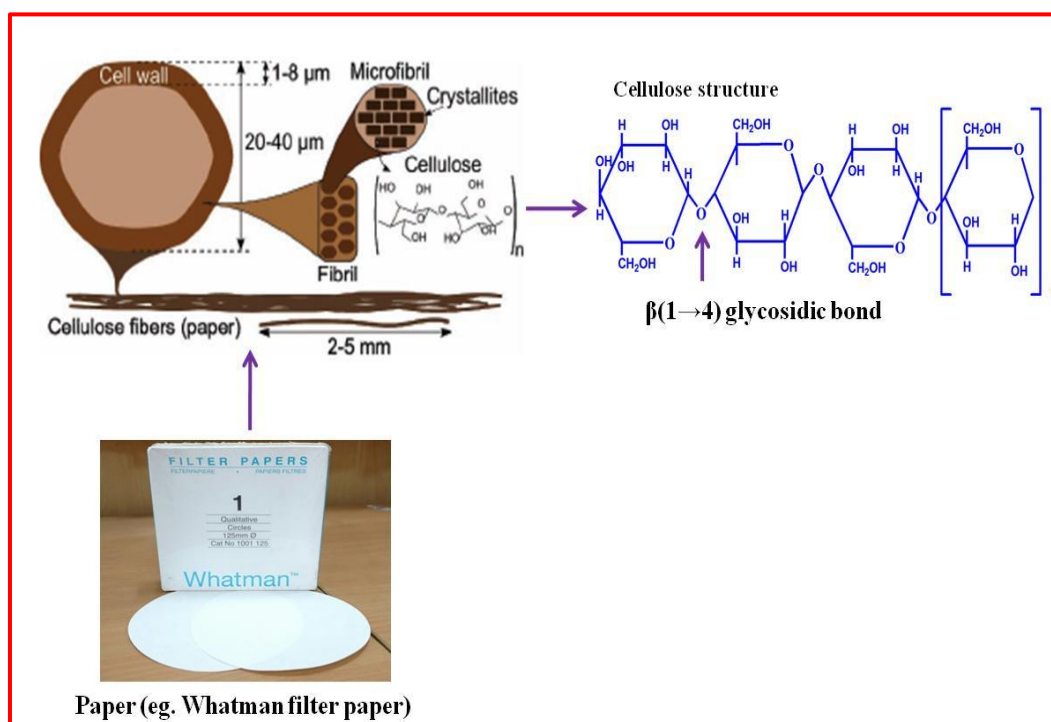


Fig. 1.7: Constituents of a paper. The cellulose fibers in paper are wood cells (or parts of wood cells), which can be up to 2–5 mm long and 20–40 μm wide depending on their origin. The cellulose-based cell wall consists of smaller fibrils, which in turn are made of microfibrils that have a diameter of around 3–20 nm. While the amorphous parts between the fibrils mainly consist of hemicellulose and lignin, the microfibrils consist of cellulose chains that partly form crystalline regions of cellulose and are held together by hydrogen bonding. Cellulose is a polysaccharide consisting of thousands of β -linked glucose units, corresponding to a 5 μ m long linear chain [90].

1.5.1 Conducting paper

Researchers have recently conceptualized a new dimension of paper based electronics which can reduce the cost of device fabrication. Besides this, their mass production, disposability, flexibility, lightweight and ease in processing could meet

the increasing demand of smart electronic devices. Conducting paper (CP) has been considered an efficient platform for transport of both electronic and ionic charge carriers. The CP has thus received enormous attention in many technological applications including capacitors, batteries, displays, thin film transistors, touch pad, and biosensors [90, 93-94]. Both organic and inorganic materials can be used to make paper conducting. The organic materials are preferred due to the flexibility, low cost, and simple processing. However, inorganic materials often have a better electrical performance but some of the drawbacks are high material cost, processing difficulties and cracks in film during bending/sintering. A compromise can perhaps be made by using a composite material, for example, by mixing metal or metal oxide nanoparticles with conducting polymers. Siegel *et al.* used a variety of metals (Al, Zn, Cu, Pb, Ni, Sb, Sn, Ti, Ag, Bi, In, Au and Pt) to produce electrical conductive pathways on paper and studied their electrical conductivity, mechanical property, melting point, and cost etc. [95]. For this purpose authors used a variety of techniques (depending on the material behavior) to deposit metal over paper. Au, Ag can be deposited by sputtering, Sn, Zn are deposited by evaporation and spray deposition is used to deposit Ni and Ag. Besides this, organic materials have been reported to make paper conducting. Zhou *et al.* used poly(3,4-ethylenedioxythiophene)/poly(4-styrene sulfonate) (PEDOT/PSS) for the fabrication of conducting paper [96]. Mäkelä *et al.* used polyaniline-dodecylbenzenesulfonic acid (PANI-DBSA) on the paper substrate via printing method for making paper conducting [97].

1.5.2 Nanomaterials modified conducting paper

Conventional paper-based analytical devices mostly give qualitative or semi-quantitative yes/no (i.e., positive/negative) results and are often limited to screening applications [98]. This is because conventional detection method is based on the

visual observation. However, much effort has been made to improve accuracy and to quantify test results. In this context conducting paper can play an important role in ongoing transition towards the flexible, lightweight, portable, cost effective and disposable devices. There is a great deal of scope to improve the performance of conducting paper based devices by integrating it with nanomaterials. This is because nanomaterials exhibit unique electrical properties, optical properties, large surface-to-volume ratio, high surface reaction activity, high catalytic efficiency and strong adsorption ability. Therefore integration of nanomaterials with paper is likely to exhibit unique physical and chemical properties arises due to nanomaterial as well as flexibility, lightweight, low-cost, disposability and environment friendliness due to paper. Nanomaterial modified conducting paper can be utilized to improve the conduction of electronic and ionic charge carrier within 3D hierarchical structure of cellulose paper that play a major role in energy storage devices, electronic and biomedical application.

Many techniques have been developed to produce conducting paper/nanomaterial modified conducting paper (**Fig. 1.8**) in desired shape and size. These include printing, sputtering, spin coating and dip coating etc. Most of these processes require conducting materials or their templates.

Printing is a fast, low-cost, and widely used method to integrate conducting material in/on to paper. The inks used in conventional printing usually have a rather high viscosity (0.05–100 Pa s) and contain many different components such as solvents, pigments, binders, and additives. When conducting ink/materials are to be printed, the choice of solvents and ink concentration is often limited and the electrical conductivity is typically decreased if binders or additives are used. Furthermore, since the cellulose fibers are hygroscopic, swelling of the substrate during the printing

process might cause problems with the resolution and registration of subsequent layers.

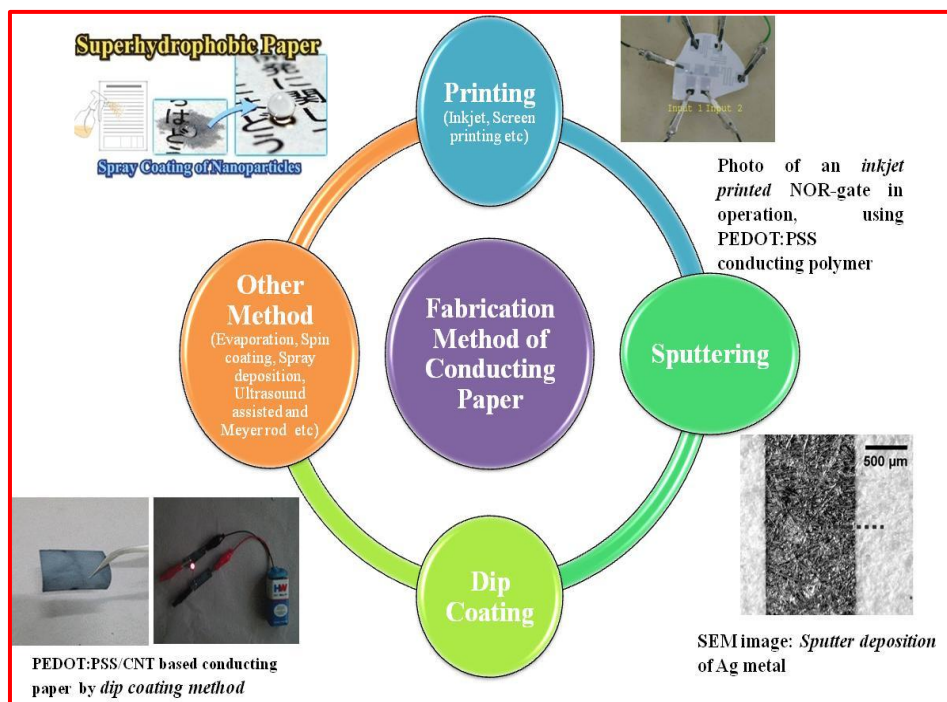


Fig. 1.8: Fabrication of conducting paper via different techniques [95, 99-101].

Mannerbro *et al.* fabricated electrochemical organic transistors on photo paper using desktop inkjet printer [100]. They used conducting polymer, poly(3,4-ethylenedioxythiophene):poly(styrene sulfonate) and the electrolyte suspension as a ink material. Harting *et al.* demonstrated the use of a screen printing approach for the fabrication of paper based field effect transistors using interconnecting silicon nanoparticle [102]. In another work, a screen printed conducting paper electrode was fabricated using graphite and silver ink on the paper substrate followed by electrochemical deposition of polyaniline for the detection of a cardiac marker (cTnI) and a cancer biomarker (sIL2R α) [103-104]. In the screen printing method, high ink viscosity (1-50 Pa) and a large amount of conducting materials are required. Siegel *et*

al. fabricated paper based printed circuit boards (PCBs) by sputter silver and gold on surfaces of paper [95]. Carvalhal *et al.* sputtered gold on Whatman paper for fabrication of patterned electrode using a physical mask made of copper [105]. Further, this patterned paper electrode could be used for quantitative detection of electroactive compounds, such as ascorbic and uric acid. An important advantage of sputter deposition is that even materials with very high melting points can be easily sputtered. This technique requires vacuum and only metallic/alloyed material can be sputtered, which in turn limits their application. Some of other methods used include evaporation [106], spin coating [107] and spray deposition [99] based coating to render the electrical conductivity to a paper. These techniques are instrument dependent, require skilled personal, and necessitate addition of additives and compatibility of instrument with materials. In this context, dip-coating methods are frequently employed to fabricate conducting paper using conducting ink and sol-gel precursors. This technique is instrument independent and can be used to coat organic as well as inorganic material. In this method precision controlled immersion and withdrawal of any substrate into a reservoir of liquid is utilized for the purpose of depositing a layer of material. Many factors contribute to the final state of the dip coating of a thin film. A large variety of repeatable dip coated film structures and thicknesses can be fabricated by controlling factors such as functionality of the initial substrate surface, submersion time, withdrawal speed, number of dipping cycles, solution composition, concentration and temperature, number of solutions in each dipping sequence, and environment humidity etc. The dip coating technique can yield uniform, high quality films even on bulky, complex shapes. There are reports wherein this technique has been used to modify paper for various applications. Lyth *et al.* reported homogenously coated paper substrate with multiwalled carbon nanotube by

dip coating method for photodiode application [108]. Gong *et al.* reported a wearable and highly sensitive pressure sensor by sandwiching ultrathin gold nanowire-impregnated tissue paper (dip coated) between two thin polydimethylsiloxane sheets [109]. This sensor can enable real-time monitoring of blood pulses as well as detection of small vibration forces from music. Wang *et al.* coated filter paper with single walled carbon nanotubes via dip coating method and modified the filter paper used for toxin detection (microcystin-LR) [110].

1.5.3 Applications of nanomaterial modified conducting paper

In the past decade, research on nanomaterial modified paper has increased dramatically due to the potential applications in electronics, energy storage devices, biomedical and biosensors devices. Integration of nanomaterials with paper exhibit unique physical and chemical properties (i.e., thermal, electrical conductivity, optical properties, high mechanical strength and electrochemical behaviors) arises due to nanomaterial as well as flexibility, lightweight, low-cost, disposability and environment friendliness due to paper. Following Sections pertain to some of the potential applications of nanomaterial modified paper.

(a) Electronic applications

Development of nanostructured materials in the form of nanocrystals, nanowires, and nanotubes provides a list of functional inks used for integration into paper. The conductive paper can be used as a flexible platform onto which an electronic structure can be fabricated. The electrical conduction in a modified paper is due to the presence of charge carriers (ions and electrons), and their short range mobility. The charge carriers are believed to be heterogeneous, involving many species as the paper material is chemically heterogeneous [111-112]. Paper is a versatile material. Its chemical and mechanical stability under atmospheric conditions

and ability to absorb ink readily remain unmatched by other materials used in large abundance. Its bulk and surface properties can be easily tuned to a desired level by modifying the fiber, adding chemical additives, and surface treatment [113-115]. Furthermore, the abundance of cellulosic material on this planet makes conductive paper a renewable and sustainable component for electronic devices such as capacitive touch pad [116], memory devices [117], field effect transistor [118], circuit board [95], and frequency identification tags (FID) [119] .

The ongoing efforts are to replace glass based thin film transistor (TFT) screens with a less expensive, lightweight, flexible and thermally stable substrate. Silver nanowire integrated paper was used to fabricate paper based capacitive touch pads [116]. In another report, polyimide based PCBs was replaced by paper based flexible PCBs (Printed Circuit Board) [95]. Fortunato *et al.* developed an oxide based semiconductor thin film Field effect transistor (FET) where paper was used as a dielectric layer. Hybrid FETs with device on both sides of the paper was developed with excellent operating characteristics such as high channel saturation mobility of $>30 \text{ cm}^2/\text{Vs}$ and subthreshold gate voltage swing of 0.8 V/decade [118]. With recent advancements in flexible electronics, printed paper based memory devices (PPMDs) have gained much attention. Lien *et al.* at the National Taiwan University (NTU) worked on PPMDs and successfully fabricated a printed paper based resistive random access memory (RRAM) device on A4 sheet with storage capacity in gigabytes (GB) [117]. The PPMD showed excellent endurance, reliable retention and operating capability under extreme bending condition. Unlike regular silicon based storage devices, PPMDs showed excellent ease of data handling, disposability, switching endurance and reliable retention. There is growing interest in exploiting the potential of paper as a substrate for ultra high frequency (UHF) and microwave applications

such inexpensive, reliable, and durable wireless radio frequency identification (RFID) tags. RFID tags have been used in logistics, monitoring of supply-chain, healthcare, pharmaceuticals, space and anti-counterfeiting. Yang *et al.* reported paper based radio frequency identification (RFID) tags integrated with silver nanoparticles [119]. The use of paper as a substrate for RFID tags has successfully reduced its cost and is eco-friendly.

(b) Energy storage devices

The 3D hierarchical structure of cellulose paper has been found to play an important role towards development of an energy storage system that involves liquid electrolytes, since the interconnected porosity allows fast access of ionic species to the electrode surfaces. In order to render electrical conductivity to the cellulose paper, conducting materials such as metal oxides, graphene, carbon nanotubes (CNTs), metal nanowires, and conductive polymers can be utilized [90, 120]. These nanomaterial based conducting papers have been predicted to have applications in energy storage devices such as electrochemical batteries [121], lithium-ion batteries [122], supercapacitors [123], biofuel cells [124] and nanogenerators [106]. Lithium ion batteries and supercapacitors are known to be good power sources for high power electronics whereas nanogenerators are useful for wearable electronics including sports clothing and military uniforms. Biofuel cells have proved handy for small power electronics such as microfluidics paper analytical devices (μ PADs) and biosensors where the energy requirement is minimal.

Compared with plastics, paper substrates themselves dramatically improved film adhesion, greatly simplified the coating process and significantly lowered the cost. It has been known that conductive paper can be used as an excellent light weight current collector in Li-ion batteries to replace the existing metallic chemical

counterparts. Wang *et al.* developed a flexible single walled carbon nanotube/polycellulose paper for Li-ion battery with first discharge capacity of 153.3 mAhg⁻¹ with columbic efficiencies, 90.6% at 0.1 C and discharge capacity of 102.6 mAhg⁻¹ at high rate (10 C) [122]. Chou *et al.* integrated MnO₂ nanowires with CNTs paper using cyclic voltammetry for demonstration of supercapacitor application [123]. This supercapacitor displayed specific capacitance as high as 167.5 Fg⁻¹ at a current density of 77 mA g⁻¹. After 3000 cycles, the composite paper retained more than 88% of initial capacitance. Cui *et al.* used CNTs and silver nanowire with commonly available commercial paper to fabricate a high efficient supercapacitors and Li-ion battery [125]. Moreover, Kim *et al.* developed the first paper based mechanical nanogenerator where piezoelectric active layer of ZnO rods were introduced on cellulose substrate using low-temperature aqueous solution methods [126]. Nanogenerators are energy harvesting devices that convert mechanical energy into electrical energy. This paper based nanogenerator produced a current density of 2 μ A cm⁻² and an output voltage of 75 mV with stable current output after 10 mechanical bending cycles. These nanogenerators have proved to be an ideal power source for self powered system as an energy source for application in micro-electro-mechanical systems (MEMS). Fraiwan *et al.* developed the first paper based microbial fuel cell (MFC) with rapid electricity generation, an improvement over the conventional MFCs with long startup time usually several days to a week [124]. Choi *et al.* fabricated battery stack using MFC that was able to power a red LED for 30 minutes [93]. This new paper battery is simple, cost effective and is a user friendly power source for single-use paper-based diagnostic devices. There is bright future for MFCs as even O₂ can be used as electron acceptor instead of conventionally used toxic ferricyanide that could perhaps be used for development of paper electronics.

(c) Biomedical applications

The fluidic properties, three dimensional geometry, white background, biocompatible surface, ability to separate analyte, low cost and easy to dispose properties of paper make it an ideal platform for biomedical applications [91, 127]. Integration of a nanomaterial with paper may lead to improved quality of the paper based devices such as enhanced separation, color contrast and loading of the biomolecules etc. The characteristics of the modified paper have found applications in bioassays [128], drug screening [129], ELISA [130], cell culture studies [131], scaffolds [132] and biosensing [133] application.

For ECG recording, the wet gel adhesives are needed that make them inconvenient for long term monitoring. Mostafalu *et al.* fabricated a patterned paper electrode using platinum, nickel and copper nanowire. This nanomaterial modified flexible electrode can be utilized for recording of electrocardiogram (ECG) signals [134]. The high surface area and low impedance of the proposed paper based electrodes were found to facilitate ease of recording even with a dry attachment to the skin. Further same electrode has been used as a cathode in a battery for energy harvesting from natural acidic environments such as body fluids (gastric juice, sweat, urine etc.). Kuzmenko *et al.* fabricated scaffolds by modifying electrospun cellulose with MWCNTs and carbon nanofiber for enhanced neural tissue growth [132]. This platform had the properties to mimic the neural extra cellular matrix (ECM) environment including its structural, topographical and mechanical features that support adhesion, growth and differentiation of neural cells, which could be used in the development of a future disease screening model or a biomaterial for the regeneration of neural tissue *in vitro*. Liu *et al.* developed a plasmonic filter paper by dipping paper in gold nanorods (GNRs) solution. This platform was used to

differentiate normal and cancerous cell using surface-enhanced raman scattering (SERS) [135]. Ornatska *et al.* modified paper with ceria nanoparticles for naked eye detection of glucose [136]. In this method glucose oxidase was immobilized on ceria nanoparticles modified paper. In the presence of glucose, the enzymatically generated hydrogen peroxide induced a visual color change onto the modified paper, from white-yellowish to dark orange, in a concentration-dependent manner. This assay utilized redox behavior of cerium oxide as a colorimetric probe indicator and could be use for 10 consecutive cycles and stability of 79 days. In another study, zirconia nanotubes modified filter paper was utilized to bind oligonucleotides via a coordination effect between zirconia and the phosphate group of probe DNAs. This platform (zirconia/paper) was further used for the sensitive and repetitive recognition of the corresponding complementary target DNA on the nanomolar level [92]. Thus using paper as an assay platform can be an interesting substitute for existing assay platforms since this would open up new possibilities in the biomedical field. **Fig. 1.9** summarizes applications of nanomaterial integrated paper in various fields.

For the fabrication of a biosensor, various electrodes such as indium tin oxide, glassy carbon, silicon wafer, and gold electrodes are being used [45, 87, 138-139]. However, the rigidity, brittleness and cost limit their applications towards the development of a wearable, flexible and cost effective point of care device. In addition to the aforementioned problems conventional electrode require very high temperature for their processing and expertise. Recently, paper based electrochemical biosensors have been attracting considerable attention because of their light weight, flexibility, portability, high sensitivity, fast response time and disposability [46, 94, 128]. Therefore, conducting paper is becoming a suitable substrate for electrochemical biosensing applications.

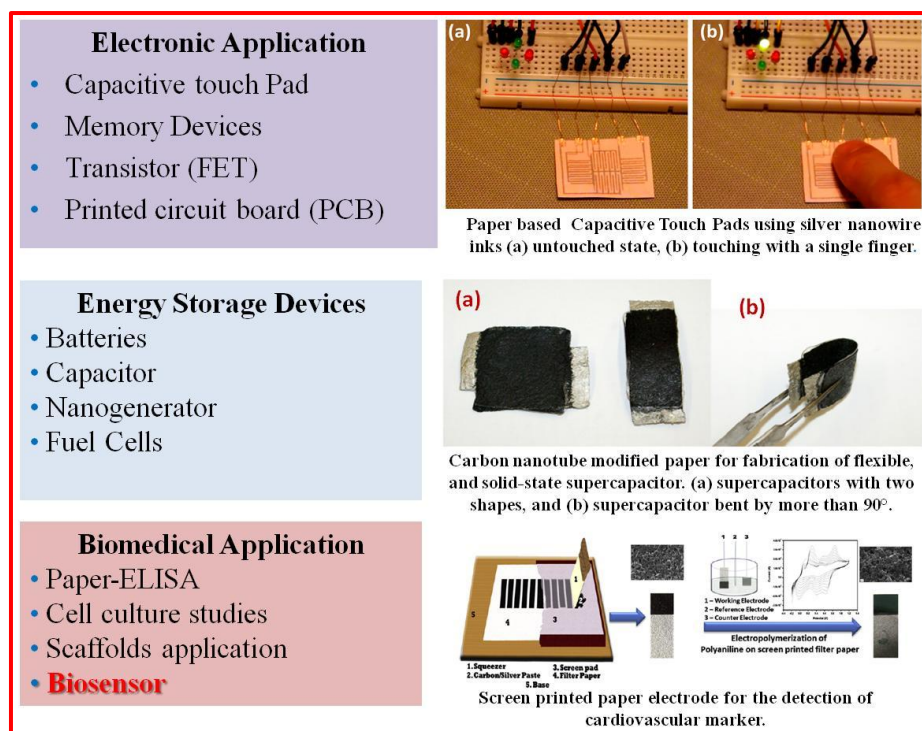


Fig. 1.9: Application of conducting paper in various fields [104, 116, 137].

The advantages of conducting paper as a sensor substrate compared to the conventional electrodes are listed in **Table 1.2**. It is also beneficial in terms of cost, renewable raw material and has a porous structure that are useful for modification of paper substrate for sensing application [91]. Conducting paper (CP) has been considered an efficient platform for conduction of both electronic and ionic charge carriers that play a major role for communication with biomolecule during the biosensing process [94]. For the fabrication of an efficient biosensing platform, immobilizing matrix plays a crucial role. A successful matrix should immobilize or integrate biomolecules at a transducer surface and efficiently maintain the functionality of the biomolecules, while providing accessibility towards the target analyte and an intimate contact with the transducer surface. In this context, the incorporation of a nanomaterial may modulate the performance of conducting paper in terms of electrochemical kinetics, signal stability, and biomolecules loading and

sensitivity. This is because nanomaterials exhibit interesting properties such as a large surface-to-volume ratio, high surface reaction activity, high catalytic efficiency and strong adsorption ability that make them potential candidate materials to play a catalytic role for the fabrication of a biosensor [42-43]. The large surface area of the nanomaterial integrated paper is likely to provide a better matrix for the immobilization of desired biomolecules leading to its increased loading. **Table 1.3** summarizes the materials and techniques used for fabrication of paper based electrochemical biosensors and their characteristics as reported in literature. Besides this, there is a considerable scope for development of a simple, low cost, flexible, lightweight, and environment friendly biosensors with improved sensing characteristics using nanomaterial modified paper platform.

Table 1.2: Comparison between conventional electrodes and paper electrodes.

S. No.	Properties	Conventional electrode (Indium tin oxide and gold coated glass, Glassy carbon, Silicon)	Conducting Paper
1	Cost	Very high	Very low
2	Flexibility	No	Yes
3	Disposability	No	Yes
4	Biocompatibility	No	Yes
5	Modification and Functionalization	Difficult	Easy
6	Fluid flow	Forced	Capillary action
7	Surface by Volume ratio	Low	High
8	Fabrication and High throughput production	No	Yes

Table 1.3: Paper based electrochemical biosensors: fabrication and characteristics.

S.No.	Substrate	Materials	Fabrication Method	Biomarker used	Detection technique	Sensing parameter	References
1.	Whatman filter paper 1	Screen printed carbon electrode	Drop casting	Glucose	Amperometry	[L]= 1-5mM [LOD]= 0.18mM [T]= 4 months	[140]
2.	Whatman filter paper 1	Ag/AgCl ink, Carbon ink, Wax, Graphene, AuNP	Wax printing, Screen Printing	DNA	Differential pulse voltammetry	[L]= 0.0008-500pM [LOD]= 0.2 fM [T]= 4 months	[141]
3.	Whatman filter paper 1	Ag/AgCl ink, Carbon ink, SU-8	Photolithography, Screen Printing	Glucose Pb(II)	Chronoamperometry Anodic stripping voltammetry	Glucose [L]= 0-22.2mM [LOD]= 0.22mM [S]= 0.43 μ AmM ⁻¹ mm ⁻² Pb (II) [L]= 5-100 ppb [LOD]= 1 ppb [S]= 0.17 μ Appb ⁻¹	[142]
4.	Whatman filter paper 1	Graphene, Polyvinyl Pyrrolidone, Polyaniline (G/PVP/PANI), carbon ink, Ag/AgCl ink	Electrospraying Wax printing Screen printing	Cholesterol	Amperometric	[L]= 0.05-10mM [LOD]= 1 μ M [S]= 34.77 μ AmM ⁻¹ cm ⁻² [T]= 2 Weeks	[143]
5.	Platinum sputtered glass	Nitrocellulose paper, Polyester cellulose blend,	Drop casting	Glucose	Amperometric	-	[144]
6.	Whatman paper 1	ITO coated glass Wax, Purssian blue	Drop casting	Glucose	Electrochromic	-	[145]

7.	Filter paper	Gold Nanorods	Dip Coating	oral squamous cell carcinoma (OSCC) cell line CAL-27	Surface-enhanced Raman scattering (SERS)	Intensity ratio of particular raman peak	[135]
8.	Filter paper	Carbon Nanotubes (CNTs)	Dip coating	Microcystin-LR (MC-LR)	Amperometry	[L]= 1-10 ngmL ⁻¹ [LOD]= 0.6 ngmL ⁻¹	[110]
9.	Whatman filter paper 1	Screen printed carbon electrode	Drop Casting	Pb (III)	Anodic striping voltammetry	[L]= 10-100 ppb [T]= 3 months	[146]
10.	Whatman filter paper 1	Gold	Sputtering	Uric Acid (UA) Ascorbic Acid (AA)	Amperometry	[L]= 0-40 pmols [LOD]=0.02 mmol L ⁻¹ AA [S]=152 nA L mmol ⁻¹ UA [S]=64 nA L mmol ⁻¹	[105]
11.	Whatman filter paper 1	Carbon ink	Screen Printing	Glucose Lactate Uric Acid	Chronoamperometry	Glucose [L]=0-100 mM [LOD]=0.21 ± 0.02mM [S]=64 µAmM ⁻¹ Lactate [L]=0-50 mM [LOD]= 0.36 ± 0.03mM [S]=40 µAmM ⁻¹ Uric Acid [L]=0-35 mM [LOD]=1.38 ± 0.13mM [S]= 6 µAmM ⁻¹	[147]

12.	Whatman filter paper 1	Carbon ink, Prussian blue	Wax Screen Printing	Glucose	Chronoamperometry	[L]=0.5-5 mM [S]=1 μAmM^{-1}	[148]
13.	Whatman filter paper 1	Carbon ink	Solid Wax Printing Screen Printing	Glucose	Chronoamperometry	[L]=0-20 mM [LOD]=0.35mM [S]=0.041 μAmM^{-1}	[149]
14.	Whatman filter paper 1	Gold and platinum NPs on SPE	Wax Printing	Single Stranded DNA	Amperometry Cyclic voltammetry	[L]= 10.0fM-100nM [LOD]= 6.3fM	[150]
15.	Whatman filter paper 1	Pencil drawn Electrode, Carbon Paste	Wax Printing	Ascorbic Acid, Dopamine, Paracetamol	Amperometry	-	[151]
16.	Whatman filter paper 1	Graphite Pencil	Wax Printing	Glucose	Chronoamperometry	[L]=0.01-1.5 mM [LOD]= 0.38 μM [T]= 5days	[152]
17.	Whatman filter paper 1	CdS quantum dot and CNTs on SPE	Wax Printing	Adenosine Triphosphate (ATP)	Cyclic voltammetry	[L]= 1–1000pM [LOD]= 0.2 pM [S]= 27nApM ⁻¹ [T]= 4 weeks	[153]
18.	Whatman filter paper 1	Gold NPs on Carbon	Wax Printing, SlipPAD technique	Single stranded DNA, Thrombin	Alternating Current voltammetry	ssDNA [LOD]= 30nM Thrombin [LOD]= 16nM [T]= 4 weeks	[154]
19.	Japanese Paper	Screen Printed Electrode	Screen Printing	Glucose	Amperometry	[L]= 10-100 mM [S]= 0.055 $\mu\text{A mM}^{-1}$	[155]

20.	Whatman filter paper 1	Gold NPs on SPE	Wax Printing Screen Printing	Microcystin-LR	Differential Pulse voltammetry	[L]= 0.01–200 $\mu\text{g mL}^{-1}$ [LOD]= 0.004 $\mu\text{g mL}^{-1}$ [T]= 2 months	[156]
21.	Whatman filter paper 1	Carbon graphite ink on SPE	Screen Printing	Nicotinamide adenine dinucleotide (NADH) Nitrite	Cyclic voltammetry	NADH [L]= 10–100 mM [LOD]= 1.8 μM Nitrite [L]= 10–100 mM [LOD]= 15.1 μM	[157]
22.	Whatman filter paper 1	Chitosan-Silver on SPE	Screen Printing	Cancer Antigen 125 (CA125) Carcinoma Antigen (CA199)	Square Wave voltammetry	CA125 [L]= 0.1–100 U mL^{-1} [LOD]= 0.02 mU mL^{-1} [S]= 2.56 $\mu\text{A mL U}^{-1}$ [T]= 21 days CA 199 [L]= 0.1–100 U mL^{-1} [LOD]= 0.04 mU mL^{-1} [S]= 0.91 $\mu\text{A mL U}^{-1}$ [T]= 21 days	[158]
23.	Whatman filter paper 1	Gold-Manganese oxide NPs on SPE	Wax Printing Screen Printing	Prostate Protein Antigen (PSA)	Differential Pulse voltammetry	[L]= 0.005–100 ng mL^{-1} [LOD]= 0.0012 ng mL^{-1} [T]= 4 weeks	[159]
24.	Whatman filter paper 1	Polyaniline(PANI) on SPE, Graphite and silver paste	Screen Printing	Human Troponin I	Cyclic voltammetry	[L]= 1–100 ng mL^{-1} [S]= 5.5 $\mu\text{A ng}^{-1} \text{mL cm}^{-2}$	[104]

25.	Whatman filter paper 1	SPE, graphite carbon and silver paste	Screen Printing	2-(dibutylamino) ethanol NADH	Cyclic voltammetry	DBAE [L]=3-5000 μ M [LOD]=0.9 μ M NADH [L]=0.2–10 mM [LOD]=72 μ M	[160]
26.	Whatman filter paper 1	Nafion/graphene Oxide on SPE	Photolithography Screen Printing	DNA Mismatches	Electrochemi-luminescence	[L]= 10 nM-5 μ M [LOD]= 1 nM [T]= 3 Months	[161]
27.	Whatman filter paper 1	Tin Oxide QDs/ RGO/Gold NPs on SPE	Screen Printing	ATP	Electrochemical Impedence Spectroscopy [EIS]	[L]= 0.1 pM-100 nM [LOD]= 0.025 pM [T]= 5 Weeks	[162]
28.	Filter paper	SWCNTs	CNTs ink Painting	Human Immunoglobulin G (HIgG)	Amperometry	[L]= 6.3– 62 pM [S]=−70.8 pApmols ⁻¹ L	[163]

Abbreviations: [L]= Linear Detection Range, [LOD]= Lower Detection Limit; [S]= Sensitivity; [T]= Stability; Ag/AgCl= Silver/Silver chloride; SPE= Screen Printed Carbon Electrode; ITO= Indium Tin Oxide; NP= Nanoparticle; CdS= cadmium sulfide; CNTs= Carbon nanotubes; SWCNTs= Single walled Carbon Nanotubes; PAD= Paper Analytical Device; QD= Quantum Dot; RGO= Reduced graphene Oxides; DNA= deoxyribose nucleic acid

1.6 OBJECTIVES OF THE STUDIES

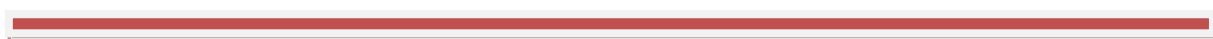
The aim of the research is to develop a substitute for conventional electrode (ITO, gold and glassy carbon), that have limitations for application in smart POC devices and their application in biosensor for carcinoembryonic antigen (CEA) detection.

To achieve this objective, the following experiments have been undertaken:

1. Selection of promising conducting material (PEDOT:PSS) for paper substrate.
2. Optimization of PEDOT:PSS coated paper via treatment with various solvents.
3. Incorporation of RGO, CNTs and PEDOT:PSS electrospun nanofibers in PEDOT:PSS coated paper.
4. Characterizations of nanomaterials modified conducting paper electrodes.
5. Immobilization of anti-carcinoembryonic antigen (anti-CEA) on nanomaterial modified conducting paper.
6. Electrochemical response studies of the fabricated paper based immunoelectrode.
7. Validation through real sample from cancer patients via the immunoassay technique.

The next chapter (**Chapter 2**) contains details of the various materials and methods used for fabrication of paper sensor for cancer biomarker (CEA) detection. And the principles of various experimental techniques that have been utilized for the characterization of modified paper electrodes. Further, efforts have been made on selection of suitable materials and solvents for obtaining improved characteristics of the paper electrode. The fabricated PEDOT:PSS/RGO (**Chapter 3**), PEDOT:PSS/CNTs (**Chapter 4**) and PEDOT:PSS nanofibers modified paper (**Chapter 5**) are

efficiently be utilized in the development of flexible, cost effective, disposable and environment friendly platform for electrochemical biosensor. Incorporation of nanomaterials with paper results in improved electrochemical characteristics towards CEA sensing.



CHAPTER 2

Materials and Characterization Techniques

2.1 INTRODUCTION

This Chapter describes details of the various materials used for the fabrication of paper based biosensors for carcinoembryonic antigen (CEA) detection using electrochemical technique. Further, the analytical techniques used for characterization of the conducting paper (CP), nanomaterial modified CP and immuno-electrodes have been discussed. Attempts have also been made to describe the procedures and protocols used to immobilize antibodies and to estimate various parameters related to the characteristics of paper based biosensors.

2.2 MATERIALS

Details of materials (chemicals and biochemicals) used while pursuing different experiment are as follows:

Poly(3,4-ethylenedioxythiophene:poly(4-styrenesulfonate) (PEDOT:PSS, 1.3 wt%, PEDOT content: 0.5wt%, PSS content: 0.8 wt%) (Catalog No. 483095), carcinoembryonic antibody monoclonal (anti-CEA, from mouse) (Catalog No. C2331), carcinoembryonic antigen (CEA) (Catalog No. 4835), 1-ethyl-(dimethylaminopropyl)-carbodiimide hydrochloride (EDC, $C_8H_{17}N_3.HCl$) (Catalog No. 03449), albumin (acetylated, bovine serum) (Catalog No. B2518), graphite flakes ($\sim 45\mu m$, >99.99 wt %) (Catalog No. 332461) and polyvinyl alcohol (PVA) (Catalog No. 341584) were procured from **Sigma Aldrich** (USA). Sodium dihydrogen phosphate dihydrate (NaH_2PO_4) (Catalog No. 61784505001730), di-sodium hydrogen phosphate dihydrate (Na_2HPO_4) (Catalog No. 61790905001730), potassium ferrocyanide [$K_4(Fe(CN)_6)$](Catalog No. 61843505001730), potassium ferricyanide [$K_3(Fe(CN)_6)$] (Catalog No. 61843605001730), and ethanol (C_2H_5OH , 99%) (Catalog No. 100983) have been purchased from **Merck**. N-hydroxysuccinimide (NHS,

C₄H₅NO₃) (Catalog No. 084718, >97 wt %) and sodium chloride (NaCl) (Catalog No. 1949134) have been purchased from **SRL** (India). Hydrazine hydrate (N₂H₄, 80%) (Catalog No. 100983), ethylene glycol (C₂H₆O₂, 98%) (Catalogue No. 23405), formic acid (CH₂O₂, 85%) has been purchased from **CDH**, **Fisher scientific** and **Rankem**, India respectively. Besides this, deionized water (Resistivity ~18.2 MΩCm⁻¹) was obtained through **Milli-Q** system and Whatman filter paper 1 was procured from **GE Healthcare**, UK.

2.3 CHARACTERIZATION TECHNIQUES

This thesis includes the various tasks related to (1) fabrication of PEDOT:PSS-RGO, PEDOT:PSS-CNTs nanocomposite and PEDOT:PSS-PVA nanofibers based conducting paper electrode (2) immobilization of monoclonal antibodies (anti-CEA) onto paper based electrodes to explore their applications for cancer biomarker (CEA) detection. At various stages of preparation, these fabricated conducting paper electrodes/bioelectrodes were characterized using various techniques such as four points probe conductivity measurement, X-Ray diffraction (XRD), Fourier transform infrared (FT-IR) spectroscopy, Raman spectroscopy, X-ray photoelectron spectroscopy (XPS), Scanning electron microscopy (SEM), Energy dispersive X-Ray spectroscopy, Transmission electron microscopy (TEM), and Electrochemical techniques [Chronoamperometry technique and Electrochemical impedance spectroscopy (EIS)].

2.3.1 Four points probe conductivity measurement

Four points probe is used for measurement of resistivity of bulk and thin film specimen. It consists of four equally spaced tungsten metal tips and from the outer two tip a high impedance current is applied while a voltmeter measures the potential

across the inner two tips which determine the specimen resistivity [164-165]. The instruments used for conductivity measurement consist of a PID controller oven unit, a constant current source, a low current source and a D.C. microvoltmeter. PID controller oven unit is a high quality temperature controlled oven which can give fast heating and cooling rates. PID avoids the wastage of power by using a pulse width modulated (PMW) switch. By having the advantage of both on-off controller and linear PID controller, it provides a stable and accurate temperature control. Constant current source unit is basically used for samples having low to medium resistivity, it functions to provide a constant current to the outer probes irrespective of the variation in resistance of sample due to change in temperature. It uses feedback mechanism to limit the load current of supply to preset maximum value. Low current source unit is used for high resistivity samples. This higher resistance can cause the resistivity measurement prone to noise pick-up from the mains and elsewhere. This unit reduces the problem by having a battery operated source. Also a transistor circuit is used instead of operational amplifier based circuit which offers a reduction of the battery count and is also simple. D.C. microvoltmeter setup is used for measurement of low dc voltage. It uses a very well designed chopper stabilized IC amplifier which offers exceptionally low offset voltage and input bias parameters, combined with excellent speed characteristics. **Fig. 2.1** shows the (a) Schematic of a four probes that measure voltage (V) and supply current (I) to the surface of the sample and (b) assembly of four points probe technique.

Bulk resistivity (ρ_0) can be obtained by using below equation:

$$\rho_0 = \frac{V}{I} \times 2\pi S \quad \dots\dots\dots \text{Eq. 2.1}$$

If thickness of the sample (thin film non conducting bottom surface) is small compared to the probe distance ($W/S < 0.25$) a correction factor for it has to be applied *i.e.* $(2S/W) \log_e 2$.

Where S = distance between equally spaced probe (in our case it is 0.2 cm) and W = thickness of the sample

$$\text{Corrected } \rho = \rho_0 / \text{correction factor} \quad \dots\dots\dots \text{Eq. 2.2}$$

$$\text{Conductivity } (\sigma) = \frac{1}{\rho} \quad \dots\dots\dots \text{Eq. 2.3}$$

The conductivity of the conducting paper was measured using the four points probe technique with a low current source (**LCS-02**), digital microvoltmeter (**DMV-001**) and PID controlled oven (**PID-200**), **SES Instruments**, India. Prior to performing the four points probe experiments on conducting papers, we measured the resistivity of standard samples such as aluminum foil (2.9×10^{-6} ohm.cm) and silicon chip (n-type, 6.5 ohm.cm) and we have observed the nearly similar result as reported in the User Manual [166].

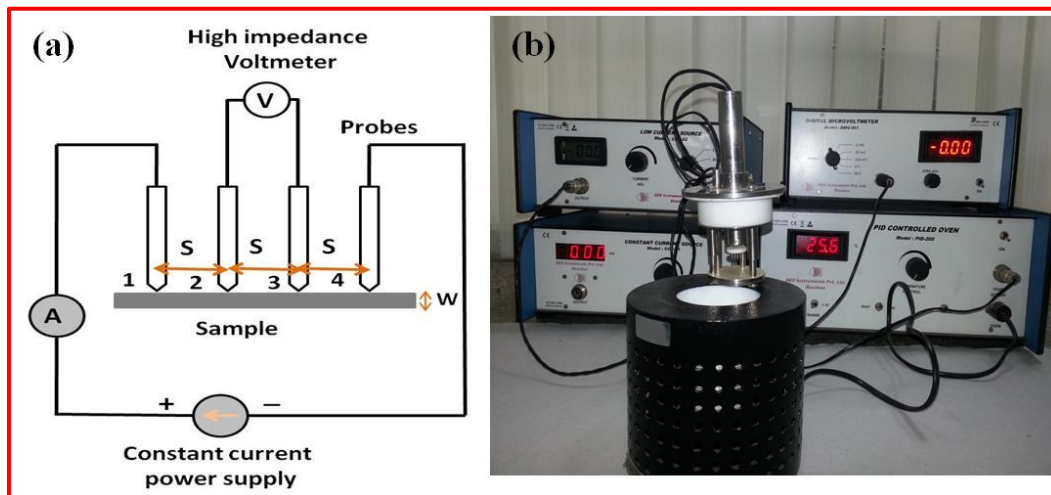


Fig. 2.1: (a) Schematic of four probe that measure voltage (V) and supply current (A) to the surface of the sample and (b) assembly of four point probe technique.

Precautions:

- i) The high resistance ($> 1\text{M}\Omega$) may cause high off-set in D.C microvoltmeter that cannot be adjusted with the knob provided-Note it down and treat it zero error.
- ii) Unstable voltage reading may be due to bad contacts of a probe with the sample.
- iii) In case of semiconductor, like Si though the resistivity of the sample may not be high but because of contact resistance, its effective resistance is usually very high.

2.3.2 X-Ray diffraction (XRD) technique

X-ray diffraction is an effective tool in studying the structure of crystalline substances. The interaction of the X-rays with the crystalline sample produces constructive interference and a diffracted ray when conditions satisfy Bragg's Law (Eq. 2.4):

$$2d \sin\theta = n\lambda \quad \dots\dots\dots \text{Eq. 2.4}$$

Where λ is the wavelength of electromagnetic radiation, θ is the diffraction angle and d is the lattice spacing in a crystalline sample. **Fig. 2.2a** indicates that the diffracted X-rays make angle 2θ with the incident X-rays, where θ is the angle between incident ray and the scatter plane (incident angle). This technique is used to characterize the crystallographic structure, crystallite size (grain size) and preferred orientation in polycrystalline or powder solid samples [167-168]. XRD can be applied to characterize the heterogeneous solid mixture to determine relative abundance of a crystalline compound.

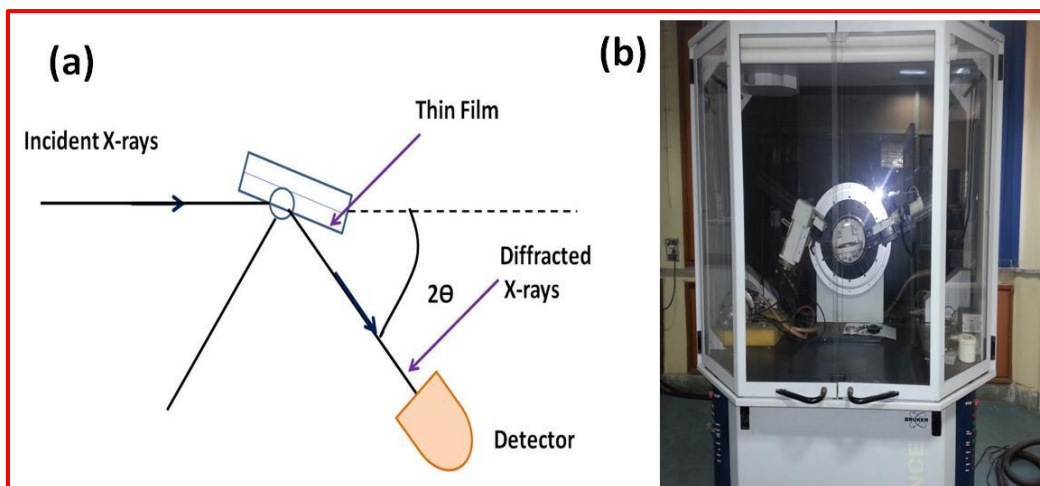


Fig. 2.2: (a) The diffracted X-rays make angle 2θ with the incident X-rays, where Θ is the angle between incident rays and scatter plane (incident angle) and (b) optical image of XRD Bruker model, D-8 advance.

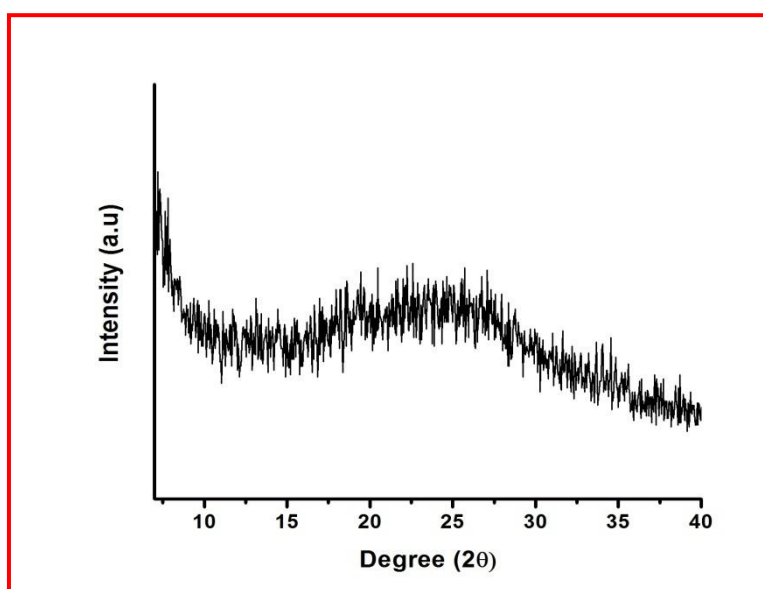


Fig. 2.3: XRD pattern of PEDOT:PSS.

XRD patterns were recorded on X-ray diffractometer (**Bruker D-8 Advance**, **Fig. 2.2b**) with Cu $K\alpha$ radiation 1.54 \AA . The voltage and the current of X-ray tube were 40 KV and 40 mA, respectively. The scanning was done with a step size of 0.02° /step and the integration time of 8 s/step. The sample under study can be either a thin layer of crystal or in powder form. **Fig. 2.3** shows the XRD pattern of PEDOT:PSS

polymer. There are no sharp diffraction peaks observed in the PEDOT:PSS polymer indicating its amorphous nature which are in agreement with the literature [169-170]. XRD studies were used to identify the crystal structure of CNTs and PEDOT:PSS-CNTs composite (**Chapter 4**).

Precautions:

- i) The film should be considerably thick to eliminate the substrate interference.
- ii) To perform the powder XRD, there should be adequate quantity of sample so that the perfect diffraction is achieved.
- iii) Do not expose any part of body to primary beam.

2.3.3 Fourier transform infrared (FT-IR) spectroscopy

Fourier transform infrared spectroscopy is a powerful tool to confirm the presence of functional group in the chemical compound. When quanta of infra red light interact with the molecule, it may absorb energy and vibrate faster. This phenomenon is the basis of FT-IR spectroscopy[171]. Infra red absorption occurs when infrared radiation interacts with a molecule undergoing a change in dipole, and when the incoming photon has sufficient energy for the transition to the next allowed vibrational energy states. The presence of a particular functional group in a given organic compound can be identified, since every functional group has unique vibration energy, the IR spectra can be seen as their fingerprints. As each material exhibits a unique combination of atoms and IR monitors the frequencies of vibrations between the bonds of the atoms making up the material therefore IR spectrum for different materials is distinguishable [172].

A detailed instrumental diagram of a single- beam FT-IR is shown in **Fig. 2.4**. An IR source in the near region (12800 to 4000 cm^{-1}), mid region (4000 - 200 cm^{-1}) or

far region ($200\text{--}10\text{ cm}^{-1}$) sends IR radiation into the interferometer where it travels through the beam splitter into a stationary and movable mirror. Once the IR radiation impacts a mirror, the radiation travels into the sample compartment and to the IR detector. The two beams of radiation produced by the beam splitter can interact with each other resulting in an interferogram. Once the signal has impacted the detector, the interferogram is Fourier transformed into the resulting spectrum of a desired material being analyzed as a function of wavelength or wave number of incident radiation. The laser is used as a calibration technique for the movable mirror in the interferometer. The most common interferometer used in FT-IR spectroscopy is a Michelson interferometer. When the IR radiation travels to the beam-splitter, it is either transmitted or reflected. Half of the radiation beam will impact either a fixed or moving mirror and will be reflected back to the beam-splitter where beam interaction can occur. The motion of the movable mirror causes the radiation to fluctuate when it reaches the detector. Depending on the distance of the movable mirror, the fluctuation can be either destructive or constructive. The difference in the path lengths of the two mirrors is called the retardation. An interferogram is the retardation plotted against the output power of the detector. The interferogram will eventually get Fourier Transformed, outputting a spectrum [173].

The molecules in which the vibrations or rotations within themselves cause a net change in their dipole moment are IR active. The interaction of alternating electrical field of radiation with molecular dipole moment fluctuations permits absorption of the matching vibrational frequency, which causes a change in the amplitude of molecular vibration. Each functional group has specific range of vibrational frequency that is sensitive to the chemical environment, thus providing

valuable information regarding the presence of certain functional groups in the sample. The frequency of vibration is given by **Eq. 2.5**:

$$\nu = \frac{1}{2\pi} \sqrt{\frac{k}{\mu}} \quad \dots\dots\dots \text{Eq. 2.5}$$

Where k is force constant and μ is reduced mass.

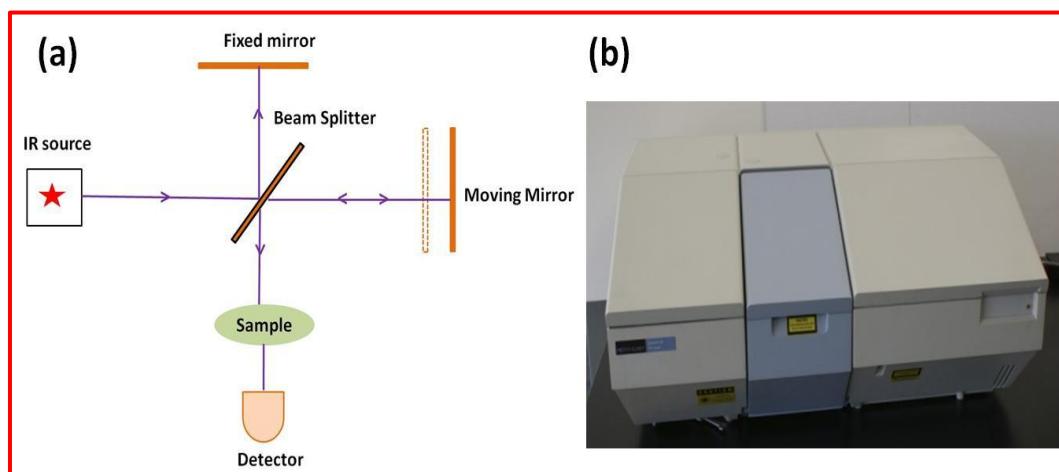


Fig. 2.4: (a) Schematic of optical layout of Michelson Interferometer and (b) optical image of FT-IR spectrophotometer (Perkin Elmer, spectrum BX II).

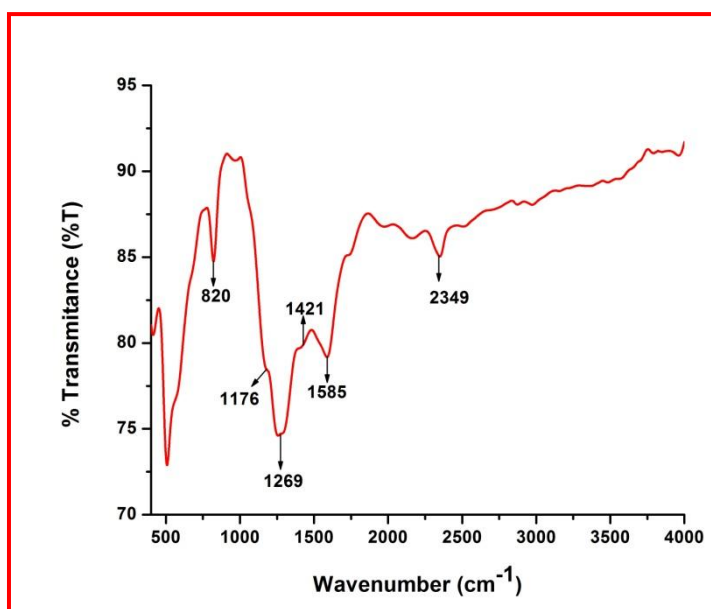


Fig. 2.5: FT-IR spectrum of polyaniline (PANI) modified paper electrode (band observed at 1421, 1585, 1269, 1176 and 820 cm^{-1} are due to benzenoid ring, quinoid ring, C-N stretching, C-H in plane bending and C-H out of plane bending respectively. The peak at the 2349 cm^{-1} corresponds to the NH stretching frequency of $\text{NH}\dots\text{Cl}$ hydrogen bond during electrochemical polymerization of PANI) [104].

FTIR spectra of desired samples (**Chapter 3**) were carried out using **Perkin Elmer Spectrum BX-II** spectrophotometer (**Fig. 2.4b**) with diffuse reflectance accessory in the wavenumber range $400\text{--}4000\text{ cm}^{-1}$. Each was recorded over 64 scans with the resolution of 4 cm^{-1} and interval of 1 cm^{-1} . Prior to conducting FT-IR experiments on desired conducting paper electrodes, we recorded FT-IR of the PANI modified paper electrode (**Fig. 2.5**) and we obtained similar results as reported in literature [104].

Precautions:

- i) Prior to the experiment, IR chamber should be flushed with nitrogen in order to avoid interference of CO_2 and water.
- ii) The sample spectrum should be taken after recording the fresh background.
- iii) The powder sample and KBr must be grinded to reduce the particle size to less than 5 mm diameter.
- iv) Pellet or film should not be too thick to hinder the light to pass through it.

2.3.4 Raman spectroscopy

Raman spectroscopy is an important technique for the analysis of molecules or particles. This is also sensitive to the vibration spectrum of molecules and is complementary to the IR analysis. Unlike IR active molecules, Raman active molecules do not depend upon the presence of a dipole moment but on the polarizability of the molecule. The technique is based on the Raman effect discovered by Sir C.V. Raman in 1928. Whenever scattering of the light occurs, the scattered light consists of two types viz. Rayleigh scattering and Raman Scattering. Rayleigh scattering is strong and has the same frequency (elastic scattering) as the incident

beam (ν_0), and the other is called Raman scattering. Raman scattering is inelastic scattering and has frequencies $\nu_0 \pm \nu_m$ where ν_m is a vibrational frequency of a molecule. Raman scattering is very weak ($\sim 10^{-5}$ of the incident beam). The decreased frequency ($\nu_0 - \nu_m$) and increased frequency ($\nu_0 + \nu_m$) lines are called the Stokes and anti-Stokes lines, respectively. The scattering is described as an excitation of the molecule to a virtual state which is lower in energy than a real electronic transition, with nearly coincident de-excitation and a change in vibrational energy. The scattering event occurs in 10^{-14} s or less. In Raman spectroscopy, the vibrational frequency (ν_m) is measured as a shift from the incident beam frequency ν_0 . This shift provides information about vibrational, rotational and other low frequency transitions in molecules. Raman spectroscopy can be used to study solid, liquid and gaseous samples.

The Raman effect is based on molecular deformations in electric field E determined by molecular polarizability, α . The laser beam can be considered as an oscillating electromagnetic wave with electrical vector E . On interaction with the sample it induces electric dipole moment (P) = αE which deforms molecules [174].

Fig. 2.6a shows the various possibilities of scattering after irradiation of the sample. A Raman spectrometer comprises of four components (1) excitation source (laser), (2) sample illumination and collection system, (3) wavelength selector and (4) detector and computer processing system. The FT-Raman spectrometer is preferred over the normal Raman spectrometer due to the advantage of measuring information of all frequencies at the same time. The instrumentation of FT-Raman spectrometer is similar to the normal Raman spectrometer with inclusion of a Michelson interferometer, which enables the simultaneous acquisition of signals of all frequencies along with the improved resolution. The laser is incident on the sample by

means of a lens and a parabolic mirror. The scattered light from the sample is collected and passed to a beam splitter and to the moving and fixed mirrors in the interferometer head. It is then passed through a series of filters and focused onto a liquid-nitrogen-cooled detector [167]. Raman spectra have been recorded on a **Varian 7000 FT-Raman** (**Fig 2.6b**) and discussed in **Chapter 3** and **5**. Prior to conducting Raman experiments on desired materials (PEDOT:PSS, PEDOT:PSS-CNTs and PEDOT:PSS-PVA), we recorded Raman of the reduced graphene oxide (**Fig 2.7**) and we obtained similar results as reported earlier [175].

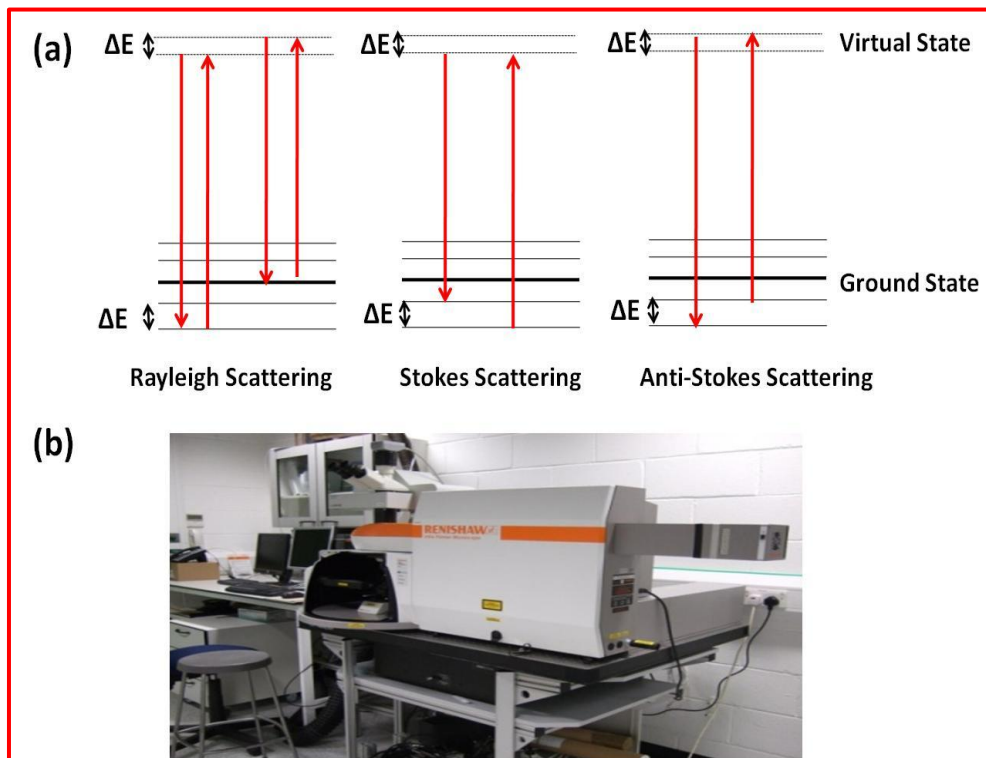


Fig. 2.6: (a) Energy level diagram for Raman scattering including Rayleigh, Stokes and anti-Stokes scattering and (b) optical image of Raman spectrophotometer (Varian 7000 FT-Raman).

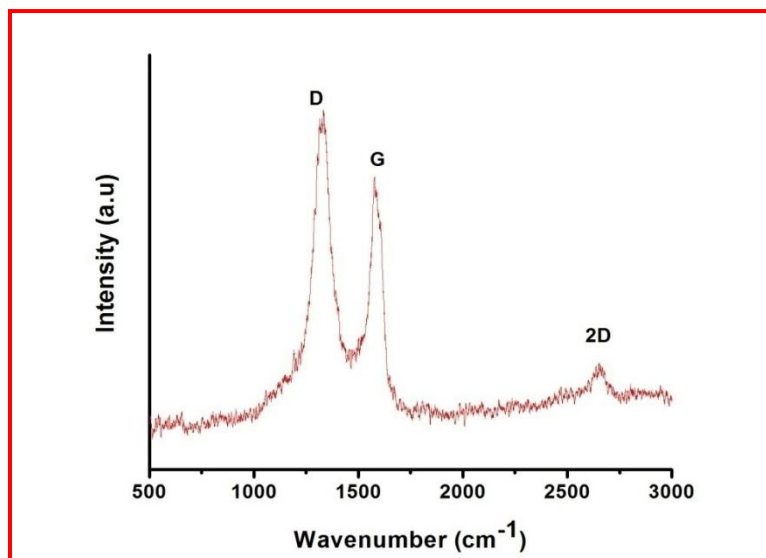


Fig. 2.7: Raman spectra of reduced graphene oxide (RGO). The D (disorder), G (graphite) and 2D (second harmonic motion of D band) bands observed at $\sim 1330\text{cm}^{-1}$, $\sim 1580\text{ cm}^{-1}$ and 2645 cm^{-1} indicate the presence of RGO[175].

Precautions:

- i) For safety reasons, the Laser key should always be in the OFF position, whenever the experiments are not being carried out.
- ii) Ensure that the chamber of the sample compartment is always clean after the experiments have been carried out. This is to prevent contamination that may affect measurements of subsequent spectra of other samples.

2.3.5 X-ray photoelectron spectroscopy (XPS)

X-ray photoelectron spectroscopy (XPS) is a surface-sensitive quantitative spectroscopic technique that measures the elemental composition, empirical formula, chemical state and electronic state of the elements that exist within a material. XPS technique is based on photoelectric effect which refers to the emission of the electrons from the sample surface in response to exposure by soft x-ray incident light. This incident light gives sufficient energy to electrons of sample to be ‘knocked’ out from

the surface of the sample producing electrons (photoelectrons) of discrete energy containing chemical information about the surface analyte. The XPS process is schematically represented in **Fig. 2.8a** for the emission of an electron from the 1s shell of an atom. For each and every element, there is a characteristic binding energy associated with each core atomic orbital i.e. each element gives rise to a characteristic set of peaks in the photoelectron spectrum at kinetic energies determined by the photon energy and the respective binding energies. The presence of peaks at particular energies, therefore, indicates the presence of a specific element in the sample under study. Variation in elemental binding energies (chemical shift) arises from differences in the chemical potential and polarizability of compounds. These chemical shifts can be used to identify the chemical state of materials being analyzed. Furthermore, intensity of the peaks is related to the concentration of the element within the sampled region. XPS is not sensitive to hydrogen and helium, but can detect all other elements. The analysis and detection of photoelectrons in XPS requires the sample to be placed in a high-vacuum chamber. Since the photoelectron energy depends on X-ray energy, the excitation source must be monochromatic [176]. XPS measurements were performed using **Kratos, Axis-Nova** instrument (**Fig. 2.8b**) and has been discussed in **Chapter 3, 4** and **5**. Prior to conducting XPS experiments on desired paper electrodes, we have recorded XPS of the electrochemically deposited polyaniline (**Fig. 2.9**) and the observed peaks well matched with the data reported in literature [103].

Precaution:

- i) Liquid, volatile samples or any substance, which contaminate the chamber of the XPS instrument under the vacuum conditions, cannot be used to conduct XPS studies.
- ii) The wave length of the X-rays should be decided according to the material.

iii) Monochromatic X-ray sources should be used for non biological samples.

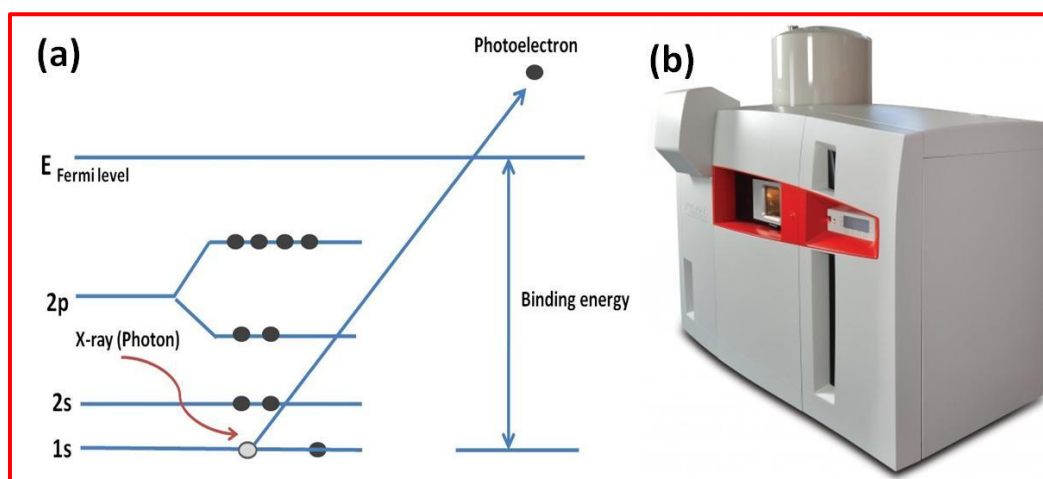


Fig. 2.8: (a) Schematic of the XPS process and (b) optical image of XPS instrument (Kratos, Axis-Nova).

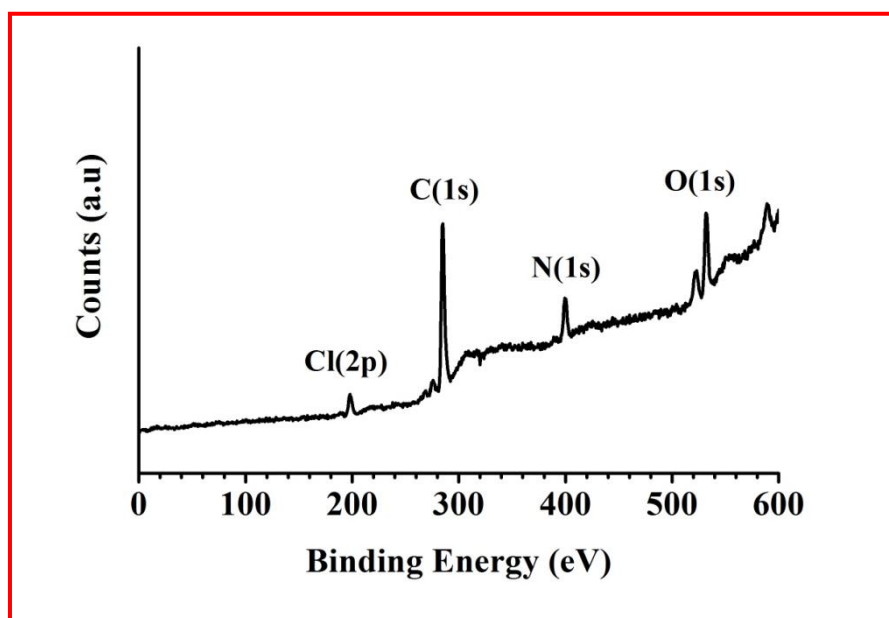


Fig. 2.9: XPS survey scan spectra for electrochemically deposited polyaniline. The analysis of the PANI films shows the presence of N (1s) (~400 eV), C (1s) (~285 eV), Cl (2p) (~199 eV) and O (1s) (~532 eV). The elements carbon and nitrogen originate from the PANI backbone, whereas the element chlorine is a counter ion in the case of the protonated PANI samples [103].

2.3.6 Scanning electron microscopy (SEM)

The scanning electron microscope (SEM) uses a focused beam of high-energy electrons via electrostatic lenses or magnetic lenses to examine objects on a very fine scale. The signals that derive from electron-sample interactions reveal information about the sample including external morphology (texture, shape and size), chemical composition and crystallographic information (orientation of materials making up the sample). In most applications, data are collected over a selected area of the surface of the sample and a 2-dimensional image is generated that displays spatial variations in these properties. The accelerated electrons in an SEM carry significant amount of kinetic energy and this energy is dissipated as a variety of signals produced by electron-sample interactions when the incident electrons are decelerated in the solid sample. These signals include secondary electrons (that produce SEM images), backscattered electrons and X-rays. **Fig. 2.10** shows a Schematic revealing the components of SEM. An electron gun at the top of the microscope produces a beam of electrons. Normally tungsten is used for thermionic electron gun owing to its highest melting point and lowest vapor pressure of all metals. The electron beam is confined and focused using magnetic lenses into a thin, focused to obtain a monochromatic beam. This beam is focused onto the sample. The electron beam is scanned over the specimen in a series of lines and frames called a raster. Once the beam hits the sample, electrons and X-rays are ejected from the sample. Detector converts them into a signal that is sent to a screen [177-178].

SEM analysis is known to be non-destructive. The X-rays generated by electron interactions do not lead to volume loss of the sample, hence it is possible to analyze the same materials repeatedly. One disadvantage of the electron microscope is that insulating samples cannot be analyzed directly as they get charged due to incident

electrons and images become blurred/faulty. Therefore insulating solids are coated with a very thin metal film like gold or platinum ($<10\text{ nm}$) making them conducting without altering any essential details of the sample. The metal film is usually sputter coated on the sample to be investigated prior to the introduction into the electron microscope.

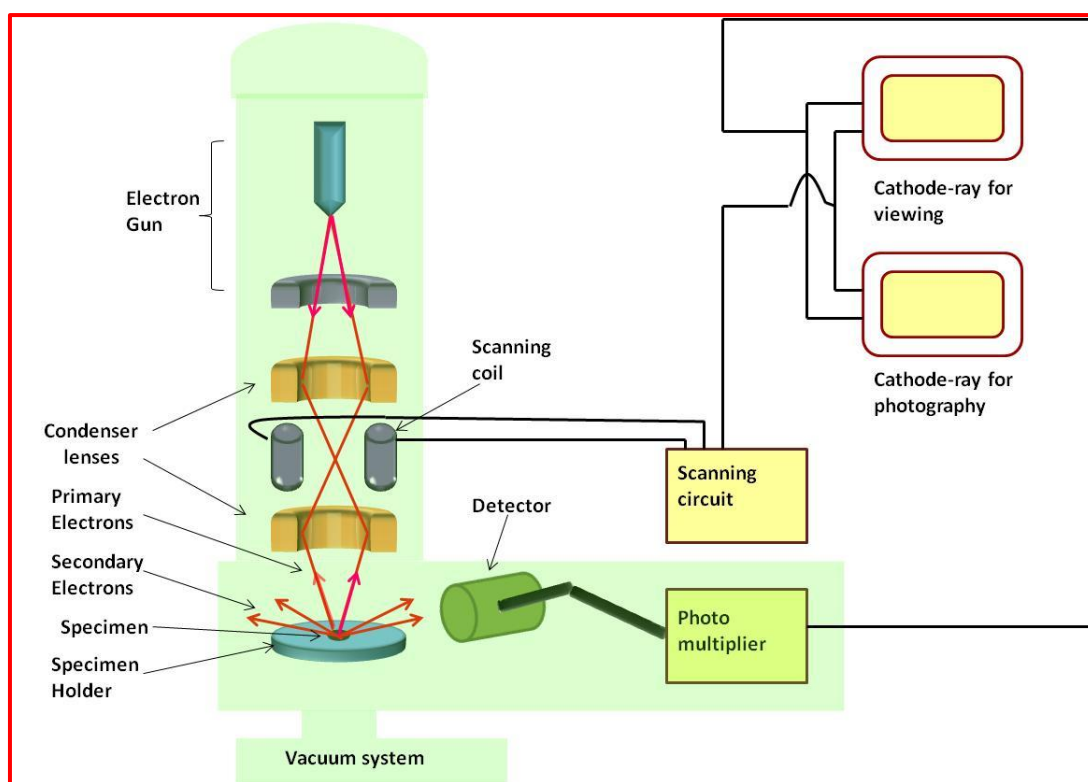


Fig. 2.10: Schematic representation of scanning electron microscope.



Fig. 2.11: (a) Optical image of SEM Hitachi model S-3700N and (b) SEM image of Whatman filter paper 1.

Electron microscopes can be used for elemental analysis of sample using an attachment known as energy dispersive analysis of X-rays (EDX) spectroscopy. The high energy electrons striking the sample produce characteristic X-rays of atoms with which they interact. When analysis of the energies and intensities of such characteristic X-rays are compared, one can obtain the composition analysis of the sample under investigation. The display is a histogram of the X-ray energy received by the detector, with individual peaks, the heights of which are proportional to the amount of a particular element in the specimen being analyzed. SEM and EDX measurements were performed using **Hitachi S-3700N** instrument (**Fig. 2.11a**) and have been discussed in **Chapter 3, 4 and 5**. Prior to obtained the scanning electron micrograph of modified paper electrodes, we have obtained SEM image of Whatman filter paper 1(**Fig. 2.11b**) and observed the same results as reported earlier [179].

Precautions:

- i) If the electrical conductance of the sample is poor, then a few Å thick conductive gold coating should be done by sputtering to obtain better resolution.
- ii) The dimensions of the sample should be $\sim 0.5 \text{ cm} \times 0.5 \text{ cm}$.

2.3.7 Transmission electron microscopy (TEM)

Transmission electron microscope is used for investigating the morphology, composition and crystallographic information of nanomaterials. This technique provides high resolution ($\sim 0.5 \text{ nm}$). The accelerated electrons in TEM are transmitted through the specimen. Thicker parts allow lesser number of electrons to be transmitted and will thus appear darker on hitting the fluorescent screen, as compared to the thinner counterparts of the same specimen. Thus obtained final image is

displayed in real time on the computer monitor. Electrons of very high energy (typically >50 KeV) are used which pass through a series of magnetic lenses. Schematic of TEM is shown in **Fig. 2.12**. The basic components of TEM are electrons source, condenser lens, specimen, objective lens, diffraction lens, intermediate lens, projector lens and a fluorescent screen in the given order. TEM is housed in a chamber having high vacuum $\sim 10^{-3}$ – 10^{-4} Pa for its proper functioning[167]. Moreover, TEM has an additional advantage to obtain diffraction patterns of the sample, by enabling it to understand the detailed crystal structure analysis of the sample. Using diffraction analysis we can be used to find out size dependent changes in the lattice parameters as well as defects in the sample. It is also possible to analyze single particles of very small (nanometer) dimensions. In our present work ,the TEM samples were prepared by dispersing powder/liquid sample in ethanol and a small drop of this solution is cast onto carbon coated copper grid. TEM studies were carried out using **JEOL JEM**, TEM system (**Fig. 2.13a**) at accelerating voltage of 200 KeV. Before conducting TEM of the synthesized nanomaterials we performed TEM of the nanostructured zirconia (ZrO_2) grafted reduced graphene oxide (RGO) (shown in **Fig. 2.13b**) and it is well matched with reported literature [180]. The results of TEM studies of the synthesized nanomaterials have been discussed in **Chapter 3** and **4**, respectively.

Precautions:

- i) Selection of the solvent for TEM analysis should be such a way that it does neither interfere with the sample nor damage the grid.
- ii) The energy of the electrons beam should be optimized as per the need of the sample.

- iii) TEM specimen must be $\sim 1000 \text{ \AA}$ or less in thickness in the area of interest.

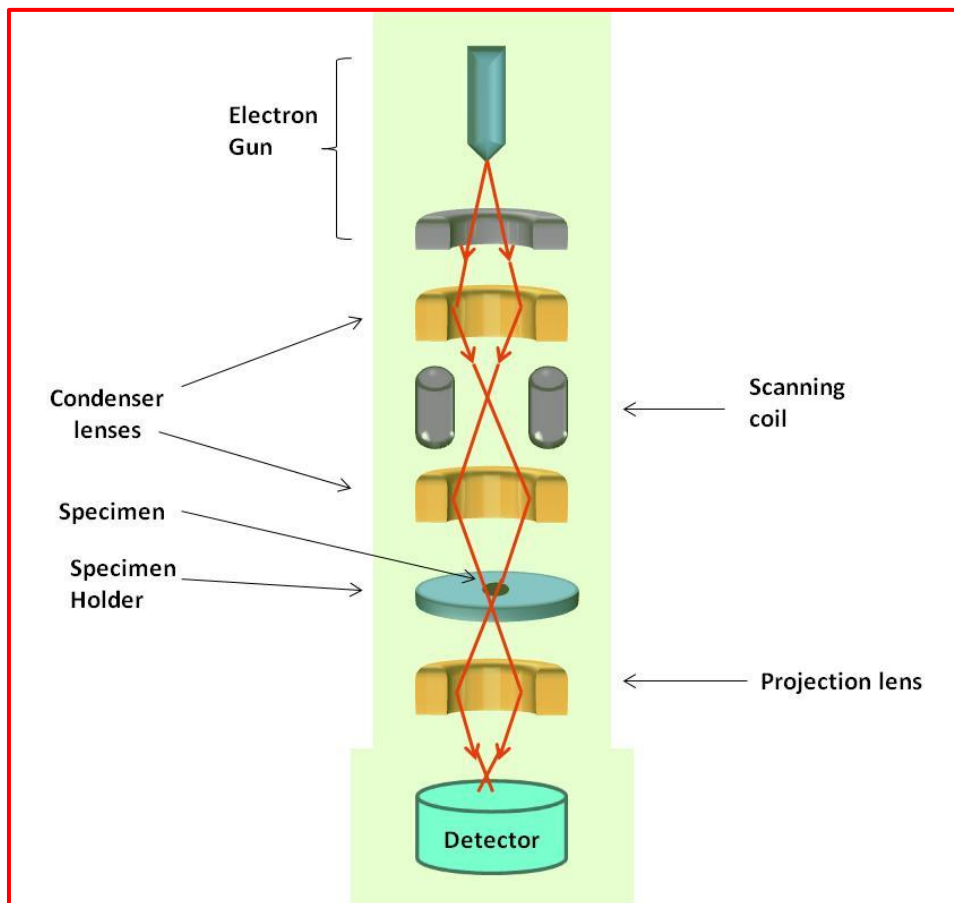


Fig. 2.12: A schematic showing various components of TEM.

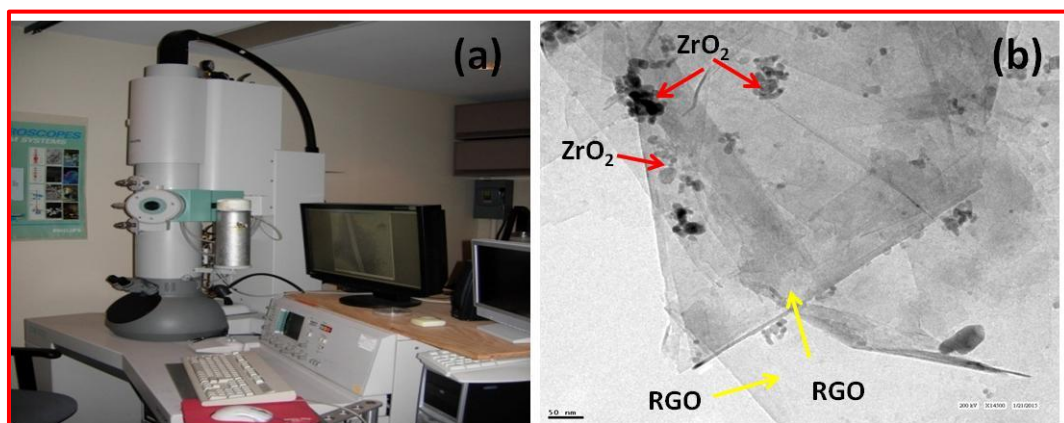


Fig. 2.13: (a) Optical image of JEOL JEM, TEM instrument and (b) TEM image of nanostructured zirconia (ZrO_2) grafted reduced graphene oxide (RGO).

2.3.8 Tensile measurements

Tensile measurement is the most fundamental type of mechanical test that can be performed on materials. In this measurement, materials are pulled in a controlled manner while measuring the applied load and elongation of the material over some distance. The obtained curve reflects the behavior of materials under stress condition [181]. This curve can be converted into a stress versus strain curve by dividing the load and elongation by constant values (material dimensions). Therefore, load-elongation curve has the same shape as the stress-strain curve and it is unique for each material. Tensile tests are used to determine tensile strength, tensile modulus, extension of break and other tensile properties. A typical stress-strain curve is shown below:

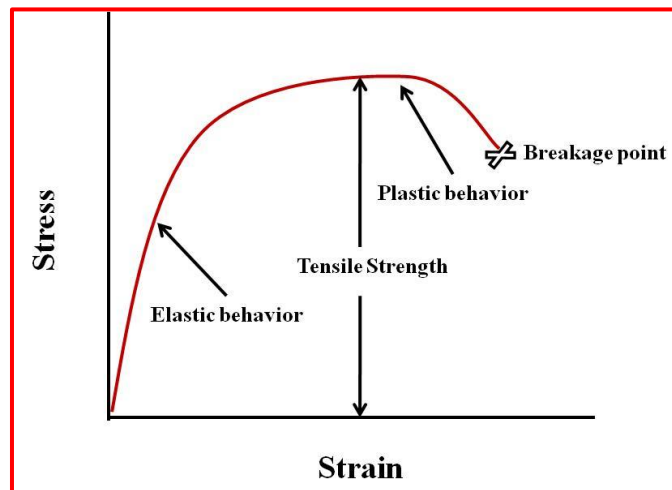


Fig. 2.14: A typical stress-strain curve.

The stress-strain plot can be divided into two distinct regions; plastic deformation and elastic deformation. The deformation which occurs in elastic region is temporary and is revived when the load (stress) is removed whereas the deformation in the plastic region is permanent even after the load (stress) is removed. Moreover, tensile strength is defined as the maximum stress the material can withstand. It is indicative of the strength obtained from determinants such as fiber

strength, fiber length, and bonding. Fracture point is the point where material breaks apart.

The most common testing machine used in tensile testing is the universal testing machine. This type of machine has two crossheads; one is adjusted for the length of the material and the other is driven to apply tension to the test material. In present work, universal testing machine (**UTM, Instron 3369, Fig. 2.15a**) has been utilized to investigate the tensile strength properties of modified paper. The preconditioned test samples ($50 \times 10 \times 0.18$ mm) were mounted between grips of the machine with span length 27 mm and pulled at cross head speed of 5 mm min^{-1} . Before conducting tensile measurement of modified paper electrode, we performed the tensile measurement of the Whatman filter paper 1(**Fig. 2.15b**) and it well matches with reported literature [182]. The results of the tensile measurements of the modified paper electrodes are discussed in **Chapter 5**.

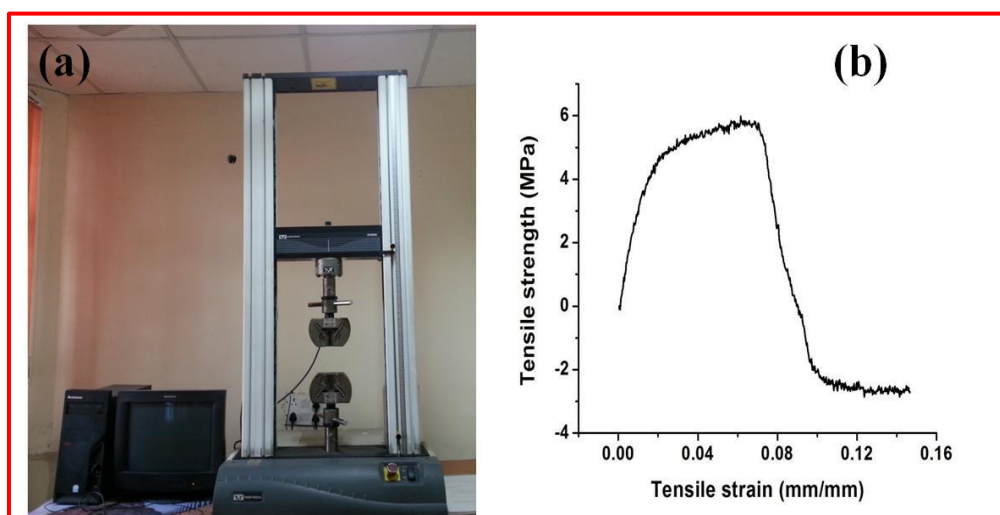


Fig. 2.15: (a) Optical image of universal testing machine (UTM, Instron 3369) and (b) Tensile strength versus strain curve of Whatman filter paper 1.

Precaution:

- i) Test material should be properly aligned so that proper reading could be obtained.
- ii) If the initial portion of the stress–strain curve is curved and not linear, it indicates the specimen is misaligned in the testing machine.

2.3.9 Contact angle (CA) measurement

Contact angle (CA) is the angle at which a liquid/vapor interface meets a solid surface. The CA is specific for any given system and is determined by the interactions across an interface. It depends upon surface roughness, surface condition and surface material. CA describes the shape of a liquid droplet resting on a solid surface. When a tangent line is drawn from a droplet to touch the solid surface, the angle between the tangent line and the solid surface is known as the contact angle. This technique is surface sensitive and has the ability to detect surface properties such as surface energy, wettability and adhesion [183]. The contact angle measurements were carried out to investigate the hydrophilic/hydrophobic character of the surface that can be correlated to material behavior/deposition as well as the immobilization of biomolecule onto the electrodes by Sessile drop method [184]. The Sessile drop method is used to estimate wetting properties of a localized region on a solid surface by measuring the angle between the baseline of the drop and the tangent at the drop boundary. Interaction between liquid and solid surface is very important. When the contact angle is less than 90° , the surface is known as hydrophilic and if it is more than 90° , it is hydrophobic. If the angle is above $\sim 150^\circ$, it is superhydrophobic and if it is less than $\sim 20^\circ$, it is superhydrophilic. The angle which distinguishes between

superhydrophilic and hydrophilic or hydrophobic and superhydrophobic is not very precise and can vary within 5° – 10° .

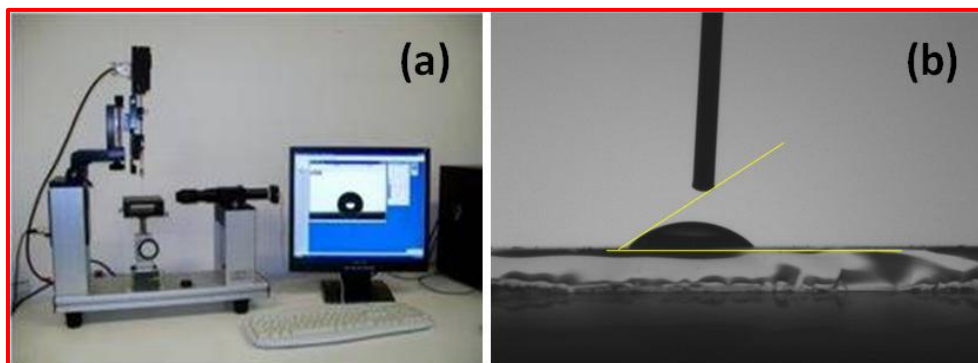


Fig. 2.16: (a) Optical image of CA meter (Data Physics OCA15EC) and (b) CA image of ITO electrode.

The CA measurements were taken by the Sessile drop method using **Data Physics OCA15EC** (**Fig. 2.16a**). **Fig. 2.16b** shows the contact angle of the standard ITO electrode indicating its hydrophilic nature of surface [184]. The results of CA measurements conducted on the modified paper electrodes have been discussed in **Chapter 5**.

Precautions:

- i) Calibration of the instrument should be done using a photographic film standard (sapphire ball standard) because it is a 3D object that requires proper lighting and camera angle. Even more importantly, it demands finding the baseline accurately, which is the difficult part of contact angle measurements.
- ii) The needle tip must be small compared to the drop such that fluid adhesion does not distort the drop shape.

- iii) The expansion or contraction of volume must be slow enough that equilibrium conditions prevail.
- iv) The measurements should be carried out soon after the drop shape stabilizes.

2.3.10 Electrochemical techniques

Electrochemistry is an analytical technique that is used to measure the potential, charge or current to characterize chemical reactivity of an analyte or to determine the analyte concentration [185]. The electrochemical techniques deal with the processes that occur in a system on application of electric potential or current. In most electrochemical techniques, there are three electrodes; the working electrode (WE), the reference electrode (RE) and the counter (or auxiliary) electrode (CE). The three electrodes are connected to a potentiostat, an instrument that controls the potential of the working electrode and measures the resulting current. In a typical electrochemical experiment, a potential is applied to the working electrode and the resulting current is measured and plotted versus time. In another, the potential is varied and the resulting current is plotted versus the applied potential. During the electrochemical reaction (in a solution), the equilibrium concentration of the reduced and oxidized forms of a redox couple are linked to the potential (E) via Nernst's equation:

$$E = E_0 + \frac{RT}{nF} \ln \frac{C_{\text{oxi}}}{C_{\text{red}}} \quad \dots\dots\dots \text{Eq. 2.6}$$

where E_0 is equilibrium potential, F is Faraday's constant, T is absolute temperature, C_{oxi} and C_{red} are concentrations of oxidation and reduction centres. For each redox couple, there is a standard potential (E_0) at which the reduced and oxidized forms are present in equal concentration. If the potential (E) with respect to the reference

electrode is applied to the working electrode, the redox couples present at the electrode respond to this change and adjust their concentration ratios according to **Eq. 2.6**.

We used chronoamperometry and electrochemical impedance spectroscopy (EIS) techniques for the electrochemical characterization of different paper electrodes and immune-electrodes (**Chapter 3, 4 and 5**). For this purpose, a Potentiostat/Galvanostat from **Autolab** (EcoChemie, Netherlands) (**Fig. 2.17**) using a three electrode system with a Ag/AgCl as a reference electrode, platinum wire as the counter electrode and modified paper as a working electrode were used. All measurements were recorded in a clean environment and under unstirred buffer conditions to minimize the errors.



Fig. 2.17: Optical image of Autolab Potentiostat/Galvanostat, EcoChemie, Netherlands.

(a) Chronoamperometry technique

Chronoamperometry uses a step potential that is applied between the working and reference electrode while the steady state current is measured as a function of time [186]. During this process a diffusion layer is formed between the surface of electrode and solution, which controls the transfer of analyte from the bulk solution of higher concentration to the electrode. There is thus a concentration gradient from

solution media to the electrode surface. Chronoamperometric measurement yields a better signal to noise ratio than other electrochemical techniques [142]. In the chronoamperometric measurement, charge transfer to/from the redox-active species as a function of time at constant applied voltages begins with an initially large capacitive current. On the decay of the initial capacitive current, Faradic current (the current that is proportional to the concentration of the analyte) dominates. The current (i) decays as function of time ($t^{1/2}$) as described by the Cottrell equation (**Eq. 2.7**) [142].

$$i = \frac{nFAD^{1/2}C}{\pi^{1/2}t^{1/2}} \dots\dots\dots \text{Eq. 2.7}$$

Where n = stoichiometric number of electrons involved in the reaction, F = Faraday's constant, A = electrode area, C = initial concentration of the reactant and D = diffusion constant of analyte.

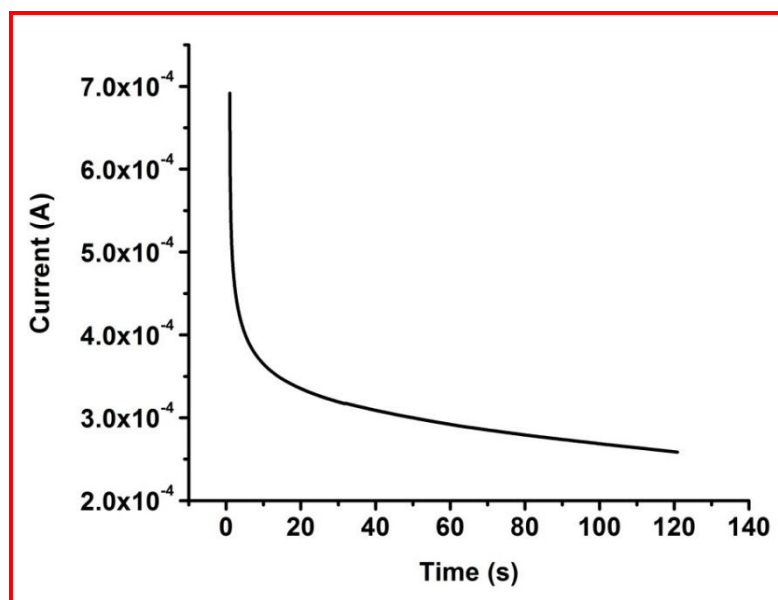


Fig. 2.18: Chronoamperometry plot obtained for PEDOT:PSS/ITO electrode.

Fig. 2.18 shows the chronoamperometric curve of ITO and PEDOT:PSS/ITO electrodes recorded at 2V in phosphate buffer saline (PBS, 50mM, pH 7.0, 0.9% NaCl) containing 5mM $[\text{Fe}(\text{CN})_6]^{3-/4-}$ for 120 s, which is in agreement with literature [187]. It was observed that, initially large electrochemical current was produced

which decays within a few seconds after which faradic current dominate and stable current is generated.

(b) Electrochemical impedance spectroscopy (EIS)

Electrochemical impedance spectroscopy (EIS) is an effective tool to measure the impeded flow of ions through solution, interface and coatings, for studying interfacial properties of the surface-modified electrodes. The EIS technique is commonly applied for the investigations of electrode kinetics, adsorption behavior and interaction of biomolecule with the electrode surface. Electrochemical impedance is usually measured by applying an AC potential (sinusoidal alternating voltage) of different frequencies to an electrochemical cell and measuring the current through the cell. The resulting current signal lags the voltage by a phase of ϕ . The time dependent signal $Z(t)$ is converted into a frequency dependent signal $Z(\omega)$ by a Laplace transformation, whereby the impedance becomes a complex number and can be calculated as follows **(Eq. 2.8)** [188].

$$Z(\omega) = E / I = E_0 \cos(\omega t) / I_0 \cos(\omega t + \phi) = Z_0 \exp(i\phi) = Z_0 (\cos \phi + i \sin \phi)$$

..... **Eq. 2.8**

ω : frequency of the applied potential, ϕ : phase angle, E : alternating voltage, E_0 : amplitude of the alternating voltage, I : alternating current and I_0 : amplitude of the alternating current

$$Z^2 = Z_{im}^2 + Z_{real}^2$$

.....**Eq. 2.9**

However, Nyquist plot (**Fig. 2.19**) represents the real part of impedance at X-axis and imaginary part at y-axis. This Nyquist plot can be modeled by an equivalent circuit (Randles circuit) comprising of the solution resistance (R_s), charge transfer resistance (R_{ct}), Warburg impedance (Z_w) and double layer capacitance (C_{dl}) (**Fig. 2.20**).

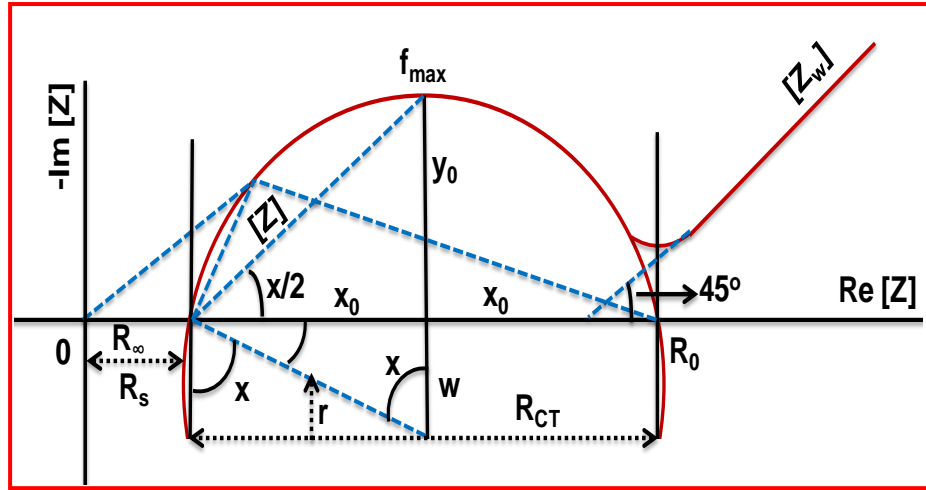


Fig. 2.19: Nyquist plot with depressed arc where, the polarization is due to combination of kinetic and diffusion processes [189].

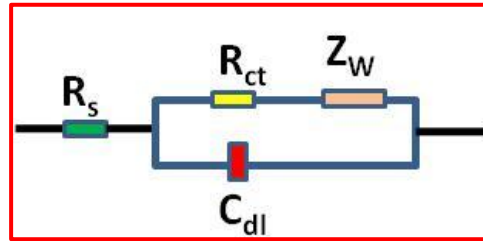


Fig. 2.20: The electrode-solution interface can be modeled by an equivalent circuit (Randles circuit) comprising of the solution resistance (R_s), charge transfer resistance (R_{ct}), Warburg impedance (Z_w) and double layer capacitance (C_{dl}) [190].

Nyquist plot, (a faradic impedance spectrum) includes a semicircle region observed at higher frequency corresponding to electron- transfer limited process and is followed by a linear straight line at 45° to the real axes at lower frequencies, revealing diffusion-limited electron transfer process as shown in **Fig. 2.19**. The semicircle diameter of EIS spectra gives value of R_{ct} that reveals electron-transfer kinetics of redox probe at the electrode interface. Moreover, R_s and Warburg impedance (Z_w) represent bulk properties of the electrolyte solution and diffusion of applied redox probe, respectively. Z_w can be estimated from the Nyquist plot to describe the electrical response at electrode. It can be expressed as an intercept of the straight line having slope of 45° .

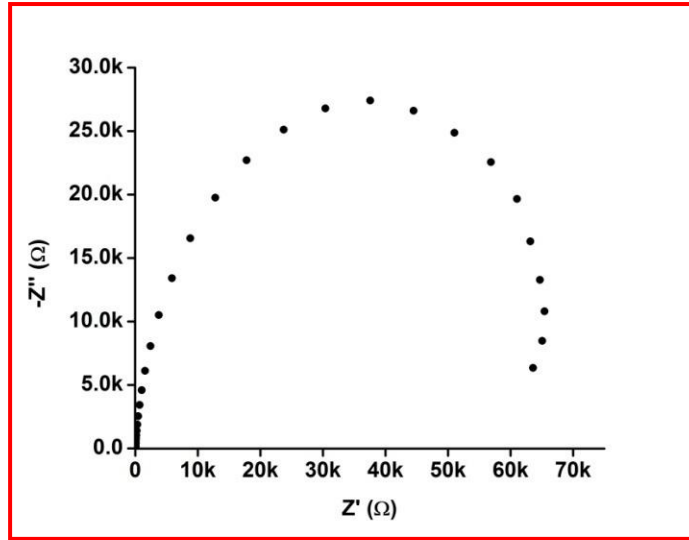


Fig. 2.21: Electrochemical impedance spectra of PEDOT:PSS/ITO electrode recorded in PBS solution (pH 7, 50 mM, 0.9% NaCl) containing 5 mM $[\text{Fe}(\text{CN})_6]^{3-/4-}$ as redox probe .

Fig. 2.21 shows the Nyquist plot obtained for PEDOT:PSS coated ITO in PBS solution containing 5mM $[\text{Fe}(\text{CN})_6]^{3-/4-}$ at 0.01 V biasing potential conducted in the frequency range, 100 KHz to 0.01 Hz. The diameter of the semicircle in the Nyquist plot gives magnitude of the charge transfer resistance (R_{ct}), which is in agreement with previous literature[191]. The charge transfer resistance (R_{ct}) of electrode depends on the dielectric characteristics of the electrode/electrolyte interface.

The heterogeneous electron transfer rate constant (K_{ct}) of various modified conducting paper can be evaluated using equation **Eq. 2.10**.

$$K_{ct} = \frac{RT}{n^2 F^2 A R_{ct} [S]} \quad \text{.....Eq. 2.10}$$

where R is the gas constant, T is absolute temperature (K), F is the Faraday constant, A is the electrode area (cm^2), R_{ct} is the charge transfer resistance obtained from Nyquist plot (EIS), [S] is the bulk concentration of redox probe (mol/cm^3) and n is the number of transferred electron per molecule of the redox probe.

Precautions:

- i) The solution should not be under stirring condition.
- ii) There should be no reacting species present in electrolyte that may compete with redox probe for electrons.
- iii) In case, Ag/AgCl is used as a reference electrode, the solution containing the electrolyte must be kept unstirred while taking observations.

2.4 METHODS OF IMMOBILIZATION OF ANTIBODIES ONTO MODIFIED PAPER SUBSTRATE

An important factor towards the development of paper based biosensor is the stability of the biomolecule. In order to obtain stabilized biomolecule with activity for long periods, these are fixed onto desired solid supports. The process is known as immobilization. The selection of the immobilization technique used to attach the biological material to a transducer surface is crucial to the operational behavior of a biosensor as the success of a biosensor relies on how well a biomolecule (antibodies, enzymes, DNA, aptamer etc) bonds to a desired biosensor surface and remains active during a desired application. Commonly used methods include physical adsorption, entrapment and covalent binding using activators or cross-linkers. Among these physical adsorption and covalent immobilization, are most frequently used (Fig. 2.22).

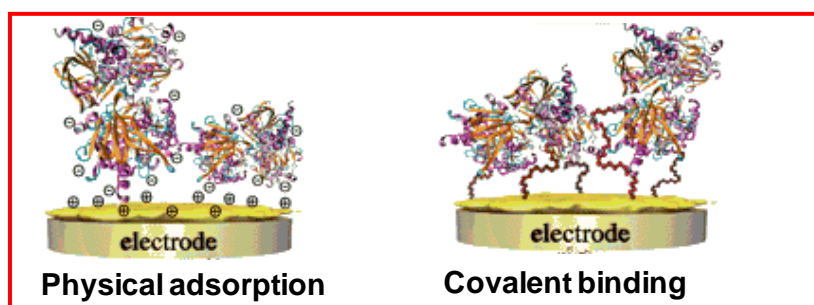


Fig. 2.22: Schematic presentation of developed immobilization methods.

2.4.1 Physical adsorption

This method of immobilization involves the physisorption of biomolecule onto the matrix and the forces involved are mostly electrostatic, such as *vander Waals* forces, ionic and hydrogen bonding interactions, although hydrophobic bonding is also significant [192]. These forces are very weak, but sufficiently large in number to enable reasonable binding. The advantages of this immobilization technique are: (a) It causes little or no conformational change in the biomolecule, (b) No reagents and only a minimum of activation steps are required (c) reversible to allow regeneration with fresh antibody/nucleic acid/enzymes/cells. This method can be used for immobilization of a biomolecule onto the modified paper surface due to strong adsorption properties of paper. We have employed this method in PEDOT:PSS-RGO, PEDOT:PSS-CNTs and PEDOT:PSS-PVA electrospun nanofibers modified paper substrate for anti-CEA immobilization (**Chapter 3, 4 and 5**). Physical adsorption may also lead to non-specific binding and overloading of the biomolecule on the matrix.

2.4.2 Covalent immobilization

Covalent binding of biomolecule to a surface is another method of immobilization and is based on the binding of functional group (such as -NH_2 , -SH , -OH etc.) of biomolecule and matrix via covalent bonds. This method can be employed to improved uniformity, density and distribution of the bound proteins, as well as reproducibility on the surfaces. However, it overcomes the problems of instability, diffusion and aggregation of enzymes in entrapment or adsorption techniques. The two main precautions which should be taken during covalent attachment are: (a) the binding reaction must be performed under conditions that do not cause loss of biomolecule activity, and (b) the active site of an enzyme must be unaffected by the reagents used. Considering the presence of -COOH groups in the

CNTs, PEDOT:PSS-CNTs modified paper matrix used for covalent immobilization of antibodies (anti-CEA) (**Chapter 4**). This immobilization method involves amide bond formation between -NH_2 group of aminated antibodies and COOH group of CNTs using EDC (0.4 M) as coupling agent and NHS (0.1 M) as activator.

2.4.3 Chemical cross-linking

Cross-linking of a biomolecule with the matrix occurs by means of a bi- or multifunctional reagent, such as glutaraldehyde and toluene di-isocyanate. Since the biomolecule is covalently linked to the support matrix, very little or no desorption occurs. Glutaraldehyde (Glu) is one of the most commonly used cross-linker for immobilization of biomolecule via -NH_2 group [193].

2.4.4 Physical entrapment

Immobilization by entrapment differs from adsorption and covalent binding where the enzyme molecules are free in solution, but restricted in movement within the layers of matrix or membrane[194]. It is accomplished in such a way that matrix retains the desired biomolecule, yet at the same time it allows free movement of substrates and products. One of the drawbacks of this technique is the large diffusion barrier to the transport of substrate and product results in increase of response time of the system as compared to other techniques.

2.5 CHARACTERISTICS OF A BIOSENSOR

2.5.1 Linear range, sensitivity and detection limit

The range of concentration over which current response varies proportionally as a function of analyte concentration is called linear detection range of the biosensor. We used chronoamperometry technique to estimate the linear detection range (**Chapter 3, 4 and 5**). The sensitivity is defined as “current response per unit change

of analyte concentration” and it can be estimated from the slope of the linearity curve. Further the limit of detection (LOD) has been determined by **Eq. 2.11**.

$$\text{LOD} = 3\sigma/m \quad \text{..... Eq. 2.11}$$

Where m is slope and σ is standard deviation of the linearity curve.

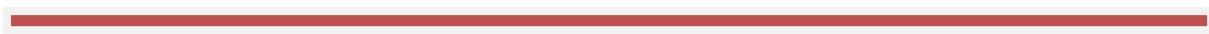
2.5.2 Shelf life and reproducibility of the bioelectrode

The life time of the biosensor can be determined by measuring parameters like shelf-life (storage stability; duration for which the sensor is considered suitable for use or it can retain maximum activity) and reproducibility (measure of the scatter or the drift in a series of observations or results performed over a period of time)[195]. Materials utilized for the sensor fabrication, morphology of the fabricated film and method of biomolecule immobilization are some of the factors that may affect the stability of the bioelectrode. Shelf life can be calculated by measuring the current response of the bioelectrodes at the regular interval of time whereas to estimate the reproducibility the number of times the bioelectrode can be utilized is important.

2.6 CONCLUSIONS

The X-ray diffraction, Raman spectroscopy, Fourier transform infrared spectroscopy, X-ray photoelectron spectroscopy, Scanning electron microscopy and Transmission electron microscopy techniques described in this Chapter were utilized for the structural and morphological analysis of nanocomposites, fabricated nanomaterial modified paper electrode and functionalized paper based bioelectrodes. Electrochemical impedance spectroscopy and chronoamperometry techniques were used to reveal the electrochemical behavior and to study the biosensing response of nanomaterial modified conducting paper immune-electrodes towards the carcinoembryonic antigen (CEA) detection. The various methods employed for the

immobilization of the desired biomolecules and the protocols used for the estimation of various parameters relating to the performance of the paper biosensor have also been discussed in the present Chapter. The next Chapter deals with the studies relating to the fabrication of a paper based sensor comprising of PEDOT:PSS-RGO composite for carcinoembryonic antigen detection.



CHAPTER 3

Reduced Graphene Oxide Modified Conducting Paper Sensor for Cancer Detection

3.1 INTRODUCTION

Graphene is an allotrope of carbon that is tightly packed into a two dimensional (2D) honeycomb lattice. Each carbon atom in graphene has four bonds, three in plane σ bond and one out of plane π bond that are associated with the neighboring carbon atoms. Besides this, each carbon atom is separated by 1.42 Å. Its stability is due to its tightly packed carbon atoms and a sp^2 hybridization wherein the combination of S, P_x and P_y orbitals constitute the σ -bond. The final P_z electron makes the π -bond and the π -bonds hybridize together to form the π -band and π^* -bands. These bands are responsible for most of its notable electronic properties arising due to the half-filled band that permits free-moving electrons [196-197]. Reduced graphene oxide (RGO), a derivative of graphene has been found to have interesting properties such as high surface area, increased concentration of defects, electroactive sites and presence of oxygen containing functional group (especially carboxyl) [15]. Its abundant defects and chemical group facilitate charge transfer and offer the convenience and flexibility for functionalization to enhance the electrochemical performance of the sensor. Several works have been reported on the use of RGO to fabricate improved biosensing platforms. Srivastava *et al.* used RGO for electrochemical detection of food toxin. This biosensor shows high sensitivity and improved stability [175]. Du *et al.* used functionalized graphene for fabrication of electrochemical biosensor to detect α fetoprotein, AFP (the cancer biomarker). The increased response was achieved due to increased loading of the biomolecule [198]. Wu *et al.* reported highly sensitive electrochemical immunosensor for cancer biomarker (carcinoembryonic antigen, CEA) detection using reduced graphene oxide-tetraethylene pentamine (RGO-TEPA) modified glass carbon electrode. The RGO-TEPA was used to enhance the concentration of amino groups that were used to form

covalent bond with the antibodies [88]. Elshafey *et al.* fabricated a sensitive and label free electrochemical biosensor based on gold nanoparticles integrated reduced graphene oxide (Au-RGO) modified electrode for the prognosis of cancer biomarker (p53). This fabricated electrode provided a large surface area, stability and preserve the bioactivity of the biomolecule for immobilization of p53 antigen [199]. In spite of these developments, there is enough scope to improve the performance of the electrochemical biosensor by integrating RGO with suitable matrix.

Paper is a flexible, lightweight, low cost, recyclable and biodegradable material. Initially it was being used in packaging, display and storing information. It has recently been used as a sensor substrate. In 79 A.D. Pliny the Elder in his *Historia Nature (encyclopedia)* described a papyrus (Latin word of paper) based method for detection of tyrian purple dye and ferrous sulphate [200]. Gay-Lussac in 18th century described the litmus paper test for acids and Hugo Schiff reported the first spot test for uric acid [91]. In 19th century, many researchers developed dip stick and dry chemistry test using paper [201]. In 1903, Tsweet demonstrated the use of filter paper to isolate leaf pigments differentially from solution and Janos Plesch in 1906 used paper for sensitive detection of bilirubin in urine [200]. Further in 1950s electrophoresis on paper became a breakthrough for the separation of protein [202]. Martin and Synge were awarded the Noble prize (1952) in chemistry for invention of paper chromatography. In 1964 Ames Company launched first commercial paper test for blood glucose detection called Dextrostix. Following this in 1988, Unipath launched its first home pregnancy test kits [91, 203]. In 1995, US patent was filed on laminated assay device for detection of cholesterol by modifying paper substrate with hydrophobic printing [204]. With advancement in techniques and exploration of different materials paper has recently been rediscovered as a sensor substrate in 21st

century leading to the development of paper based devices [205-206]. Recently, paper based electrochemical biosensors are rapidly evolving for desired analytical and clinical applications since these are predicted to be simple, cost-effective, flexible, portable, consume low power and are disposable. These devices have potential applications in healthcare, detection of toxicants, explosives and environmental studies. Compared to conventional laboratory assays, these devices can be helpful for making speedy decision for therapeutics. Besides this, the testing can be performed near the vicinity of a patient [62, 103, 207-208]. To ensure the application of paper in an electrochemical sensor, it is essential to make it conducting. Many methods such as screen printing, inkjet printing, spin coating etc. have been used to incorporate conducting ink on a paper substrate [90, 104]. These methods require complex fabrication steps, additional instrumentation, and skilled personnel and are time-consuming. Conducting polymers have been considered a promising candidate to obtain conducting paper due to delocalization of π electrons since they are known to facilitate rapid electron transfer, mechanical flexibility and solution processability [209-210]. Doping of a conducting polymer has been found to enhance its electronic, optical, physical, chemical and electrochemical properties [20]. Among the various conducting polymers, poly(3,4ethylenedioxythiophene):poly(styrenesulfonate) (PEDOT:PSS) has been considered to be a interesting candidate for the development of a conducting paper due to its homogeneous entrapment in/on a paper using simple dip coating method (Chapter 1). Moreover, the conductivity of PEDOT:PSS based paper can be significantly enhanced and tuned by treatment with a desired solvent. Further, incorporation of RGO in the PEDOT:PSS matrix may modulate the performance of a conducting paper in terms of electrochemical kinetics or signal stability and sensitivity [211-212].

This Chapter pertains to results of the studies relating to the fabrication of a paper based sensor based on poly(3,4-ethylenedioxythiophene):poly(styrenesulfonate) (PEDOT:PSS) and reduced graphene oxide (RGO) composite for carcinoembryonic antigen (CEA) detection .

3.2 EXPERIMENTAL DETAILS

3.2.1 Fabrication of PEDOT:PSS based conducting paper

The conducting paper (1cm×3cm) was prepared using a simple dip coating method. The PEDOT:PSS aqueous solution (1.3 wt%, PEDOT content 0.5 wt.%, PSS content 0.8 wt.%) purchased from Sigma Aldrich was ultrasonicated prior to use after which 3% ethylene glycol (EG) was added to the aqueous suspension of PEDOT:PSS. This solution was used to dip coat the Whatman filter paper 1 (procured from GE healthcare UK) rendering it conductive. It was then dried in a hot air oven at 100 °C and was termed as conducting paper.

3.2.2 Preparation of reduced graphene oxide (RGO) and PEDOT:PSS/RGO composite

Graphene oxide (GO) was synthesized via improved Hummers method [213]. It was reduced to RGO via hydrothermal method. Firstly, 100 mg of GO was dispersed in 70 mL of de-ionized water via ultrasonication. Subsequently, 80% aqueous solution of hydrazine hydrate was gradually added into this solution under constant stirring for 1 h. The resulting solution was poured into a 100 mL Teflon vessel and then placed in a stainless steel tank for hydrothermal treatment at 150 °C for 15 h. Once the reaction reached completion, the system was allowed to cool down to room temperature (27 °C). Thus obtained product was purified by repeated centrifugation using de-ionized water and ethanol, and subsequently dried at 60 °C overnight resulting in black powder of RGO.

For the preparation of PEDOT:PSS/RGO composite, PEDOT:PSS aqueous solution (1.3 wt%, PEDOT content 0.5 wt.%, PSS content 0.8 wt.%) was ultrasonicated prior to use after which 3 % ethylene glycol was added into the aqueous suspension of PEDOT:PSS. Thereafter, the prepared RGO (7 mg) was added into 20 mL of the PEDOT:PSS solution. It was found that RGO got highly dispersed without sedimentation in PEDOT:PSS solution on being subjected to ultrasonication for 30 min.

3.2.3 Fabrication of PEDOT:PSS/RGO based electroactive paper

The Whatman paper (1cm×1cm) was dipped in PEDOT:PSS/RGO aqueous suspension (1.3 wt% of PEDOT:PSS , 0.035wt% of RGO) containing 3% EG for 1 h and then dried at 100 °C in a hot air oven. Thereafter it was treated with EG by dipping in EG solution for 20 min. The EG treated conducting paper was finally dried at 100 °C for about 1 h. A Schematic of the experiment is demonstrated in **Fig. 3.1**.

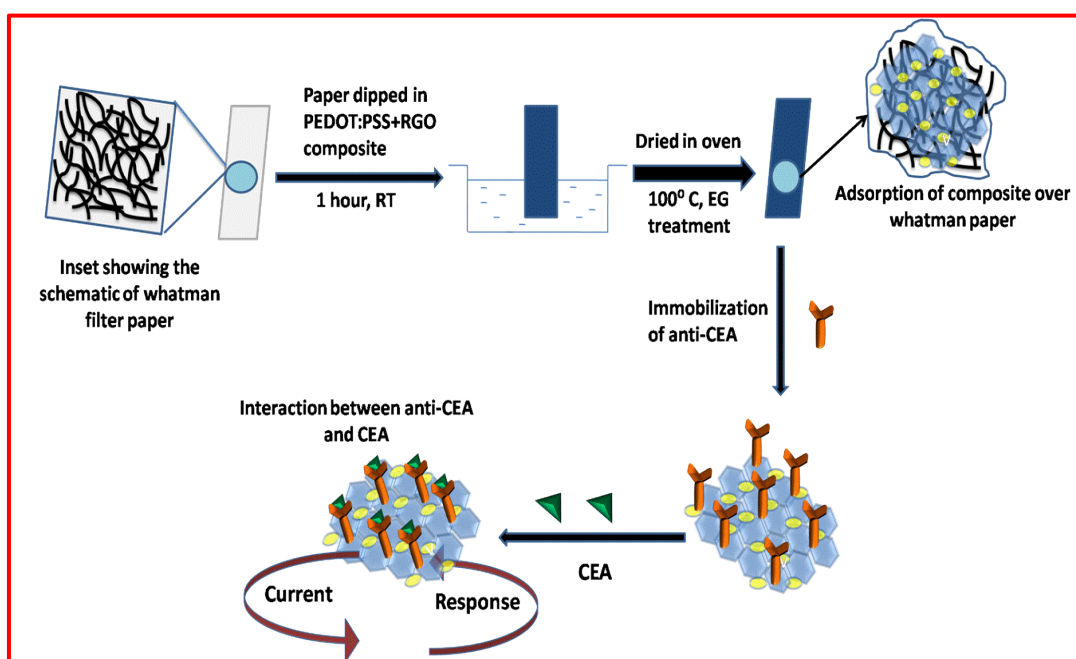


Fig. 3.1: Schematic of proposed electroactive paper sensor.

3.3 RESULTS AND DISCUSSION

3.3.1 Electron microscopy studies

Transmission electron micrograph of the RGO exhibits curved sheet like structure with a fairly smooth surface (**Fig. 3.2A**). The observed lighter and darker regions indicate the presence of RGO. The lighter region pertains to a few layered graphene whereas the darker region corresponds to the multilayered graphene. The wrinkles and folds pertaining to the graphene sheet (sub-microns in size) are clearly visible. The selected area electron diffraction (SAED) pattern of RGO reveals hexagonal atomic structure and crystalline nature of the RGO sheets (**Fig. 3.2B**). The inner six member ring represents the [1100] plane. The visible six diffraction spots corresponding to [0001] indicate hexagonal symmetry of the [0001] diffraction of the RGO [214]. The RGO sheets appear to be uniformly covered with PEDOT: PSS (**Fig. 3.2C**). The PSS molecules perhaps assist RGO dispersion via edge-to-face aromatic interactions between the RGO surface and the aromatic rings of the polymer which inhibits the hydrophobic graphene nanoplates from agglomeration, leading to a stable RGO dispersion in the polar solvent [215]. The diffused ring like structure observed (**Fig. 3.2D**) in the SAED pattern of PEDOT:PSS/RGO composite is because of the amorphous nature of PEDOT:PSS covering the RGO sheets. The SEM of PEDOT: PSS (**Fig. 3.2E**) coated paper indicates uniform adsorption of PEDOT: PSS over cellulose fibers of the paper. Because of the high porosity and tiny interfiber air spaces in Whatman paper, the PEDOT:PSS gets adsorbed into the paper through capillary action and after drying it produces uniform and stable film of PEDOT:PSS on the paper. **Fig. 3.2F** shows SEM of PEDOT:PSS/RGO coated paper. PEDOT: PSS/RGO is found to be uniformly adsorbed onto the cellulose fiber wherein some of RGO sheets are entangled in the fibrous network of Whatman paper.

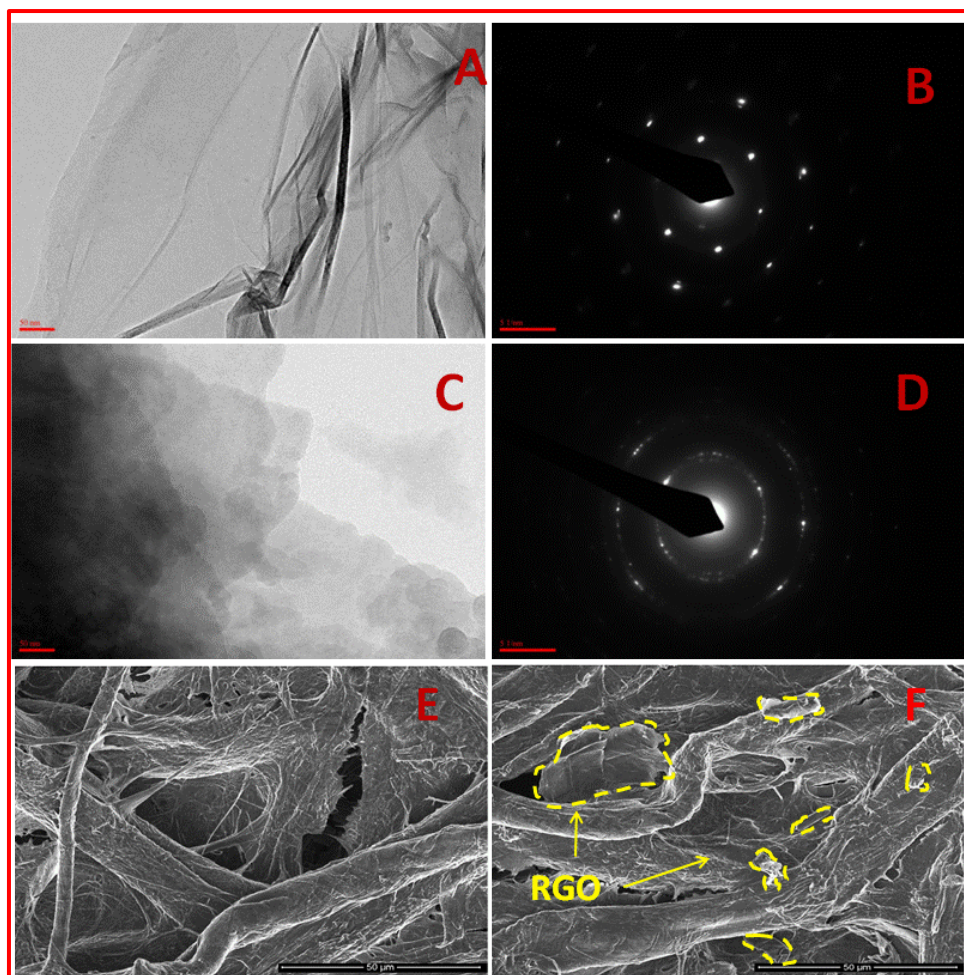


Fig. 3.2: (A) TEM image of synthesized reduced graphene oxide (RGO) where darker region correspond to multilayer and lighter region corresponds to a few layer graphene (B) SAED of RGO, which confirms the hexagonal atomic structure and crystalline nature of the sheets. (C) TEM image of PEDOT:PSS/RGO. (D) SAED pattern of PEDOT:PSS/RGO composite (E) SEM of PEDOT:PSS adsorbed onto Whatman paper (F) SEM of PEDOT:PSS/RGO Whatman coated paper.

3.3.2 Electrical conductivity studies

The PEDOT:PSS coated paper has been found to have conductivity of $1.16 \times 10^{-4} \text{ Scm}^{-1}$. However, on addition of 3% ethylene glycol (EG) in PEDOT:PSS solution, the value of conductivity increases to $1.43 \times 10^{-3} \text{ Scm}^{-1}$. This is due to decreased columbic interactions between PEDOT and PSS molecules that perhaps contribute to reorientation of the polymer chains resulting in improved charge carrier mobility [216]. Further, all studies were done with PEDOT:PSS doped with 3%

EG[217]. The PEDOT:PSS doped with 3% EG coated Whatman paper is termed as conducting paper.

The enhancement in the conductivity of PEDOT:PSS film (coated on glass substrate) has been recently reported when the film is dipped in methanol and H₂SO₄ [218-219]. This is due to ejection of the PSS ions from the PEDOT:PSS film dipped in the solvent, inducing conformational rearrangement of the PEDOT chains leading to higher conductivity. In the present case, effect of solvents such as methanol, H₂SO₄ and ethylene glycol (EG) on electrical conductivity of the conducting paper has been investigated. We observed that EG treated flexible substrate (Whatman paper 1) shows the highest value of conductivity ($3.57 \times 10^{-2} \text{ Scm}^{-1}$) in comparison to methanol ($6.8 \times 10^{-3} \text{ Scm}^{-1}$), and H₂SO₄ ($8.1 \times 10^{-3} \text{ Scm}^{-1}$). This is in accordance with a similar report wherein the effect of flexibility of material and polyelectrolyte adhesion to substrate was studied [220]. The increased flexibility of the EG treated conducting paper due to ejection of PSS results in strong non-covalent cooperative interactions between PEDOT and cellulose molecules leading to higher conductivities. We incorporated RGO in the PEDOT:PSS matrix for electrochemical studies since RGO is known to exhibit excellent electrochemical properties [15]. The PEDOT:PSS/RGO based conducting paper dipped in EG (electroactive paper) shows almost similar conductivity value ($3.12 \times 10^{-2} \text{ Scm}^{-1}$). The as-prepared electroactive paper shows greater degree of flexibility and efficient conductivity as demonstrated in **Fig. 3.3**.

The effect of folding (-180° to 180°), repeated folding and unfolding on conductivity of the electroactive paper was investigated. **Fig. 3.3D** describes results of flexibility studies conducted on the electroactive electrode; wherein the positive and negative angle clearly reveal electrode folding in upward and downward direction, respectively. Relative conductivity [(ratio of measured conductivity (σ_{meas}) to initial

conductivity (σ_0)] of electroactive electrode was measured as a function of folding angle.

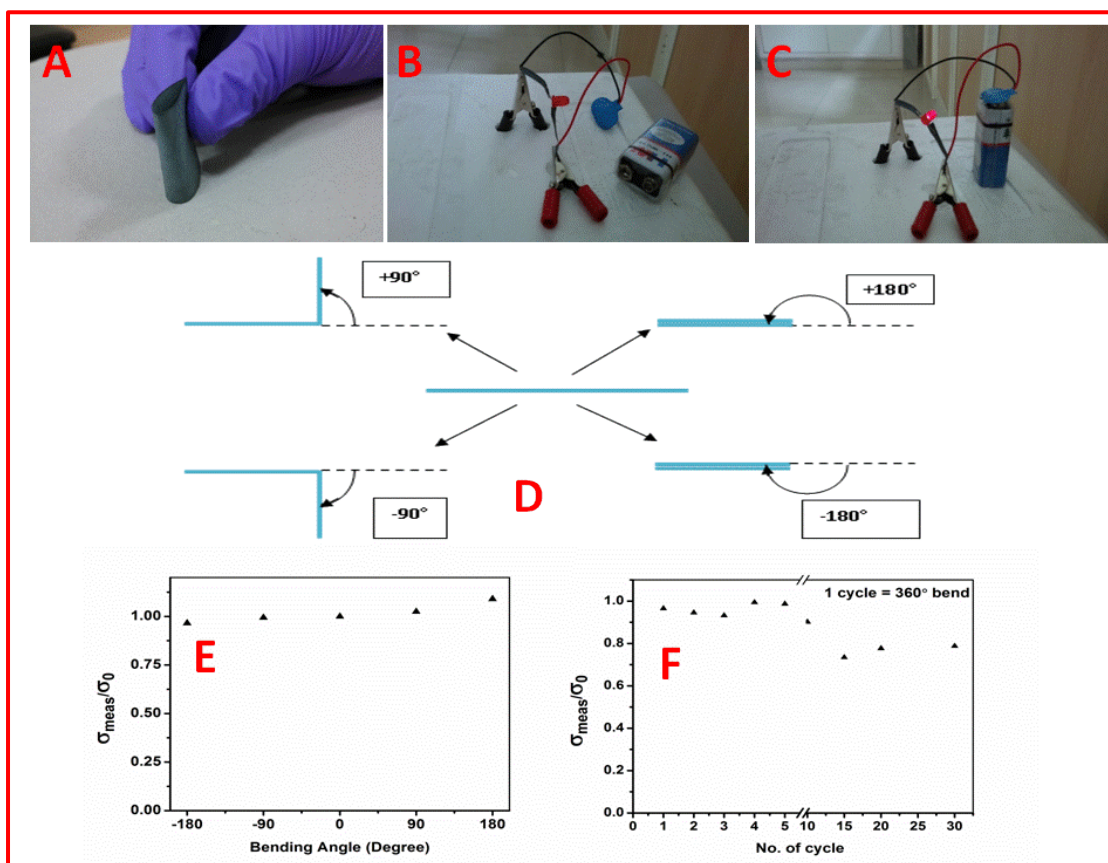


Fig. 3.3: Optical image of electroactive paper (A) foldable nature of electroactive paper (B, C) demonstration of LED emission when current flow through electroactive paper. Flexibility studies of PEDOT:PSS/RGO based electroactive electrode (D) Schematic diagram of electrode folding at different deformation angle. (E) The ratio of measured conductivity (σ_{meas}) to initial conductivity (σ_0) of electroactive paper with respect to folding angle. (F) The ratio of measured conductivity (σ_{meas}) to initial conductivity (σ_0) of electroactive paper versus folding cycle (1 cycle = 360°).

Fig. 3.3E displays variation of the relative conductivity of electroactive electrode indicating deviation of upto 4% under different folding angles. This reveals that electrodes are flexible and there is negligible change in the conductivity. The variation of relative conductivity of electrode with repeated cycle of folding and unfolding (manually) is shown in **Fig 3.3F**. It may be noted that the conducting paper folded after 30 cycles (1 cycle = 360° rotation) shows decrease of about 20% in relative conductivity due to tearing of the cellulose threads. A video pertaining to the

lighting of an LED lamp when current is passed through the multiple times folded electroactive paper is shown in **video 3.1 (Please see the attached CD)**.

Fig. 3.4A represents Schematic of the observed mechanism, showing enhanced conductivity of the EG treated conducting paper. The conducting paper comprises of PEDOT:PSS polymer chains wherein PEDOT molecules present in the core of the insulating PSS are highly conductive in nature. On being treated with ethylene glycol, the core-shell structure of the conducting paper becomes partially linear due to ejection of the PSS molecules. This exclusion of PSS from the surface is perhaps responsible for conformational changes in the polymer film that in turn results in increased conductivity. This has been further confirmed by Fourier transform infrared (FT-IR) spectroscopy and X-ray photoelectron spectroscopy (XPS) studies.

3.3.3 FT-IR and XPS studies

FT-IR spectra of PEDOT:PSS/Whatman paper (curve i), conducting paper (curve ii) and conducting paper treated with EG (curve iii) are shown in **Fig. 3.4B**. FT-IR spectrum of PEDOT:PSS coated on Whatman paper (spectra i) exhibits characteristic absorption bands at near 670 cm^{-1} and 1060 cm^{-1} , corresponding to C-S and C-O stretching vibration of the thiophene ring in PEDOT [221]. The bands seen at 1010 cm^{-1} , 1045 cm^{-1} and 1160 cm^{-1} represent SO_3^- symmetric and asymmetric stretching vibrations, respectively due to PSS [218]. The bands found at 1392 cm^{-1} and 1537 cm^{-1} are due to C-C and C=C, respectively. In the FT-IR spectrum of conducting paper (curve ii), the intense absorption band at 1060 cm^{-1} is due to addition of EG that causes conformational changes in the polymer structure. The absorption band at 1104 cm^{-1} and 1160 cm^{-1} represent SO_3^- asymmetric stretching

vibration whereas disappearance of $-\text{SO}_3^-$ symmetric stretching suggests molecular rearrangement in the PEDOT:PSS leading to increased electrical conductivity.

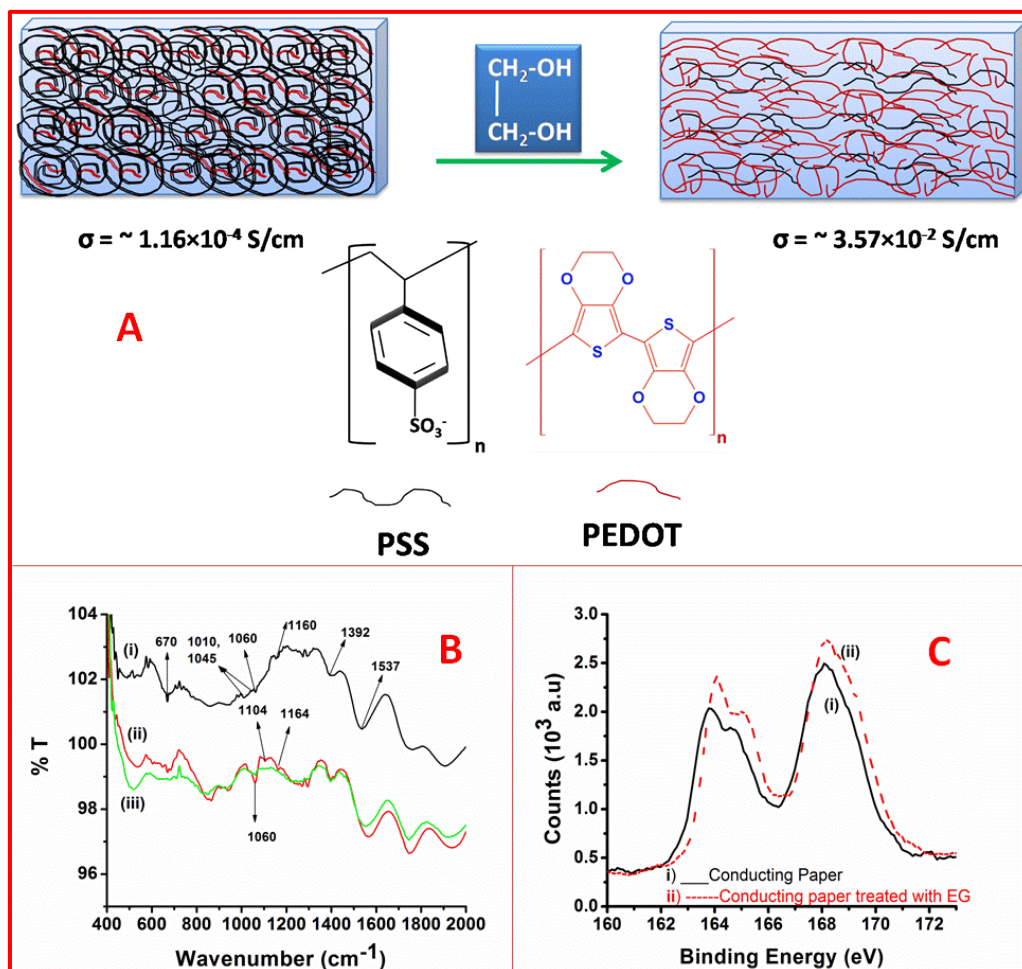


Fig. 3.4: (A) The schematic illustration of the mechanism of conductivity enhancement on conducting paper surface by EG treatment. (B) The FT-IR spectra of (i) PEDOT: PSS/Whatman paper (ii) conducting paper (iii) conducting paper treated with EG (C) X-ray photoelectron spectra (XPS) of (i) conducting paper (ii) conducting paper treated with ethylene glycol.

These results are in agreement with those observed for the conductivity measurements wherein increase in conductivity from $\sim 1.16 \times 10^{-4} \text{ Scm}^{-1}$ to $\sim 1.43 \times 10^{-3} \text{ Scm}^{-1}$ occurred when EG was added into PEDOT:PSS. In the FT-IR of the EG treated conducting paper (curve iii), the characteristic bands seen at 1104 cm^{-1} and 1160 cm^{-1}

pertaining to the -SO^{3-} stretch of PSS are absent. This indicates removal of PSS from the conducting paper after EG treatment. This removal of PSS after EG treatment is perhaps responsible for the higher conductivity of the conducting paper due to increased exposure of PEDOT.

Fig. 3.4C shows XPS spectra of i) conducting paper ii) EG treated conducting paper. The S(2p) binding energy peak seen at 168 eV corresponds to sulfur due to presence of PSS, and the doublet peak seen at 163.8 eV and 164.5 eV correspond to the presence of sulfur in PEDOT[22]. The S2p XPS intensity ratio of PEDOT/PSS increases from 0.721 to 0.760 after the conducting paper is treated with EG. This change indicates the removal of some of the PSS chains from the film. That perhaps causes conformational change in PEDOT:PSS due to the transition from coiled to linear form leading to increased exposure of PEDOT chains (**Fig. 3.4A**) [218]. The change in C/S molar ratio evaluated from the scan spectra decreases from 9.63 to 8.17 after the conducting paper is treated with EG, is consistent with the removal of some PSS from the film.

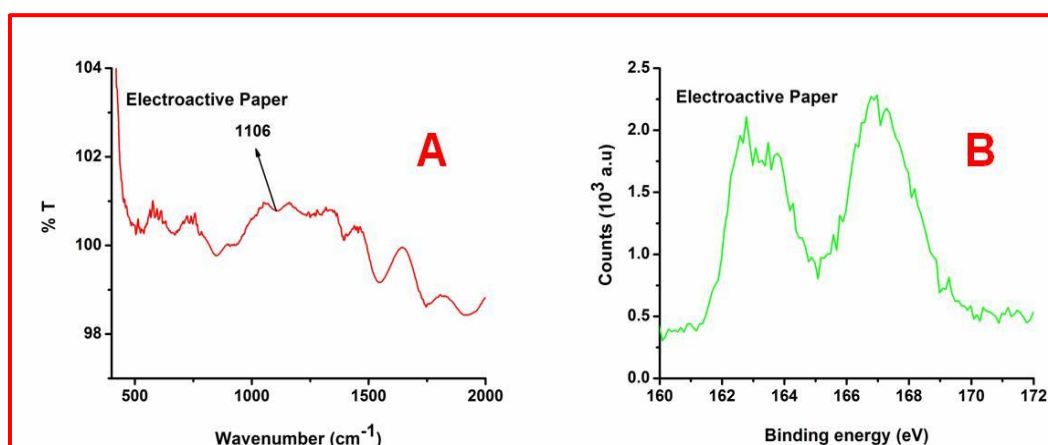


Fig. 3.5: (A) FT-IR spectra of electroactive paper (B) XPS spectra of electroactive paper

FT-IR and XPS spectra obtained for the electroactive paper are shown in **Fig. 3.5**. FT-IR spectra of electroactive paper (**Fig. 3.5A**) indicate an additional broad

absorption band at 1106 cm^{-1} that is attributed to C-OH stretching of graphene oxide. Further, the other observed IR bands are the same as seen in **Fig. 3.4B**, curve iii. XPS of electroactive paper is shown in **Fig. 3.5B**. The S2p XPS intensity ratio of PEDOT/PSS present in electroactive paper increases to 0.82. However, the conductivity of electroactive paper is almost equivalent to that of the conducting paper after EG treatment. This may perhaps be attributed to the presence of discontinuous and non-uniform RGO sheet resulting in increased distance between PEDOT chains within the fiber network. Further, the C/S molar ratio increases to 10.1 due to presence of carbon content of RGO.

3.3.4 Electrochemical studies

To investigate the charge transfer phenomenon at the conducting paper/solution interface, the electrochemical impedance spectroscopy (EIS) studies were conducted at biasing potential of 0.01V in the frequency range, 100 KHz to 1Hz. The Randles circuit is an equivalent electrical circuit that is commonly used to measure the electrochemical impedance comprising of an active electrolyte resistance R_s in series with R_{ct} (charge transfer resistance) in parallel combination of the double-layer capacitance C_{dl} or constant phase element (CPE) of a Faradaic reaction. The diameter of the semicircle in the Nyquist plot gives magnitude of the charge transfer resistance (R_{ct}) at the electrode surface [222]. **Fig. 3.6A** shows EIS spectra of the (i) conducting paper, (ii) conducting paper treated with EG, (iii) electroactive paper. The curve fitting was done assuming Randles circuit [$R_s (R_{ct} C_{dl})$] of the electrochemical cell. The R_{ct} obtained for conducting paper is $48\text{ K}\Omega$ which is maximum (curve i). However, the significant decrease in R_{ct} value upto $7\text{ K}\Omega$ (curve ii) was observed in EG treated conducting paper. This is assigned to the conformational changes of the PEDOT:PSS chains from coiled to linear form leading to the higher conductivity due

to enhanced electron transfer between solution/electrode interface. It is observed that the R_{ct} value further decreases to $2.8\text{ K}\Omega$ (curve iii) in case of the electroactive paper. This may be attributed to excellent electrochemical properties and larger 2D surface area of RGO incorporated in the PEDOT:PSS matrix that increases the permeability of $[\text{Fe}(\text{CN})_6]^{3-/4-}$ to the surface of paper electrode. The heterogeneous electron transfer rate constant (K_{ct}) of EG treated conducting paper and electroactive paper has been calculated using Eq. 3.1 [223].

$$K_{ct} = \frac{RT}{n^2 F^2 A R_{ct} [S]} \quad \dots\dots\dots \text{Eq. 3.1}$$

where R is the gas constant, T is absolute temperature, F is the Faraday constant, A is the electrode area (cm^2), [S] is the concentration of redox probe (mol/cm^3) and n is the number of transferred electrons per molecule of the redox probe. The heterogeneous electron transfer rate constant (K_{ct}) value of the electroactive paper has been estimated as $1.9 \times 10^{-5} \text{ cm s}^{-1}$ which is 2.5 times better as compared to conducting paper treated with EG ($7.6 \times 10^{-6} \text{ cm s}^{-1}$). This indicates that the RGO present in electroactive paper electrode exhibits faster electron transfer kinetics as compared to the EG treated conducting paper. Thus incorporation of the RGO results in improved electrochemical activity of the electroactive paper as compared to that of EG treated conducting paper.

Fig. 3.6B shows results of the chronoamperometric studies (current vs. time) conducted on conducting paper and EG treated conducting paper at 2V every 0.1s. The higher value of the current observed for EG treated conducting paper electrode than that of conducting paper indicates increased electron transfer between solution and electrode due to conformational rearrangement in PEDOT polymeric chains. Further increase in the value of the electrochemical current in case of the electroactive paper electrode is attributed to enhanced permeability of the redox couple $[\text{Fe}(\text{CN})_6]^{3-/4-}$ resulting due to RGO doping. It may be noted that electroactive paper

electrode exhibits improved electrochemical performance and signal stability than that of the EG treated conducting paper.

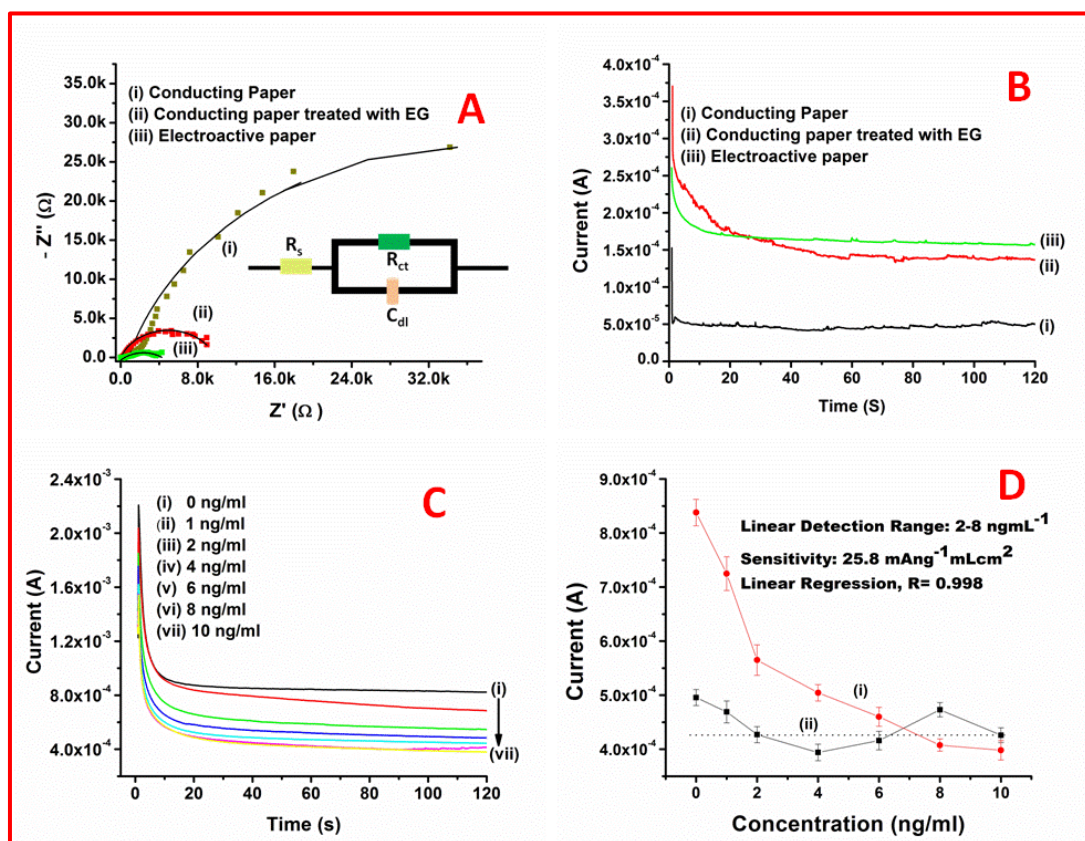


Fig. 3.6: Electrochemical studies conducted on paper electrode (A) Electrochemical impedance spectra (B) Chronoamperometric plot obtained for (i) conducting paper (ii) conducting paper treated with EG (iii) electroactive paper (C) Electrochemical response studies of anti-CEA immobilized electroactive paper at different concentration of CEA (D) Calibration plot between the magnitudes of current recorded and CEA concentration (curve i); control experiment in absence of antibody (curve ii). Conducting paper: EG doped PEDOT: PSS solution coated onto whatman paper; Electroactive paper: EG and RGO doped PEDOT:PSS solution coated onto Whatman paper further treated with EG.

3.3.5 Electrochemical response studies

Electroactive paper has been used to detect the presence of cancer biomarker, CEA. The monoclonal carcinoembryonic antibodies (anti-CEA) (procured from Sigma Aldrich) are physically absorbed onto the PEDOT:PSS/RGO based electroactive paper (**Fig. 3.1**). The anti-CEA immobilized paper bioelectrode is

washed with phosphate buffer (PBS, 50 mM, 0.9% NaCl; pH 7.4) to remove any unbound antibodies. Different concentrations of the carcinoembryonic antigen (CEA) (1-10 ngmL⁻¹) are prepared via further dilution of the stock solution (25µgmL⁻¹). The response studies of anti-CEA/electroactive paper obtained as a function of CEA concentration (1-10 ngmL⁻¹), were carried out in phosphate buffer saline (PBS, 50 mM, pH 7.4) containing 5 mM [Fe(CN)₆]^{3-/4-}. 10µL of diluted antigen solution was added into the electrochemical cell for each antigen concentration. After adding each CEA concentration the current-time curve was recorded after every 300 s to ensure completion of the immunoreaction. The variation of the response current recorded as a function of CEA (1-10 ngmL⁻¹) is shown in **Fig. 3.6C**. The decrease in amperometric current occurs upto a maximum of 10 ngmL⁻¹. This can be attributed to the formation of antigen–antibody complex causing significant rearrangement over the electrode surface that diminishes charge transfer via [Fe(CN)₆]^{3-/4-} leading to reduction in amperometric current [110, 224]. **Fig. 3.6D** indicates the calibration plot obtained between response current and CEA concentration (curve i). Furthermore, a control experiment was performed to check cross reactivity of the electroactive paper with CEA antigen in absence of the antibodies (curve ii). However, no significant change in current response was observed for the electroactive paper in the absence of antibodies as a function of CEA concentration. A linear relationship was observed in the range, 2-8 ngmL⁻¹ with a sensitivity of 25.8 µAng⁻¹mLcm⁻² and follows the Eq. 3.2.

$$I(A) = -25.8 \mu A \text{ mL ng}^{-1} \times [\text{CEA concentration}] + 613.5 \mu A; R^2 = 0.99$$

..... **Eq. 3.2**

We compared the sensing performance of the electroactive paper with the conducting paper treated with EG. For this, the electrochemical response studies were

carried out on the anti-CEA immobilized conducting paper treated with EG, in presence of different concentration of antigen. It was found that the electroactive paper was almost 6 times more sensitive than the conducting paper treated with EG for CEA detection.

3.3.6 Stability, selectivity and reproducibility studies

Fig. 3.7A shows variation of response current of the immuno-electrode (anti-CEA immobilized electroactive paper) taken at a regular interval of 2 days. It was found that magnitude of current decreased to ~7% after 21 days. This indicated that the paper sensor exhibited good stability upto 21 days. The selectivity study of this paper sensor was investigated in the presence of cardiac troponin I (cTnI), cytokeratin-19 fragment (CYFRA-21-1), and endotheline-1 protein (ET-1) (2ngmL^{-1}).

Fig. 3.7B shows observed decrease in current response on addition of CEA (2ngmL^{-1}) after which we do not observe any significant current change on addition of other antigen indicating high selective of the biosensor. The reproducibility of the five different immuno-electrodes fabricated under similar conditions was investigated in presence of 2ngmL^{-1} CEA concentration (**Fig. 3.7C**). It was found that this paper electrode showed good reproducibility for five different electrodes with constant surface area as is evident by low value of relative standard deviation (RSD) of 7.6% (mean value = $609\mu\text{A}$). Further each measurement (**Fig. 3.7C**) was repeated 4 times for each electrode and the error bars were included accordingly. The low RSD obtained for each electrode (less than 5 %) indicates appreciable repeatability of the biosensor.

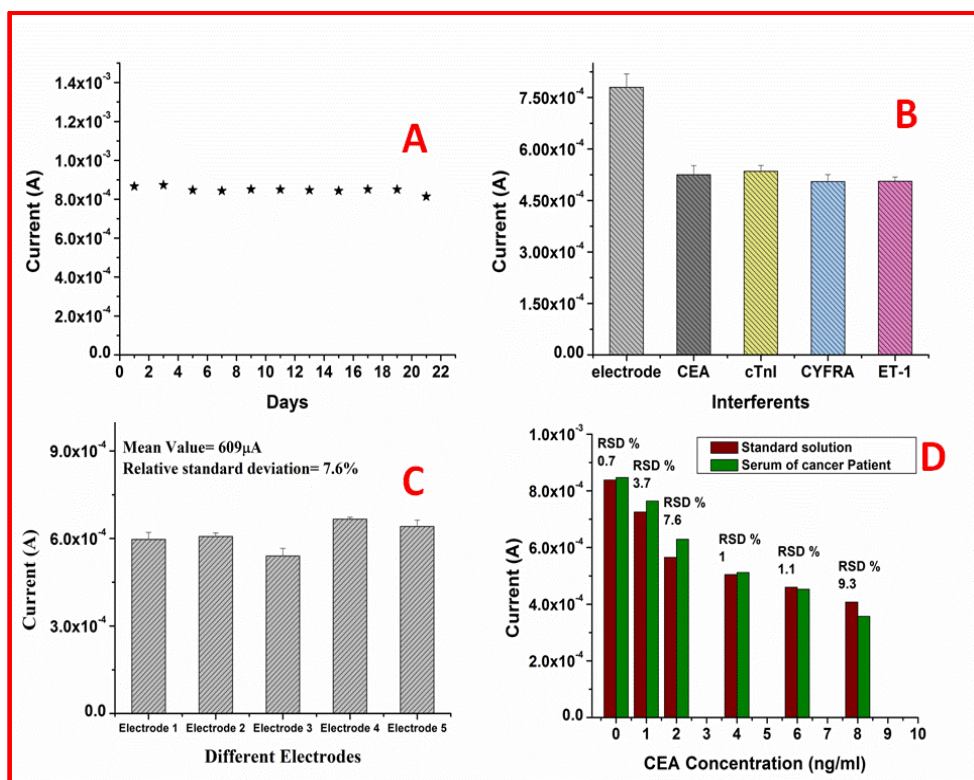


Fig. 3.7: (A) Electrochemical current response of anti-CEA immobilized electroactive paper electrode (immuno-electrode) measured as a function of time (day) (B) Electrochemical current response of immuno-electrode in the presence of other analytes (C) Electrochemical current response of different immuno-electrode fabricated via the same set of procedure in presence of CEA (2 ng mL^{-1}) and (D) CEA concentration values obtained by immunoassay and the electroactive paper method.

3.3.7 Real sample analysis

The results obtained for serum sample of cancer patients using this electroactive paper sensor were validated using ELISA. The blood samples collected from patient and processed at the Rajiv Gandhi Cancer Institute & Research Centre (RGCi & RC) in Rohini, Delhi, India. Concentration of CEA in the serums of cancer patients was measured at RGCi&RC using the VITROS CEA reagent Pack and the VITROS CEA Calibrators on the VITROS ECi/ECiQ Immunodiagnostic Systems, VITROS 3600 Immunodiagnostic System and VITROS 5600 Integrated System using Intellicheck® Technology. It can be seen that a reasonable correlation occurs between the CEA concentration value obtained by immunoassay and the electroactive paper

based electrochemical method (**Fig. 3.7D**). As shown in **Fig. 3.7D**, the electroactive paper affords good recoveries and acceptable relative standard deviation.

The sensing characteristics of the electroactive paper based electronic paper sensor are summarized in **Table 3.1** along with those reported in literature. It may be noted that this low cost flexible electroactive paper sensor can be easily decomposed by simple incineration (**video 3.2, please see the attached CD**). Keeping in view the production of the medical diagnostics kits, this is an added advantage of this new environment friendly disposable electroactive paper sensor.

Table 3.1: The sensing characteristics of electroactive paper have been summarized along with some of those reported in literature.

S. No.	substrate	Material	Fabrication Method	Detection Method	Linear range and Sensitivity	Stability	Cost	Reference
1.	Array of Gold electrode	Thiol based self assembled monolayer	Dip Coating	Amperometry	0-200 ngmL ⁻¹ and 3.8 nAmLng ⁻¹	30	High	[225]
2.	Gold electrode	AuNP, O-aminophenol	Drop cast	Electrochemical Impedance Spectroscopy	0.5-20 ngmL ⁻¹ and 1.08×10 ⁵ Ωng ⁻¹ mL	-	High	[86]
3.	Glassy carbon electrode	AuNP, MWCNTs, Chitosan	Drop Casting	Differential pulse voltammetry	0.3-2.5 & 2.5- 20 ngmL ⁻¹ -----	30	Moderate	[87]
4.	Glassy carbon electrode	Reduced graphene oxide-tetraethylene pentamine (RGO-TEPA)	Drop Casting	Differential pulse voltammetry	0.05-20 ngmL ⁻¹ -----	10	Moderate	[88]
5.	ITO	AuNP, Hyperbranched polyester	Dip coating	Linear sweep stripping voltammetry	0.01-80 ngmL ⁻¹ -----	30	Moderate	[226]
6.	ITO	Au-chitosan	Drop cost	Cyclic voltametry	2-20 ngmL ⁻¹ -----	14	Moderate	[85]
7.	Whatman paper 1	PEDOT:PSS/RGO	Dip coating	Amperometry	2-8 ngmL ⁻¹ and 25.8 μAng ⁻¹ mL	21	Low Cost	Present Work

3.4 CONCLUSIONS

We have demonstrated a flexible and highly conducting paper sensor, based on composite of poly(3,4-ethylenedioxythiophene):poly(styrenesulfonate) (PEDOT:PSS) and reduced graphene oxide (RGO). It has been found that conductivity of the PEDOT:PSS conducting paper increases by 2 order of magnitude when it is treated with ethylene glycol. The incorporation of RGO in PEDOT:PSS conducting paper film indicates excellent electrochemical activity and faster charge transfer kinetics. This low cost, flexible and environment friendly conducting paper has been used for cancer biomarker detection. The fabricated PEDOT:PSS/RGO based electroactive paper shows sensitivity of $25.8 \mu\text{Ang}^{-1}\text{mLcm}^{-2}$ in the detection range of 2-8 ngmL^{-1} . The results obtained for serum samples of cancer patients using this paper based sensor have been validated using ELISA. However, this paper sensor exhibit low detection range and there is considerable scope to improve the performance of conducting paper by selection of suitable solvent and dopant. The next Chapter contains results of studies relating to the development of an electrochemical conducting paper sensor based on formic acid treated carbon nanotubes.

The results of these studies have been published in Biosensors and Bioelectronics, 2015, 73, 114-22.

CHAPTER 4

Carbon Nanotube Modified Conducting Paper Sensor for Cancer Detection

4.1 INTRODUCTION

Carbon nanotubes (CNTs) are allotropes of carbon consisting of one-atom-thick sheets of carbon (graphene) arranged in a long, hollow and cylindrical structure. This one dimensional nanostructure has high aspect ratio, where diameter is of the order of nanometer and length may comprise of several hundred micrometers [227]. Individual nanotubes align themselves into rope like structure *via Van der Waals* force, more specifically by pi-stacking. Chemical bonding of a carbon nanotube is entirely composed of sp^2 nature, which is stronger than the sp^3 bonds found in diamonds resulting in extraordinary strength, unique electrical and thermal properties of nanotubes [227-228]. The edge localized -COOH and -NH₂ groups generated upon oxidation of CNTs can be utilized for covalent attachment of desired biomolecules, polymers and metallic particles [10, 229-230]. These excellent properties of CNTs have attracted considerable interest in biomedical applications such as drug delivery, tissue engineering, theranostics, electrochemical and biological sensor etc. [231-232].

For biosensing application, CNTs have been predicted to have a wide range of applications because of their excellent electrochemical properties, large surface area, ballistic electron transport and high mechanical strength. In addition, CNTs-modified electrodes can be employed to immobilize biomolecules and to minimize surface fouling effects [233]. There are several reports where CNTs have been employed to enhance the electrochemical performance of a biosensor. Singh *et al.* used functionalized CNTs for fabrication of electrochemical biosensor for food toxin detection. The fabricated biosensor shows high sensitivity and improved detection limit [233]. Rusling *et al.* used CNTs have been used to fabricate an ultrasensitive electrochemical biosensor to detect oral cancer biomarker, IL-6. This fabricated biosensor utilized CNTs as an immobilization matrix as well as to tag enzyme

(horseradish peroxidase, HRP) with secondary antibody to enhance sensitivity and detection limit [234]. Akter *et al.* used similar strategy to amplify signal of electrochemical biosensor by tagging secondary antibody with multiple HRP integrated CNTs for detection of cancer biomarker (prostate specific antigen, PSA). Herein, gold integrated CNTs were used to immobilize the primary antibody which enhances the long term stability of fabricated electrode [235]. Huang *et al.* fabricated a rapid, sensitive and highly stable electrochemical biosensor based on gold integrated chitosan modified CNTs electrode for prognosis of cancer biomarker (CEA) [87]. There is thus a lot of scope to improve the performance of electrochemical biosensor by integrating CNTs with a suitable matrix. In the above discussed report, conventional conducting substrate (indium tin oxide, gold, glassy carbon etc.) have been used for the fabrication of various electrochemical biosensor. These electrodes have high cost, are rigid, brittle, and their fabrication requires high temperature processing and expertise. Besides this, disposability of these materials continues to be a major challenge. Therefore, there is increased demand for the development of a paper based biosensor for clinical application as these are predicted to be simple, low cost, flexible, lightweight, biocompatible, and it can be easily disposed off by incineration [91, 236-237]. A conducting paper has been found to play an important role in the ongoing transition to the development of paper based electrochemical biosensors. Coupling of paper electronic devices (such as electrodes and transistors) with biological systems provides an efficient platform for conduction of both electronic and ionic charge carriers that play a major role for communication with a desired biomolecule [110, 143, 238-239]. Ge *et al.* used carbon nanotubes and glutaraldehyde modified paper to fabricate the electrode array of Ag/AgCl reference and carbon counter electrodes for cancer biomarker detection [240]. Lei *et al.*

fabricated CNTs modified paper for detection of biotin-avidin binding and pH measurements. This method used a metal mask, vacuum filtration unit and polydimethyl siloxane (PDMS) for development of sensor on paper [241-242]. Koo *et al.* grew carbon nanotubes using chemical vapour deposition (CVD) on wax-printed Origami paper chip for potential application in electroanalytical devices [243]. Wang *et al.* fabricated CNTs modified paper sensor via dip coating method for detection of environmental toxin, Microcystin-LR (MC-LR) [110]. However, CNTs are known to be insoluble in most solvents and difficulties in forming uniform film over large areas. The grafting of CNTs with polymer may improve the solubility of CNTs, prevent restacking of CNTs layer, and form free standing film with improved electrochemical properties [244-245]. The poly (3,4-ethylene dioxythiophene) /poly(styrenesulfonate) (PEDOT/PSS) is considered a promising conducting material for fabricating conducting paper due to its high conductivity, solution processability, uniform film forming ability, thermal stability, mechanical flexibility and homogenous adsorption on paper by simple dip coating method [90, 246]. The conductivity of the PEDOT:PSS can be tuned by chemical modification that depends on nature and the degree of doping [217-218, 247-248]. Keeping in view these advantages, we have fabricated a PEDOT:PSS/CNTs based efficient conducting paper *via* simple dip coating method to improve the electrochemical performance of conducting paper sensor for carcinoembryonic antigen (CEA) detection.

4.2 EXPERIMENTAL DETAILS

4.2.1 Fabrication of PEDOT:PSS based conducting paper

The PEDOT:PSS aqueous solution doped with 5% EG was used to fabricate the conducting paper. The Whatman Paper 1 (1cm×3 cm) was dipped in aqueous

suspension of PEDOT:PSS (1.3wt%, 5% ethylene glycol) for 1 h and was then dried at 100°C in a hot air oven, was termed as conducting paper (CP) after which it was further treated with formic acid by dipping it in formic acid for 20 min. The formic acid (FA) treated conducting paper (FA@CP) was finally dried at 100 °C for about 1 h.

4.2.2 Fabrication of CNTs doped conducting paper (CNTs/FA@CP)

Firstly, 5 mg CNTs was doped into 10 ml of PEDOT:PSS aqueous solution (1.3wt%, 5% EG). Next, PEDOT:PSS/CNTs composite (1.3wt%, 5% EG, 0.05wt% CNTs) ultrasonicated for 1 h. It was found that CNTs were highly dispersed without sedimentation in PEDOT:PSS solution. Further, Whatman paper 1 was dipped in PEDOT:PSS/CNTs composite for 1 h and was then dried at 100 °C in a hot air oven after which it was further treated with formic acid by dipping it in the formic acid for 20 min. The formic acid treated conducting paper was finally dried at 100 °C for about 1 h. A Schematic of the experiment is demonstrated in **Fig. 4.1**.

4.2.3 Fabrication of CNTs doped conducting paper sensor (anti-CEA/CNTs/FA@CP)

Anti-CEA monoclonal (20 μ L, 100 μ g mL^{-1}) antibodies were immobilized over the CNTs doped conducting paper treated with formic acid electrode (CNTs/FA@CP) via formation of a covalent bond between the carboxylic group of CNTs and the NH_2 -terminal of the antibody via EDC-NHS coupling reaction. The anti-CEA were physically adsorbed over CNTs/FA@CP electrode *via* electrostatic interactions between biomolecules and the conducting paper. The electrode was then rinsed with phosphate buffer (PBS, 50 mM, pH 7.2, 0.9% NaCl) to remove any unbound antibodies. 0.1% of bovine serum albumin (BSA) in PBS was added to the antibody-modified electrode to block the unspecific sites. After rinsing again with PBS, the electrodes were stored at 4 °C before carrying out the sensing studies.

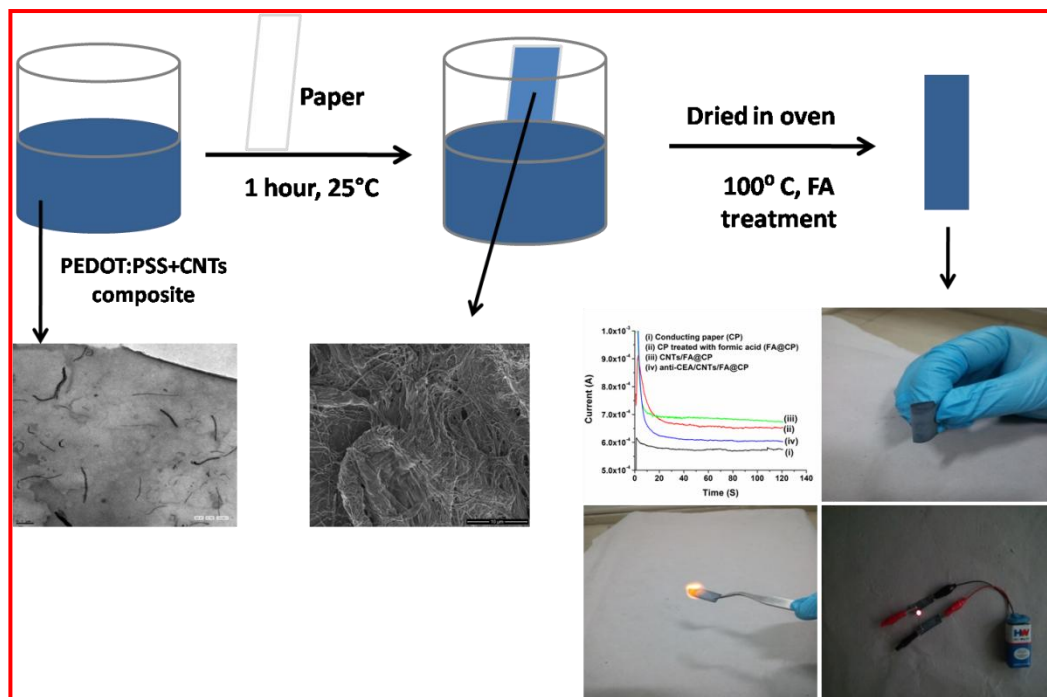


Fig. 4.1: Fabrication and characterization of CNTs/FA@CP modified paper electrode.

4.3 RESULTS AND DISCUSSION

4.3.1 Transmission electron microscopic studies

Fig. 4.2a shows TEM image of the carbon nanotube indicating linear and a tubular structure with a few microns in length. The tubular structure with diameter ranging from ~25-30 nm can be seen in the inset of **Fig. 4.2a**. It appears that CNTs are uniformly dispersed in PSS via non-covalent stabilization. Hydrophobic portion of polymeric chains appear to cover the CNTs surface via edge-to-face aromatic interactions where as the hydrophilic part interacts with water molecules to make homogeneous dispersion of CNTs [249]. TEM image of PEDOT:PSS-CNTs nanocomposite is shown in **Fig. 4.2b** wherein uniformly dispersed CNTs are clearly visible at the PEDOT:PSS surface.

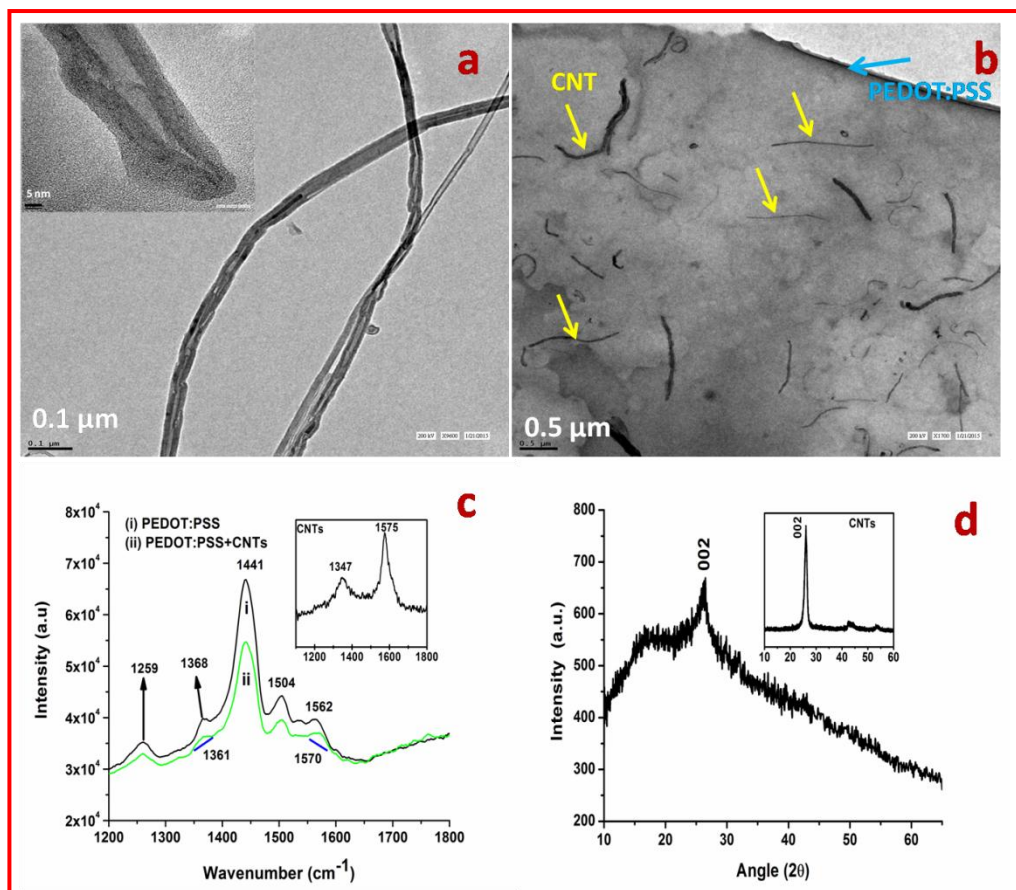


Fig. 4.2: TEM image of (a) carbon nanotube (b) CNTs/PEDOT:PSS composite (c) Raman spectrum of (i) PEDOT:PSS and (ii) PEDOT:PSS/CNTs composite [Inset shows the Raman of CNTs] (d) XRD pattern of PEDOT:PSS/CNTs composite and inset showing XRD of CNTs.

4.3.2 Raman and X-ray diffraction studies

The Raman peaks seen at 1259 cm⁻¹, 1368 cm⁻¹, and 1441 cm⁻¹ are associated with C-C in-plane symmetric stretching, C-C stretching deformation and C_α=C_β symmetric stretching vibration respectively. The C_α=C_β asymmetric stretching vibration gives rise to bands at 1504 and 1562 cm⁻¹, corresponding to thiophene rings in the middle and at the end of the chains (**Fig. 4.2c**) [250-251]. Inset of **Fig. 4.2c** shows characteristic peak of CNTs at 1347 cm⁻¹ due to D band and 1575 cm⁻¹ attributed to G band [233]. The Raman spectrum of the PEDOT:PSS/CNTs hybrid shows peak shift from 1368 to 1361 cm⁻¹ and 1562 to 1570 cm⁻¹ indicating existence of interactions between the CNTs and the conjugated thiophene ring of PEDOT:PSS,

that can be associated with electronic density transfer between constituent [250-251]. Similarly XRD spectra also shows a sharp peak centered on 2θ value 26.2° corresponding to the (002) plane of CNTs (inset of **Fig. 4.2d** shows XRD of CNTs confirming the presence of CNTs in PEDOT:PSS amorphous polymer [252].

4.3.3 Scanning electron microscopic studies

The surface morphology of the various modified electrode was investigated using scanning electron microscopy (SEM) (**Fig. 4.3**). Image a shows SEM of the PEDOT:PSS coated paper, wherein conducting polymer is found to be uniformly adsorbed over the cellulose fibers of the paper. However, morphology of the PEDOT:PSS-CNTs coated paper (Image b) suggests that CNTs are incorporated throughout the surface. Most CNTs are entangled with PEDOT:PSS and cellulose fibers while some of these are clearly visible on the surface of the polymer coated paper. However, after the antibody functionalization (image c), surface morphology of the PEDOT:PSS-CNTs coated paper electrode exhibits a shiny appearance due to accumulation of the static charge, indicating successful immobilization of the antibodies. It appears that the antibody molecules cover the pores of the PEDOT:PSS-CNTs coated paper surface.

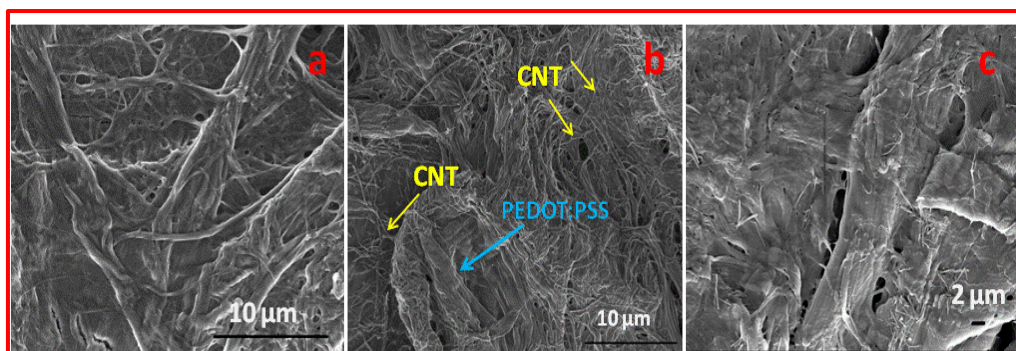


Fig. 4.3: SEM image of (a) PEDOT:PSS coated paper (b) CNTs/PEDOT:PSS coated paper (c) anti-CEA/CNTs/PEDOT:PSS paper sensor

4.3.4 Electrical conductivity studies

The PEDOT:PSS coated paper shows electrical conductivity of $6.5 \times 10^{-4} \text{ Scm}^{-1}$ whereas after doping with 5% ethylene glycol, the conductivity increases to $2.1 \times 10^{-3} \text{ Scm}^{-1}$. This is attributed to decreased columbic interactions between the positively charged PEDOT molecules and the negatively charged PSS that facilitate reorientation of the polymer chains resulting in enhanced charge carrier mobility. The increased crystal ordering and crystal size on addition of EG results in improved carrier mobility and electrical conductivity [216-217]. On treatment of this paper with formic acid, EG doped conducting paper electrode shows the highest electrical conductivity value ($2.4 \times 10^{-2} \text{ Scm}^{-1}$) by 2 orders of magnitude compared to other solvent (methanol and sulphuric acid). The electrical conductivity enhancement is known to strongly depend on the dielectric constant of the chemicals used for treatment [218, 248]. The high dielectric constant of formic acid (58.5) screens the columbic interaction between positively charged conducting PEDOT and the negatively charged non- conducting PSS resulting in phase separation between them leading to removal of the PSSH and formation of interconnected PEDOT chains and enhanced conductivity. Further, we incorporated CNTs in the PEDOT:PSS solution (1.3wt%, 5% EG, 0.05wt% CNTs) for electrochemical studies since CNTs are known to exhibit excellent electrochemical activity, fast electron transfer and large surface area [253-254]. Formic acid treated CNTs doped conducting paper (CNTs/FA@CP) retains almost similar order of conductivity value ($2.2 \times 10^{-2} \text{ Scm}^{-1}$) as compared to that of the formic acid treated conducting paper (FA@CP).

The optical image of the CNTs modified conducting paper treated with formic acid (CNTs/FA@CP) shows high flexibility and conductivity as demonstrated in **video 4.1 (Please see the attached CD)** and **Fig. 4.4 (a-d)**. Its fabrication does not

require any additional steps and it can be cut into desired shape and size. This platform holds great potential for application in the paper based electrochemical devices. In **Fig. 4.4 (c-d)** we demonstrate an efficient conductivity of paper electrode by lighting an LED when current is passed through multiple times folded conducting paper (**video 4.1, Please see attached CD**). It may be noted that this low-cost conducting platform can be easily decomposed by simple burning/incineration [**Fig. 4.4 (e-f)**]. This is an additional advantage for electronic and biomedical waste management.

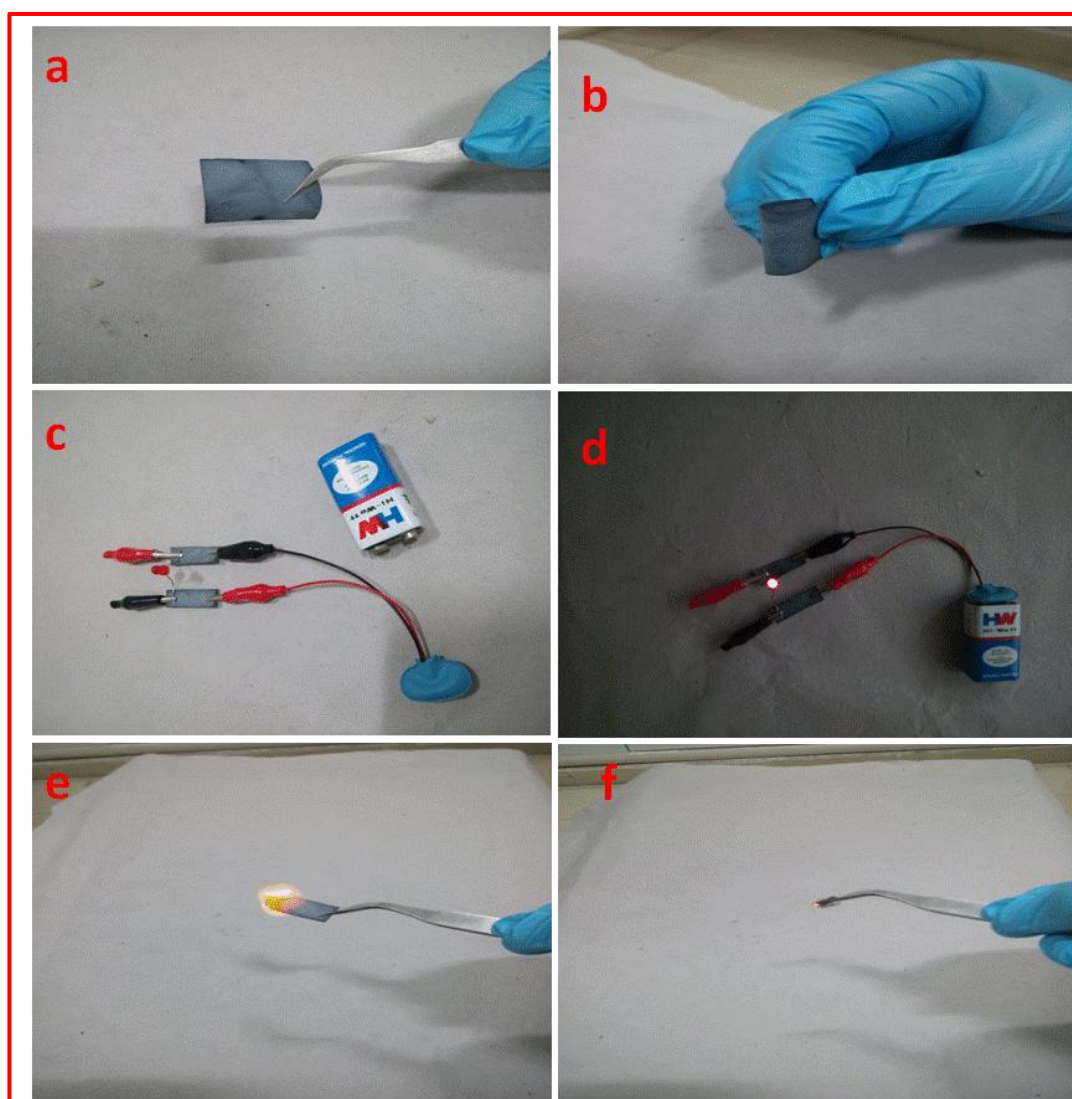


Fig. 4.4: (a) Optical image of conductive and electrochemically active paper (CNTs/FA@CP) showing (b) high flexibility (c-d) Lighting an LED lamp (e-f) easy to dispose off.

4.3.5 X-ray photoelectron spectroscopic studies

In PEDOT:PSS, both PEDOT and PSS contain one sulfur atom per monomer. In PSS, sulfur is present as sulfonate moiety whereas PEDOT contains sulfur in thiophene ring and thus provides different chemical environments since S(2p) electrons of PEDOT and PSS have different binding energies [22]. The S 2p band of PEDOT is found at lower binding energy whereas S 2p band of PSS is observed at higher binding energy. Each band splits into doublet of S 2p_{3/2} and S 2p_{1/2} component due to spin-orbital splitting of sulfur atom. **Fig. 4.5a** shows XPS spectra of the pristine PEDOT:PSS coated paper (curve i), EG doped PEDOT:PSS paper (conducting paper) (curve ii), formic acid treated conducting paper (curve iii). The observed slight change in peak intensity of conducting paper as compared to that of the PEDOT:PSS coated paper may be assigned to the conformational changes in PEDOT:PSS polymer. However after formic acid treatment there is decrease in peak intensity of PSS indicating exfoliation of PSS from conducting paper surface. **Fig. 4.5b** shows XPS spectra of the pristine PEDOT:PSS coated paper that has been deconvoluted into the characteristic binding energy peaks. The S 2p_{3/2}(S 2p_{1/2}) peak at the binding energy near 163.7 (164.8) eV corresponds to sulfur atom of the PEDOT and the S 2p_{3/2}(S 2p_{1/2}) peak seen at the binding energy near 168.3 (169.6) eV is due to sulfur atom present in PSS [191, 255]. The binding energy positions of these bands are almost same as in the case of the conducting paper (**Fig. 4.5c**). However, after the formic acid treatment, S 2p peak of PSS is shifted to lower energy level (**Fig. 4.5d**). It is observed that PSS peak of CNTs/FA@CP (**Fig. 4.5e**) is shifted towards the lower binding energy as compared to that of FA@CP around -0.3. The presence of (-0.5) eV is due to high electron density in PSS because of charge transfer from CNTs to

electronegative sulfur atom indicating existence of interactions between the CNTs and the conjugated thiophene ring of PEDOT:PSS [252].

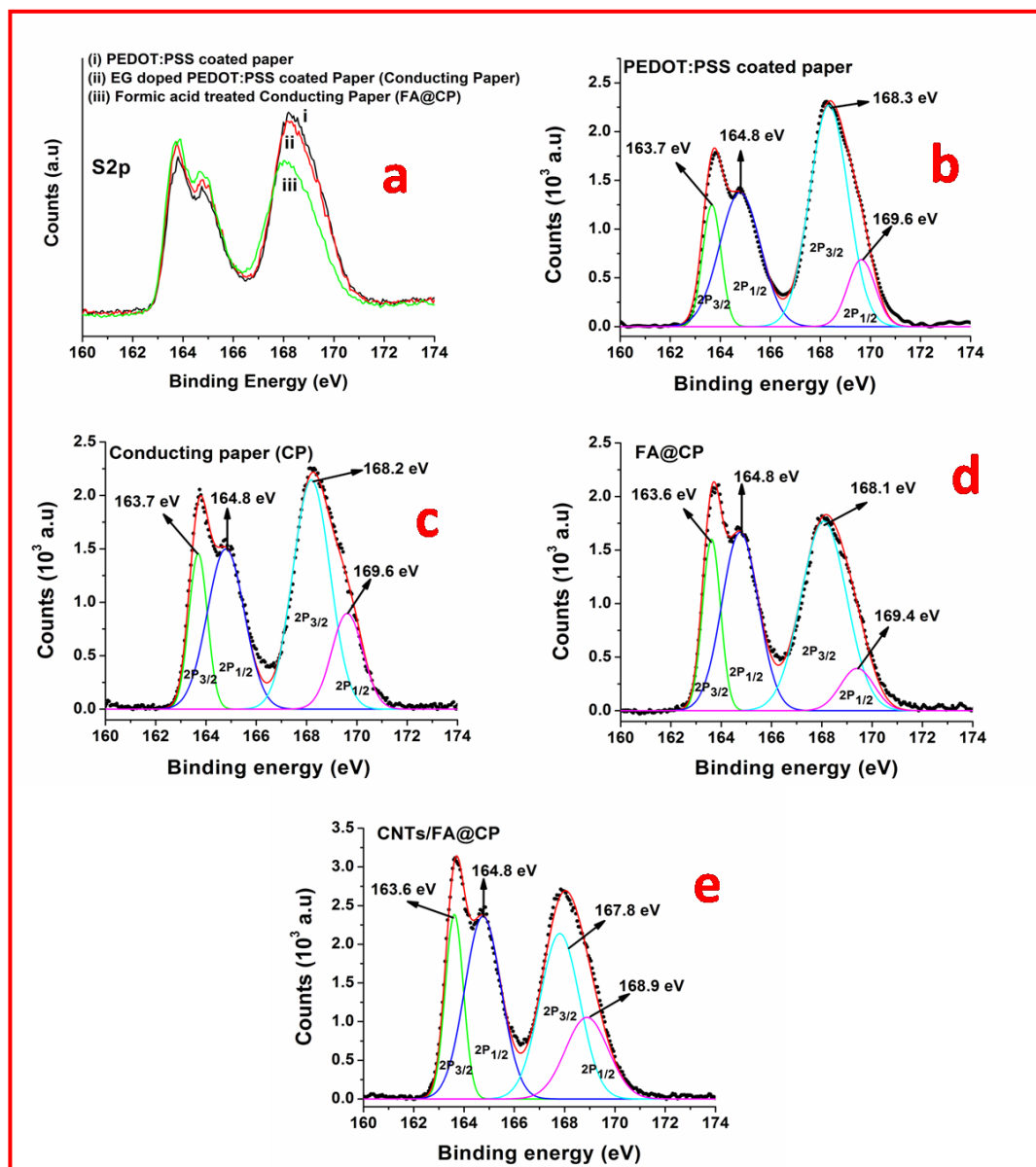


Fig. 4.5: S (2p) XPS spectra of (a) modified papers, XPS curve fitting of (b) PEDOT:PSS coated Paper (c) Ethylene glycol doped PEDOT: PSS coated over paper *i.e.* conducting paper (d) conducting paper treated with formic acid (FA@CP) (e) CNTs doped conducting paper treated with formic acid.

In PEDOT:PSS, PEDOT molecules are conductive in nature and are surrounded by the non-conductive PSS molecules [246]. On being treated with formic

acid, this core-shell structure of the PEDOT:PSS in conducting paper changes from coiled to partially linear due to ejection of PSS molecules that are perhaps responsible for enhanced connectivity between PEDOT chains. Therefore energy barrier for charge hopping is lowered resulting in enhanced charge transfer among the PEDOT chains. The ratio of PEDOT to PSS can be estimated from area under the curve. It is found that, there is no significant change in PEDOT to PSS ratio between PEDOT:PSS coated paper (1/1.33) and conducting paper (1/1.30). However, the ratio of PEDOT to PSS increases from 1/1.30 to 1/1.04 after conducting paper is treated with formic acid confirming removal of ~20% PSS from the surface. It appears that exclusion of PSS due to formic acid treatment is perhaps responsible for better connectivity between PEDOT chain that in turn result in increased conductivity.

4.3.6 Electrochemical studies

Fig. 4.6a shows results of the chronoamperometric studies obtained for (i) conducting paper, [CP] (ii) conducting paper treated with formic acid, [FA@CP] (iii) CNTs doped conducting paper treated with formic acid, [CNTs/FA@CP] (iv) anti-CEA immobilized over CNTs/FA@CP, [anti-CEA/CNTs/FA@CP] at 2V on every 0.1 s. The increased electrochemical response current of the FA@CP electrode (~0.65 mA) than that of the CP electrode (~0.57 mA) is attributed to increased conductivity of the electrode due to removal of PSS from the film surface. Further increase in the electrochemical current value of CNTs/FA@CP electrode (~0.68 mA) can be assigned to high electrochemical activity of CNTs that enhances permeability of the redox couple $[\text{Fe}(\text{CN})_6]^{3-/4-}$. Next, decrease in the value of electrochemical current observed after immobilization of anti-CEA onto CNTs/FA@CP electrode (~0.60 mA) is attributed to the hindrance caused by the CEA antibodies to the electron transport indicating immobilization of anti-CEA.

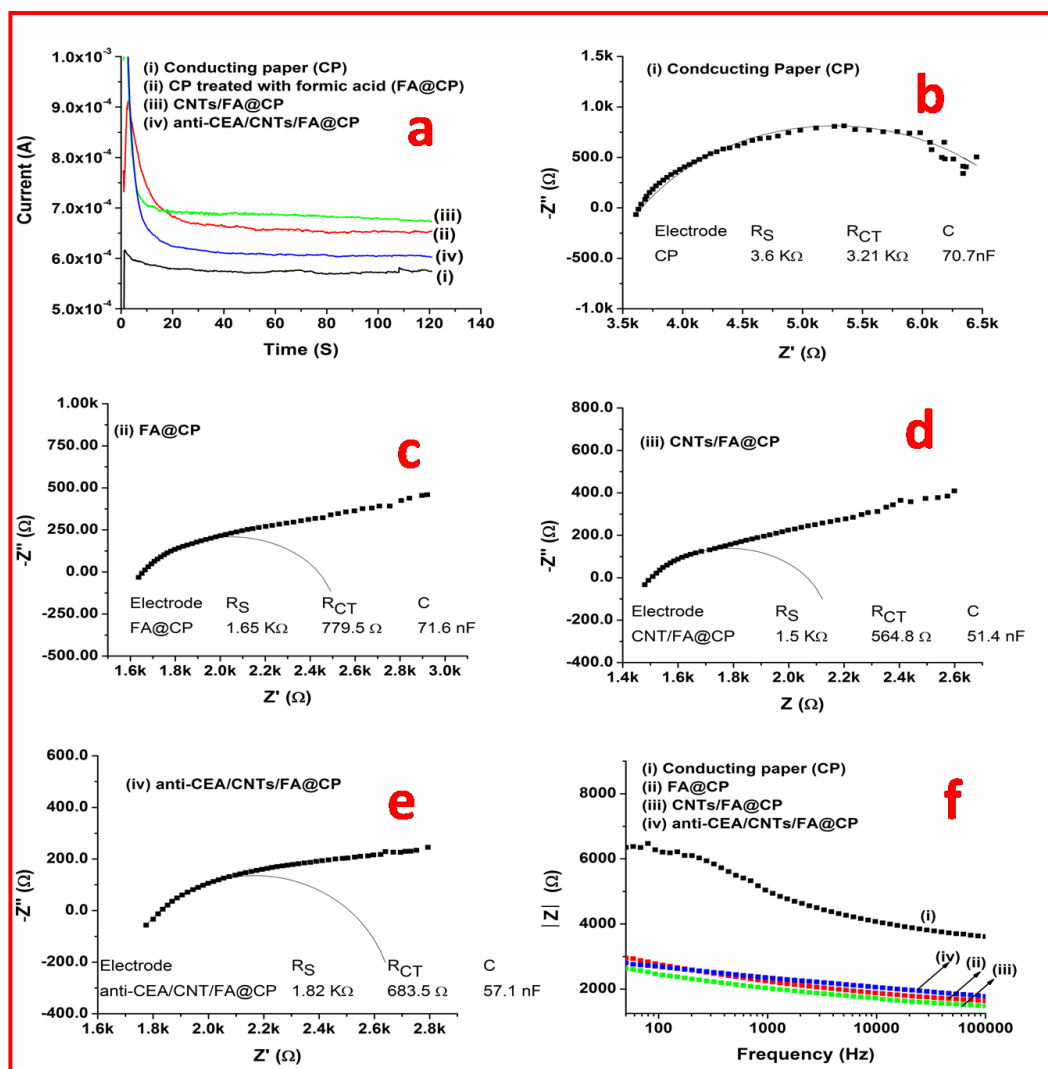


Fig. 4.6: Electrochemical characterization of modified paper electrode (a) chronoamperometric studies of modified paper electrode. Impedance spectra of (b) conducting paper (c) conducting paper treated with formic acid (FA@CP) (d) CNTs modified conducting paper treated with formic acid (CNTs/FA@CP) (e) anti-CEA/CNTs/FA@CP paper electrode and circuit were fitted with equivalent randles circuit $R_S(R_{ct} C)$. (f) Bode plot of different modified electrode.

The electrochemical impedance spectroscopy (EIS) is an effective tool for investigating interfacial properties of the surface modified electrodes. **Fig. 4.6** shows the Nyquist plot obtained for (b) conducting paper, [CP] (c) conducting paper treated with formic acid, [FA@CP] (d) CNTs doped FA@CP, [CNTs/FA@CP] and (e) anti-CEA immobilized over CNTs/FA@CP, [anti-CEA/CNTs/FA@CP] in PBS solution containing 5 mM $[\text{Fe}(\text{CN})_6]^{3-/4-}$ at 0.03V (biasing potential) in the frequency range,

100KHz to 50 Hz. The diameter of the semicircle in the Nyquist plot yields magnitude of the charge transfer resistance (R_{ct}) of electrode that depends on the dielectric features of the electrode/electrolyte interface. It can be seen that R_{ct} value of the conducting paper electrode (3.2 K Ω , **Fig. 4.6b**) decreases after the formic acid treatment (779.5 Ω , **Fig. 4.6c**). This is assigned to the high dielectric constant of the formic acid that facilitates decreased columbic interaction between PEDOT and PSS leading to removal of the PSS molecule. The exclusion of PSS (negatively charged and non-conducting in nature) from the conducting paper provides increased exposure of the inter-connected PEDOT chains (positively charged and conducting in nature) that promotes permeability of redox probe, $[\text{Fe}(\text{CN})_6]^{3-/4-}$ to the surface of FA@CP electrode. The value of R_{ct} (564.8 Ω , **Fig. 4.6d**) for the CNTs/FA@CP electrode is smaller than that of the FA@CP electrode (779.5 Ω). This may be attributed to excellent electrochemical properties and larger surface area of CNTs that are incorporated in the PEDOT:PSS matrix resulting in increased permeability of the $[\text{Fe}(\text{CN})_6]^{3-/4-}$ to the surface of CNTs/FA@CP paper electrode. Further, increase in the value of R_{ct} (683.5 Ω , **Fig. 4.6e**) of anti-CEA/CNTs/FA@CP is attributed to the hindrance caused by the macromolecular structure of the antibodies that perhaps obstruct electron transfer owing to their insulating nature. These results also confirm functionalization of the CNTs/FA@CP electrode with anti-CEA. The heterogeneous electron transfer rate constant (K_{ct}) of CNTs/FA@CP and FA@CP electrode can be calculated using Eq. 4.1 [223].

$$K_{ct} = \frac{RT}{n^2 F^2 A R_{ct} [S]} \quad \text{.....Eq. 4.1}$$

where R is the gas constant, T is absolute temperature, F is the Faraday constant, A is the electrode area (cm^2), [S] is the concentration of redox probe (mol/cm^3) and n is the number of transferred electrons per molecule of the redox probe. The heterogeneous

electron transfer rate constant (K_{ct}) value of the CP, FA@CP and CNTs/FA@CP has been found to be $1.66 \times 10^{-7} \text{ cm s}^{-1}$, $6.83 \times 10^{-5} \text{ cm s}^{-1}$ and $9.43 \times 10^{-5} \text{ cm s}^{-1}$, respectively. This indicates that the CNTs/FA@CP electrode exhibits faster electron transfer kinetics as compared to that of the other modified paper electrodes. Thus incorporation of CNTs results in improved electrochemical activity of the paper electrode (CNTs/FA@CP). Interestingly, K_{ct} of CNTs/FA@CP electrode is found to be nearly 5 times higher compared to our previous work where in PEDOT:PSS-RGO composite was used to fabricate conducting paper using ethylene glycol [256].

The solution resistance (R_s) is found to be the highest (3.6 $K\Omega$) for CP electrode as compared to that of the other modified electrodes FA@CP (1.6 $K\Omega$), CNTs/FA@CP (1.5 $K\Omega$) and anti-CEA/CNTs/FA@CP (1.8 $K\Omega$). R_s depends on the type of ions, ionic concentration, temperature and the electrode surface [257]. This suggests that after the formic acid treatment, morphology of CP electrode changes due to the removal of PSS leading to lower R_s value. **Fig. 4.6f** shows the Bode plot representing the impedance modulus ($|Z|$) vs. frequency for the modified paper electrodes. The FA@CP, CNTs/FA@CP and anti-CEA/CNTs/FA@CP electrodes exhibit low $|Z|$ compared to CP in the frequency range, 50 Hz to 100 KHz, confirming increased electrochemical activity due to removal of non conducting PSS molecule. The values of electrical conductivity and electrochemical properties of modified paper electrodes are summarized in **Table 4.1**.

4.3.7 Electrochemical response studies

The electrochemical response studies (**Fig. 4.7a**) were conducted by varying the concentration of carcinoembryonic antigen (CEA) from 1 to 100 ng mL^{-1} in PBS (50mM, pH 7.4, 0.9% NaCl) containing 5 mM $[\text{Fe}(\text{CN})_6]^{3-/4-}$ using chrono-amperometry with an incubation time of 15 min. The magnitude of current decreases

on addition of CEA due to formation of electrically insulating antigen–antibody complexes produced due to specific interaction of the CEA and anti-CEA that may block the electron transfer via redox probe, $[\text{Fe}(\text{CN})_6]^{3-/4}$ at the paper electrode surface.

Table 4.1: Conductivity and electrochemical properties of modified paper electrode.

S.No.	Material coated on Paper	Conductivity	Charge transfer resistance (R_{CT})	Solution Resistance (R_s)	Heterogeneous electron transfer rate constant (K_{et})
1.	PEDOT:PSS+ EG (CP)	$2.1 \times 10^{-3} \text{ Scm}^{-1}$	3.21 K Ω	3.6 K Ω	$1.66 \times 10^{-7} \text{ cm s}^{-1}$
2.	PEDOT:PSS+ EG Treated with Formic acid (FA@CP)	$2.4 \times 10^{-2} \text{ Scm}^{-1}$	779.5 Ω	1.65 K Ω	$6.83 \times 10^{-5} \text{ cm s}^{-1}$
3.	PEDOT:PSS+ EG + CNTs treated with Formic acid (CNTs/ FA@CP)	$2.2 \times 10^{-2} \text{ Scm}^{-1}$	564.8 Ω	1.5 K Ω	$9.43 \times 10^{-5} \text{ cm s}^{-1}$

Fig. 4.7b shows the calibration curve obtained between response current and CEA concentration (curve i). It is found that the amperometric current decreases upto 25 ngmL⁻¹ after which it increases and reaches saturation upto 100 ngmL⁻¹. However, a linear relationship obtained between 2-15 ngmL⁻¹ with a sensitivity of 7.7 $\mu\text{Ang}^{-1} \text{ mLcm}^{-2}$ and follows Eq. 4.2.

$$I(\text{A}) = -7.8 \mu\text{A mL ng}^{-1} \times [\text{CEA concentration}] + 528 \mu\text{A}; R^2 = 0.95$$

.....Eq. 4.2

A control experiment was performed to check cross reactivity of the paper sensor with CEA antigen in the absence of antibodies (curve ii). However, no significant change in current response was observed for the BSA/CNTs/FA@CP in the absence of antibodies as a function of CEA concentration. The repeatability of bioelectrode

was confirmed by repeating each experiment 3 times and the error bars are included based on RSD value.

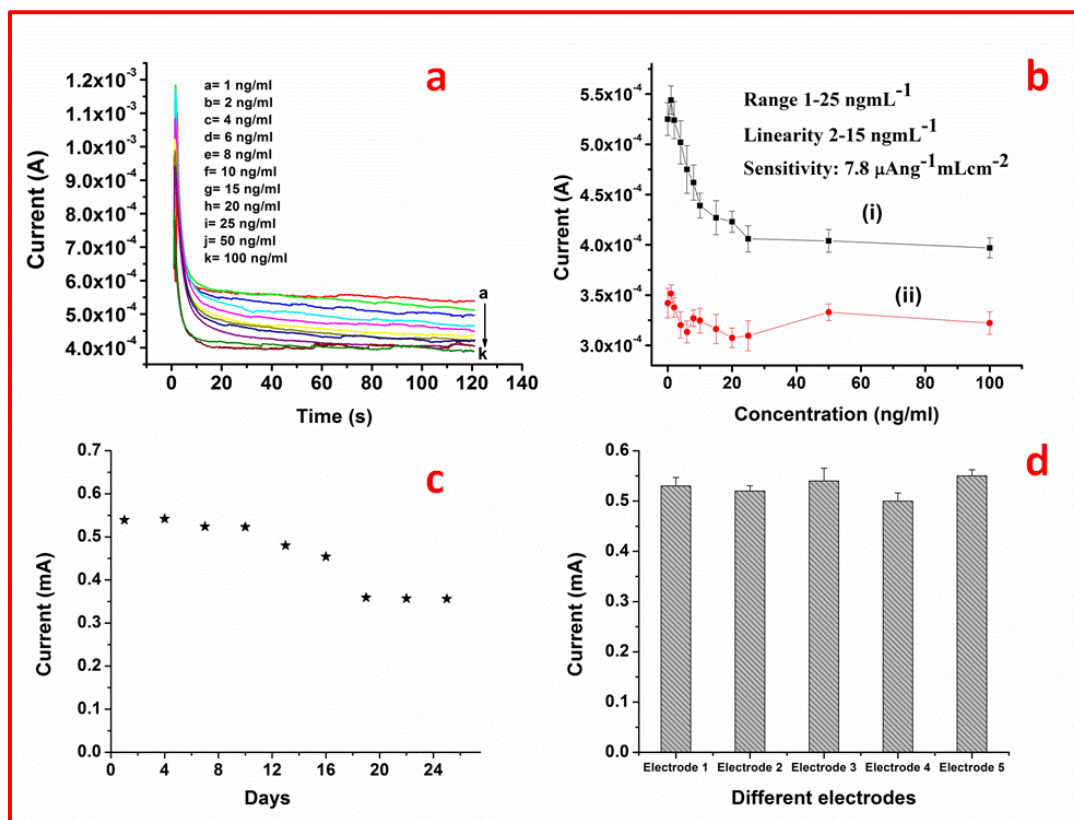


Fig. 4.7: (a) Electrochemical response studies of the BSA/anti-CEA/CNTs/FA@CP paper electrode obtained as a function of CEA concentration ($1\text{--}100 \text{ ng mL}^{-1}$) using chronoamperometry and (b) calibration plot between the magnitudes of current recorded and CEA concentration (curve i); control experiment in absence of antibody (curve ii). (c) Current response time of BSA/anti-CEA/CNTs/FA@CP paper electrode as a function of time (day) (d) Current response time of five different BSA/anti-CEA/CNTs/FA@CP paper electrodes fabricated using the same set of procedure in presence of CEA concentration (2 ng mL^{-1}).

4.3.8 Real sample analysis

CEA is traditionally determined by gold standard technique for proteinaceous molecules *i.e.* ELISA to diagnose and monitor cancer. This method usually involves a complex procedure, is time-consuming and is expensive. It is thus desirable to develop techniques that are low cost, easy to use, are rapid, sensitive and do not require any laboratory infrastructure for the CEA estimation. Therefore attempts have been made to estimate CEA concentration in serum by using BSA/anti-CEA/

CNTs/FA@CP bioelectrode to evaluate the feasibility of the proposed paper sensor as discussed in chapter 3. It can be seen that a reasonable correlation exists between (a) CEA concentration in serum samples determined by immunometric immunoassay technique and (b) standard concentration of CEA (**Table 4.2**). The results exhibit reasonable relative standard deviation (%RSD) indicating high accuracy of paper sensor.

Table 4.2: Determination of carcinoembryonic antigen concentration in serum samples using BSA/anti-CEA/CNTs/ FA@CP paper electrode.

S. No.	CEA concentration (ngmL ⁻¹) Determined using ELISA	Amperometric current (mA) obtained with Standard CEA sample	Amperometric current (mA) obtained with serum sample	%RSD
1	2.37	0.518	0.517	0.2
2	4.03	0.501	0.507	0.8
3	5.57	0.485	0.487	0.3
4	5.96	0.474	0.493	2.81
5	10	0.439	0.482	6.5

4.3.9 Stability and reproducibility studies

The storage stability of this paper sensor was monitored at an interval of 3 days as shown in **Fig 4.7c**. It was found that the paper immuno-electrode (BSA/anti-CEA/CNTs/FA@CP) retained about 82% activity even after 18 days when stored at 4°C after which the current response decreased to less than 70% in about 25 days. This indicates that the fabricated paper immuno-electrode exhibits reasonably good stability at least for 18 days. **Fig.4.7d** indicates electrochemical response of five different paper immuno-electrodes (BSA/anti-CEA/CNTs/FA@CP) fabricated under the same set of conditions in presence of CEA concentration (2 ngmL⁻¹). It is found that this paper immuno-electrode shows good reproducibility for five different

electrodes with constant surface area as is evident by standard error of less than 5% (mean value = 528 μ A). Further, each measurement was repeated 3 times for each electrode and the error bars are included accordingly.

The sensing characteristics of the CNTs modified conducting paper sensor are summarized in **Table 4.3** along with those reported in literature. It can be seen that sensitivity of the paper electrode is much higher than that of the other reported electrodes (gold, glassy carbon and ITO electrode) and can be used to differentiate two lower value of CEA concentration. These results show that paper based electrochemical sensor is a better candidate over conventional electrodes.

4.3.10 Disposability studies

To attest the environment friendliness, these paper electrodes were decomposed by incineration. The resulting ash was investigated by energy dispersive X-ray (EDX) technique. EDX results confirm the presence of only carbon, oxygen, sodium, phosphorous and potassium; no toxic metals were detected (**Fig. 4.7**).

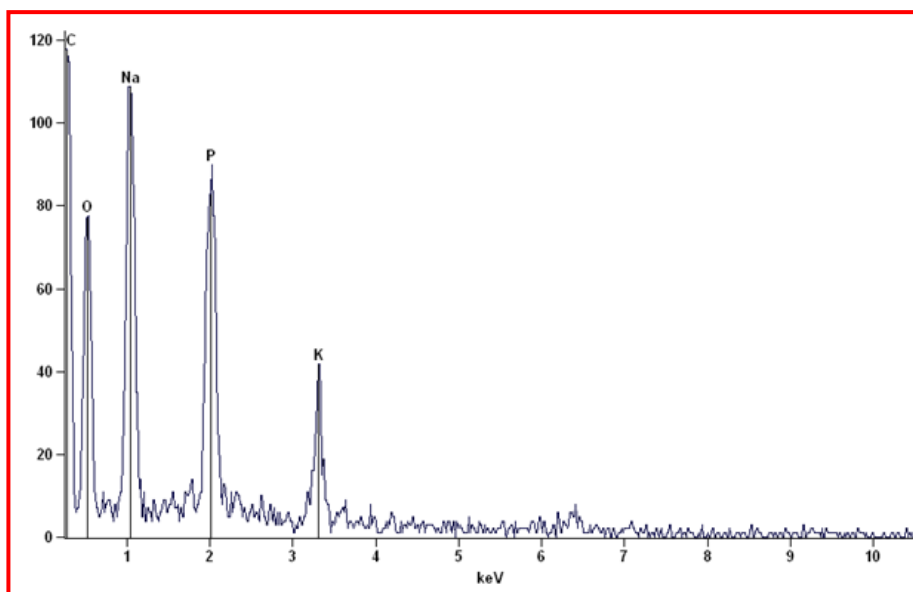


Fig. 4.8: Energy dispersive X-ray (EDX) analysis.

Table 4.3 shows response characteristics of BSA/anti-CEA/CNTs/FA@CP electrode along with those reported in literature.

S. No.	Substrate	Material	Fabrication Method	Detection Method	Linear range and Sensitivity	Stability (days)	Cost	Ref.
1.	Array of Gold electrode	Thiol based Self assembled monolayer	Dip Coating	Amperometry	0-200 ngmL ⁻¹ and 3.8 nAmLng ⁻¹	30	High	[225]
2.	Gold electrode	AuNP, O-aminophenol	Drop cast	Electrochemical Impedance Spectroscopy	0.5-20 ngmL ⁻¹ and 1.08×105 Ωng ⁻¹ mL	-	High	[138]
3.	Glassy carbon electrode	AuNP, MWCNT, Chitosan	Drop Casting	Differential pulse voltammetry	0.3-2.5 & 2.5- 20 ngmL ⁻¹ -----	30	Moderate	[87]
4.	Glassy carbon electrode	Reduced graphene oxide-tetraethylene pentamine (RGO-TEPA)	Drop cast	Differential pulse voltammetry	0.05-20 ngmL ⁻¹	10	Moderate	[88]
5.	ITO	AuNP, Hyperbranched polyester	Dip coating	Linear sweep stripping voltammetry	0.01-80 ngmL ⁻¹ -----	30	Moderate	[226]
6.	ITO	Au-chitosan	Drop cost	Cyclic voltammetry	2-20 ngmL ⁻¹ -----	14	Moderate	[85]
7.	Whatman paper 1	PEDOT:PSS/RGO, Ethylene Glycol	Dip coating	Amperometry	2-8 ngmL ⁻¹ and 25.8 μAng ⁻¹ mLcm ²	21	Low	[46]
8.	Whatman paper 1	PEDOT:PSS/CNTs, Formic acid	Dip coating	Amperometry	2-15 ngmL ⁻¹ and 7.8 μAng ⁻¹ mLcm ²	18	Low	Present Work

4.4 CONCLUSIONS

The nanocomposite of poly(3,4-ethylenedioxythiophene):poly(styrene-sulfonate) (PEDOT:PSS) and carbon nanotubes (CNTs) have been used to fabricate conducting paper (CNTs/CP). It has been found that conductivity of this paper increases by 2 orders of magnitude on being treated with formic acid (CNTs/FA@CP) due to removal of the non-conducting molecule PSS from electrode surface. This fabricated paper is efficient conductive, flexible, electrochemical active, and it can be easily disposed off by simple incineration. Further, this smart conducting platform has been used for conjugation of the anti-carcinoembryonic antigen (CEA) protein for quantitative estimation of CEA. It was observed that incorporation of carbon nanotubes improved heterogeneous electron transfer rate constant (5 times) and linear detection range (2–15 ngmL⁻¹) with respect to PEDOT:PSS-RGO based conducting paper (**Chapter 3**). However this paper sensor does not cover whole physiological range (3-20 ngmL⁻¹). The next chapter pertains to the results relating to the performance of biosensor by modifying the conducting paper with suitable matrix that may provide enhanced biomolecule loading with better orientation.

The results of the studies described in this Chapter have been published in Journal of Materials Chemistry B, 2015, 3, 9305-9314.

CHAPTER 5

PEDOT:PSS/PVA Nanofibers Decorated Conducting Paper Sensor for Cancer Detection

5.1 INTRODUCTION

Nanostructured materials are being explored as immobilization matrices for the development of an efficient biosensing platform [258]. In this context, nanofibers of PEDOT:PSS have been predicted as a promising immobilization matrix for development of paper based electrochemical biosensors due to rapid electron transfer, excellent electrochemical properties, high surface-to-volume ratio, mechanical flexibility, thermal stability, film forming ability and homogenous entrapment on a paper substrate. Electrospun nanofibers (EsNf) of PEDOT:PSS have been predicted to provide a suitable matrix to obtain enhanced physical contact by providing increased number of sites for biochemical interaction, improved biomolecule loading with better orientation of biomolecules resulting in enhanced capturing of the bio-analyte [259-260]. One of the methods that can be used for fabrication of polymeric nanofiber is electrospinning wherein high voltage is applied to the tip of the syringe which contains polymeric solution. As a result, polymer solution becomes charged at high electric field causing the solvent to evaporate and form polymeric nanofiber jets. It provides long ultrafine fibers of a very high surface to volume ratio and relatively defect free fibers at molecular level [261-262]. However, PEDOT:PSS is mechanically weak and has low viscosity which resist the formation of ultrafine fibers [263].

Polyvinyl alcohol (PVA) is a water soluble, nontoxic and biocompatible synthetic polymer. It has excellent film forming, emulsifying, and adhesive properties. The electrospinning of PVA solution forms ultrafine nanofibers that have high tensile strength and good flexibility [264]. These properties of PVA have attracted considerable interest in biomedical application such as drug delivery, tissue engineering, therapy and biosensors [265-266]. Recently, nanofibers of PVA and their

composite have been proposed as immobilization matrix for biosensing application. Wang *et al.* fabricated gold nanoparticle modified PVA electrospun nanofibers immobilized with horseradish peroxidase (HRP). This fabricated biosensor showed a highly sensitive detection of H_2O_2 with a detection limit of $0.5\ \mu\text{M}$ [267]. Su *et al.* fabricated chitosan modified PVA based electrospun nanofibers for glucose detection. The fabricated matrix provides three dimensional network, large porosity and high surface to volume ratio which improve the detection range, detection limit and Michaelis-Menten constant [268]. Zhao *et al.* fabricated hyaluronic acid functionalized PVA/polyethyleneimine electrospun nanofibers for capturing circulating tumor cell for early cancer detection. The fabricated nanofibers matrix exhibit superior capability to capture cancer cells [269]. Thus PEDOT:PSS polymer blends can be modified by cross-linking with PVA to fabricate electrospun fibers with enhanced flexibility, improved mechanical and electrochemical characteristics. This Chapter contains results of the studies relating to the fabrication of PEDOT:PSS/PVA electrospun nanofiber decorated conducting paper *via* electrospinning technique for cancer biomarker (carcinoembryonic antigen, CEA) detection.

5.2 EXPERIMENTAL DETAILS

5.2.1 Fabrication of conducting paper (CP)

Conducting paper was fabricated as described earlier (**Chapter 3**) [256]. In brief, the Whatman paper ($1\text{cm}\times 3\text{cm}$) was dipped in PEDOT:PSS aqueous suspension [1.3 wt%, 3% ethylene glycol (EG)] for 1 h and was then dried at $100\ ^\circ\text{C}$ in a hot air oven. Thereafter it was treated with EG by dipping it in the EG solution for 20 min. The EG treated conducting paper was finally dried at $100\ ^\circ\text{C}$ for about 1h.

5.2.2 Fabrication of PEDOT:PSS/PVA electrospun nanofiber (EsNf) decorated conducting paper (PEDOT:PSS/PVA-EsNf/CP)

The PEDOT:PSS/PVA nanofibers were synthesized using electrospinning (Fig. 5.1a) [26]. Briefly, 0.3g of polyvinyl alcohol (PVA) powder was added to 5 mL of PEDOT:PSS in a vial and magnetically stirred and heat at 60°C for 1-2 h to ensure that the solution was homogenous. The PVA was used as a polymeric carrier material to prepare PEDOT:PSS based electrospun nanofiber. Besides this, PVA is nontoxic, environment friendly polymer that can be helpful to attest the environmental concern of paper sensor [270]. The black viscous solution was kept overnight to remove the air bubbles. Thereafter, the as-prepared viscous solution was transferred into syringe for electrospinning. During the electrospinning process, a direct current voltage of 20 KV was applied to the syringe needle and a feed rate of 1.4 mL/h was used. The distance between the needle tip and the conducting paper (collector) was kept as 10 cm.

5.2.3 Biofunctionalization of PEDOT:PSS/PVA electrospun nanofiber decorated conducting paper (anti-CEA/PEDOT:PSS/PVA-EsNf/CP)

For biofunctionalization, the monoclonal carcinoembryonic antibodies (anti-CEA) solution of 100 $\mu\text{g mL}^{-1}$ was uniformly spread over the PEDOT:PSS/PVA-EsNf/CP electrode (anti-CEA/PEDOT:PSS/PVA-EsNf/CP). The anti-CEA was physically absorbed onto the PEDOT:PSS/PVA-EsNf/CP electrode. The anti-CEA/PEDOT:PSS/PVA-EsNf/CP electrodes thus formed were washed with phosphate buffer (PBS, 50 mM, pH 7.0) to remove any unbound antibodies. Further, to block unspecific sites 0.1% of bovine serum albumin (BSA) was added to the anti-CEA functionalized PEDOT:PSS/PVA-EsNf/CP electrode. After rinsing again with PBS, the fabricated paper electrodes (BSA/anti-CEA/PEDOT:PSS/PVA-EsNf/CP)

were stored at 4 °C before carrying out the sensing studies. A schematic of the experiment is shown in **Fig. 5.1**.

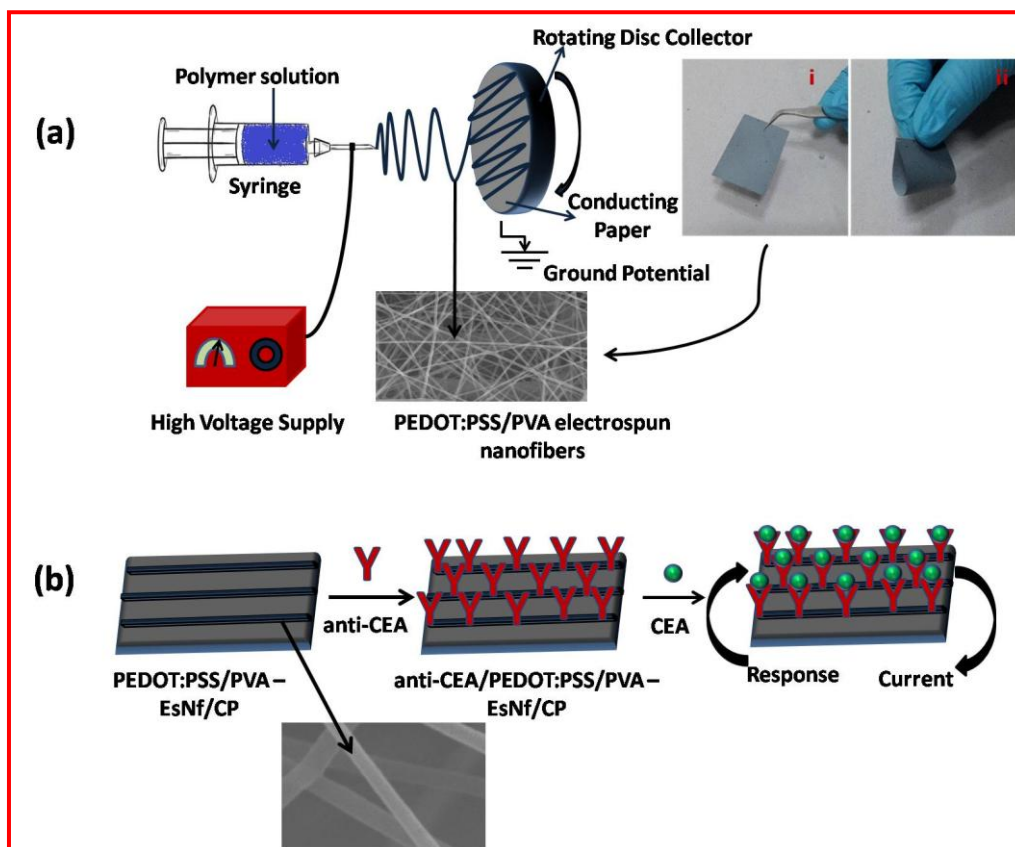


Fig. 5.1: (a) Schematic representation of the electrospinning setup for the synthesis of PEDOT:PSS/PVA nanofibers (Inset showing (i) optical image of electrospun modified paper with (ii) high degree of flexibility) and (b) bio functionalized electrospun PEDOT:PSS/PVA nanofiber for carcinoembryonic antigen detection.

5.3 RESULTS AND DISCUSSION

5.3.1 Raman spectroscopic and zeta potential studies

Fig. 5.2 shows the Raman spectrum of the PEDOT:PSS (curve i) and PEDOT:PSS/PVA hybrid (curve ii), which is nearly identical because of resonating behavior of PEDOT:PSS that enhances the Raman scattering. No PVA peaks were observed due to the presence of dominant PEDOT:PSS intensity peak. The peaks seen at 1257, 1372 and 1440 cm^{-1} are associated with $\text{C}_\alpha\text{-C}_\alpha$ inter-ring stretching, $\text{C}_\beta\text{-C}_\beta$ stretching and $\text{C}_\alpha=\text{C}_\beta$ ($-\text{O}$) symmetric stretching vibration, respectively. The $\text{C}_\alpha=\text{C}_\beta$

asymmetric stretching vibration gives rise to the band at 1502 cm^{-1} and 1565 cm^{-1} corresponding to the thiophene rings of PEDOT:PSS chain [101, 271]. It can be seen that the Raman spectrum of the PEDOT: PSS/PVA hybrid (curve ii) shows peak shift from 1373 to 1366 cm^{-1} and 1500 to 1506 cm^{-1} due to interaction between PEDOT:PSS and PVA. Next, the surface charge of the PEDOT:PSS and PEDOT:PSS/PVA hybrid suspension was characterized by measuring the zeta potential. The observed zeta potential of PEDOT:PSS suspension in water at -24.9 mV is due to presence of sulfonyl group in the PSS molecule [179]. However, zeta potential of PEDOT:PSS/PVA hybrid is found to be shifted towards more negative value (-28.5 mV) due to anionic behavior of PVA chain, indicating interaction between PEDOT:PSS and PVA chain [272].

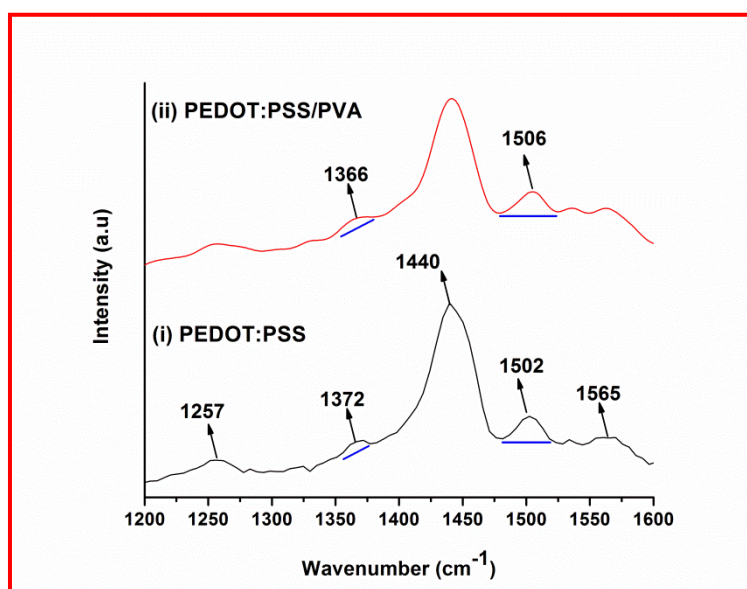


Fig. 5.2: Raman spectrum of (i) PEDOT:PSS and PEDOT:PSS/PVA composite.

5.3.2 X-ray photoelectron spectroscopic studies

In the PEDOT:PSS polymer, both PEDOT and PSS molecules contain one sulfur atom per monomer. In the PEDOT, sulfur is present in thiophene ring, whereas PSS contains sulfur in the sulfonate moiety attached with styrene ring of the polymer.

It appears that the changed chemical environment is perhaps responsible for the observed binding energy of sulfur in PEDOT and PSS polymer. As shown in **Fig. 5.3**, the XPS bands seen between 166 and 172 eV are assigned to the S 2p band of the sulfur atoms present in PSS, whereas the XPS bands between 162 and 166 eV refer to the S 2p band of the sulfur atoms present in PEDOT [219].

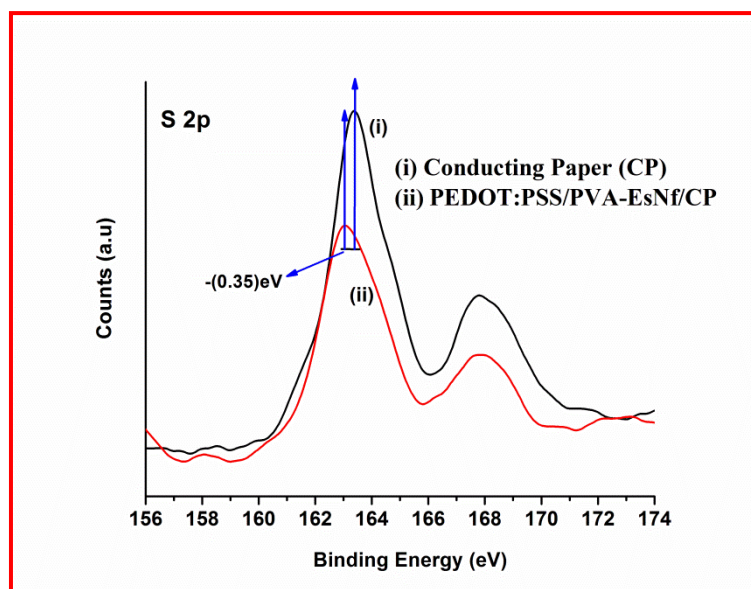


Fig. 5.3: S 2p XPS spectra of (i) conducting paper (CP) (ii) PEDOT:PSS/PVA electrospun nanofiber coated CP

S 2p band of CP (curve i) and PEDOT:PSS/PVA-EsNf/CP (curve ii) is visible in **Fig. 5.3**. It can be seen that the PEDOT peak of PEDOT:PSS/PVA-EsNf/CP is slightly shifted towards the lower binding energy $[-(0.35) \text{ eV}]$ suggesting the presence of interaction between positively charge PEDOT molecules and negatively charge PVA molecules which affect the electronic environment. Moreover, the atomic percentage of S 2p decreases from 2 to 1.1 after the CP is decorated with PEDOT:PSS/PVA-EsNf/CP. This result is consistent with the presence of PVA molecule.

5.3.3 Mechanical behavior

Fig. 5.4a shows optical image of the conducting paper modified with PEDOT:PSS/PVA electrospun nanofiber that has high flexibility. It can be folded and cut into desired shape and size. Additionally, this platform can be easily decomposed by simple incineration.

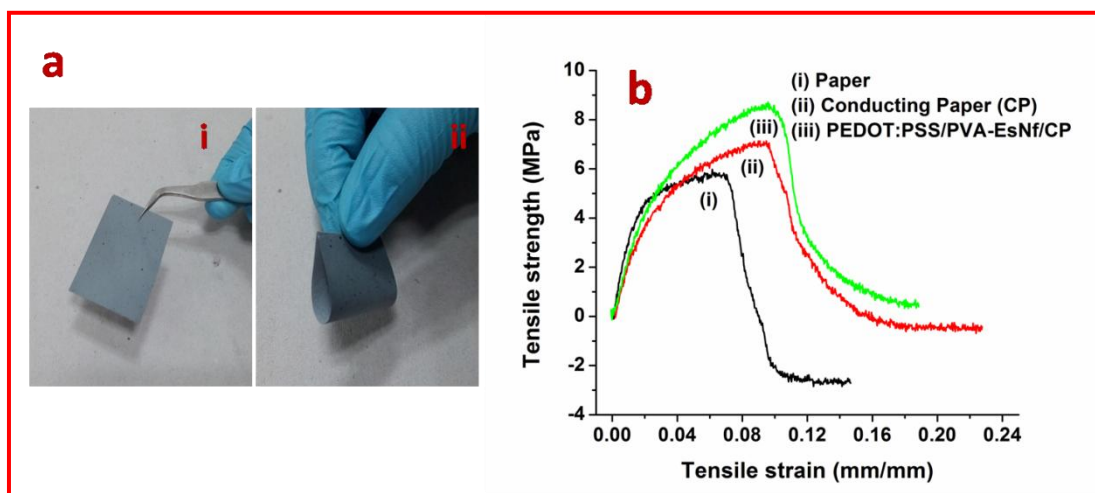


Fig. 5.4: (a) (i) Optical image of conducting paper coated with PEDOT:PSS/PVA electrospun nanofiber showing (ii) high flexibility (b) Stress-strain curve of different modified paper.

The mechanical properties of the Whatman paper, conducting paper (CP) and PEDOT:PSS/PVA nanofibers deposited conducting paper (PEDOT:PSS/PVA-EsNf/CP) were evaluated through stress-strain relationship (**Fig. 5.4b**). The tensile strength and the tensile modulus were found to be 5.9 & 314 MPa, 7 and 198 MPa, and 8.71 & 232 MPa, respectively. The increased tensile strength of the conducting paper may be attributed to the uniform adsorption of PEDOT:PSS molecules onto cellulose fibers of Whatman paper resulting in enhanced interfacial adherence with a high extensibility and reduced stiffness. Further, nanofiber coated conducting paper (PEDOT:PSS/PVA-EsNf/CP) exhibits high tensile strength and modulus but reduced extensibility than the CP. This decrease in extensibility is due to the increased

stiffness of the CP paper owing to coating of the nanofibrous network. **Table 5.1** summarizes the mechanical properties of the modified conducting paper.

Table 5.1: Mechanical properties of modified paper.

Sample	Tensile Strength (MPa)	Tensile Modulus (MPa)	Extension at Break (mm)
Paper	5.9	314	3.8
Conducting Paper (CP)	7	198	6.0
PEDOT:PSS/PVA-EsNf/CP	8.7	232	5.5

5.3.4 Contact angle studies

To investigate the hydrophilic/hydrophobic properties of the modified paper electrode, contact angle (CA) measurements were carried out using the sessile drop method (**Fig. 5.5**).

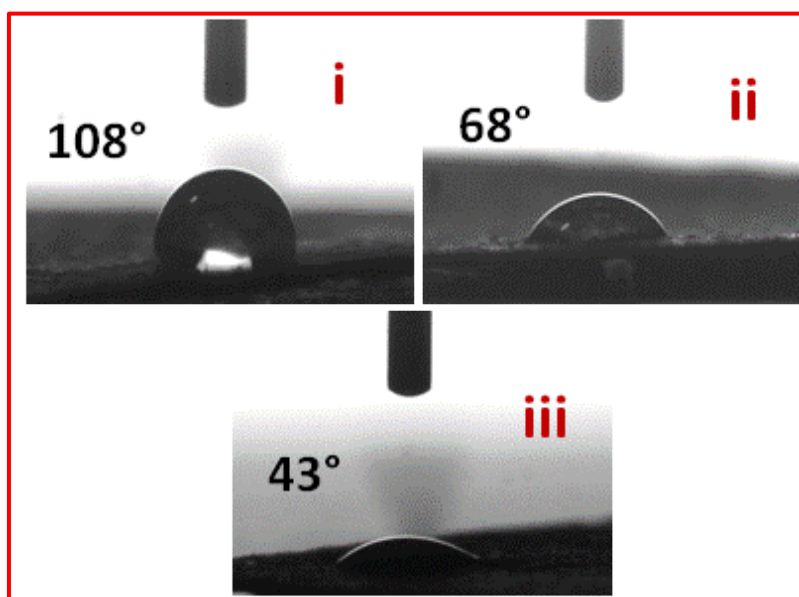


Fig. 5.5: Contact angle measurement of (i) conducting Paper (CP) (ii) PEDOT:PSS electrospun nanofibers coated over conducting paper (PEDOT:PSS/PVA-EsNf/CP) (iii) anti-CEA immobilized PEDOTE:PSS/PVA-EsNf/CP.

There is a large decrease in the CA value of the conducting paper (108° , image i) after electrospinning it with the PEDOT:PSS/PVA polymer (68° , image ii). This decrease in the CA value may be attributed to the presence of the hydrophilic group in poly (styrenesulfonate) (PSS), hydroxyl group of PVA and pores created due to random orientation of the PEDOT:PSS/PVA nanofiber. The CA decreases to 43° (image iii) after the immobilization of anti-CEA. The decrease in the value of contact angle is attributed to the hydrophilic nature of the surface and confirms the immobilization of antibody on the PEDOT:PSS/PVA-EsNf/CP electrode surface.

5.3.5 Electron microscopic studies

The surface morphology of the various modified paper electrodes (**Fig. 5.6**) was investigated using scanning electron microscopy (SEM). Image a-c shows SEM of the PEDOT:PSS/PVA-EsNf deposited on CP at different magnification scale ($30\text{ }\mu\text{m}$, $5\text{ }\mu\text{m}$ and 500 nm). It can be seen that continuous, well separated and homogenous electrospun nanofiber (EsNf) network covers the conducting paper. The average diameter of EsNf calculated by Image J software is found to be $150\text{--}200\text{ nm}$. The EsNf has enhanced specific surface area of CP that perhaps plays an important role in the orientation and enhanced loading of biomolecule. However, after antibody functionalization (image d) surface morphology of the PEDOT:PSS/PVA-EsNf/CP exhibits porous and homogeneously covered surface, indicating successful immobilization of antibody (anti-CEA). It appears that anti-CEA are entangled and covered over EsNf that may provide easier access of analyte.

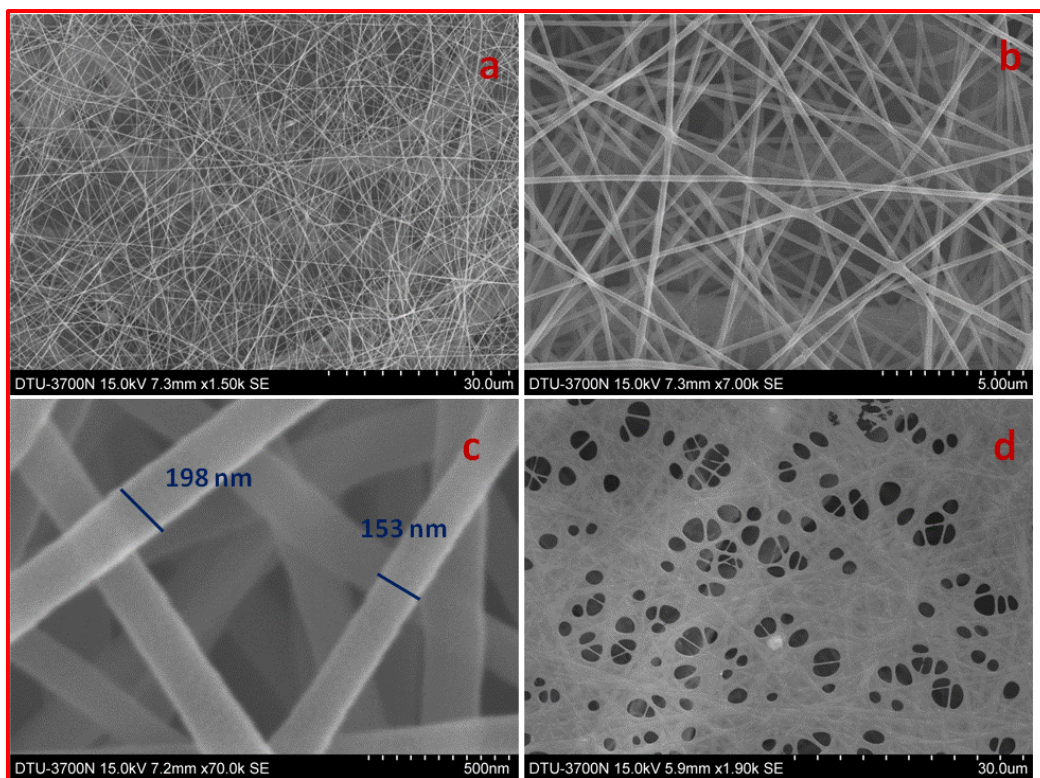


Fig. 5.6: SEM images of (a,b,c) PEDOT:PSS/PVA-EsNf/CP at different magnification (d) anti-CEA/PEDOT:PSS/PVA-EsNf/CP.

5.3.6 Electrochemical studies

Fig. 5.7a shows results of the chronoamperometric studies (current versus time) obtained for CP (a), PEDOT:PSS/PVA-EsNf/CP (b), anti-CEA/PEDOT:PSS/PVA-EsNf/CP (c), BSA/anti-CEA/PEDOT:PSS/PVA-EsNf/CP (d) at 2V every 0.1 s. The increased value of electrochemical current (0.88 mA) of the PEDOT:PSS/PVA-EsNf/CP electrode than that of CP electrode (0.74 mA) indicates deposition of the as-spun nanofiber onto the CP. The increase in the electrochemical current value can be attributed to conducting behavior of the PEDOT:PSS where high surface-to-volume ratio of nanofibers on CP results in enhanced permeability of the redox couple $[\text{Fe}(\text{CN})_6]^{-3/-4}$ towards CP electrode. Further increase in the value of amperometric current (1.05 mA) observed after anti-CEA immobilization onto the PEDOT:PSS/PVA-EsNf/CP electrode is attributed to well oriented antibodies layer that facilitates

electron transfer between solution and electrode. Since bovine serum albumin (BSA) was used to block non-specific site on anti-CEA/PEDOT:PSS/PVA-EsNf/CP electrode, the observed amperometric current (0.97mA) decreases due to macromolecular structure and insulating nature of BSA. It was found that amperometric current of paper sensor (BSA/anti-CEA/PEDOT:PSS/PVA-EsNf/CP) remained constant and hence could be utilized for biosensing application.

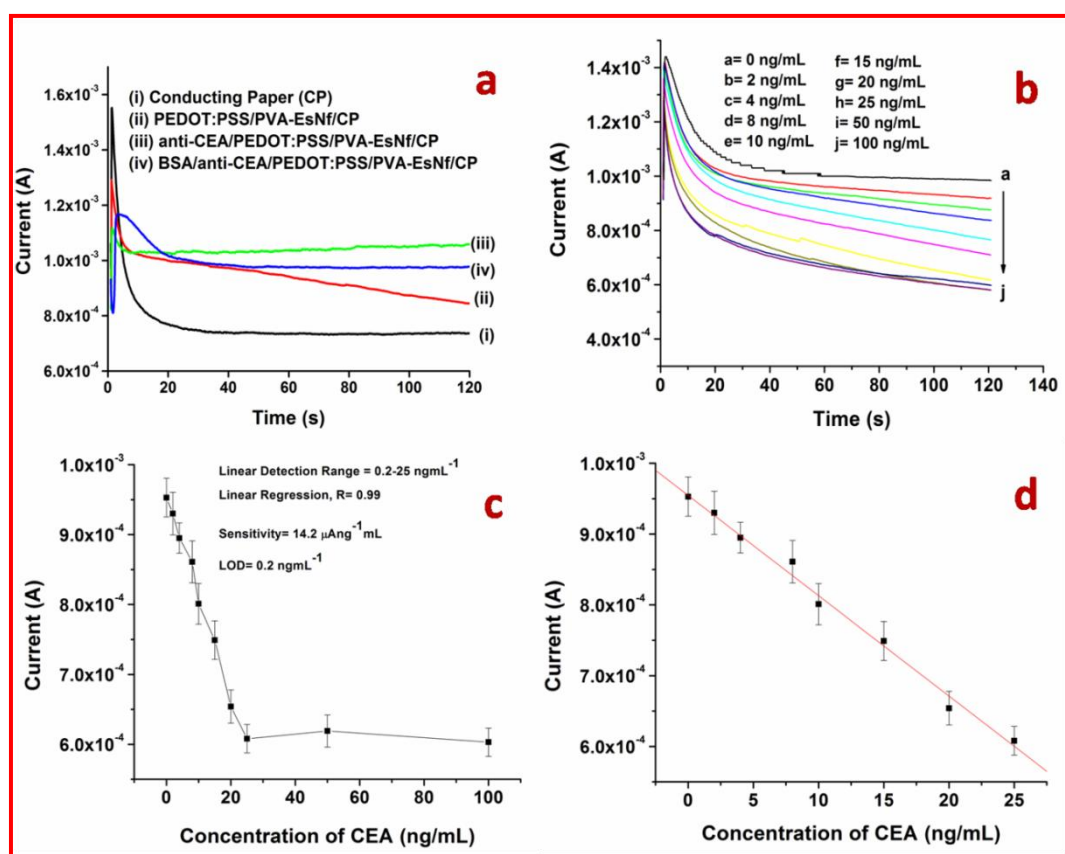


Fig. 5.7: Electrochemical characterization of modified paper electrode (a) chronoamperometric plot obtained for (i) conducting paper, CP (ii) PEDOT:PSS/PVA-EsNf/CP (iii) anti-CEA/PEDOT:PSS/PVA-EsNf/CP (iv) BSA/anti-CEA/PEDOT:PSS/PVA-EsNf/CP. (b) Electrochemical response studies of BSA/anti-CEA/PEDOT:PSS/PVA-EsNf/CP electrode at different concentration (0-100 ng/mL) of CEA (c) calibration plot between the magnitudes of current recorded and CEA concentration (d) linearity plot of paper sensor (BSA/anti-CEA/PEDOT:PSS/PVA-EsNf/CP) with linear regression coefficient $R = 0.99$.

5.3.7 Electrochemical response studies

The amperometric response studies of the BSA/anti-CEA/PEDOT:PSS/PVA-EsNf/CP bioelectrode were carried out with successive addition of human carcinoembryonic antigen (CEA) concentration up to 100 ngmL⁻¹ in PBS (50 mM, pH 7.0, 0.9% NaCl) containing 5 mM [Fe(CN)₆]^{3-/4-} under static condition. For this, 10 µL of different antigen concentration was added into the electrochemical cell one by one and the current-time (0 to 120 s) curve was recorded after incubation of 10 min for each cycle. The variation of the amperometric response current recorded as a function of CEA (0-100 ngmL⁻¹) is shown in **Fig. 5.7b**. It can be seen that (**Fig. 5.7c**) at concentration up to 25 ngmL⁻¹ amperometric current decreases and saturation current is obtained at higher concentration (50, 100 ngmL⁻¹). This can be understood by immunoreactions, wherein CEA first reacts with anti-CEA on paper surface and forms the antigen-antibody complex resulting in decreased charge transfer via [Fe(CN)₆]^{3-/4-} leading to reduction in the amperometric current. This can be assigned to rearrangement of the molecules in the matrix. A linear relationship is observed between magnitude of amperometric current and CEA concentration in the range 0-25 ngmL⁻¹ (**Fig. 5.7d**) with regression coefficient of 0.996 as given in following Eq. 5.1.

$$I(A) = -14.2 \mu A m L n g^{-1} \times [CEA \text{ concentration}] + 954 \mu A; R^2 = 0.99$$

..... **Eq. 5.1**

The sensitivity of the BSA/anti-CEA/PEDOT:PSS/PVA-EsNf/CP bioelectrode estimated from slope of the curve has been found to be 14.2 µAng⁻¹mLcm⁻² and the lower detection limit (LD) has been determined to be 0.2 ngmL⁻¹ using Eq. 5.2.

$$\text{Detection limit} = \frac{3\sigma}{m} \quad \text{.....Eq. 5.2}$$

Where σ is standard deviation and m is the slope of the curve. A control experiment was conducted using the PEDOT:PSS/PVA-EsNf/CP electrode as a function of CEA concentration in the absence of antibodies. It was observed that there was no significant change in the amperometric current of PEDOT:PSS/PVA-EsNf/CP electrode with increasing concentration of CEA. It appears that the PEDOT:PSS/PVA-EsNf/CP electrode does not bind the antigen molecule and hence the amperometric current does not exhibit significant change on PEDOT:PSS/PVA-EsNf/CP electrode surface.

5.3.8 Selectivity, stability and reproducibility studies

The selectivity of BSA/anti-CEA/PEDOT:PSS/PVA-EsNf/CP bioelectrode was investigated in the presence of other analytes such as endotheline-1 protein (ET-), cardiac troponin I (cTnI) and cytokeratin-19 fragment (CYFRA-21-1), (2 ngmL⁻¹) (**Fig. 5.8a**). It was found that magnitude of amperometric current decreased on addition of CEA (2 ngmL⁻¹). However, there was no significant change in amperometric current on addition of another antigen indicating high selectivity of the paper sensor towards CEA. **Fig. 5.8b** shows the reproducibility of five different paper electrode (BSA/anti-CEA/PEDO:PSS/PVA-EsNf/CP) fabricated under similar conditions investigated in presence of 2 ngmL⁻¹ CEA concentration. It was found that BSA/anti-CEA/PEDOT:PSS/PVA-EsNf/CP bioelectrode showed good reproducibility for five different electrodes with constant surface area as evident by low value of relative standard deviation (RSD) of 3.1% (mean value = 980 μ A). Further, each measurement was repeated 3 times for each electrode and the error bars were included accordingly. The shelf life of BSA/anti-CEA/PEDOT:PSS/PVA-EsNf/CP bioelectrode (**Fig. 5.8c**) was determined by measuring the amperometric response current at regular interval of 2-3 days. It was found that no significant change

occurred in the amperometric current up to about 22 days after which the amperometric current decreased to 21%. This indicated that paper electrode (BSA/anti-CEA/PEDOT:PSS/PVA-EsNf/CP) exhibits good stability up to 22 days.

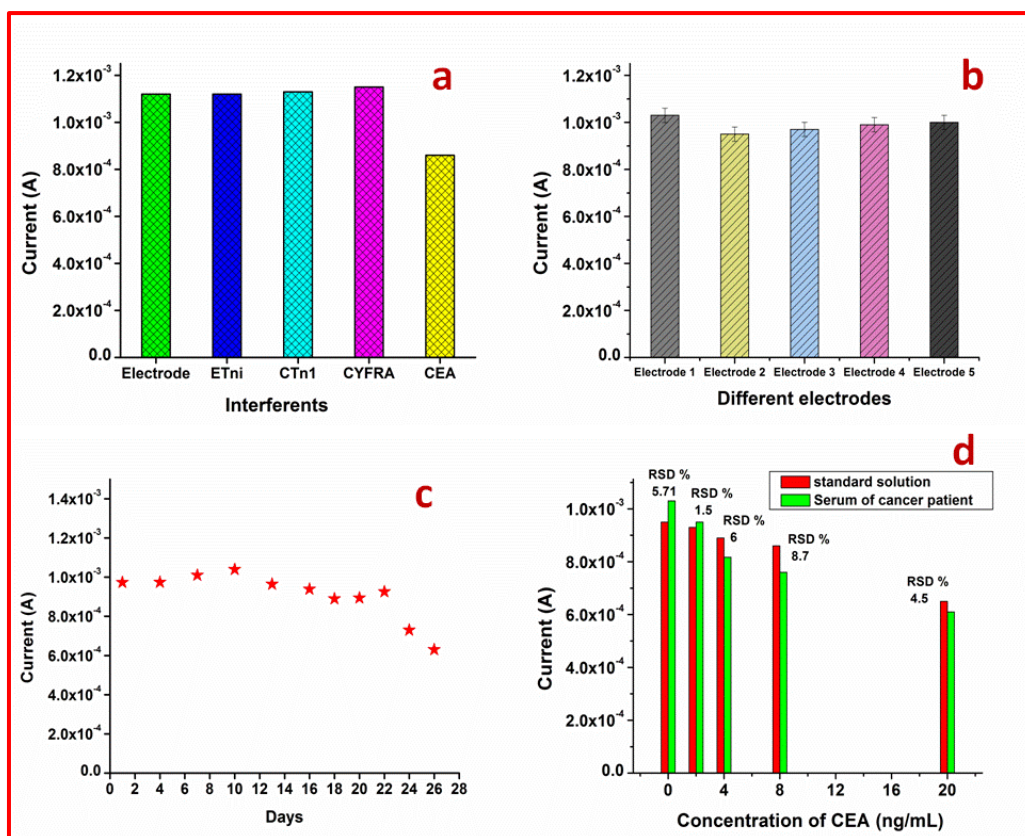


Fig. 5.8: (a) Interferents studies conducted via measurement of electrochemical current response of BSA/anti-CEA/PEDOT:PSS/PVA-EsNf/CP bioelectrode (paper sensor) in the presence of other analytes (b) Electrochemical current response of different immunoelectrode fabricated under similar condition in presence of CEA (2 ng mL^{-1}). (c) Electrochemical current response of BSA/anti-CEA/PEDOT:PSS/PVA-EsNf/CP bioelectrode measured as a function of time (day) and (d) CEA concentration values obtained by immunoassay and the BSA/anti-CEA/PEDOT:PSS/PVA-EsNf/CP bioelectrode.

5.3.9 Real sample analysis

Quantification of CEA in serum of cancer patients was conducted at Rajiv Gandhi Cancer Institute & Research Centre (RGCI&RC) in Delhi, India using the VITROS CEA Reagent Pack and the VITROS CEA Calibrators on the VITROS

ECi/ECiQ Immunodiagnostic Systems, the VITROS 3600 Immunodiagnostic System and the VITROS 5600 Integrated System using Intellicheck® Technology. The blood samples of patients were collected and processed at RGCI&RC after ethical approval by the Institutional Review board. It was found that a reasonable correlation exists between magnitude of amperometric current response of the BSA/anti-CEA/PEDOT:PSS/PVA-EsNf/CP bioelectrode in presence of (a) standard concentration of CEA and (b) CEA concentration in serum samples obtained by RGCI&RC (**Fig. 5.8d**). The observed results exhibit reasonable (less than 9%) relative standard deviation (%RSD) indicating high accuracy of paper sensor.

The sensing characteristics of this paper sensor are summarized in **Table 5.2** and the results have been compared with some conventional electrode such as gold, glassy carbon and ITO reported in literature for CEA detection. It can be seen that fabricated paper electrodes (BSA/anti-CEA/PEDOT:PSS/PVA-EsNf/CP) covers broad detection range and display improved sensing parameters compared to conventional electrodes (gold, glassy carbon and ITO electrode).

5.3.10 Disposability studies

The fabricated paper sensor (BSA/anti-CEA/PEDOT:PSS/PVA-EsNf/CP) can be easily decomposed by incineration (**video 5.1, please see the attached CD**), which is a major drawback in disposal of expensive conventional electrodes such as gold, glassy carbon and ITO electrodes.

The resulting ash was investigated by energy dispersive X-ray (EDX) technique. EDX results confirm the presence of carbon, oxygen, sulfur, potassium, calcium and iron. No traces of toxic metals were detected (**Fig. 5.9**). It shows that the proposed paper sensors is disposable, environment friendly and a promising platform for point of care diagnostics.

Table 5.2 shows response characteristics of the BSA/anti-CEA/PEDOT:PSS/PVA-EsNf/ CP bioelectrode along with those reported in literature.

S. No.	Substrate	Material	Fabrication Method	Detection Method	Linear range and Sensitivity	Stability (days)	Cost	References
1.	Array of Gold electrode	Thiol based Self assembled monolayer	Dip Coating	Amperometry	0-200 ngmL ⁻¹ and 3.8 nAng ⁻¹ mL	30	High	[225]
2.	Gold electrode	AuNP, O-aminophenol	Drop cast	Electrochemical Impedance Spectroscopy	0.5-20 ngmL ⁻¹ and 1.08×105 Ωng ⁻¹ mL		High	[138]
3.	Glassy carbon electrode	AuNP, MWCNT, Chitosan	Drop Casting	Differential pulse voltammetry	0.3-2.5 & 2.5- 20 ngmL ⁻¹ -----	30	Moderate	[87]
4.	Glassy carbon electrode	Reduced graphene oxide-tetraethylene pentamine (RGO-TEPA)	Drop cast	Differential pulse voltammetry	0.05-20 ngmL ⁻¹	10	Moderate	[88]
5.	ITO	AuNP, Hyperbranched polyester	Dip coating	Linear sweep stripping voltammetry	0.01-80 ngmL ⁻¹ -----	30	Moderate	[226]
6.	ITO	Au-chitosan	Drop cost	Cyclic voltametry	2-20 ngmL ⁻¹ -----	14	Moderate	[85]
7.	Whatman paper 1	PEDOT:PSS/RGO, Ethylene Glycol	Dip coating	Amperometry	2-8 ngmL ⁻¹ and 25.8 μAng ⁻¹ mLcm ²	21	Low	[46]
8.	Whatman paper 1	PEDOT:PSS/CNTs, Formic acid	Dip coating	Amperometry	2-15 ngmL ⁻¹ and 7.8 μAng ⁻¹ mLcm ²	18	Low	[101]
9.	Whatman paper 1	PEDOT:PSS/PVA electrospun nanofiber	Electrospinning method	Amperometry	0.2-25 ngmL ⁻¹ and 14.2 μA ng ⁻¹ mLcm ²	22	Low	Present Work

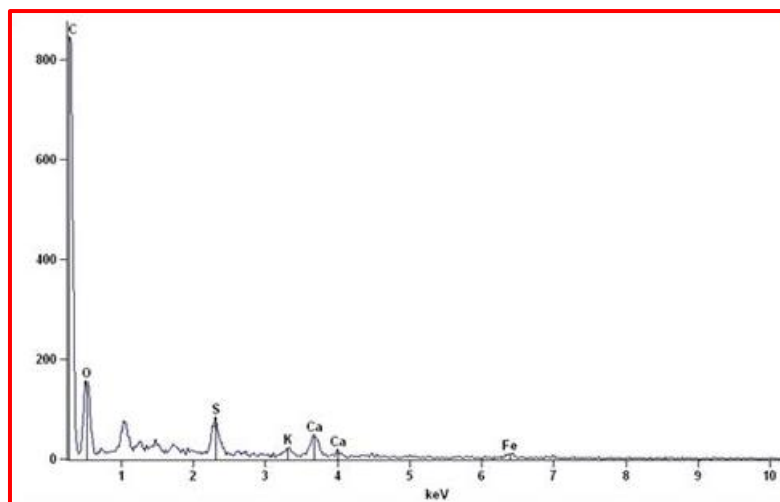


Fig. 5.9: Energy dispersive X-ray (EDX) analysis of incinerated paper electrode (BSA/anti-CEA/PEDOT:PSS/PVA-EsNf/CP).

5.4 CONCLUSIONS

We have demonstrated the fabrication of a flexible, cost-effective, lightweight, label free and environment friendly electrochemical sensor. For this, nanofiber of PEDOT:PSS/PVA have been grown on conducting paper (CP) platform using electrospinning technique. The deposition of EsNf results in improved mechanical strength and electrochemical properties. In addition high aspect ratio of PEDOT:PSS/PVA-EsNf results in improved charge transfer between electrode and solution resulting in higher sensitivity towards the electrochemical detection of cancer biomarker (CEA). The results of the amperometric response studies indicate that the paper electrode (BSA/anti-CEA/PEDO:PSS/PVA-EsNf/CP) can be used to estimate the CEA from 0.2 to 25 ngmL⁻¹, has high sensitivity (14.2 $\mu\text{Ang}^{-1}\text{mLcm}^{-2}$) and shelf life of 22 days. In comparison to previous discussed work (**Chapter 3** and **4**), this paper sensor cover the whole physiological range of CEA secreted in serum sample (< 3 to 20 ngmL⁻¹) with improved lower detection limit. This modified conducting paper electrode is a promising alternative over expensive conventional electrodes (ITO, gold and glassy carbon) for fabrication of smart point of care devices. This

EsNf decorated CP shows excellent electrochemical behavior and has the potential use in the development of electrochemical biosensors for detection of other analytes including cholesterol, urea, environment pollutant chemical etc. Next chapter contains the summary of research work described in the thesis and also presents the future prospects of conducting paper sensors.

The results of the studies contained in this Chapter have been published in Advanced Materials Technologies, 2016 (doi:10.1002/admt.201600056).

CHAPTER 6

Summary and Future Prospects

6.1 SUMMARY

There is increased demand for availability of paper based devices due to their application in capacitors, batteries, displays, thin film transistors, touch pad and biosensors. It has been predicted that fabrication of paper based electronic devices is highly cost effective and environment friendly. Besides this, their mass production, disposability, flexibility and ease in processing may perhaps meet the increasing demand of desired smart electronic devices. For biosensing applications, a wide range of conducting substrates such as glassy carbon, indium tin oxide and gold coated glass substrate are currently being used. These electrodes are costly, rigid and can easily break during bending, making them difficult to be used for fabrication of desired flexible electronic devices and smart point of care devices. Conducting paper (CP) has been found to play an important role in the ongoing transition to the development of paper based electrochemical biosensors due to their high flexibility, cost-effectiveness, light weight and disposability. Moreover, coupling of paper based electrode with biological entity provides an efficient platform for conduction of both electronic and ionic charge carriers that play a major role in efficient signal transduction. Further, incorporation of a nanomaterial may modulate the performance of a conducting paper in terms of electrochemical kinetics, signal stability and sensitivity. Recently nanomaterials such as reduced graphene oxide (RGO), carbon nanotubes (CNTs), polymeric (PEDOT:PSS) electrospun nanofibers have recently aroused much interest in electrochemical sensors. This is due to their large surface area, enhanced biomolecule loading and excellent electrochemical properties. Therefore incorporation of nanomaterials in the conducting paper may further improve electrochemical performance of the desired paper sensor.

Cancer is currently a serious concern and a medical threat to the contemporary world. According to a recent report, there have been 8.2 million cancer deaths, 14.1 million new cancer cases and 32.6 million people are living with cancer necessitating its early detection. Carcinoembryonic antigen (CEA) is an important biomarker for the diagnosis and routine monitoring of cancer because it is associated with colon, lung, ovarian and breast cancer that are responsible for more than half of all cancer deaths each year. It plays an important role in early monitoring, screening and disease recurrence. In this context, determination of CEA in serum has been proposed for clinical diagnosis and monitoring of a cancer. Present thesis deals with the fabrication of nanomaterials modified paper biosensor for CEA detection.

We have conducted detailed studies on the fabrication of a paper based sensor comprising of poly(3,4-ethylenedioxythiophene):poly(styrenesulfonate) (PEDOT:PSS) and reduced graphene oxide (RGO) composite. The effect of various solvents like methanol, ethylene glycol and H_2SO_4 on the electrical conductivity of PEDOT:PSS coated Whatman paper has been investigated. The conductivity of this solution processed conducting paper significantly increases by 2 orders of magnitude on treatment with ethylene glycol. The observed significant increase in electrical conductivity is due to conformational rearrangement in the polymer and due to strong non-covalent cooperative interaction between PEDOT and the cellulose molecules. Moreover the variation of relative conductivity of paper electrode with folding angle and folding cycle was studied. It was observed that 4% relative conductivity deviation during -180° to 180° folding angle and 20% conductivity deviation after 30 cycle of folding and unfolding (1 cycle = 360° rotation) was observed. Further, incorporation of RGO into the conducting paper results in improved electrochemical performance and signal stability. This paper electrode was used for the immobilization of

monoclonal antibody against carcinoembryonic antigen (anti-CEA). This low cost, flexible and environment friendly conducting paper based biosensor was utilized for cancer biomarker (carcinoembryonic antigen, CEA) detection, that reveals high sensitivity of $25.8 \mu\text{Ang}^{-1}\text{mLcm}^{-2}$ in the linear detection range of $2\text{--}8 \text{ ngmL}^{-1}$ with a good storage stability (21 days). The response of paper electrode was validated using CEA concentration of serum sample of cancer patient. This paper electrode can be decomposed by simple incineration and has immense potential as a smart medical diagnostic kit or point of care biosensor. In order to further improve the performance of conducting paper, formic acid and CNTs was used as a suitable solvent and dopant respectively. Metallic impurities that are present in CNTs have been found to improve the electrochemistry of CNTs as compare to RGO.

We have fabricated a paper based sensor comprising of poly (3,4-ethylenedioxythiophene):poly(styrenesulfonate) (PEDOT:PSS) and carbon nanotubes (CNTs) composite via dip coating. It is found that conductivity of this paper increases by 2 orders of magnitude on being treated with formic acid due to removal of the non-conducting molecule PSS from electrode surface. This fabricated paper is efficient conductive, flexible, electrochemical active, and it can be easily disposed off by simple incineration. Further, this smart conducting platform has been used for conjugation of the anti-carcinoembryonic antigen (CEA) protein for quantitative estimation of CEA. The PEDOT:PSS-CNTs based electrochemical paper immunosensor exhibits sensitivity ($7.8 \mu\text{Ang}^{-1}\text{mLcm}^{-2}$) with improved linear detection range of $2\text{--}15 \text{ ngmL}^{-1}$ and feasibility of paper electrode was also validated with CEA concentration in serum sample of cancer patient. To attest the environment friendliness, these paper electrodes were decomposed by incineration. The resulting ash was investigated by the energy dispersive X-ray (EDX) technique. EDX results

confirm the presence of only carbon, oxygen, sodium, phosphorous and potassium; no toxic metals were detected. Moreover, it was observed that incorporation of carbon nanotubes improved heterogeneous electron transfer rate constant (5 times) and linear detection range with respect to PEDOT:PSS-RGO based conducting paper. CEA biomarker release in serum of healthy person is $< 3 \text{ ngmL}^{-1}$ with a cut-off value 5 ngmL^{-1} and for cancer patient it is usually reported to maximal of 20 ngmL^{-1} .

We have developed a conducting paper modified with PEDOT:PSS/PVA nanofibers via electrospinning technique. The deposition of electrospun nanofibers (EsNf) is found to result in improved mechanical strength, large surface area, enhanced biomolecule loading and electrochemical characteristics. Therefore, this platform results in improved charge transfer between electrode and solution resulting in higher sensitivity towards the electrochemical detection of cancer biomarker (CEA). The results of the amperometric response studies indicate that the paper electrode (BSA/anti-CEA/PEDO:PSS/PVA-EsNf/CP) can be used to estimate CEA in the range 0.2 to 25 ngmL^{-1} , has high sensitivity of $14.2 \mu\text{Ang}^{-1}\text{mLcm}^{-2}$ and shelf life of 22 days. This paper sensor covers the entire physiological range of CEA secreted in serum sample (< 3 to 20 ngmL^{-1}) with improved lower detection limit. This modified conducting paper electrode is a promising alternative over expensive conventional electrodes (ITO, gold and glassy carbon) for fabrication of smart point of care devices.

The sensing characteristic of RGO, CNTs and PEDOT:PSS/PVA electrospun nanofibers integrated conducting paper (PEDOT:PSS coated paper), utilized in the present thesis work has been summarized in **Table 6.1**.

Table 6.1: Sensing characteristic of RGO, CNTs and PEDOT:PSS/PVA electrospun nanofibers integrated conducting paper electrode for CEA detection.

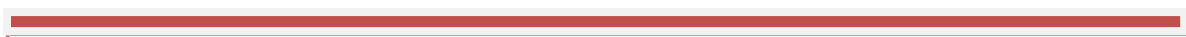
Paper electrodes	Sensitivity ($\mu\text{Ang}^{-1}\text{mLcm}^{-2}$)	Detection range (ngmL^{-1})	Stability (days)
PEDOT:PSS/RGO	25.8	2-8	21
PEDOT:PSS/CNTs	7.8	2-15	18
PEDOT:PSS/PVA nanofibers	14.2	0.2-25	22

6.2 FUTURE PROSPECTS

The experimental investigations reveal that the RGO, CNTs and PEDOT:PSS electrospun nanofibers integrated conducting paper (PEDOT:PSS coated paper) can be utilized for the development of flexible, cost effective, disposable and environment friendly platform for electrochemical biosensing platform. Efforts should be made to improve the stability, detection range of the paper sensor for CEA detection. There is enough scope to improve the characteristics of conducting paper by selection of suitable solvent and nanomaterials (Au, Pt, NiO, Fe_2O_3 , nanostructured polymer). Moreover, this platform could be utilized for detection of other analytes including cholesterol, urea, environment pollutant chemicals etc. The results of the studies described in this thesis have implications towards the application of other area such as microfluidics, energy storage devices, flexible and dissolvable electronics.

Efforts should be made for the fabrication of transparent and conducting paper platform. This novel concept breaks new ground in the creation of next-generation paper electronics. We believe that this class of platforms will prove valuable for displaying analytical information in diverse fields such as diagnostics, environmental

monitoring and food safety. It could also be used as wearable optical sensors and could even be integrated into novel theranostic devices.



REFERENCES

- [1] A. Alagarasi, Introduction to Nanomaterials. 2013, Chapter.
- [2] C.P. Poole Jr, F.J. Owens, Introduction to nanotechnology: John Wiley & Sons; 2003.
- [3] F. Caruso, Nanoengineering of particle surfaces, *Advanced Materials*, 13(2001) 11-22.
- [4] V. Pokropivny, V. Skorokhod, Classification of nanostructures by dimensionality and concept of surface forms engineering in nanomaterial science, *Materials Science and Engineering: C*, 27(2007) 990-3.
- [5] E. Comini, Metal oxide nano-crystals for gas sensing, *Analytica chimica acta*, 568(2006) 28-40.
- [6] V.V. Mody, R. Siwale, A. Singh, H.R. Mody, Introduction to metallic nanoparticles, *Journal of Pharmacy and Bioallied Sciences*, 2(2010) 282.
- [7] M. Jesus, V. Grazu, Nanobiotechnology: Inorganic Nanoparticles Vs Organic Nanoparticles: Elsevier; 2012.
- [8] L. Dai, Carbon nanotechnology: recent developments in chemistry, physics, materials science and device applications: Elsevier; 2006.
- [9] S. Iijima, Helical microtubules of graphitic carbon, *Nature*, 354(1991) 56-8.
- [10] J.N. Coleman, U. Khan, W.J. Blau, Y.K. Gun'ko, Small but strong: a review of the mechanical properties of carbon nanotube–polymer composites, *Carbon*, 44(2006) 1624-52.
- [11] J. Wen, Y. Xu, H. Li, A. Lu, S. Sun, Recent applications of carbon nanomaterials in fluorescence biosensing and bioimaging, *Chemical Communications*, 51(2015) 11346-58.
- [12] J.N. Wohlstadter, J.L. Wilbur, G.B. Sigal, H.A. Biebuyck, M.A. Billadeau, L. Dong, et al., Carbon nanotube-based biosensor, *Advanced Materials*, 15(2003) 1184-7.
- [13] K.S. Novoselov, A.K. Geim, S. Morozov, D. Jiang, Y. Zhang, S.a. Dubonos, et al., Electric field effect in atomically thin carbon films, *science*, 306(2004) 666-9.
- [14] D.A. Dikin, S. Stankovich, E.J. Zimney, R.D. Piner, G.H. Dommett, G. Evmenenko, et al., Preparation and characterization of graphene oxide paper, *Nature*, 448(2007) 457-60.
- [15] M. Pumera, Graphene in biosensing, *Materials today*, 14(2011) 308-15.
- [16] Y. Shao, J. Wang, H. Wu, J. Liu, I.A. Aksay, Y. Lin, Graphene based electrochemical sensors and biosensors: a review, *Electroanalysis*, 22(2010) 1027-36.
- [17] M. Gerard, A. Chaubey, B. Malhotra, Application of conducting polymers to biosensors, *Biosensors and Bioelectronics*, 17(2002) 345-59.
- [18] J.L. Bredas, G.B. Street, Polarons, bipolarons, and solitons in conducting polymers, *Accounts of Chemical Research*, 18(1985) 309-15.
- [19] V. Saxena, B. Malhotra, Prospects of conducting polymers in molecular electronics, *Current Applied Physics*, 3(2003) 293-305.
- [20] C. Dhand, M. Das, M. Datta, B. Malhotra, Recent advances in polyaniline based biosensors, *Biosensors and Bioelectronics*, 26(2011) 2811-21.

- [21] L. Groenendaal, F. Jonas, D. Freitag, H. Pielartzik, J.R. Reynolds, Poly (3, 4-ethylenedioxythiophene) and its derivatives: past, present, and future, *Advanced Materials*, 12(2000) 481-94.
- [22] X. Crispin, F. Jakobsson, A. Crispin, P. Grim, P. Andersson, A. Volodin, et al., The origin of the high conductivity of poly (3, 4-ethylenedioxythiophene)-poly (styrenesulfonate)(PEDOT-PSS) plastic electrodes, *Chemistry of Materials*, 18(2006) 4354-60.
- [23] X. Zhang, A.G. MacDiarmid, S.K. Manohar, Chemical synthesis of PEDOT nanofibers, *Chem Commun*, (2005) 5328-30.
- [24] J. Ouyang, C.W. Chu, F.C. Chen, Q. Xu, Y. Yang, Polymer Optoelectronic Devices with High-Conductivity Poly (3, 4-Ethylenedioxythiophene) Anodes, *Journal of Macromolecular Science, Part A*, 41(2004) 1497-511.
- [25] S.W. Dutse, N.A. Yusof, H. Ahmad, M.Z. Hussein, Z. Zainal, An electrochemical DNA biosensor for ganoderma boninense pathogen of the Oil palm utilizing a New ruthenium complex, [Ru (dppz) ₂ (qtpy)] Cl₂, *Int J Electrochem Sci*, 7(2012) 8105-15.
- [26] N. Liu, G. Fang, J. Wan, H. Zhou, H. Long, X. Zhao, Electrospun PEDOT: PSS–PVA nanofiber based ultrahigh-strain sensors with controllable electrical conductivity, *Journal of Materials Chemistry*, 21(2011) 18962-6.
- [27] A.G. Del Mauro, M. GraziaáMaglione, Nanostructured PEDOT: PSS film with two-dimensional photonic quasi crystals for efficient white OLED devices, *Journal of Materials Chemistry C*, 3(2015) 147-52.
- [28] D.R. Thévenot, K. Toth, R.A. Durst, G.S. Wilson, Electrochemical biosensors: recommended definitions and classification, *Biosensors and Bioelectronics*, 16(2001) 121-31.
- [29] B.M. Paddle, Biosensors for chemical and biological agents of defence interest, *Biosensors and Bioelectronics*, 11(1996) 1079-113.
- [30] D. Ivnitiski, I. Abdel-Hamid, P. Atanasov, E. Wilkins, Biosensors for detection of pathogenic bacteria, *Biosens Bioelectron*, 14(1999) 599-624.
- [31] D.W. Morrison, M.R. Dokmeci, U. Demirci, A. Khademhosseini, *Clinical applications of micro-and nanoscale biosensors*: John Wiley & Sons, Inc.: Hoboken, NJ, USA; 2007.
- [32] J.R. North, Immunosensors: antibody-based biosensors, *Trends in biotechnology*, 3(1985) 180-6.
- [33] B. Hames, N. Hooper, *Instant Notes in Biochemistry*, Bios Scientific Pub, Springer.
- [34] R.S. Sethi, Transducer aspects of biosensors, *Biosensors and Bioelectronics*, 9(1994) 243-64.
- [35] J. Wang, Electrochemical biosensors: towards point-of-care cancer diagnostics, *Biosens Bioelectron*, 21(2006) 1887-92.
- [36] J. Wang, Amperometric biosensors for clinical and therapeutic drug monitoring: a review, *J Pharm Biomed Anal*, 19(1999) 47-53.

- [37] L. Feng, Y. Chen, J. Ren, X. Qu, A graphene functionalized electrochemical aptasensor for selective label-free detection of cancer cells, *Biomaterials*, 32(2011) 2930-7.
- [38] J. Chen, J. Zhang, Y. Guo, J. Li, F. Fu, H.-H. Yang, et al., An ultrasensitive electrochemical biosensor for detection of DNA species related to oral cancer based on nuclease-assisted target recycling and amplification of DNAzyme, *Chem Commun*, 47(2011) 8004-6.
- [39] W.H. Scouten, J.H. Luong, R.S. Brown, Enzyme or protein immobilization techniques for applications in biosensor design, *Trends in biotechnology*, 13(1995) 178-85.
- [40] A. Sassolas, L.J. Blum, B.D. Leca-Bouvier, Immobilization strategies to develop enzymatic biosensors, *Biotechnology Advances*, 30(2012) 489-511.
- [41] T. Ahuja, I.A. Mir, D. Kumar, Biomolecular immobilization on conducting polymers for biosensing applications, *Biomaterials*, 28(2007) 791-805.
- [42] N.J. Ronkainen, S.L. Okon, Nanomaterial-based electrochemical immunosensors for clinically significant biomarkers, *Materials*, 7(2014) 4669-709.
- [43] J. Wang, Nanomaterial-based electrochemical biosensors, *Analyst*, 130(2005) 421-6.
- [44] X. Yu, B. Munge, V. Patel, G. Jensen, A. Bhirde, J.D. Gong, et al., Carbon nanotube amplification strategies for highly sensitive immunodetection of cancer biomarkers, *Journal of the American Chemical Society*, 128(2006) 11199-205.
- [45] S. Kumar, S. Kumar, S. Tiwari, S. Srivastava, M. Srivastava, B.K. Yadav, et al., Biofunctionalized nanostructured zirconia for biomedical application: a smart approach for oral cancer detection, *Advanced Science*, 2(2015).
- [46] S. Kumar, S. Kumar, S. Srivastava, B.K. Yadav, S.H. Lee, J.G. Sharma, et al., Reduced graphene oxide modified smart conducting paper for cancer biosensor, *Biosensors and Bioelectronics*, 73(2015) 114-22.
- [47] M. Emami, M. Shamsipur, R. Saber, R. Irajirad, An electrochemical immunosensor for detection of a breast cancer biomarker based on antiHER2–iron oxide nanoparticle bioconjugates, *Analyst*, 139(2014) 2858-66.
- [48] P. Norouzi, V.K. Gupta, F. Faridbod, M. Pirali-Hamedani, B. Larijani, M.R. Ganjali, Carcinoembryonic antigen admittance biosensor based on Au and ZnO nanoparticles using FFT admittance voltammetry, *Analytical chemistry*, 83(2011) 1564-70.
- [49] M.A. Ali, K. Mondal, C. Singh, B.D. Malhotra, A. Sharma, Anti-epidermal growth factor receptor conjugated mesoporous zinc oxide nanofibers for breast cancer diagnostics, *Nanoscale*, 7(2015) 7234-45.
- [50] Z. Veisi, M. Ceylan, A. Mahapatro, R. Asmatulu, An electrospun polyaniline nanofiber as a novel platform for real-time COX-2 biomarker detection, *ASME 2013 International Mechanical Engineering Congress and Exposition*, American Society of Mechanical Engineers 2013, pp. V03BTA028-V03BT03A.
- [51] B. Stewart, C.P. Wild, World cancer report 2014, World, (2015).
- [52] L.H. Hartwell, M.B. Kastan, Cell cycle control and cancer, *science*, 266(1994) 1821-8.

- [53] A.G. Knudson, Two genetic hits (more or less) to cancer, *Nature Reviews Cancer*, 1(2001) 157-62.
- [54] H. Lodish, A. Berk, P. Matsudaira, C.A. Kaiser, Monty Kreiger, Mathew P. Scott, S. Lawerance Zipursky, James Darnell, “, *Molecular Cell Biology*”, 5th edition, WH Freeman & Company, 101-45.
- [55] S. Mehta, A. Shelling, A. Muthukaruppan, A. Lasham, C. Blenkiron, G. Laking, et al., Predictive and prognostic molecular markers for cancer medicine, *Ther Adv Med Oncol*, 2(2010) 125-48.
- [56] C.O. Madu, Y. Lu, Novel diagnostic biomarkers for prostate cancer, *J Cancer*, 1(2010) 150-77.
- [57] M. De Palma, D. Hanahan, The biology of personalized cancer medicine: Facing individual complexities underlying hallmark capabilities, *Mol Oncol*, 6(2012) 111-27.
- [58] N.L. Henry, D.F. Hayes, Cancer biomarkers, *Mol Oncol*, 6(2012) 140-6.
- [59] S.S. Hori, S.S. Gambhir, Mathematical Model Identifies Blood Biomarker-Based Early Cancer Detection Strategies and Limitations, *Sci Transl Med*, 3(2011) 109ra16-ra16.
- [60] L. Wu, X. Qu, Cancer biomarker detection: recent achievements and challenges, *Chem Soc Rev*, 44(2015) 2963-97.
- [61] M.A. Gillette, S.A. Carr, Quantitative analysis of peptides and proteins in biomedicine by targeted mass spectrometry, *Nat Methods*, 10(2013) 28-34.
- [62] S. Kumar, S. Kumar, M. Ali, P. Anand, V.V. Agrawal, R. John, et al., Microfluidic-integrated biosensors: Prospects for point-of-care diagnostics, *Biotechnology journal*, 8(2013) 1267-79.
- [63] V. Kulasingam, E.P. Diamandis, Strategies for discovering novel cancer biomarkers through utilization of emerging technologies, *Nature clinical practice Oncology*, 5(2008) 588-99.
- [64] M.J. Duffy, Carcinoembryonic antigen as a marker for colorectal cancer: is it clinically useful?, *Clinical chemistry*, 47(2001) 624-30.
- [65] M.S. Pepe, R. Etzioni, Z. Feng, J.D. Potter, M.L. Thompson, M. Thornquist, et al., Phases of biomarker development for early detection of cancer, *Journal of the National Cancer Institute*, 93(2001) 1054-61.
- [66] H.J. Wanebo, B. Rao, C.M. Pinsky, R.G. Hoffman, M. Stearns, M.K. Schwartz, et al., Preoperative carcinoembryonic antigen level as a prognostic indicator in colorectal cancer, *New England Journal of Medicine*, 299(1978) 448-51.
- [67] J. Kulpa, E. Wójcik, M. Reinfuss, L. Kołodziejwski, Carcinoembryonic antigen, squamous cell carcinoma antigen, CYFRA 21-1, and neuron-specific enolase in squamous cell lung cancer patients, *Clinical chemistry*, 48(2002) 1931-7.
- [68] R.E. Myers, D.J. Sutherland, J.W. Meakin, J.A. Kellen, D.G. Malkin, A. Malkin, Carcinoembryonic antigen in breast cancer, *Cancer*, 42(1978) 1520-6.
- [69] J. Wang, C. Lu, K. Chu, C. Ma, D. Wu, H. Tsai, et al., Prognostic significance of pre-and postoperative serum carcinoembryonic antigen levels in patients with colorectal cancer, *European Surgical Research*, 39(2007) 245-50.

- [70] B.K. Banin Hirata, J.M.M. Oda, R. Losi Guembarovski, C.B. Ariza, C.E.C.d. Oliveira, M.A.E. Watanabe, Molecular Markers for Breast Cancer: Prediction on Tumor Behavior, Dis Markers, 2014(2014) 12.
- [71] <http://www.mayomedicallaboratories.com/test-catalog/Clinical+and+Interpretive/8521>.
- [72] P. Gold, S.O. Freedman, SPECIFIC CARCINOEMBRYONIC ANTIGENS OF THE HUMAN DIGESTIVE SYSTEM, The Journal of Experimental Medicine, 122(1965) 467-81.
- [73] S. Hammarström, The carcinoembryonic antigen (CEA) family: structures, suggested functions and expression in normal and malignant tissues, Semin Cancer Biol, 9(1999) 67-81.
- [74] D.M. Goldenberg, R.M. Sharkey, F.J. Primus, Immunocytochemical detection of carcinoembryonic antigen in conventional histopathology specimens, Cancer, 42(1978) 1546-53.
- [75] S. Von Kleist, E. Chany, P. Burtin, M. King, J. Fogh, Immunohistology of the antigenic pattern of a continuous cell line from a human colon tumor, J Natl Cancer Inst, 55(1975) 555-60.
- [76] D.M. Goldenberg, E.E. Kim, F.H. DeLand, S. Bennett, F.J. Primus, Radioimmunoassay of cancer with radioactive antibodies to carcinoembryonic antigen, Cancer Res, 40(1980) 2984-92.
- [77] D. Thomson, J. Krupey, S. Freedman, P. Gold, The radioimmunoassay of circulating carcinoembryonic antigen of the human digestive system, Proceedings of the National Academy of Sciences, 64(1969) 161-7.
- [78] R.-S. Lai, H.-K. Hsu, J.-Y. Lu, L.-P. Ger, N.-S. Lai, CYFRA 21-1 enzyme-linked immunosorbent assay: evaluation as a tumor marker in non-small cell lung cancer, CHEST Journal, 109(1996) 995-1000.
- [79] F. Zhou, M. Wang, L. Yuan, Z. Cheng, Z. Wu, H. Chen, Sensitive sandwich ELISA based on a gold nanoparticle layer for cancer detection, Analyst, 137(2012) 1779-84.
- [80] D. Xu, X.-f. Li, S. Zheng, W.-z. Jiang, Quantitative real-time RT-PCR detection for CEA, CK20 and CK19 mRNA in peripheral blood of colorectal cancer patients, Journal of Zhejiang University Science B, 7(2006) 445-51.
- [81] Y. Yonemura, Y. Endou, T. Fujimura, S. Fushida, E. Bandou, K. Kinoshita, et al., Diagnostic value of preoperative RT-PCR-based screening method to detect carcinoembryonic antigen-expressing free cancer cells in the peritoneal cavity from patients with gastric cancer, ANZ J Surg, 71(2001) 521-8.
- [82] F.L. Flanagan, F. Dehdashti, O.A. Ogunbiyi, I.J. Kodner, B.A. Siegel, Utility of FDG-PET for investigating unexplained plasma CEA elevation in patients with colorectal cancer, Ann Surg, 227(1998) 319.
- [83] C.-S. Liu, Y.-Y. Shen, C.-C. Lin, R.-F. Yen, C.-H. Kao, Clinical impact of [18F] FDG-PET in patients with suspected recurrent breast cancer based on asymptotically elevated tumor marker serum levels: a preliminary report, Jap J Clin Oncol, 32(2002) 244-7.

- [84] R. Wang, X. Chen, J. Ma, Z. Ma, Ultrasensitive detection of carcinoembryonic antigen by a simple label-free immunosensor, *Sensors and Actuators B: Chemical*, 176(2013) 1044-50.
- [85] J. Lin, W. Qu, S. Zhang, Electrochemical immunosensor for carcinoembryonic antigen based on antigen immobilization in gold nanoparticles modified chitosan membrane, *Analytical Sciences*, 23(2007) 1059-63.
- [86] H. Tang, J. Chen, L. Nie, Y. Kuang, S. Yao, A label-free electrochemical immunoassay for carcinoembryonic antigen (CEA) based on gold nanoparticles (AuNPs) and nonconductive polymer film, *Biosensors and Bioelectronics*, 22(2007) 1061-7.
- [87] K.-J. Huang, D.-J. Niu, W.-Z. Xie, W. Wang, A disposable electrochemical immunosensor for carcinoembryonic antigen based on nano-Au/multi-walled carbon nanotubes–chitosans nanocomposite film modified glassy carbon electrode, *Anal Chim Acta*, 659(2010) 102-8.
- [88] D. Wu, A. Guo, Z. Guo, L. Xie, Q. Wei, B. Du, Simultaneous electrochemical detection of cervical cancer markers using reduced graphene oxide-tetraethylene pentamine as electrode materials and distinguishable redox probes as labels, *Biosensors and Bioelectronics*, 54(2014) 634-9.
- [89] C. Hagiopol, J.W. Johnston, *Chemistry of modern papermaking*: CRC Press; 2011.
- [90] D. Tobjörk, R. Österbacka, Paper electronics, *Advanced Materials*, 23(2011) 1935-61.
- [91] E.W. Nery, L.T. Kubota, Sensing approaches on paper-based devices: a review, *Analytical and bioanalytical chemistry*, 405(2013) 7573-95.
- [92] W. Xiao, J. Huang, Immobilization of oligonucleotides onto zirconia-modified filter paper and specific molecular recognition, *Langmuir*, 27(2011) 12284-8.
- [93] T.H. Nguyen, A. Fraiwan, S. Choi, Paper-based batteries: A review, *Biosensors and Bioelectronics*, 54(2014) 640-9.
- [94] C. Desmet, C.A. Marquette, L.J. Blum, B. Doumèche, Paper electrodes for bioelectrochemistry: Biosensors and biofuel cells, *Biosensors and Bioelectronics*, 76(2016) 145-63.
- [95] A.C. Siegel, S.T. Phillips, M.D. Dickey, N. Lu, Z. Suo, G.M. Whitesides, Foldable printed circuit boards on paper substrates, *Advanced Functional Materials*, 20(2010) 28-35.
- [96] J. Zhou, T. Fukawa, H. Shirai, M. Kimura, Anisotropic motion of electroactive papers coated with PEDOT/PSS, *Macromolecular Materials and Engineering*, 295(2010) 671-5.
- [97] T. Mäkelä, S. Jussila, M. Vilkinen, H. Kosonen, R. Korhonen, Roll-to-roll method for producing polyaniline patterns on paper, *Synthetic metals*, 135(2003) 41-2.
- [98] D.D. Liana, B. Raguse, J.J. Gooding, E. Chow, Recent advances in paper-based sensors, *Sensors*, 12(2012) 11505-26.

- [99] H. Ogihara, J. Xie, J. Okagaki, T. Saji, Simple method for preparing superhydrophobic paper: spray-deposited hydrophobic silica nanoparticle coatings exhibit high water-repellency and transparency, *Langmuir*, 28(2012) 4605-8.
- [100] R. Mannerbro, M. Ranlöf, N. Robinson, R. Forchheimer, Inkjet printed electrochemical organic electronics, *Synthetic metals*, 158(2008) 556-60.
- [101] S. Kumar, M. Willander, J.G. Sharma, B.D. Malhotra, A solution processed carbon nanotube modified conducting paper sensor for cancer detection, *Journal of Materials Chemistry B*, 3(2015) 9305-14.
- [102] M. Härting, J. Zhang, D. Gamota, D. Britton, Fully printed silicon field effect transistors, *Applied Physics Letters*, 94(2009) 193509.
- [103] S. Kumar, K.K. Jagadeesan, A.G. Joshi, G. Sumana, Immuno-CoPS (conducting paper strips) for futuristic cost-effective cancer diagnostics, *RSC Advances*, 3(2013) 11846-53.
- [104] K.K. Jagadeesan, S. Kumar, G. Sumana, Application of conducting paper for selective detection of troponin, *Electrochemistry Communications*, 20(2012) 71-4.
- [105] R.F. Carvalho, M. Simão Kfour, M.H. de Oliveira Piazzetta, A.L. Gobbi, L.T. Kubota, Electrochemical detection in a paper-based separation device, *Analytical chemistry*, 82(2010) 1162-5.
- [106] Q. Zhong, J. Zhong, B. Hu, Q. Hu, J. Zhou, Z.L. Wang, A paper-based nanogenerator as a power source and active sensor, *Energy & Environmental Science*, 6(2013) 1779-84.
- [107] A. Manekkathodi, M.Y. Lu, C.W. Wang, L.J. Chen, Direct Growth of Aligned Zinc Oxide Nanorods on Paper Substrates for Low-Cost Flexible Electronics, *Advanced Materials*, 22(2010) 4059-63.
- [108] S. Lyth, R. Hatton, S. Silva, Efficient field emission from Li-salt functionalized multiwall carbon nanotubes on flexible substrates, *Applied Physics Letters*, 90(2007) 013120.
- [109] S. Gong, W. Schwalb, Y. Wang, Y. Chen, Y. Tang, J. Si, et al., A wearable and highly sensitive pressure sensor with ultrathin gold nanowires, *Nature communications*, 5(2014).
- [110] L. Wang, W. Chen, D. Xu, B.S. Shim, Y. Zhu, F. Sun, et al., Simple, rapid, sensitive, and versatile SWNT– paper sensor for environmental toxin detection competitive with ELISA, *Nano letters*, 9(2009) 4147-52.
- [111] E. Montibon, M. Lestelius, L. Järnström, K.T. Love, Electroconductive paper: a study of polymer deposition and conductivity influenced by sheet forming and fibre beating, *Nordic Pulp & Paper Research Journal*, 25(2010) 473-80.
- [112] L. Zhang, P. Zhu, F. Zhou, W. Zeng, H. Su, G. Li, et al., Flexible Asymmetrical Solid-State Supercapacitors Based on Laboratory Filter Paper, *ACS nano*, (2015).
- [113] S. Song, M. Zhang, Z. He, J.Z. Li, Y. Ni, Investigation on a novel fly ash based calcium silicate filler: Effect of particle size on paper properties, *Industrial & Engineering Chemistry Research*, 51(2012) 16377-84.
- [114] A. Baptista, I. Ferreira, J. Borges, Cellulose-based bioelectronic devices, *Cellulose-Medical, Pharmaceutical and Electronic Applications: InTech*, (2013).

- [115] A. Barhoum, H. Rahier, R.E. Abou-Zaied, M. Rehan, T. Dufour, G. Hill, et al., Effect of cationic and anionic surfactants on the application of calcium carbonate nanoparticles in paper coating, *ACS applied materials & interfaces*, 6(2014) 2734-44.
- [116] R.-Z. Li, A. Hu, T. Zhang, K.D. Oakes, Direct writing on paper of foldable capacitive touch pads with silver nanowire inks, *ACS applied materials & interfaces*, 6(2014) 21721-9.
- [117] D.-H. Lien, Z.-K. Kao, T.-H. Huang, Y.-C. Liao, S.-C. Lee, J.-H. He, All-printed paper memory, *ACS nano*, 8(2014) 7613-9.
- [118] E. Fortunato, N. Correia, P. Barquinha, L. Pereira, G. Gonçalves, R. Martins, High-performance flexible hybrid field-effect transistors based on cellulose fiber paper, *Electron Device Letters, IEEE*, 29(2008) 988-90.
- [119] L. Yang, A. Rida, R. Vyas, M.M. Tentzeris, RFID tag and RF structures on a paper substrate using inkjet-printing technology, *Microwave Theory and Techniques, IEEE Transactions on*, 55(2007) 2894-901.
- [120] G. Zheng, Y. Cui, E. Karabulut, L. Wågberg, H. Zhu, L. Hu, Nanostructured paper for flexible energy and electronic devices, *MRS bulletin*, 38(2013) 320-5.
- [121] G. Nyström, A. Razaq, M. Strømme, L. Nyholm, A. Mihranyan, Ultrafast all-polymer paper-based batteries, *Nano letters*, 9(2009) 3635-9.
- [122] J. Wang, L. Li, C.L. Wong, S. Madhavi, Flexible single-walled carbon nanotube/polycellulose papers for lithium-ion batteries, *Nanotechnology*, 23(2012) 495401.
- [123] S.-L. Chou, J.-Z. Wang, S.-Y. Chew, H.-K. Liu, S.-X. Dou, Electrodeposition of MnO₂ nanowires on carbon nanotube paper as free-standing, flexible electrode for supercapacitors, *Electrochemistry Communications*, 10(2008) 1724-7.
- [124] A. Fraiwan, S. Mukherjee, S. Sundermier, H.-S. Lee, S. Choi, A paper-based microbial fuel cell: instant battery for disposable diagnostic devices, *Biosensors and Bioelectronics*, 49(2013) 410-4.
- [125] L. Hu, J.W. Choi, Y. Yang, S. Jeong, F. La Mantia, L.-F. Cui, et al., Highly conductive paper for energy-storage devices, *Proceedings of the National Academy of Sciences*, 106(2009) 21490-4.
- [126] K.H. Kim, K.Y. Lee, J.S. Seo, B. Kumar, S.W. Kim, Paper-Based Piezoelectric Nanogenerators with High Thermal Stability, *Small*, 7(2011) 2577-80.
- [127] A.W. Martinez, S.T. Phillips, G.M. Whitesides, Three-dimensional microfluidic devices fabricated in layered paper and tape, *Proceedings of the National Academy of Sciences*, 105(2008) 19606-11.
- [128] Y.-H. Chen, Z.-K. Kuo, C.-M. Cheng, Paper—a potential platform in pharmaceutical development, *Trends in biotechnology*, 33(2015) 4-9.
- [129] Z. Zhang, W. Xu, N.E. Manicke, R.G. Cooks, Z. Ouyang, Silica coated paper substrate for paper-spray analysis of therapeutic drugs in dried blood spots, *Analytical chemistry*, 84(2011) 931-8.
- [130] M.-Y. Hsu, C.-Y. Yang, W.-H. Hsu, K.-H. Lin, C.-Y. Wang, Y.-C. Shen, et al., Monitoring the VEGF level in aqueous humor of patients with ophthalmologically relevant diseases via ultrahigh sensitive paper-based ELISA, *Biomaterials*, 35(2014) 3729-35.

- [131] R. Derda, S.K. Tang, A. Laromaine, B. Mosadegh, E. Hong, M. Mwangi, et al., Multizone paper platform for 3D cell cultures, *PloS one*, 6(2011) e18940.
- [132] V. Kuzmenko, T. Kalogeropoulos, J. Thunberg, S. Johannesson, D. Hägg, P. Enoksson, et al., Enhanced growth of neural networks on conductive cellulose-derived nanofibrous scaffolds, *Materials Science and Engineering: C*, 58(2016) 14-23.
- [133] X. Ge, A.M. Asiri, D. Du, W. Wen, S. Wang, Y. Lin, Nanomaterial-enhanced paper-based biosensors, *TrAC Trends in Analytical Chemistry*, 58(2014) 31-9.
- [134] P. Mostafalu, S. Sonkusale, A high-density nanowire electrode on paper for biomedical applications, *RSC Advances*, 5(2015) 8680-7.
- [135] Q. Liu, J. Wang, B. Wang, Z. Li, H. Huang, C. Li, et al., Paper-based plasmonic platform for sensitive, noninvasive, and rapid cancer screening, *Biosensors and Bioelectronics*, 54(2014) 128-34.
- [136] M. Ornatska, E. Sharpe, D. Andreescu, S. Andreescu, Paper bioassay based on ceria nanoparticles as colorimetric probes, *Analytical chemistry*, 83(2011) 4273-80.
- [137] S. Hu, R. Rajamani, X. Yu, Flexible solid-state paper based carbon nanotube supercapacitor, *Applied Physics Letters*, 100(2012) 104103.
- [138] Z. Liu, Z. Ma, Fabrication of an ultrasensitive electrochemical immunosensor for CEA based on conducting long-chain polythiols, *Biosens Bioelectron*, 46(2013) 1-7.
- [139] S.W. Lee, K. Hosokawa, S. Kim, O.C. Jeong, H. Lilja, T. Laurell, et al., A Highly Sensitive Porous Silicon (P-Si)-Based Human Kallikrein 2 (hK2) Immunoassay Platform toward Accurate Diagnosis of Prostate Cancer, *Sensors*, 15(2015) 11972-87.
- [140] C.S.K. Lawrence, S.N. Tan, C.Z. Floresca, A “green” cellulose paper based glucose amperometric biosensor, *Sensors and Actuators B: Chemical*, 193(2014) 536-41.
- [141] J. Lu, S. Ge, L. Ge, M. Yan, J. Yu, Electrochemical DNA sensor based on three-dimensional folding paper device for specific and sensitive point-of-care testing, *Electrochimica Acta*, 80(2012) 334-41.
- [142] Z. Nie, C.A. Nijhuis, J. Gong, X. Chen, A. Kumachev, A.W. Martinez, et al., Electrochemical sensing in paper-based microfluidic devices, *Lab on a Chip*, 10(2010) 477-83.
- [143] N. Ruecha, R. Rangkupan, N. Rodthongkum, O. Chailapakul, Novel paper-based cholesterol biosensor using graphene/polyvinylpyrrolidone/polyaniline nanocomposite, *Biosensors and Bioelectronics*, 52(2014) 13-9.
- [144] J. Lankelma, Z. Nie, E. Carrilho, G.M. Whitesides, Paper-based analytical device for electrochemical flow-injection analysis of glucose in urine, *Analytical chemistry*, 84(2012) 4147-52.
- [145] H. Liu, R.M. Crooks, Paper-based electrochemical sensing platform with integral battery and electrochromic read-out, *Analytical chemistry*, 84(2012) 2528-32.
- [146] S.N. Tan, L. Ge, W. Wang, Paper disk on screen printed electrode for one-step sensing with an internal standard, *Analytical chemistry*, 82(2010) 8844-7.
- [147] W. Dungchai, O. Chailapakul, C.S. Henry, Electrochemical detection for paper-based microfluidics, *Analytical chemistry*, 81(2009) 5821-6.

- [148] W. Dungchai, O. Chailapakul, C.S. Henry, A low-cost, simple, and rapid fabrication method for paper-based microfluidics using wax screen-printing, *Analyst*, 136(2011) 77-82.
- [149] C. Zhao, M.M. Thuo, X. Liu, A microfluidic paper-based electrochemical biosensor array for multiplexed detection of metabolic biomarkers, *Science and Technology of Advanced Materials*, (2016).
- [150] Y. Wang, L. Ge, C. Ma, Q. Kong, M. Yan, S. Ge, et al., Self-Powered and Sensitive DNA Detection in a Three-Dimensional Origami-Based Biofuel Cell Based on a Porous Pt-Paper Cathode, *Chemistry—A European Journal*, 20(2014) 12453-62.
- [151] N. Dossi, R. Toniolo, E. Piccin, S. Susmel, A. Pizzariello, G. Bontempelli, Pencil-Drawn Dual Electrode Detectors to Discriminate Between Analytes Comigrating on Paper-Based Fluidic Devices but Undergoing Electrochemical Processes with Different Reversibility, *Electroanalysis*, 25(2013) 2515-22.
- [152] M. Santhiago, L.T. Kubota, A new approach for paper-based analytical devices with electrochemical detection based on graphite pencil electrodes, *Sensors and Actuators B: Chemical*, 177(2013) 224-30.
- [153] L. Ge, P. Wang, S. Ge, N. Li, J. Yu, M. Yan, et al., Photoelectrochemical lab-on-paper device based on an integrated paper supercapacitor and internal light source, *Analytical chemistry*, 85(2013) 3961-70.
- [154] J.C. Cunningham, N.J. Brenes, R.M. Crooks, Paper electrochemical device for detection of DNA and thrombin by target-induced conformational switching, *Analytical chemistry*, 86(2014) 6166-70.
- [155] I. Shitanda, T. Yamaguchi, Y. Hoshi, M. Itagaki, Fully screen-printed paper-based electrode chip for glucose detection, *Chemistry Letters*, 42(2013) 1369-70.
- [156] S. Ge, W. Liu, L. Ge, M. Yan, J. Yan, J. Huang, et al., In situ assembly of porous Au-paper electrode and functionalization of magnetic silica nanoparticles with HRP via click chemistry for Microcystin-LR immunoassay, *Biosensors and Bioelectronics*, 49(2013) 111-7.
- [157] J.P. Metters, S.M. Houssein, D.K. Kampouris, C.E. Banks, Paper-based electroanalytical sensing platforms, *Analytical Methods*, 5(2013) 103-10.
- [158] W. Li, L. Li, S. Ge, X. Song, L. Ge, M. Yan, et al., Multiplex electrochemical origami immunodevice based on cuboid silver-paper electrode and metal ions tagged nanoporous silver–chitosan, *Biosensors and Bioelectronics*, 56(2014) 167-73.
- [159] L. Li, J. Xu, X. Zheng, C. Ma, X. Song, S. Ge, et al., Growth of gold-manganese oxide nanostructures on a 3D origami device for glucose-oxidase label based electrochemical immunosensor, *Biosensors and Bioelectronics*, 61(2014) 76-82.
- [160] J.L. Delaney, C.F. Hogan, J. Tian, W. Shen, Electrogenenerated chemiluminescence detection in paper-based microfluidic sensors, *Analytical chemistry*, 83(2011) 1300-6.
- [161] Y. Xu, B. Lou, Z. Lv, Z. Zhou, L. Zhang, E. Wang, Paper-based solid-state electrochemiluminescence sensor using poly (sodium 4-styrenesulfonate) functionalized graphene/nafion composite film, *Analytica chimica acta*, 763(2013) 20-7.

- [162] Y. Wang, J. Xu, C. Ma, S. Li, J. Yu, S. Ge, et al., A chemiluminescence excited photoelectrochemistry aptamer-device equipped with a tin dioxide quantum dot/reduced graphene oxide nanocomposite modified porous Au-paper electrode, *Journal of Materials Chemistry B*, 2(2014) 3462-8.
- [163] M. Pozuelo, P. Blondeau, M. Novell, F.J. Andrade, F.X. Rius, J. Riu, Paper-based chemiresistor for detection of ultralow concentrations of protein, *Biosensors and Bioelectronics*, 49(2013) 462-5.
- [164] C. Kittel, *Introduction to solid state physics*: Wiley; 2005.
- [165] L. Valdes, *Handbook of semiconductor electronics*: LP Hunter (Editor): McGraw-Hill, New York, 1962. 871 pp., \$18.50, Pergamon 1962.
- [166] Measurement of Resistivity of thin film by four probe method, User Manual, SES instrument Pvt Ltd UK, India 2014.
- [167] S.K. Kulkarni, *Nanotechnology: principles and practices*: Springer; 2015.
- [168] B. Culity, S. Stock, *Elements of X-ray Diffraction*, 2nd, Addison-Wesley, MA, London, (1978).
- [169] J. Li, J. Liu, C. Gao, J. Zhang, H. Sun, Influence of MWCNTs doping on the structure and properties of PEDOT: PSS films, *International Journal of Photoenergy*, 2009(2009).
- [170] L. Zhan, Z. Song, J. Zhang, J. Tang, H. Zhan, Y. Zhou, et al., PEDOT: Cathode active material with high specific capacity in novel electrolyte system, *Electrochimica Acta*, 53(2008) 8319-23.
- [171] B.C. Smith, *Fundamentals of Fourier transform infrared spectroscopy*: CRC press; 2011.
- [172] J.M. Chalmers, P.R. Griffiths, *Handbook of Vibrational Spectroscopy*, (2001).
- [173] F.J.H. Douglas A. Skoog, *Principles of Instrumental Analysis*, 6th Edition, (2007).
- [174] S. Ewen, G. Dent, *Modern Raman spectroscopy: a practical approach*, New York: John Wiler & Sons, (2005).
- [175] S. Srivastava, V. Kumar, M.A. Ali, P.R. Solanki, A. Srivastava, G. Sumana, et al., Electrophoretically deposited reduced graphene oxide platform for food toxin detection, *Nanoscale*, 5(2013) 3043-51.
- [176] K.D. Bomben, J.F. Moulder, P.E. Sobol, W.F. Stickle, *Handbook of X-ray photoelectron spectroscopy*, Perkin-Elmer Corporation, Physical Electronics Division, (1992).
- [177] J.J. Bozzola, L.D. Russell, *Electron microscopy: principles and techniques for biologists*: Jones & Bartlett Learning; 1999.
- [178] R. Egerton, *Physical principles of electron microscopy: an introduction to TEM, SEM, and AEM*: Springer Science & Business Media; 2006.
- [179] M. Horikawa, T. Fujiki, T. Shirosaki, N. Ryu, H. Sakurai, S. Nagaoka, et al., The development of a highly conductive PEDOT system by doping with partially crystalline sulfated cellulose and its electric conductivity, *Journal of Materials Chemistry C*, 3(2015) 8881-7.

- [180] Q. Zhou, J. Huang, J. Wang, Z. Yang, S. Liu, Z. Wang, et al., Preparation of a reduced graphene oxide/zirconia nanocomposite and its application as a novel lubricant oil additive, *RSC Advances*, 5(2015) 91802-12.
- [181] J.R. Davis, *Tensile testing: ASM international*; 2004.
- [182] D. Van der Reyden, C. Hofmann, M. Baker, Effects of aging and solvent treatments on some properties of contemporary tracing papers, *Journal of the American Institute for Conservation*, 32(1993) 177-206.
- [183] D.Y. Kwok, A.W. Neumann, Contact angle measurement and contact angle interpretation, *Advances in colloid and interface science*, 81(1999) 167-249.
- [184] S. Kumar, J. Singh, V. Agrawal, M. Ahamad, B. Malhotra, Biocompatible self-assembled monolayer platform based on (3-glycidoxypopyl) trimethoxysilane for total cholesterol estimation, *Analytical Methods*, 3(2011) 2237-45.
- [185] A.J. Bard, L.R. Faulkner, J. Leddy, C.G. Zoski, *Electrochemical methods: fundamentals and applications: Wiley New York*; 1980.
- [186] C.G. Zoski, *Handbook of electrochemistry: Elsevier*; 2006.
- [187] C.-W. Kuo, L.-M. Huang, T.-C. Wen, A. Gopalan, Enhanced electrocatalytic performance for methanol oxidation of a novel Pt-dispersed poly (3, 4-ethylenedioxythiophene)–poly (styrene sulfonic acid) electrode, *Journal of power sources*, 160(2006) 65-72.
- [188] M. Moisel, M.L. de Mele, W.D. Müller, Biomaterial interface investigated by electrochemical impedance spectroscopy, *Advanced engineering materials*, 10(2008) B33-B46.
- [189] J.R. McDonald, *Impedance spectroscopy: emphasizing solid materials and systems, Impedance Spectroscopy Emphasizing Solid Materials and Systems*, (1987).
- [190] B.-Y. Chang, S.-M. Park, Electrochemical impedance spectroscopy, *Annual Review of Analytical Chemistry*, 3(2010) 207-29.
- [191] H.-S. Park, S.-J. Ko, J.-S. Park, J.Y. Kim, H.-K. Song, Redox-active charge carriers of conducting polymers as a tuner of conductivity and its potential window, *Scientific reports*, 3(2013).
- [192] B.D. Malhotra, A. Turner, *Advances in biosensors: Perspectives in biosensors: Elsevier*; 2003.
- [193] Y. Miao, S.N. Tan, Amperometric hydrogen peroxide biosensor based on immobilization of peroxidase in chitosan matrix crosslinked with glutaraldehyde, *Analyst*, 125(2000) 1591-4.
- [194] J. Wang, M. Musameh, Carbon-nanotubes doped polypyrrole glucose biosensor, *Analytica Chimica Acta*, 539(2005) 209-13.
- [195] D.R. Thevenot, K. Toth, R.A. Durst, G.S. Wilson, Electrochemical biosensors: recommended definitions and classification, *Pure and Applied Chemistry*, 71(1999) 2333-48.
- [196] M.J. Allen, V.C. Tung, R.B. Kaner, Honeycomb carbon: a review of graphene, *Chemical reviews*, 110(2009) 132-45.
- [197] D.R. Cooper, B. D'Anjou, N. Ghattamaneni, B. Harack, M. Hilke, A. Horth, et al., Experimental review of graphene, *ISRN Condensed Matter Physics*, 2012(2012).

- [198] D. Du, Z. Zou, Y. Shin, J. Wang, H. Wu, M.H. Engelhard, et al., Sensitive immunosensor for cancer biomarker based on dual signal amplification strategy of graphene sheets and multienzyme functionalized carbon nanospheres, *Analytical Chemistry*, 82(2010) 2989-95.
- [199] R. Elshafey, M. Siaj, A.C. Tavares, Au nanoparticle decorated graphene nanosheets for electrochemical immunosensing of p53 antibodies for cancer prognosis, *Analyst*, 141(2016) 2733-40.
- [200] E. Morgan, I. Wilson, An early description of paper chromatography?, *Chromatographia*, 60(2004) 135-6.
- [201] R.M. Rocco, *Landmark papers in clinical chemistry*: Elsevier; 2005.
- [202] H.G. Kunkel, A. Tiselius, Electrophoresis of proteins on filter paper, *The Journal of general physiology*, 35(1951) 89-118.
- [203] H. Liu, Y. Xiang, Y. Lu, R.M. Crooks, Aptamer-based origami paper analytical device for electrochemical detection of adenosine, *Angewandte Chemie*, 124(2012) 7031-4.
- [204] M.P. Allen, Laminated assay device, Google Patents 1995.
- [205] A.W. Martinez, S.T. Phillips, M.J. Butte, G.M. Whitesides, Patterned paper as a platform for inexpensive, low-volume, portable bioassays, *Angewandte Chemie International Edition*, 46(2007) 1318-20.
- [206] B. Liu, D. Du, X. Hua, X.Y. Yu, Y. Lin, Paper-Based Electrochemical Biosensors: From Test Strips to Paper-Based Microfluidics, *Electroanalysis*, 26(2014) 1214-23.
- [207] P.B. Lippa, C. Müller, A. Schlichtiger, H. Schlebusch, Point-of-care testing (POCT): Current techniques and future perspectives, *TrAC Trends in Analytical Chemistry*, 30(2011) 887-98.
- [208] L. Gervais, N. De Rooij, E. Delamarche, Microfluidic Chips for Point-of-Care Immunodiagnosics, *Advanced Materials*, 23(2011) H151-H76.
- [209] D. Zhai, B. Liu, Y. Shi, L. Pan, Y. Wang, W. Li, et al., Highly sensitive glucose sensor based on Pt nanoparticle/polyaniline hydrogel heterostructures, *ACS nano*, 7(2013) 3540-6.
- [210] L. Li, Y. Wang, L. Pan, Y. Shi, W. Cheng, Y. Shi, et al., A nanostructured conductive hydrogels-based biosensor platform for human metabolite detection, *Nano letters*, (2015).
- [211] M. Zhang, W. Yuan, B. Yao, C. Li, G. Shi, Solution-Processed PEDOT: PSS/Graphene Composites as the Electrocatalyst for Oxygen Reduction Reaction, *ACS applied materials & interfaces*, 6(2014) 3587-93.
- [212] Y. Gao, J. Li, X. Yang, Q. Xiang, K. Wang, Electrochemiluminescence Biosensor Based on PEDOT-PSS-Graphene Functionalized ITO Electrode, *Electroanalysis*, 26(2014) 382-8.
- [213] D.C. Marcano, D.V. Kosynkin, J.M. Berlin, A. Sinitskii, Z. Sun, A. Slesarev, et al., Improved synthesis of graphene oxide, *ACS nano*, 4(2010) 4806-14.
- [214] P. Cui, J. Lee, E. Hwang, H. Lee, One-pot reduction of graphene oxide at subzero temperatures, *Chemical Communications*, 47(2011) 12370-2.

- [215] W.J. Hyun, O.O. Park, B.D. Chin, Foldable graphene electronic circuits based on paper substrates, *Advanced Materials*, 25(2013) 4729-34.
- [216] J. Ouyang, C.W. Chu, F.C. Chen, Q. Xu, Y. Yang, High-Conductivity Poly (3, 4-ethylenedioxythiophene): Poly (styrene sulfonate) Film and Its Application in Polymer Optoelectronic Devices, *Advanced Functional Materials*, 15(2005) 203-8.
- [217] Q. Wei, M. Mukaida, Y. Naitoh, T. Ishida, Morphological Change and Mobility Enhancement in PEDOT: PSS by Adding Co-solvents, *Advanced Materials*, 25(2013) 2831-6.
- [218] D. Alemu, H.-Y. Wei, K.-C. Ho, C.-W. Chu, Highly conductive PEDOT: PSS electrode by simple film treatment with methanol for ITO-free polymer solar cells, *Energy & environmental science*, 5(2012) 9662-71.
- [219] Y. Xia, K. Sun, J. Ouyang, Solution-Processed Metallic Conducting Polymer Films as Transparent Electrode of Optoelectronic Devices, *Advanced Materials*, 24(2012) 2436-40.
- [220] P. Podsiadlo, Z. Tang, B.S. Shim, N.A. Kotov, Counterintuitive effect of molecular strength and role of molecular rigidity on mechanical properties of layer-by-layer assembled nanocomposites, *Nano letters*, 7(2007) 1224-31.
- [221] F. Ely, A. Matsumoto, B. Zoetebier, V.S. Peressinotto, M.K. Hirata, D.A. de Sousa, et al., Handheld and automated ultrasonic spray deposition of conductive PEDOT: PSS films and their application in AC EL devices, *Organic Electronics*, 15(2014) 1062-70.
- [222] J.S. Daniels, N. Pourmand, Label-Free Impedance Biosensors: Opportunities and Challenges, *Electroanalysis*, 19(2007) 1239-57.
- [223] A. Bardea, E. Katz, I. Willner, Probing antigen–antibody interactions on electrode supports by the biocatalyzed precipitation of an insoluble product, *Electroanalysis*, 12(2000) 1097-106.
- [224] B.S. Shim, W. Chen, C. Doty, C. Xu, N.A. Kotov, Smart electronic yarns and wearable fabrics for human biomonitoring made by carbon nanotube coating with polyelectrolytes, *Nano letters*, 8(2008) 4151-7.
- [225] N. Laboria, A. Fragoso, W. Kemmner, D. Latta, O. Nilsson, M. Luz Botero, et al., Amperometric immunosensor for carcinoembryonic antigen in colon cancer samples based on monolayers of dendritic bipodal scaffolds, *Analytical chemistry*, 82(2010) 1712-9.
- [226] J. Miao, X. Wang, L. Lu, P. Zhu, C. Mao, H. Zhao, et al., Electrochemical immunosensor based on hyperbranched structure for carcinoembryonic antigen detection, *Biosensors and Bioelectronics*, 58(2014) 9-16.
- [227] M.J. O'connell, *Carbon nanotubes: properties and applications*: CRC press; 2006.
- [228] B.D. Malhotra, S. Srivastava, S. Augustine, *Biosensors for Food Toxin Detection: Carbon Nanotubes and Graphene*, *MRS Proceedings*, Cambridge Univ Press 2015, pp. mrsf14-1725-i05-02.
- [229] Y. Lin, W. Yantasee, J. Wang, Carbon nanotubes (CNTs) for the development of electrochemical biosensors, *Front Biosci*, 10(2005) 582.

- [230] B. Kim, W.M. Sigmund, Functionalized multiwall carbon nanotube/gold nanoparticle composites, *Langmuir*, 20(2004) 8239-42.
- [231] S. Vardharajula, S.Z. Ali, P.M. Tiwari, E. Eroğlu, K. Vig, V.A. Dennis, et al., Functionalized carbon nanotubes: biomedical applications, *International journal of nanomedicine*, 7(2012) 5361.
- [232] G. Modugno, C. Ménard-Moyon, M. Prato, A. Bianco, Carbon nanomaterials combined with metal nanoparticles for theranostic applications, *British journal of pharmacology*, 172(2015) 975-91.
- [233] C. Singh, S. Srivastava, M.A. Ali, T.K. Gupta, G. Sumana, A. Srivastava, et al., Carboxylated multiwalled carbon nanotubes based biosensor for aflatoxin detection, *Sensors and Actuators B: Chemical*, 185(2013) 258-64.
- [234] R. Malhotra, V. Patel, J.P. Vaqué, J.S. Gutkind, J.F. Rusling, Ultrasensitive electrochemical immunosensor for oral cancer biomarker IL-6 using carbon nanotube forest electrodes and multilabel amplification, *Analytical chemistry*, 82(2010) 3118-23.
- [235] R. Akter, M.A. Rahman, C.K. Rhee, Amplified electrochemical detection of a cancer biomarker by enhanced precipitation using horseradish peroxidase attached on carbon nanotubes, *Analytical chemistry*, 84(2012) 6407-15.
- [236] A.W. Martinez, S.T. Phillips, G.M. Whitesides, E. Carrilho, Diagnostics for the developing world: microfluidic paper-based analytical devices, *Analytical chemistry*, 82(2009) 3-10.
- [237] J. Hu, S. Wang, L. Wang, F. Li, B. Pingguan-Murphy, T.J. Lu, et al., Advances in paper-based point-of-care diagnostics, *Biosensors and Bioelectronics*, 54(2014) 585-97.
- [238] J.R. Windmiller, A.J. Bandodkar, G. Valdés-Ramírez, S. Parkhomovsky, A.G. Martinez, J. Wang, Electrochemical sensing based on printable temporary transfer tattoos, *Chemical Communications*, 48(2012) 6794-6.
- [239] A.C. Glavan, D.C. Christodouleas, B. Mosadegh, H.D. Yu, B.S. Smith, J. Lessing, et al., Folding Analytical Devices for Electrochemical ELISA in Hydrophobic RH Paper, *Analytical chemistry*, 86(2014) 11999-2007.
- [240] S. Wang, L. Ge, Y. Zhang, X. Song, N. Li, S. Ge, et al., Battery-triggered microfluidic paper-based multiplex electrochemiluminescence immunodevice based on potential-resolution strategy, *Lab on a Chip*, 12(2012) 4489-98.
- [241] S.-I. Yang, K.F. Lei, S.-W. Tsai, H.-T. Hsu, Development of a paper-based carbon nanotube sensing microfluidic device for biological detection, *Engineering in Medicine and Biology Society (EMBC), 2013 35th Annual International Conference of the IEEE, IEEE2013*, pp. 168-71.
- [242] K.F. Lei, K.-F. Lee, S.-I. Yang, Fabrication of carbon nanotube-based pH sensor for paper-based microfluidics, *Microelectronic Engineering*, 100(2012) 1-5.
- [243] Y. Koo, V.N. Shanov, Y. Yun, Carbon Nanotube Paper-Based Electroanalytical Devices, *Micromachines*, 7(2016) 72.
- [244] D.-J. Yun, K. Hong, S.h. Kim, W.-M. Yun, J.-y. Jang, W.-S. Kwon, et al., Multiwall carbon nanotube and poly (3, 4-ethylenedioxythiophene): polystyrene

sulfonate (PEDOT: PSS) composite films for transistor and inverter devices, *ACS applied materials & interfaces*, 3(2011) 43-9.

[245] D. Antiohos, G. Folkes, P. Sherrell, S. Ashraf, G.G. Wallace, P. Aitchison, et al., Compositional effects of PEDOT-PSS/single walled carbon nanotube films on supercapacitor device performance, *Journal of Materials Chemistry*, 21(2011) 15987-94.

[246] U. Lang, E. Müller, N. Naujoks, J. Dual, Microscopical investigations of PEDOT: PSS thin films, *Advanced Functional Materials*, 19(2009) 1215-20.

[247] J. Kim, J. Jung, D. Lee, J. Joo, Enhancement of electrical conductivity of poly (3, 4-ethylenedioxythiophene)/poly (4-styrenesulfonate) by a change of solvents, *Synthetic Metals*, 126(2002) 311-6.

[248] D.A. Mengistie, M.A. Ibrahim, P.-C. Wang, C.-W. Chu, Highly conductive PEDOT: PSS treated with formic acid for ITO-free polymer solar cells, *ACS applied materials & interfaces*, 6(2014) 2292-9.

[249] S. Razdan, P.K. Patra, S. Kar, L. Ci, R. Vajtai, A. Kukovecz, et al., Ionically self-assembled polyelectrolyte-based carbon nanotube fibers, *Chemistry of Materials*, 21(2009) 3062-71.

[250] T. Ji, L. Tan, X. Hu, Y. Dai, Y. Chen, A comprehensive study of sulfonated carbon materials as conductive composites for polymer solar cells, *Physical Chemistry Chemical Physics*, 17(2015) 4137-45.

[251] G. Guan, Z. Yang, L. Qiu, X. Sun, Z. Zhang, J. Ren, et al., Oriented PEDOT: PSS on aligned carbon nanotubes for efficient dye-sensitized solar cells, *Journal of Materials Chemistry A*, 1(2013) 13268-73.

[252] J. Li, J.-C. Liu, C.-J. Gao, On the mechanism of conductivity enhancement in PEDOT/PSS film doped with multi-walled carbon nanotubes, *Journal of polymer research*, 17(2010) 713-8.

[253] V.V. Shumyantseva, L.V. Sigolaeva, L.E. Agafonova, T.V. Bulko, D.V. Pergushov, F.H. Schacher, et al., Facilitated biosensing via direct electron transfer of myoglobin integrated into diblock copolymer/multi-walled carbon nanotube nanocomposites, *Journal of Materials Chemistry B*, 3(2015) 5467-77.

[254] S. Soylemez, F.E. Kanik, S.D. Uzun, S.O. Hacıoglu, L. Toppare, Development of an efficient immobilization matrix based on a conducting polymer and functionalized multiwall carbon nanotubes: synthesis and its application to ethanol biosensors, *Journal of Materials Chemistry B*, 2(2014) 511-21.

[255] J.P. Thomas, L. Zhao, D. McGillivray, K.T. Leung, High-efficiency hybrid solar cells by nanostructural modification in PEDOT: PSS with co-solvent addition, *Journal of Materials Chemistry A*, 2(2014) 2383-9.

[256] S. Kumar, S. Kumar, S. Srivastava, B.K. Yadav, S.H. Lee, J.G. Sharma, et al., Reduced graphene oxide modified smart conducting paper for Cancer biosensor, *Biosensors and Bioelectronics*, (2015).

[257] N. Sekar, R.P. Ramasamy, Electrochemical impedance spectroscopy for microbial fuel cell characterization, *J Microb Biochem Technol S*, 6(2013).

[258] U. Yogeswaran, S.A. Kumar, S.-M. Chen, Nanostructured materials for electrochemical biosensors: Nova Science Publ.; 2009.

- [259] A. Laforgue, L. Robitaille, Production of conductive PEDOT nanofibers by the combination of electrospinning and vapor-phase polymerization, *Macromolecules*, 43(2010) 4194-200.
- [260] J.A. Arter, D.K. Taggart, T.M. McIntire, R.M. Penner, G.A. Weiss, Virus-PEDOT nanowires for biosensing, *Nano letters*, 10(2010) 4858-62.
- [261] A. Frenot, I.S. Chronakis, Polymer nanofibers assembled by electrospinning, *Current opinion in colloid & interface science*, 8(2003) 64-75.
- [262] H. Park, S.J. Lee, S. Kim, H.W. Ryu, S.H. Lee, H.H. Choi, et al., Conducting polymer nanofiber mats via combination of electrospinning and oxidative polymerization, *Polymer*, 54(2013) 4155-60.
- [263] C.h. Chen, J.C. LaRue, R.D. Nelson, L. Kulinsky, M.J. Madou, Electrical conductivity of polymer blends of poly (3, 4-ethylenedioxythiophene): Poly (styrenesulfonate): N-methyl-2-pyrrolidinone and polyvinyl alcohol, *Journal of Applied Polymer Science*, 125(2012) 3134-41.
- [264] J.-C. Park, T. Ito, K.-O. Kim, K.-W. Kim, B.-S. Kim, M.-S. Khil, et al., Electrospun poly (vinyl alcohol) nanofibers: effects of degree of hydrolysis and enhanced water stability, *Polymer journal*, 42(2010) 273-6.
- [265] K. Shalumon, N. Binulal, N. Selvamurugan, S. Nair, D. Menon, T. Furuike, et al., Electrospinning of carboxymethyl chitin/poly (vinyl alcohol) nanofibrous scaffolds for tissue engineering applications, *Carbohydrate Polymers*, 77(2009) 863-9.
- [266] Z. Chen, Z. Chen, A. Zhang, J. Hu, X. Wang, Z. Yang, Electrospun nanofibers for cancer diagnosis and therapy, *Biomaterials science*, 4(2016) 922-32.
- [267] J. Wang, H.-B. Yao, D. He, C.-L. Zhang, S.-H. Yu, Facile fabrication of gold nanoparticles-poly (vinyl alcohol) electrospun water-stable nanofibrous mats: efficient substrate materials for biosensors, *ACS applied materials & interfaces*, 4(2012) 1963-71.
- [268] X. Su, J. Wei, X. Ren, L. Li, X. Meng, J. Ren, et al., A New Amperometric Glucose Biosensor Based on One-Step Electrospun Poly (Vinyl Alcohol)/Chitosan Nanofibers, *Journal of biomedical nanotechnology*, 9(2013) 1776-83.
- [269] Y. Zhao, Z. Fan, M. Shen, X. Shi, Hyaluronic Acid-Functionalized Electrospun Polyvinyl Alcohol/Polyethyleneimine Nanofibers for Cancer Cell Capture Applications, *Advanced Materials Interfaces*, 2(2015).
- [270] Y.-T. Jia, J. Gong, X.-H. Gu, H.-Y. Kim, J. Dong, X.-Y. Shen, Fabrication and characterization of poly (vinyl alcohol)/chitosan blend nanofibers produced by electrospinning method, *Carbohydrate Polymers*, 67(2007) 403-9.
- [271] J.S. Hwang, T.H. Oh, S.H. Kim, S.S. Han, S.J. Lee, S.G. Lee, et al., Effect of solvent on electrical conductivity and gas sensitivity of PEDOT: PSS polymer composite films, *Journal of Applied Polymer Science*, 132(2015).
- [272] H. Moayedi, A. Asadi, F. Moayedi, B.B. Huat, Zeta potential of tropical soil in presence of polyvinyl alcohol, *Int J Electrochem Sci*, 6(2011) 1294-306.

Publications Included in Thesis



Reduced graphene oxide modified smart conducting paper for cancer biosensor



Saurabh Kumar^a, Suveen Kumar^a, Saurabh Srivastava^a, Birendra K. Yadav^b,
Seung H. Lee^{c,*}, Jai G. Sharma^a, Dinesh C. Doval^b, Bansi D. Malhotra^{a,*}

^a Nanobioelectronics Laboratory, Department of Biotechnology, Delhi Technological University, Shahbad Daultpur, Delhi 110042, India

^b Rajiv Gandhi Cancer Institute and Research Centre, Rohini, Delhi 110085, India

^c Applied Materials Institute for BIN Convergence, Department of BIN Fusion Technology, Chonbuk National University, Jeonju 561-756, Republic of Korea

ARTICLE INFO

Article history:

Received 3 March 2015

Received in revised form

16 May 2015

Accepted 17 May 2015

Available online 27 May 2015

Keywords:

Conducting paper

PEDOT:PSS

Biosensor

Cancer

ABSTRACT

We report results of the studies relating to the fabrication of a paper based sensor comprising of poly (3,4-ethylenedioxythiophene):poly(styrenesulfonate) (PEDOT:PSS) and reduced graphene oxide (RGO) composite. The effect of various solvents like methanol, ethylene glycol and H₂SO₄ on the electrical conductivity of PEDOT:PSS coated Whatman paper has been investigated. The conductivity of this solution processed conducting paper significantly increases from $\sim 1.16 \times 10^{-4} \text{ S cm}^{-1}$ up to $\sim 3.57 \times 10^{-2} \text{ S cm}^{-1}$ (~ 300 times) on treatment with ethylene glycol. The observed significant increase in electrical conductivity is due to conformational rearrangement in the polymer and is due to strong non-covalent cooperative interaction between PEDOT and the cellulose molecules. Further, incorporation of RGO into the conducting paper results in improved electrochemical performance and signal stability. This paper electrode is a promising alternative over the expensive conventional electrodes (ITO, gold and glassy carbon), that are known to have limited application in smart point-of-care (POC) devices. This low cost, flexible and environment friendly conducting paper based biosensor utilized for cancer biomarker (carcinoembryonic antigen, CEA) detection reveals high sensitivity of $25.8 \mu\text{A ng}^{-1} \text{ mL cm}^{-2}$ in the physiological range, 1–10 ng mL⁻¹.

© 2015 Elsevier B.V. All rights reserved.

1. Introduction

Paper based point-of-care (POC) devices are rapidly evolving for desired analytical and clinical applications since these are predicted to be simple, cost-effective, portable, consume low power and are disposable. These devices have potential applications in healthcare, detection of toxicants, explosives and environmental studies. Compared to conventional laboratory assays, these devices are found to be very helpful for making speedy decision for therapeutics. Besides this, the testing can be performed near the vicinity of a patient and hence these devices have recently gained considerable attention in health care (Gervais et al., 2011; Kumar et al., 2013a, 2013b; Lippa et al., 2011).

Electrochemical sensors are known to play an important role in on-going transition towards the paper based POC diagnostic devices. The electrochemical techniques offer high sensitivity, high signal-to-noise ratio, portability and fast response time (Wang,

2006). Therefore, its integration with the paper may be advantageous. To ensure the application of paper in an electrochemical sensor, it is essential to make it conducting. In this context, many methods such as screen printing, inkjet printing etc. have been used to incorporate conducting ink on a paper substrate (Jagadeesan et al., 2012; Tobjörk and Österbacka, 2011). These methods require complex fabrication steps, additional instrumentation, skilled personnel and are time-consuming. Conducting polymers (CPs) have been considered a promising candidate to obtain conducting paper due to delocalization of π electrons since they are known to facilitate rapid electron transfer, mechanical flexibility and solution processability. Doping of a conducting polymer has been found to enhance its electronic, optical, physical, chemical and electrochemical properties (Dhand et al., 2011). CPs have been predicted to have enough potential for the development of a low cost and high performance biosensor materials that offer high permeability biocompatibility, and rapid electron transfer (Li et al., 2015; Zhai et al., 2013). Among the various conducting polymers, poly(3,4-ethylenedioxythiophene):poly(styrenesulfonate) (PEDOT:PSS) has been considered to be a interesting candidate for development of a conducting paper due to its homogeneous entrapment in/on a paper using a simple dip coating method with

* Corresponding authors.

E-mail addresses: lsh1@jbnu.ac.kr (S.H. Lee), bansi.malhotra@gmail.com (B.D. Malhotra).

enhanced stability. Moreover, the conductivity of PEDOT:PSS based paper can be significantly enhanced and tuned by treatment with a desired solvent. Further, doping with a nanomaterial may modulate the performance of paper in terms of electrochemical kinetics or signal stability and sensitivity. The reduced graphene oxide (RGO) has recently aroused much interest for development of electrochemical sensors. This is due to excellent electrochemical properties and large 2D surface area. Its abundant defects and chemical groups facilitate charge transfer and thus ensure increased electrochemical activity (Pumera, 2011). Hence incorporation of RGO in the PEDOT:PSS matrix may further improve electrochemical performance of a desired paper sensor (Gao et al., 2014; Zhang et al., 2014).

Cancer is currently a serious concern and a medical threat to the contemporary world. An estimated 14.1 million new cases of cancer and 8.2 million deaths were reported in 2012 necessitating early diagnosis of this dreaded disease (Cancer, 2012). Carcinoembryonic antigen (CEA) is known to be a tumor marker associated with colon, lung, ovarian and breast cancer that are responsible for more than half of all cancer deaths each year (Kulpa et al., 2002; Myers et al., 1978; Pepe et al., 2001; Wanebo et al., 1978). Determination of CEA in serum may be an interesting alternative for clinical diagnosis and monitoring of a cancer.

We report a facile method to obtain enhanced conductivity (~ 300 times) of PEDOT:PSS coated paper on treatment with ethylene glycol. Further, incorporation of RGO into the solution processed conducting paper results in improved electrochemical characteristics. This low cost, flexible and environment friendly conducting paper platform reveals high sensitivity towards a cancer biomarker (carcinoembryonic antigen, CEA) detection in the physiological range.

2. Materials and methods

2.1. Fabrication of PEDOT:PSS based conducting paper

The conducting paper ($1\text{ cm} \times 3\text{ cm}$) was prepared using a simple dip coating method. The PEDOT:PSS aqueous solution (1.3 wt%, PEDOT content 0.5 wt%, PSS content 0.8 wt%) purchased from SigmaAldrich was ultrasonicated prior to use after which 3% ethylene glycol (EG) was added to the aqueous suspension of PEDOT:PSS. This solution was used to dip coat the Whatman filter paper #1 (procured from GE healthcare UK) rendering it conductive. It was then dried in a hot air oven at 100°C and was termed as conducting paper.

2.2. Fabrication of PEDOT:PSS/RGO based electroactive paper

Preparation of the reduced graphene oxide (RGO) and PEDOT:PSS/RGO composite is given in Supporting information. The Whatman paper ($1\text{ cm} \times 1\text{ cm}$) was dipped in PEDOT:PSS/RGO aqueous suspension (PEDOT:PSS content 1.3 wt%, RGO content 0.035 wt%) containing 3% EG for 1 h and then dried at 100°C in a hot air oven. Thereafter it was treated with EG by dipping in the EG solution for 20 min. The EG treated conducting paper is finally dried at 100°C for about 1 h. A Schematic of the experiment has been demonstrated in Fig. 1.

2.3. Characterization

The conductivity of the conducting paper was measured using the four points probe technique with a low current source (LCS-02), digital microvoltmeter (DMV-001) and PID controlled oven (PID-200), SES Instruments, India. The surface morphology was investigated by the high-resolution field emission scanning electron microscopy (Nova Nano Sem450, FEI). The transmission electron microscopy (TEM) was carried out with a JEM-2200 FS (JEOL, Japan). X-ray photoelectron spectroscopy (XPS) studies were performed using Axis-Nova, Kratos Analytical Ltd., Manchester, UK. The electrochemical studies were carried out by an Autolab Potentiostat/Galvanostat (Metrohm, Netherlands) using a conventional three-electrode cell with the electroactive paper as working electrode, platinum as auxiliary electrode and Ag/AgCl as the reference electrode in phosphate buffer saline (PBS, 50 mM, pH 7.4) containing 5 mM $[\text{Fe}(\text{CN})_6]^{3-/4-}$.

3. Results and discussion

3.1. Electron microscopy and elemental analysis

Transmission electron micrograph of the RGO exhibits curved sheet like structure with a fairly smooth surface (Fig. 2A). The observed lighter and darker regions indicate the presence of RGO. The lighter region pertains to a few layered graphene whereas the darker region corresponds to the multilayered graphene. The wrinkles and folds pertaining to the graphene sheet (sub-microns in size) are clearly visible. The selected area electron diffraction (SAED) pattern of RGO reveals hexagonal atomic structure and crystalline nature of the RGO sheets (Fig. 2B). The inner six member ring represents the [1100] plane. The visible six diffraction spots corresponding to [0001] indicate hexagonal symmetry

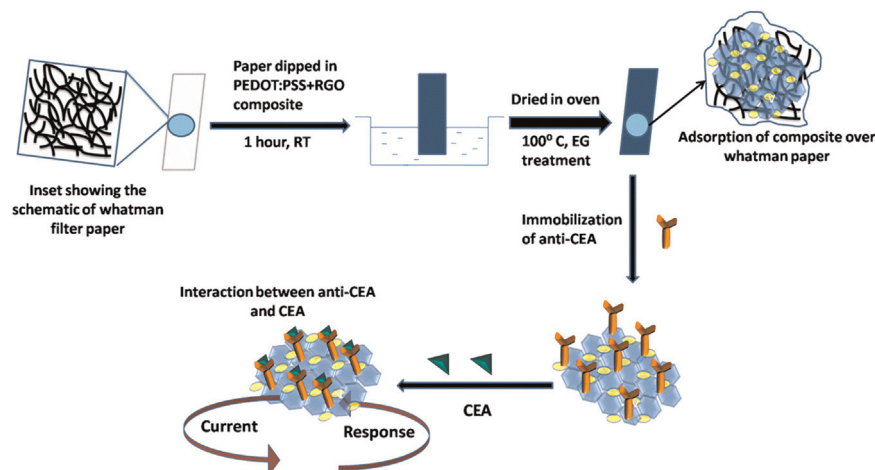


Fig. 1. Schematic of proposed electroactive paper sensor.

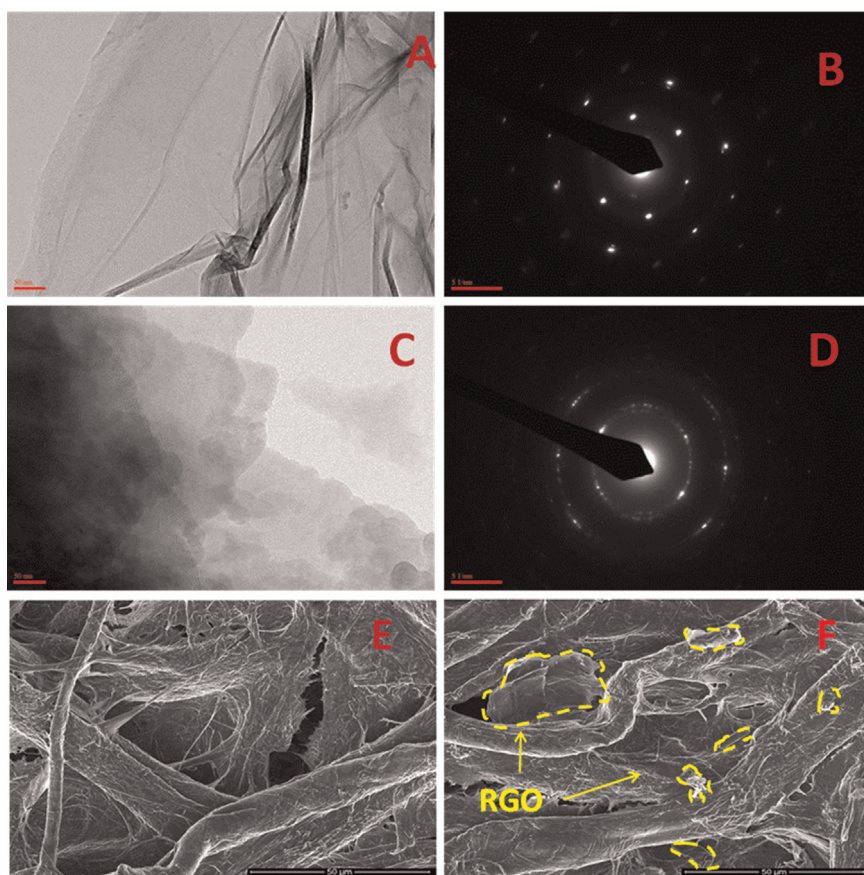


Fig. 2. (A) TEM image of synthesized reduced graphene oxide (RGO) where darker region corresponds to multilayer and lighter region corresponds to a few layer graphene. (B) SAED of RGO, which confirms the hexagonal atomic structure and crystalline nature of the sheets. (C) TEM image of PEDOT:PSS/RGO. (D) SAED pattern of PEDOT:PSS/RGO composite. (E) SEM of PEDOT:PSS adsorbed onto Whatman paper. (F) SEM of PEDOT:PSS/RGO Whatman coated paper.

of the [0001] diffraction of the RGO (Cui et al., 2011). The RGO sheets appear to be uniformly covered with PEDOT:PSS (Fig. 2C). The PSS molecules perhaps assist RGO dispersion via edge-to-face aromatic interactions between the RGO surface and the aromatic rings of the polymer which inhibit the hydrophobic graphene nanoplates from agglomeration, leading to a stable RGO dispersion in the polar solvent (Hyun et al., 2013). The diffused ring like structure observed (Fig. 2D) in the SAED pattern of PEDOT:PSS/RGO composite is because of the amorphous nature of PEDOT:PSS covering the RGO sheets. The SEM of PEDOT:PSS (Fig. 2E) coated paper indicates uniform adsorption of PEDOT:PSS over cellulose fibers of the paper. Because of the high porosity and tiny interfiber air spaces in Whatman paper, the PEDOT:PSS adsorbs into the paper through capillary action and after drying it produces uniform and stable film of PEDOT:PSS on the paper. Fig. 2F shows SEM of PEDOT:PSS/RGO coated paper. PEDOT:PSS/RGO is found to be uniformly adsorbed onto the cellulose fiber wherein some of RGO sheets are entangled in the fibrous network of Whatman paper. To further validate the formation of RGO, and its presence in PEDOT:PSS matrix, electron microscopic studies (SEM, elemental mapping and EDX) of RGO, PEDOT:PSS and PEDOT:PSS/RGO have been carried out (Supporting information Fig. S1).

3.2. Conductivity studies

The PEDOT:PSS coated paper shows conductivity of $1.16 \times 10^{-4} \text{ S cm}^{-1}$ (see Supporting information for conductivity calculation). However, on addition of 3% ethylene glycol (EG) in PEDOT:PSS solution, the value of conductivity increases to $1.43 \times 10^{-3} \text{ S cm}^{-1}$. This is due to decreased columbic interactions

between PEDOT and PSS molecules that perhaps contribute to reorientation of the polymer chains resulting in improved charge carrier mobility (Ouyang et al., 2005). Further, all studies have been done with PEDOT:PSS doped with 3% EG (Wei et al., 2013). The PEDOT:PSS doped with 3% EG coated Whatman paper has been termed as conducting paper.

The enhancement in the conductivity of PEDOT:PSS film (coated on glass substrate) has been recently reported when the film is dipped in methanol and H_2SO_4 (Alemu et al., 2012; Xia et al., 2012). This is due to ejection of the PSS ions from the PEDOT:PSS film dipped in the solvent, inducing the conformational rearrangement of PEDOT chains leading to higher conductivity. In the present case, effect of solvents such as methanol, H_2SO_4 and ethylene glycol (EG) on electrical conductivity of the conducting paper has been investigated (Supporting information Table S1). We have observed that on flexible substrate (Whatman paper 1), EG treatment shows the highest value of conductivity ($3.57 \times 10^{-2} \text{ S cm}^{-1}$) in comparison to methanol ($6.8 \times 10^{-3} \text{ S cm}^{-1}$), and H_2SO_4 ($8.1 \times 10^{-3} \text{ S cm}^{-1}$). This is in accordance with a similar report wherein the effect of flexibility of material and polyelectrolyte adhesion to substrate was studied (Podsiadlo et al., 2007). The increased flexibility of the EG treated conducting paper due to ejection of PSS results in the strong non-covalent cooperative interactions between PEDOT and cellulose molecules leading to higher conductivities. We have incorporated RGO in the PEDOT:PSS matrix for electrochemical studies since RGO exhibits excellent electrochemical properties (Pumera, 2011). PEDOT:PSS/RGO based conducting paper dipped in EG (electroactive paper) shows almost similar conductivity value ($3.12 \times 10^{-2} \text{ S cm}^{-1}$). The as-prepared electroactive paper shows greater degree of flexibility

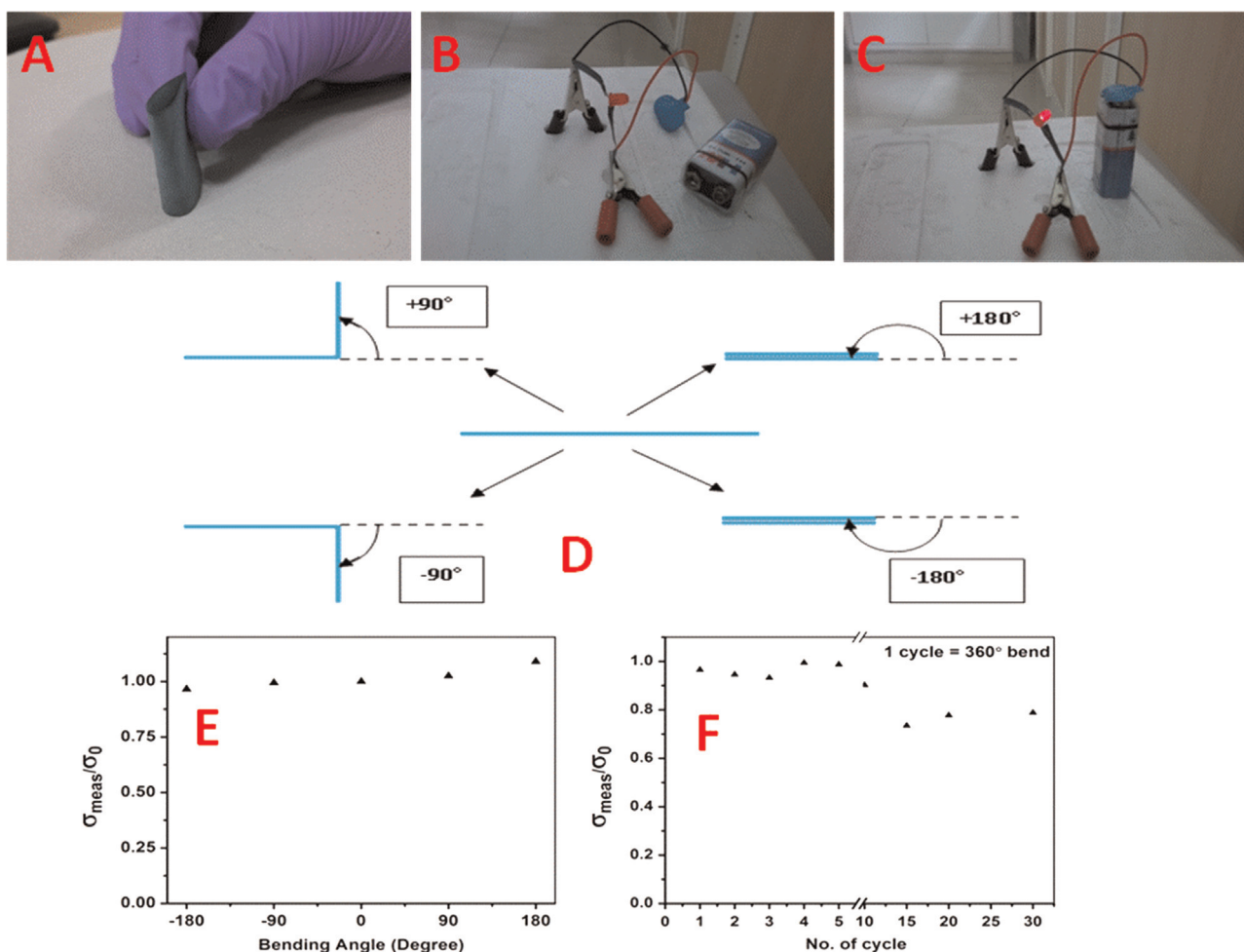


Fig. 3. Optical image of electroactive paper (A) foldable nature of electroactive paper (B, C) demonstration of LED emission when current flow through electroactive paper. Flexibility studies of PEDOT:PSS/RGO based electroactive electrode (D) Schematic diagram of electrode folding at different deformation angle. (E) The ratio of measured conductivity (σ_{meas}) to initial conductivity (σ_0) of electroactive paper with respect to folding angle. (F) The ratio of measured conductivity (σ_{meas}) to initial conductivity (σ_0) of electroactive paper versus folding cycle (1 cycle = 360°).

and efficient conductivity as demonstrated in Fig. 3.

The effect of folding (-180° to 180°), repeated folding and unfolding on conductivity of the electroactive paper has been investigated. Fig. 3D describes results of flexibility studies conducted on the electroactive electrode; wherein the positive and negative angles clearly reveal electrode folding in upward and downward direction, respectively. Relative conductivity [(ratio of measured conductivity (σ_{meas}) to initial conductivity (σ_0)] of electroactive electrode is measured as a function of folding angle. Fig. 3E displays variation of the relative conductivity of electroactive electrode indicating deviation of up to 4% under different folding angles. This reveals that electrodes are flexible and there is negligible change in the conductivity. The variation of relative conductivity of electrode with repeated cycle of folding and unfolding (manually) is shown in Fig. 3F. It may be noted that the conducting paper folded after 30 cycles (1 cycle = 360° rotation) shows decrease of about 20% in relative conductivity due to tearing of the cellulose threads. A video pertaining to the lighting of an LED lamp when current is passed through the multiple times folded electroactive paper is shown in Movie S1 in the Supporting information.

Fig. 4A presents Schematic of the observed mechanism, showing enhanced conductivity of the EG treated conducting paper. The conducting paper comprises of PEDOT:PSS polymer chains wherein PEDOT molecules present in the core of the insulating PSS are highly conductive in nature. On being treated with ethylene glycol, the core-shell structure of the conducting paper becomes

partially linear due to ejection of the PSS molecules. This exclusion of PSS from the surface is perhaps responsible for conformational changes in the polymer film that in turn results in increased conductivity. This has been further confirmed by Fourier transform infrared (FT-IR) spectroscopy and X-ray photoelectron spectroscopy (XPS) studies.

3.3. FT-IR and XPS analysis

FT-IR spectra of PEDOT:PSS/Whatman paper (curve i), conducting paper (curve ii) and conducting paper treated with EG (curve iii) are shown in Fig. 4B. FT-IR spectrum of PEDOT:PSS coated on Whatman paper (spectra i) exhibits characteristic absorption bands at near 670 cm^{-1} and 1060 cm^{-1} , corresponding to C-S and C-O stretching vibration of the thiophene ring in PEDOT (Ely et al., 2014). The bands at 1010 cm^{-1} , 1045 cm^{-1} and 1160 cm^{-1} represent SO_3^- symmetric and asymmetric stretching vibrations, respectively due to PSS (Alemu et al., 2012). The bands seen at 1392 cm^{-1} and 1537 cm^{-1} are due to C-C and C=C, respectively. In the FT-IR spectrum of conducting paper (curve ii), the intense absorption band at 1060 cm^{-1} is due to addition of EG that causes conformational changes in the polymer structure. The absorption band at 1104 cm^{-1} and 1160 cm^{-1} represents SO_3^- asymmetric stretching vibration whereas disappearance of SO_3^- symmetric stretching suggests molecular rearrangement in the PEDOT:PSS leading to increased electrical conductivity. These

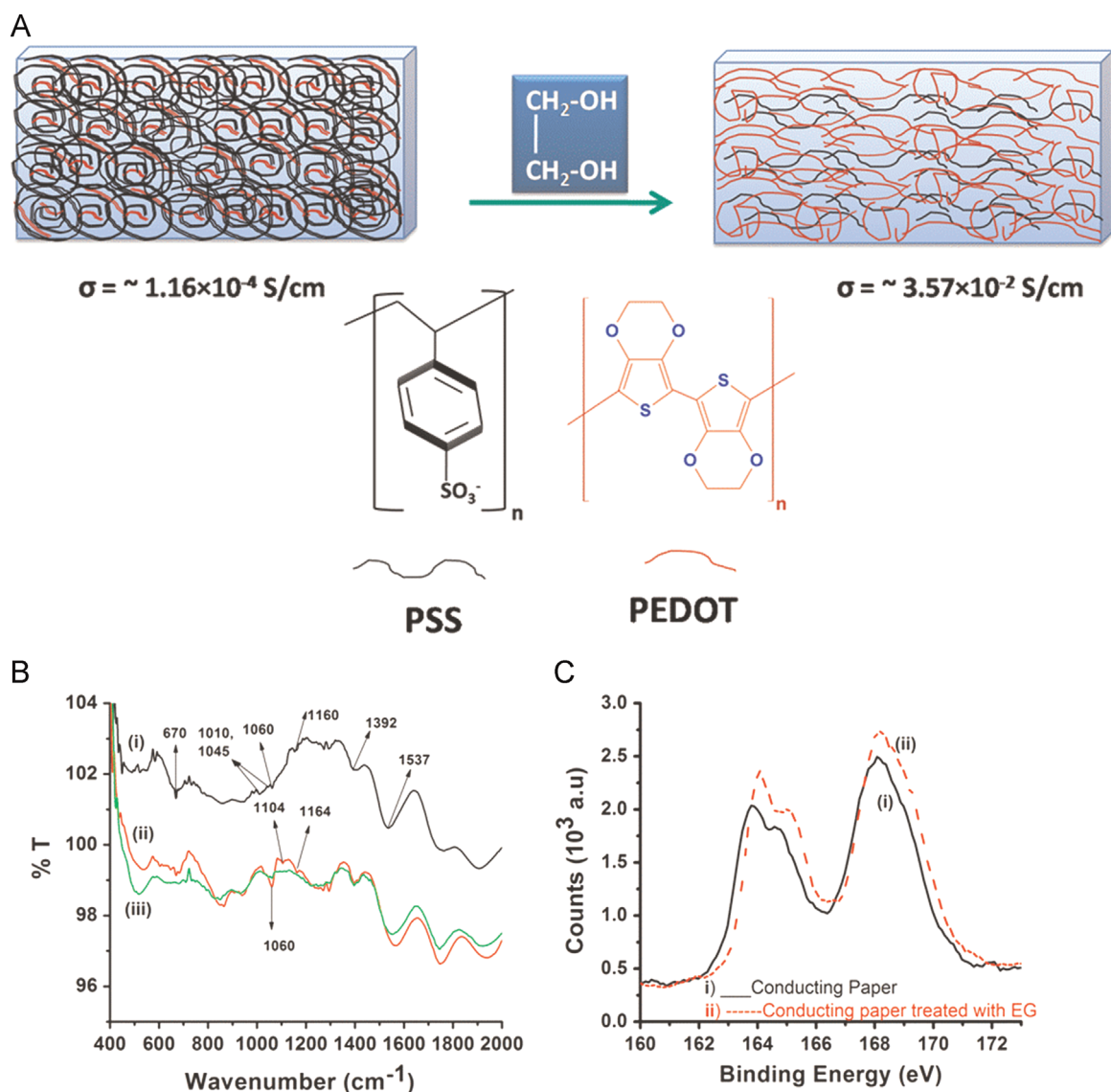


Fig. 4. (A) The schematic illustration of the mechanism of conductivity enhancement on conducting paper surface by EG treatment. (B) The FT-IR spectra of (i) PEDOT:PSS/Whatman paper (ii) conducting paper and (iii) conducting paper treated with EG. (C) X-ray photoelectron spectra (XPS) of (i) conducting paper and (ii) conducting paper treated with ethylene glycol.

results are in agreement with those observed for the conductivity measurements wherein increase in conductivity from $\sim 1.16 \times 10^{-4} \text{ S cm}^{-1}$ to $\sim 1.43 \times 10^{-3} \text{ S cm}^{-1}$ occurs when EG is added into PEDOT:PSS. In the FT-IR of the EG treated conducting paper (curve iii), the characteristic bands seen at 1104 cm^{-1} and 1160 cm^{-1} pertaining to the $-\text{SO}_3^-$ stretch of PSS are absent. This indicates removal of PSS from the conducting paper after EG treatment. This removal of PSS after EG treatment is perhaps responsible for the higher conductivity of the conducting paper due to increased exposure of PEDOT. FT-IR spectra of electroactive paper (Fig. S2(i) in Supporting information) indicate an additional broad absorption band at 1106 cm^{-1} that is attributed to C–OH stretching of graphene oxide. Further, the other observed IR bands are the same as seen in curve iii.

Fig. 4C shows XPS of i) conducting paper and ii) EG treated conducting paper. The S(2p) binding energy peak seen at 168 eV corresponds to sulfur due to the presence of PSS, and the doublet peak seen at 163.8 eV and 164.5 eV corresponds to the presence of sulfur in PEDOT (Crispin et al., 2006). The S2p XPS intensity ratio of PEDOT/PSS increases from 0.721 to 0.760 after the conducting paper is treated with EG. This change indicates the removal of

some PSS chains from the film. That may perhaps cause conformational change in PEDOT:PSS due to the transition from coiled to linear form leading to increased exposure of PEDOT chains (Fig. 3A) (Alemu et al., 2012). The change in C/S molar ratio evaluated from the scan spectra decreases from 9.63 to 8.17 after the conducting paper is treated with EG. This result is consistent with the removal of some PSS from the film. XPS of electroactive paper is shown in Fig. S2(ii) (see Supporting information). The S2p XPS intensity ratio of PEDOT/PSS present in electroactive paper increases to 0.82. However, the conductivity of electroactive paper is almost equivalent to that of the conducting paper after EG treatment. This may perhaps be attributed to the presence of discontinuous and non-uniform RGO sheet resulting in increased distance between PEDOT chains within the fiber network. Further, the C/S molar ratio increases to 10.1 due to the presence of carbon content of RGO.

3.4. Electrochemical studies

To investigate the charge transfer phenomenon at the conducting paper/solution interface, the electrochemical impedance

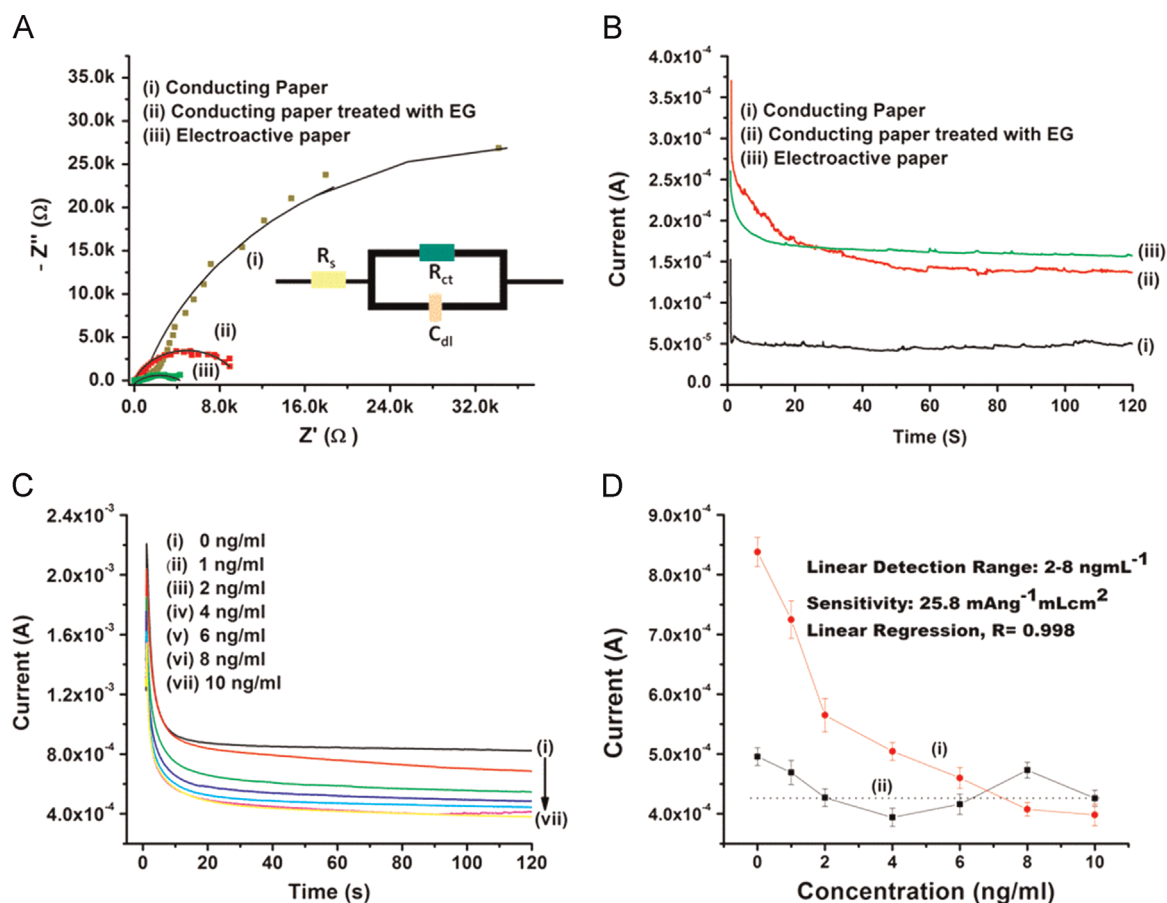


Fig. 5. Electrochemical studies conducted on paper electrode. (A) Electrochemical impedance spectra. (B) Chronoamperometry plot obtained for (i) conducting paper (ii) conducting paper treated with EG and (iii) electroactive paper. (C) Electrochemical response studies of anti-CEA immobilized electroactive paper at different concentration of CEA. (D) Calibration plot between the magnitudes of current recorded and CEA concentration (curve i); control experiment in absence of antibody (curve ii). Conducting paper: EG doped PEDOT: PSS solution coated onto whatman paper; Electroactive paper: EG and RGO doped PEDOT:PSS solution coated onto Whatman paper further treated with EG.

spectroscopy (EIS) studies have been conducted at biasing potential of 0.01 V in the frequency range, 100 kHz to 1 Hz. The Randles circuit is an equivalent electrical circuit that is commonly used to measure the electrochemical impedance comprising of an active electrolyte resistance R_s in series with R_{ct} (charge transfer resistance) in parallel combination of the double-layer capacitance C_{dl} or constant phase element (CPE) of a Faradaic reaction. The diameter of the semicircle in the Nyquist plot gives magnitude of the charge transfer resistance (R_{ct}) at the electrode surface (Daniels and Pourmand, 2007). Fig. 5A shows EIS of the (i) conducting paper, (ii) conducting paper treated with EG, and (iii) electroactive paper. Fig. 5A has been obtained using software (Nova) provided with the Autolab Potentiostat/Galvanostat. The curve fitting has been done assuming Randles circuit [$R_s(R_{ct} C_{dl})$] of the electrochemical cell. The various parameters related to the circuit element have been summarized in Table S2 alongwith % error [see Supplementary information sheet]. R_{ct} obtained for conducting paper is 48 kΩ which is maximum (curve i). However, the significant decrease in R_{ct} value up to 7 kΩ (curve ii) is observed in EG treated conducting paper. This is assigned to the conformational changes of the PEDOT:PSS chains from coiled to linear form leading to the higher conductivity due to enhanced electron transfer between solution/electrode interface. It is observed that the R_{ct} value further decreases to 2.8 kΩ (curve iii) in case of the electroactive paper. This may be attributed to excellent electrochemical properties and larger 2D surface area of RGO incorporated in the PEDOT:PSS matrix that increases the permeability of $[Fe(CN)_6]^{3-/4-}$ to the surface of paper electrode. The

heterogeneous electron transfer rate constant (K_{ct}) of EG treated conducting paper and electroactive paper has been calculated using Eq. (1) (Bardea et al., 2000)

$$K_{ct} = \frac{RT}{n^2 F^2 A R_{ct} [S]} \quad (1)$$

where R is the gas constant, T is absolute temperature, F is the Faraday constant, A is the electrode area (cm^2), $[S]$ is the concentration of redox probe (mol/cm^3) and n is the number of transferred electrons per molecule of the redox probe. The heterogeneous electron transfer rate constant (K_{ct}) value of the electroactive paper has been estimated as $1.9 \times 10^{-5} cm s^{-1}$ which is 2.5 times better as compared to conducting paper treated with EG ($7.6 \times 10^{-6} cm s^{-1}$). This indicates that the RGO present in electroactive paper electrode exhibits faster electron transfer kinetics as compared to the EG treated conducting paper. Thus the incorporation of RGO improves the electrochemical activity of the electroactive paper as compared to that of EG treated conducting paper.

Fig. 5B shows results of the chronoamperometric studies (current versus time) carried out on conducting paper and EG treated conducting paper at 2 V every 0.1 s. The higher value of the current observed for EG treated conducting paper electrode than that of conducting paper indicates increased electron transfer between solution and electrode due to conformational rearrangement in PEDOT polymeric chains. Further increase in the value of the electrochemical current in case of the electroactive paper electrode is attributed to the enhancement in permeability of the

redox couple $\{[\text{Fe}(\text{CN})_6]^{3-/4-}\}$ resulting due to RGO doping. It may be noted that electroactive paper electrode exhibits improved electrochemical performance and signal stability than that of the EG treated conducting paper. Keeping this in view, electroactive paper has been used to detect cancer biomarker, CEA. The monoclonal carcinoembryonic antibodies (anti-CEA) (procured from SigmaAldrich) are physically absorbed onto the PEDOT:PSS/RGO based electroactive paper (Fig. 1). The anti-CEA immobilized paper bioelectrode is washed with phosphate buffer (PBS, 50 mM, 0.9% NaCl; pH 7.4) to remove any unbound antibodies. Different concentrations of the carcinoembryonic antigen (CEA) ($1\text{--}10\text{ ng mL}^{-1}$) are prepared via further dilution of stock solution ($25\text{ }\mu\text{g mL}^{-1}$). The response studies of anti-CEA/electroactive paper obtained as a function of CEA concentration ($1\text{--}10\text{ ng mL}^{-1}$) have been carried out in phosphate buffer saline (PBS, 50 mM, pH 7.4) containing $5\text{ mM } [\text{Fe}(\text{CN})_6]^{3-/4-}$. $10\text{ }\mu\text{L}$ of diluted antigen solution is added into electrochemical cell for each antigen concentration. After adding each CEA concentration the current–time curve is recorded after every 300 s to ensure completion of the immunoreaction. The variation of the response current recorded as a function of CEA ($1\text{--}10\text{ ng mL}^{-1}$) is shown in Fig. 5C. The decrease in amperometric current occurs up to a maximum of 10 ng mL^{-1} . This can be attributed to the formation of antigen–antibody complex causing significant rearrangement over the electrode surface that diminishes charge transfer via $[\text{Fe}(\text{CN})_6]^{3-/4-}$ leading to reduction in amperometric current (Shim et al., 2008; Wang et al., 2009). Fig. 5D indicates the calibration plot obtained between response current and CEA

concentration (curve i). Interestingly, we obtained similar results between electrochemical current and CEA concentration via single shot incubation (different electrode was taken for each concentration) which is shown in Fig. S3. Furthermore, a control experiment was performed to check cross reactivity of the electroactive paper with CEA antigen in the absence of antibodies (curve ii). However, no significant change in current response was observed for the electroactive paper in the absence of antibodies as a function of CEA concentration. A linear relationship is observed in the range $2\text{--}8\text{ ng mL}^{-1}$ with a sensitivity of $25.8\text{ }\mu\text{A ng}^{-1}\text{ mL cm}^{-2}$ and follows Eq. (2)

$$I(A) = -25.8\text{ }\mu\text{A mL ng}^{-1} \times [\text{CEA concentration}] + 613.5\text{ }\mu\text{A};$$

$$R^2 = 0.998 \quad (2)$$

We have compared the sensing performance of the electroactive paper with the conducting paper treated with EG. For this, the electrochemical response studies have been carried out on the anti-CEA immobilized conducting paper treated with EG, in the presence of different concentrations of antigen ($1\text{--}10\text{ ng mL}^{-1}$) (see Supporting information Fig. S4). It is found that the electroactive paper is almost 6 times more sensitive than the conducting paper treated with EG for CEA detection.

3.5. Stability, selectivity and reproducibility studies

Fig. 6A shows variation of response current of the immunoelectrode (anti-CEA immobilized electroactive paper) taken at a regular interval of 2 days. It has been found that current value

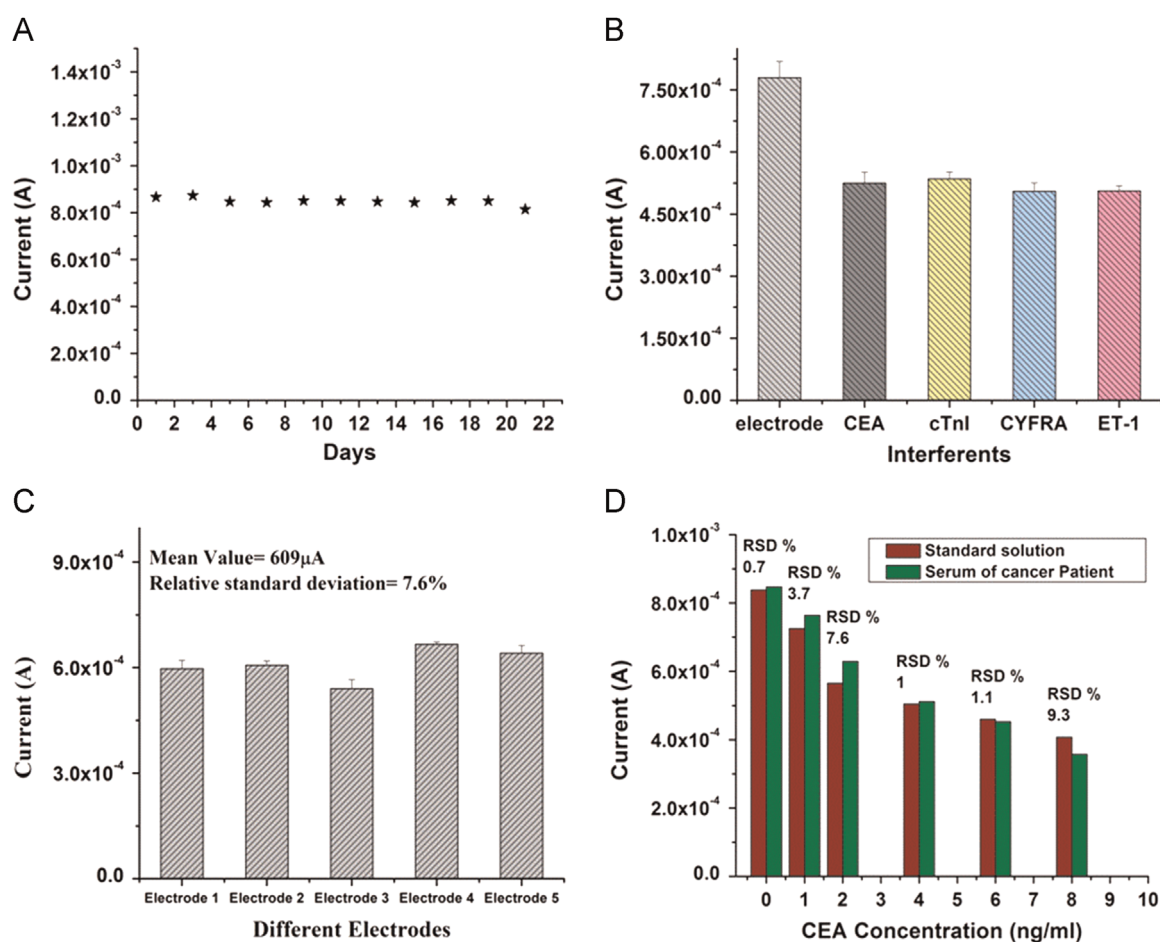


Fig. 6. (A) Electrochemical current response of anti-CEA immobilized electroactive paper electrode (immunoelectrode) measured as a function of time (day). (B) Electrochemical current response of immunoelectrode in the presence of other analytes. (C) Electrochemical current response of different immunoelectrode fabricated via the same set of procedure in the presence of CEA (2 ng mL^{-1}) and (D) CEA concentration values obtained by immunoassay and the electroactive paper method.

decreases to $\sim 7\%$ after 21 days. This indicates that the paper sensor exhibits good stability up to 21 days. The selectivity study of this paper sensor has been investigated in the presence of cardiac troponin I (cTnI), cytokeratin-19 fragment (CYFRA-21-1), and endothelin-1 protein (ET-1) (2 ng mL^{-1}). Fig. 6B shows decrease in current response on addition of CEA (2 ng mL^{-1}) after which we do not observe any significant current change on addition of another antigen indicating high selectivity of the biosensor. The reproducibility of the five different immunoelectrodes fabricated under similar conditions has been investigated in the presence of 2 ng mL^{-1} CEA concentration (Fig. 6C). It is found that this paper electrode shows good reproducibility for five different electrodes with constant surface area as is evident by low value of relative standard deviation (RSD) of 7.6% (mean value = $609 \mu\text{A}$). Further each measurement (Fig. 6C) has been repeated 4 times for each electrode and error bars are included accordingly. The low RSD obtained for each electrode (less than 5%) indicates appreciable repeatability of the biosensor.

3.6. Real sample analysis

The results obtained for serum sample of cancer patients using this electroactive paper sensor have been validated using ELISA. The blood samples collected from patient and processed at the Rajiv Gandhi Cancer Institute & Research Centre (RGCI & RC) in Rohini, Delhi, India. Concentration of CEA in the serums of cancer patients was measured at RGCI&RC using the VITROS CEA reagent Pack and the VITROS CEA Calibrators on the VITROS ECI/ECiQ Immunodiagnostic Systems, VITROS 3600 Immunodiagnostic System and VITROS 5600 Integrated System using Intellicheck[®] Technology. It can be seen that a reasonable correlation occurs between the CEA concentration value obtained by immunoassay and the electroactive paper based electrochemical method (Fig. 6D). As shown in Fig. 6D, the electroactive paper affords good recoveries and acceptable relative standard deviation.

The sensing characteristics of the electroactive paper based electronic paper sensor have been summarized in Table S3 along with those reported in the literature. It may be noted that this low cost flexible electroactive paper sensor can be easily decomposed by simple incineration (see Movie S2). Keeping in view the production of the medical diagnostics kits, this is an added advantage of this new environment friendly disposable electroactive paper sensor.

4. Conclusions

We have demonstrated a flexible and highly conducting paper sensor, based on composite of poly(3,4-ethylenedioxythiophene):poly(styrenesulfonate) (PEDOT:PSS) and reduced graphene oxide (RGO). It is found that conductivity of the PEDOT:PSS conducting paper increases by ~ 300 times when it is treated with ethylene glycol. The incorporation of RGO in PEDOT:PSS conducting paper film indicates excellent electrochemical activity and faster charge transfer kinetics. In order to further improve the performance of conducting paper, suitable selection of solvent and dopant should be investigated. This low cost, flexible and environment friendly conducting paper has been used for cancer biomarker detection. The fabricated PEDOT:PSS/RGO based electroactive paper shows sensitivity of $25.8 \mu\text{A ng}^{-1} \text{ mL cm}^{-2}$ in the detection range of $2\text{--}8 \text{ ng mL}^{-1}$. The results obtained for serum samples of cancer patients using this paper based sensor have been validated using ELISA. This simple, low cost, flexible and disposable electroactive paper based platform has immense potential for point of care biosensors, flexible electronics and energy storage devices etc.

Acknowledgments

We thank Prof. Pradeep Kumar, Vice Chancellor Delhi Technological University (DTU), Delhi, India for providing the facilities. Saurabh Kumar and Suveen Kumar are thankful to DTU for the award of financial assistance. S. Srivastava acknowledges University Grant Commission, India for providing Dr. D. S. Kothari Postdoctoral fellowship [No. F.4-2/2006 (BSR)/PH/13-14/0098]. This Research was partially supported by the Basic Research Laboratory Program (2014R1A4A1008140) through the Ministry of Science, ICT & Future Planning through the National Research Foundation of Korea (NRF) funded by Ministry of Education.

Appendix A. Supplementary material

Supplementary data associated with this article can be found in the online version at <http://dx.doi.org/10.1016/j.bios.2015.05.040>.

References

- Alemu, D., Wei, H.-Y., Ho, K.-C., Chu, C.-W., 2012. Highly conductive PEDOT:PSS electrode by simple film treatment with methanol for ITO-free polymer solar cells. *Energy Environ. Sci.* 5 (11), 9662–9671.
- Bardea, A., Katz, E., Willner, I., 2000. Probing antigen–antibody interactions on electrode supports by the biocatalyzed precipitation of an insoluble product. *Electroanalysis* 12 (14), 1097–1106.
- Cancer, I.A.F.R.O., 2012. World Cancer Factsheet. World Health Organization (<http://www.cancerresearchuk.org>).
- Crispin, X., Jakobsson, F., Crispin, A., Grim, P., Andersson, P., Volodin, A., Van Haeendonck, C., Van der Auweraer, M., Salaneck, W.R., Berggren, M., 2006. The origin of the high conductivity of poly (3, 4-ethylenedioxythiophene)-poly (styrenesulfonate)(PEDOT-PSS) plastic electrodes. *Chem. Mater.* 18 (18), 4354–4360.
- Cui, P., Lee, J., Hwang, E., Lee, H., 2011. One-pot reduction of graphene oxide at subzero temperatures. *Chem. Commun.* 47 (45), 12370–12372.
- Daniels, J.S., Pourmand, N., 2007. Label-free impedance biosensors: opportunities and challenges. *Electroanalysis* 19 (12), 1239–1257.
- Dhand, C., Das, M., Datta, M., Malhotra, B., 2011. Recent advances in polyaniline based biosensors. *Biosens. Bioelectron.* 26 (6), 2811–2821.
- Ely, F., Matsumoto, A., Zoetebier, B., Peressinotto, V.S., Hirata, M.K., de Sousa, D.A., Maciel, R., 2014. Handheld and automated ultrasonic spray deposition of conductive PEDOT:PSS films and their application in AC EL devices. *Org. Electron.* 15 (5), 1062–1070.
- Gao, Y., Li, J., Yang, X., Xiang, Q., Wang, K., 2014. Electrochemiluminescence biosensor based on PEDOT-PSS-graphene functionalized ITO electrode. *Electroanalysis* 26 (2), 382–388.
- Gervais, L., De Rooij, N., Delamarche, E., 2011. Microfluidic chips for point-of-care immunodiagnostics. *Adv. Mater.* 23 (24), H151–H176.
- Hyun, W.J., Park, O.O., Chin, B.D., 2013. Foldable graphene electronic circuits based on paper substrates. *Adv. Mater.* 25 (34), 4729–4734.
- Jagadeesan, K.K., Kumar, S., Sumana, G., 2012. Application of conducting paper for selective detection of troponin. *Electrochem. Commun.* 20, 71–74.
- Kulpa, J., Wójcik, E., Reinfuss, M., Kołodziejski, L., 2002. Carcinoembryonic antigen, squamous cell carcinoma antigen, CYFRA 21-1, and neuron-specific enolase in squamous cell lung cancer patients. *Clin. Chem.* 48 (11), 1931–1937.
- Kumar, S., Jagadeesan, K.K., Joshi, A.G., Sumana, G., 2013a. Immuno-CoPS (conducting paper strips) for futuristic cost-effective cancer diagnostics. *RSC Adv.* 3 (29), 11846–11853.
- Kumar, S., Kumar, S., Ali, M., Anand, P., Agrawal, V.V., John, R., Maji, S., Malhotra, B. D., 2013b. Microfluidic-integrated biosensors: prospects for point-of-care diagnostics. *Biotechnol. J.* 8 (11), 1267–1279.
- Li, L., Wang, Y., Pan, L., Shi, Y., Cheng, W., Shi, Y., Yu, G., 2015. A nanostructured conductive hydrogels-based biosensor platform for human metabolite detection. *Nano Lett.* 15 (2), 1146–1151.
- Luppa, P.B., Müller, C., Schlichtiger, A., Schlebusch, H., 2011. Point-of-care testing (POCT): current techniques and future perspectives. *TrAC Trends Anal. Chem.* 30 (6), 887–898.
- Myers, R.E., Sutherland, D.J., Meakin, J.W., Kellen, J.A., Malkin, D.G., Malkin, A., 1978. Carcinoembryonic antigen in breast cancer. *Cancer* 42 (S3), S1520–S1526.
- Ouyang, J., Chu, C.W., Chen, F.C., Xu, Q., Yang, Y., 2005. High-conductivity poly (3, 4-ethylenedioxythiophene): poly (styrene sulfonate) film and its application in polymer optoelectronic devices. *Adv. Funct. Mater.* 15 (2), 203–208.
- Pepe, M.S., Etzioni, R., Feng, Z., Potter, J.D., Thompson, M.L., Thornquist, M., Winget, M., Yasui, Y., 2001. Phases of biomarker development for early detection of cancer. *J. Natl. Cancer Inst.* 93 (14), 1054–1061.

- Podsiadlo, P., Tang, Z., Shim, B.S., Kotov, N.A., 2007. Counterintuitive effect of molecular strength and role of molecular rigidity on mechanical properties of layer-by-layer assembled nanocomposites. *Nano Lett.* 7 (5), 1224–1231.
- Pumera, M., 2011. Graphene in biosensing. *Mater. Today* 14 (7), 308–315.
- Shim, B.S., Chen, W., Doty, C., Xu, C., Kotov, N.A., 2008. Smart electronic yarns and wearable fabrics for human biomonitoring made by carbon nanotube coating with polyelectrolytes. *Nano Lett.* 8 (12), 4151–4157.
- Tobjörk, D., Österbacka, R., 2011. Paper electronics. *Adv. Mater.* 23 (17), 1935–1961.
- Wanebo, H.J., Rao, B., Pinsky, C.M., Hoffman, R.G., Stearns, M., Schwartz, M.K., Oettgen, H.F., 1978. Preoperative carcinoembryonic antigen level as a prognostic indicator in colorectal cancer. *N. Engl. J. Med.* 299 (9), 448–451.
- Wang, J., 2006. Electrochemical biosensors: towards point-of-care cancer diagnostics. *Biosens. Bioelectron.* 21 (10), 1887–1892.
- Wang, L., Chen, W., Xu, D., Shim, B.S., Zhu, Y., Sun, F., Liu, L., Peng, C., Jin, Z., Xu, C., 2009. Simple, rapid, sensitive, and versatile SWNT – paper sensor for environmental toxin detection competitive with ELISA. *Nano Lett.* 9 (12), 4147–4152.
- Wei, Q., Mukaida, M., Naitoh, Y., Ishida, T., 2013. Morphological change and mobility enhancement in PEDOT:PSS by adding co-solvents. *Adv. Mater.* 25 (20), 2831–2836.
- Xia, Y., Sun, K., Ouyang, J., 2012. Solution-processed metallic conducting polymer films as transparent electrode of optoelectronic devices. *Adv. Mater.* 24 (18), 2436–2440.
- Zhai, D., Liu, B., Shi, Y., Pan, L., Wang, Y., Li, W., Zhang, R., Yu, G., 2013. Highly sensitive glucose sensor based on Pt nanoparticle/polyaniline hydrogel heterostructures. *ACS Nano* 7 (4), 3540–3546.
- Zhang, M., Yuan, W., Yao, B., Li, C., Shi, G., 2014. Solution-processed PEDOT:PSS/Graphene composites as the electrocatalyst for oxygen reduction reaction. *ACS Appl. Mater. Interfaces* 6 (5), 3587–3593.

PAPER



Cite this: *J. Mater. Chem. B*, 2015, **3**, 9305

A solution processed carbon nanotube modified conducting paper sensor for cancer detection†

Saurabh Kumar,^a Magnus Willander,^b Jai G. Sharma^a and Bansi D. Malhotra^{*a}

A solution processed poly(3,4-ethylenedioxythiophene):poly(styrenesulfonate) (PEDOT:PSS)–carbon nanotube (CNT) nano-composite has been utilized for the fabrication of a conducting paper (CP) *via* dip coating. Further, high conductivity of this paper (from $\sim 6.5 \times 10^{-4}$ to $2.2 \times 10^{-2} \text{ S cm}^{-1}$) obtained by treating it with formic acid (CNT/FA@CP) is due to the removal of the non-conducting PSS molecules from its surface. This smart conducting platform has been used for the conjugation of the anti-carcinoembryonic antigen (CEA) protein for quantitative estimation of CEA, a cancer biomarker. Transmission electron microscopy (TEM), Raman spectroscopy, X-ray diffraction (XRD), scanning electron microscopy (SEM), X-ray photoelectron spectroscopy (XPS), electrochemical impedance spectroscopy (EIS) and amperometric techniques have been used to characterize the low cost, flexible and environmentally friendly conducting BSA/anti-CEA/CNT/FA@CP paper electrode that is found to be highly sensitive ($7.8 \mu\text{A ng}^{-1} \text{ ml cm}^{-2}$) in the physiological range ($2\text{--}15 \text{ ng ml}^{-1}$) of CEA. The response of the paper electrode is validated using CEA concentration of serum samples of cancer patients obtained *via* the immunoassay technique.

Received 17th October 2015,
Accepted 11th November 2015

DOI: 10.1039/c5tb02169c

www.rsc.org/MaterialsB

1. Introduction

Cancer occurs due to uncontrolled growth and spread of abnormal cells and is currently a medical threat to the mankind. According to a recent report, there have been 8.2 million cancer deaths, 14.1 million new cancer cases and 32.6 million people are living with cancer necessitating its early detection.^{1,2} Carcinoembryonic antigen (CEA) is an important biomarker for the diagnosis and routine monitoring of cancer. The human CEA gene family is clustered on chromosome 19q and it comprises of 29 genes.³ CEA (a glycoprotein), comprising of $\sim 60\%$ carbohydrates having a molecular mass of $\sim 180\text{--}200 \text{ kDa}$, is one of the most widely used cancer biomarker. It plays an important role in early monitoring, screening and disease recurrence. The existing techniques, including cytopathology, biopsy, enzyme linked immunosorbent assay, and visualization adjuncts, can be used for the detection and monitoring of cancer.^{4,5} These methods are invasive, time-consuming, expensive and require highly skilled personnel. In this context, biosensors offer a simple, reliable, and user friendly detection strategy with increased assay speed, high sensitivity, low cost and require low sample volume.^{6,7}

For the fabrication of biosensors, indium tin oxide, glassy carbon and gold electrodes can be used as the substrates. These electrodes are of high cost, are rigid, brittle, and their fabrication requires high temperature processing and expertise. Besides this, disposability of these materials continues to be a major challenge. Therefore, there is increased demand for the development of a paper based biosensor for clinical application as these are predicted to be simple, low cost, flexible, lightweight, and biocompatible.^{8–10} A conducting paper has been found to play an important role in the ongoing transition to the development of paper based electrochemical biosensors. Coupling of paper electronic devices (*e.g.* electrodes and transistors) with biological systems provides an efficient platform for the conduction of both electronic and ionic charge carriers that play a major role for communication with a desired biomolecule.^{11–14} Many methods including inkjet printing, screen printing, and spin coating to modify the paper substrate can be utilized for making a paper conducting. Manekkathodi *et al.* deposited a thin film of ZnO by spin coating on paper and used it for the fabrication of the flexible diode and UV photodetectors.¹⁵ Määttänen *et al.* utilized the inkjet printing method for the fabrication of a gold electrode over the paper substrate. Further a poly(3,4-ethylenedioxythiophene) (PEDOT) layer was electropolymerized over the gold coated paper electrode for glucose detection.¹⁶ Kumar *et al.* reported a screen printing method for producing graphite and a silver ink pattern on the paper substrate. These authors electrochemically deposited polyaniline over the screen printed paper electrode for cancer biomarker (sIL2R α) detection.¹⁷ Ge *et al.* used carbon nanotubes

^a Nanobioelectronics Laboratory, Department of Biotechnology, Delhi Technological University, Shahbad Daulatpur, Delhi-110042, India.
E-mail: bansi.malhotra@gmail.com; Fax: +91-011-45609310;
Tel: +91-011-45609152

^b Department of Science and Technology, Linköping University, SE-60174, Sweden

† Electronic supplementary information (ESI) available. See DOI: 10.1039/c5tb02169c

and a glutaraldehyde modified paper to fabricate the electrode array of Ag/AgCl reference and carbon counter electrode for cancer biomarker detection.¹⁸ Su *et al.* reported a gold nanoparticle modified paper device for aptamer based detection of cancer cells and *in situ* anticancer drug screening.¹⁹ These techniques require skilled personnel, costly conducting ink (gold, silver and graphite) paste and equipments, and are time-consuming.

Conducting polymers (CPs) are promising candidates for fabricating a conducting paper due to their low cost, mechanical flexibility and solution processability.²⁰ Poly(3,4-ethylenedioxythiophene:poly(4-styrenesulfonate) (PEDOT:PSS) has emerged as an interesting conducting material due to its film forming ability, thermal stability and homogenous adsorption on a paper by a simple dip coating method.^{21,22} PEDOT:PSS consists of hydrophobic and conducting PEDOT-rich grains encapsulated by hydrophilic and insulating PSS-rich shells. The conductivity of the PEDOT:PSS can be tuned by chemical modification that depends on nature and the degree of doping.^{23–26} There is a great deal of scope to improve the performance of a conducting paper sensor by integrating it with nanomaterials. In this context, carbon nanotubes have aroused much interest for applications in electrochemical biosensors. This is due to their excellent electrochemical properties, large surface area, ballistic electron transport and high mechanical strength.^{27,28} In addition to enhanced electrochemical reactivity, CNT-modified electrodes can be utilized to immobilize biomolecules and to minimize surface fouling.²⁹ These properties make CNTs widely attractive for the fabrication of electrochemical biosensors.

We report a facile method to obtain enhanced conductivity of a PEDOT:PSS coated paper on treatment with formic acid. Doping of CNTs into the solution processed conducting paper results in improved electrochemical characteristics of the paper electrode. This low cost, flexible and environmentally friendly CNT modified conducting paper has been utilized for the detection of a cancer biomarker (carcinoembryonic antigen, CEA).

2. Materials and methods

(I) Chemicals and reagents

PEDOT:PSS (1.3 wt%, PEDOT content: 0.5wt%, PSS content: 0.8 wt%), carcinoembryonic antibody monoclonal (anti-CEA), carcinoembryonic antigen (CEA), 1-ethyl-(dimethylaminopropyl)-carbodiimide hydrochloride (EDC), *N*-hydroxysuccinimide (NHS) and bovine serum albumin (BSA) were procured from Sigma Aldrich, India. All other chemicals like ethylene glycol and formic acid were of analytical grade and procured from Thermo Fisher Scientific, India. The deionized water obtained from Millipore water purification system was used for the preparation of buffers and solution. The Whatman Filter paper #1 (GE healthcare, UK) was used as a substrate for adsorption of PEDOT:PSS with a thickness of 0.18 mm. The carboxy functionalized CNTs were a gift and used without purification.

(II) Fabrication of the PEDOT:PSS based conducting paper

The PEDOT:PSS aqueous solution doped with 5% EG was used to fabricate the conducting paper. The Whatman Paper #1 (1 cm × 3 cm) was dipped in aqueous suspension of PEDOT:PSS (1.3 wt%, 5% ethylene glycol) for 1 h and was then dried at 100 °C in a hot air oven, and was termed as a conducting paper (CP) after which it was further treated with formic acid by dipping it in formic acid for 20 min. The formic acid (FA) treated conducting paper (FA@CP) was finally dried at 100 °C for about 1 h.

(III) Fabrication of the CNT doped conducting paper (CNT/FA@CP)

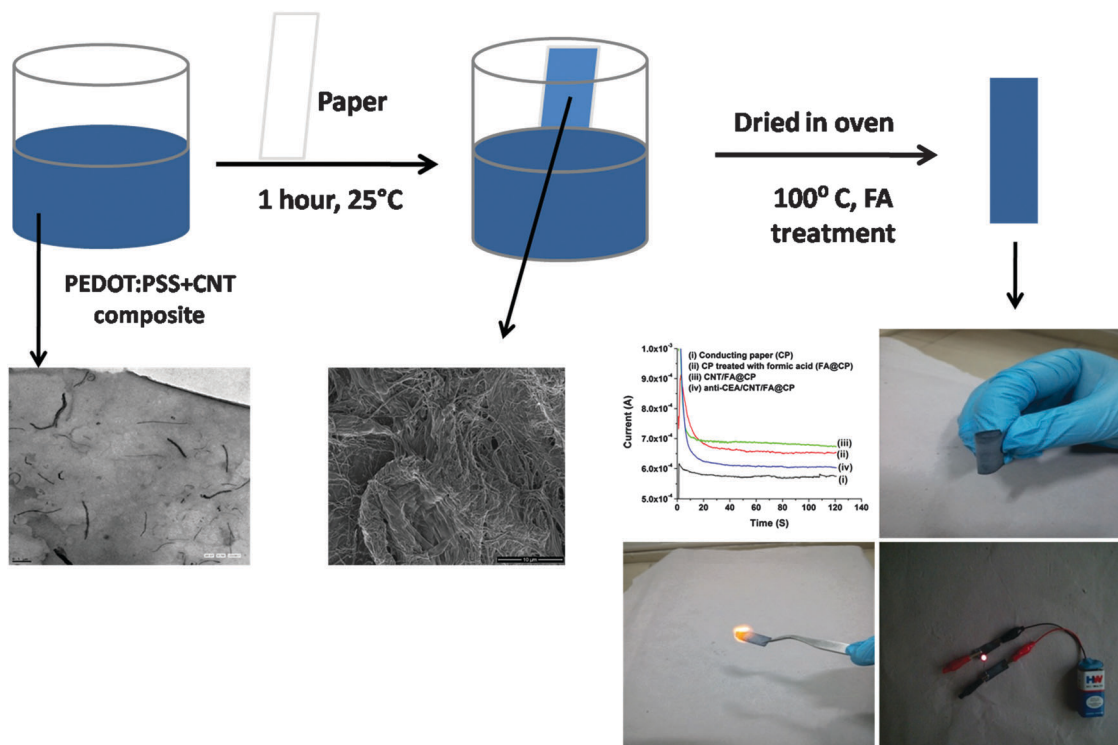
First, 5 mg CNTs was doped into 10 ml of PEDOT:PSS aqueous solution (1.3 wt%, 5% EG). Next, a PEDOT:PSS/CNT composite (1.3 wt%, 5% EG, 0.05 wt% CNT) was ultrasonicated for 1 h. It was found that CNTs got highly dispersed without sedimentation in the PEDOT:PSS solution. Further, Whatman paper #1 was dipped in the PEDOT:PSS/CNT composite for 1 h and was then dried at 100 °C in a hot air oven after which it was further treated with formic acid by dipping it in formic acid for 20 min. The formic acid treated conducting paper was finally dried at 100 °C for about 1 h. A schematic of the experiment is demonstrated in Scheme 1.

(IV) Fabrication of a paper sensor (anti-CEA/CNT/FA@CP)

Anti-CEA monoclonal (20 µL, 100 µg ml⁻¹) antibodies were immobilized over the CNT doped conducting paper treated with the formic acid electrode (CNT/FA@CP) *via* the formation of a covalent bond between the carboxylic group of CNTs and the NH₂-terminal of the antibody *via* an EDC-NHS coupling reaction. The anti-CEA was physically adsorbed over the CNT/FA@CP electrode *via* electrostatic interactions between biomolecules and the conducting paper. The electrode was then rinsed with phosphate buffer (PBS, 50 mM, pH 7.2, 0.9% NaCl) to remove any unbound antibodies. 0.1% of bovine serum albumin (BSA) in PBS was added to the antibody-modified electrode to block unspecific sites. After rinsing again with PBS, the electrodes were stored at 4 °C before carrying out the sensing studies.

(V) Characterization

The CNT/PEDOT:PSS nanocomposite was characterized using transmission electron microscopy (Tecnai G2 30, Ultratwin microscope), Raman spectroscopy (Varian 7000 FT-Raman) and X-ray diffraction spectroscopy (Bruker D-8 Advance, Cu K α , λ = 1.5406 Å). The surface morphology was investigated by scanning electron microscopy (Nova Nano Sem450 and Carl Zeiss, EVO15). The conductivity of the conducting paper was measured using the four point probe technique with a low current source (LCS-02), digital microvoltmeter (DMV-001) and PID controlled oven (PID-200), SES Instruments, India. The effect of solvent on the PEDOT:PSS structure was investigated by X-ray photoelectron spectroscopy (XPS) (Scienta ESCA 200). The electrochemical studies were carried out by an Autolab Potentiostat/Galvanostat (Metrohm, Netherlands) using a conventional three-electrode



Scheme 1 Fabrication and characterization of a CNT/FA@CP modified paper electrode.

cell with the paper electrode as a working electrode, platinum wire as an auxiliary electrode and Ag/AgCl as the reference electrode in phosphate buffer saline (PBS, 50 mM, pH 7.4) containing 5 mM $[\text{Fe}(\text{CN})_6]^{3-/4-}$.

3. Results and discussion

Fig. 1a shows the TEM image of CNTs indicating a linear and a tubular structure with a few microns in length. The tubular structure with diameter ranging from ~ 25 – 30 nm can be seen in the inset of Fig. 1a. It appears that CNTs are uniformly dispersed in PSS *via* non-covalent stabilization. The hydrophobic portion of polymeric chains appear to cover the carbon nanotube surface *via* edge-to-face aromatic interactions whereas the hydrophilic part interacts with water molecules to make homogeneous dispersion of CNTs.³⁰ A TEM image of PEDOT:PSS–CNT nanocomposite is shown in Fig. 1b wherein uniformly dispersed CNTs are clearly visible at the PEDOT:PSS surface. The Raman peaks seen at 1259 cm^{-1} , 1368 cm^{-1} , and 1441 cm^{-1} are associated with C–C in-plane symmetric stretching, C–C stretching deformation and $\text{C}_\alpha=\text{C}_\beta$ symmetric stretching vibration respectively. The $\text{C}_\alpha=\text{C}_\beta$ asymmetric stretching vibration gives rise to bands at 1504 and 1562 cm^{-1} , corresponding to thiophene rings in the middle and at the end of the chains (Fig. 1c).^{31,32} The inset in Fig. 1c shows a characteristic peak of CNTs at 1347 cm^{-1} due to a D band and 1575 cm^{-1} attributed to a G band.²⁹ The Raman spectrum of the PEDOT:PSS/CNT hybrid shows peak shift from 1368 to 1361 cm^{-1} and 1562 to 1570 cm^{-1} indicating existence of interactions between the CNTs and the

conjugated thiophene ring of PEDOT:PSS, that can be associated with electronic density transfer between constituents.^{31,32} Similarly XRD spectra also shows a sharp peak centered on 2θ value 26.2° corresponding to the (002) plane of CNTs (inset of Fig. 1d shows XRD of CNTs) confirming the presence of CNTs in the PEDOT:PSS amorphous polymer.³³

The surface morphology of various modified electrodes was investigated using scanning electron microscopy (SEM) (Fig. 2). Image (a) shows SEM of the PEDOT:PSS coated paper, wherein the conducting polymer is found to be uniformly adsorbed over the cellulose fibers of the paper. However, morphology of the PEDOT:PSS–CNT coated paper (Image b) suggests that CNTs are incorporated throughout the surface. Most CNTs are entangled with PEDOT:PSS and cellulose fibers while some of these are clearly visible on the surface of the polymer coated paper. The SEM image of CNT/PEDOT:PSS onto an ITO glass substrate confirms the presence of CNTs in PEDOT:PSS film (Fig. S1 in the ESI[†]). However, after antibody functionalization (image c), surface morphology of the PEDOT:PSS–CNT coated paper electrode exhibits a shiny appearance due to accumulation of the static charge, indicating successful immobilization of the antibodies. It appears that the antibody molecules cover the pores of the PEDOT:PSS–CNT coated paper surface.

The PEDOT:PSS coated paper shows an electrical conductivity of $6.5 \times 10^{-4}\text{ S cm}^{-1}$ whereas after doping with 5% ethylene glycol, the conductivity increases to $2.1 \times 10^{-3}\text{ S cm}^{-1}$. This is attributed to decreased coulombic interactions between the positively charged PEDOT molecules and the negatively charged PSS that facilitate reorientation of the polymer chains resulting in enhanced charge carrier mobility. The increased crystal ordering and crystal size on

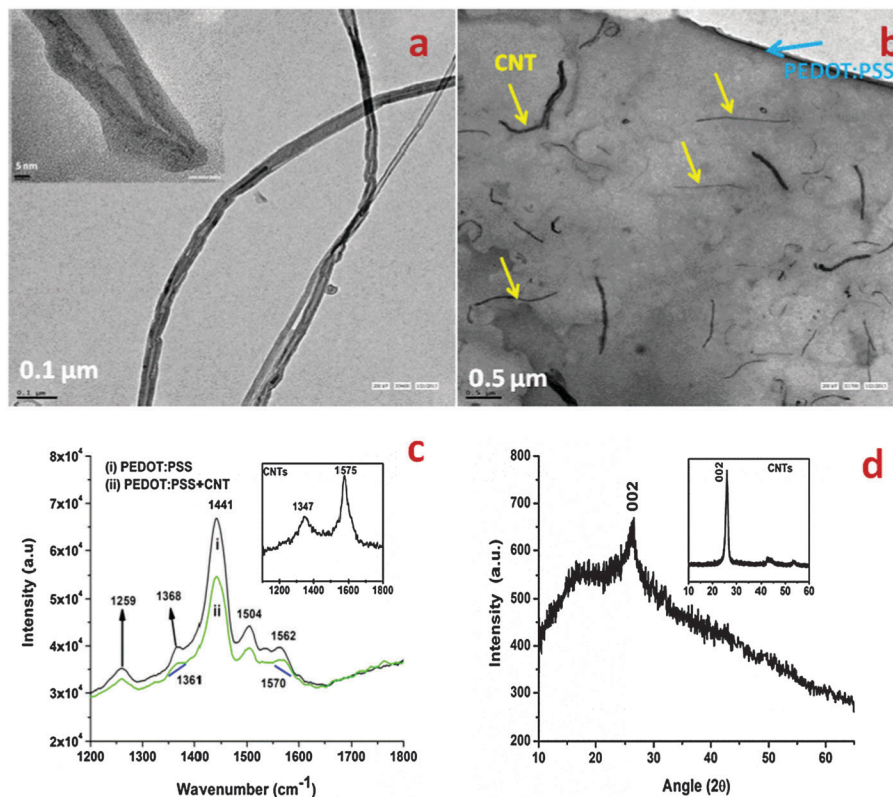


Fig. 1 TEM image of (a) carbon nanotubes, (b) CNT/PEDOT:PSS composite, (c) Raman spectrum of (i) PEDOT:PSS and (ii) PEDOT:PSS/CNT composite [the inset shows the Raman spectrum of CNTs] and (d) XRD pattern of the PEDOT:PSS/CNT composite and the inset showing XRD of CNTs.

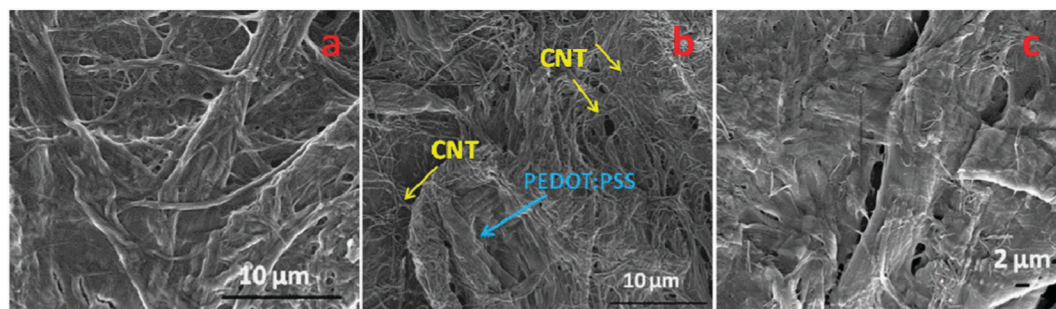


Fig. 2 SEM image of (a) PEDOT:PSS coated paper, (b) CNT/PEDOT:PSS coated paper and (c) anti-CEA/CNT/PEDOT:PSS paper sensor.

addition of EG results in improved carrier mobility and electrical conductivity.^{25,34} On treatment of this paper with formic acid, the EG doped conducting paper electrode shows the highest electrical conductivity value ($2.4 \times 10^{-2} \text{ S cm}^{-1}$) by 2 orders of magnitude compared to other solvent (methanol and sulphuric acid). The electrical conductivity enhancement is known to strongly depend on the dielectric constant of the chemicals used for treatment.^{24,26} The high dielectric constant of formic acid (58.5) screens the coulombic interaction between positively charged conducting PEDOT and the negatively charged non-conducting PSS resulting in phase separation between them leading to the removal of the PSSH and the formation of interconnected PEDOT chains and enhanced conductivity. Further, we incorporated CNTs into the PEDOT:PSS solution

(1.3 wt%, 5% EG, 0.05 wt% CNTs) for electrochemical studies since CNTs are known to exhibit excellent electrochemical activity, fast electron transfer and large surface area.^{27,28} The formic acid treated CNT doped conducting paper (CNT/FA@CP) retains almost similar order of conductivity value ($2.2 \times 10^{-2} \text{ S cm}^{-1}$) as compared to that of the formic acid treated conducting paper (FA@CP).

The optical image of the CNT modified conducting paper treated with formic acid (CNT/FA@CP) shows high flexibility and conductivity as demonstrated in Video 1 and Fig. 3a–d. Its simple fabrication does not require any additional steps and it can be cut into the desired shape and size. This platform holds great potential for application in paper based electrochemical devices. In Fig. 3c and d we demonstrate efficient conductivity

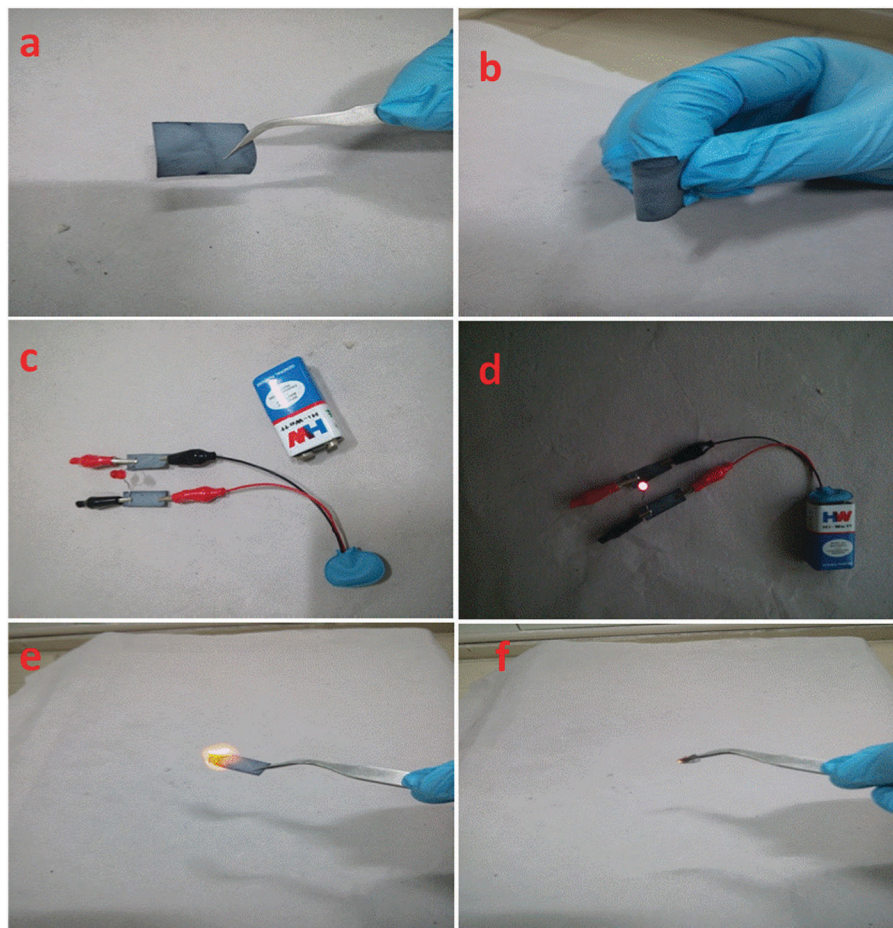


Fig. 3 (a) Optical image of conductive and electrochemically active paper (CNT/FA@CP) showing (b) high flexibility, (c and d) lighting of an LED lamp and (e and f) easy to dispose off.

of the paper electrode by lighting an LED when current is passed through multiple times folded conducting paper (Video S1, ESI†). It may be noted that this low-cost conducting platform can be easily decomposed by simple burning/incineration (Fig. 3e and f). This is an additional advantage for electronic and biomedical waste management.

In PEDOT:PSS, both PEDOT and PSS contain one sulfur atom per monomer. In PSS, sulfur is present as a sulfonate moiety whereas PEDOT contains sulfur in the thiophene ring and thus provides different chemical environments since S(2p) electrons of PEDOT and PSS have different binding energies.³⁵ The S 2p band of PEDOT is found at lower binding energy whereas the S 2p band of PSS is observed at higher binding energy. Each band splits into a doublet of S 2p_{3/2} and S 2p_{1/2} component due to spin-orbital splitting of the sulfur atom. Fig. 4a shows XPS spectra of the pristine PEDOT:PSS coated paper (curve i), EG doped PEDOT:PSS paper (conducting paper) (curve ii), and formic acid treated conducting paper (curve iii). The observed slight change in peak intensity of the conducting paper as compared to that of the PEDOT:PSS coated paper may be assigned to the conformational changes in the PEDOT:PSS polymer. However after formic acid treatment there is a decrease in peak intensity of PSS indicating exfoliation of PSS from the

conducting paper surface. Fig. 4b shows XPS spectra of the pristine PEDOT:PSS coated paper that has been deconvoluted into the characteristic binding energy peaks. The S 2p_{3/2}(S 2p_{1/2}) peak at the binding energy near 163.7 (164.8) eV corresponds to the sulfur atom of the PEDOT and the S 2p_{3/2} (S 2p_{1/2}) peak seen at the binding energy near 168.3 (169.6) eV is due to the sulfur atom present in PSS.^{36,37} The binding energy positions of these bands are almost the same as in the case of the conducting paper (Fig. 4c). However, after formic acid treatment, the S 2p peak of PSS is shifted to a lower energy level (Fig. 4d). It is observed that the PSS peak of CNT/FA@CP (Fig. 4e) is shifted towards the lower binding energy as compared to that of FA@CP around -0.3 . The presence of (-0.5) eV is due to high electron density in PSS because of charge transfer from CNTs to the electronegative sulfur atom indicating existence of interactions between the CNTs and the conjugated thiophene ring of PEDOT:PSS.³³

In PEDOT:PSS, PEDOT molecules are conductive in nature and are surrounded by the non-conductive PSS molecules.²¹ On being treated with formic acid, this core-shell structure of the PEDOT:PSS in the conducting paper changes from coiled to partially linear due to ejection of PSS molecules that are perhaps responsible for enhanced connectivity between PEDOT chains. Therefore energy barrier for charge hopping is lowered resulting

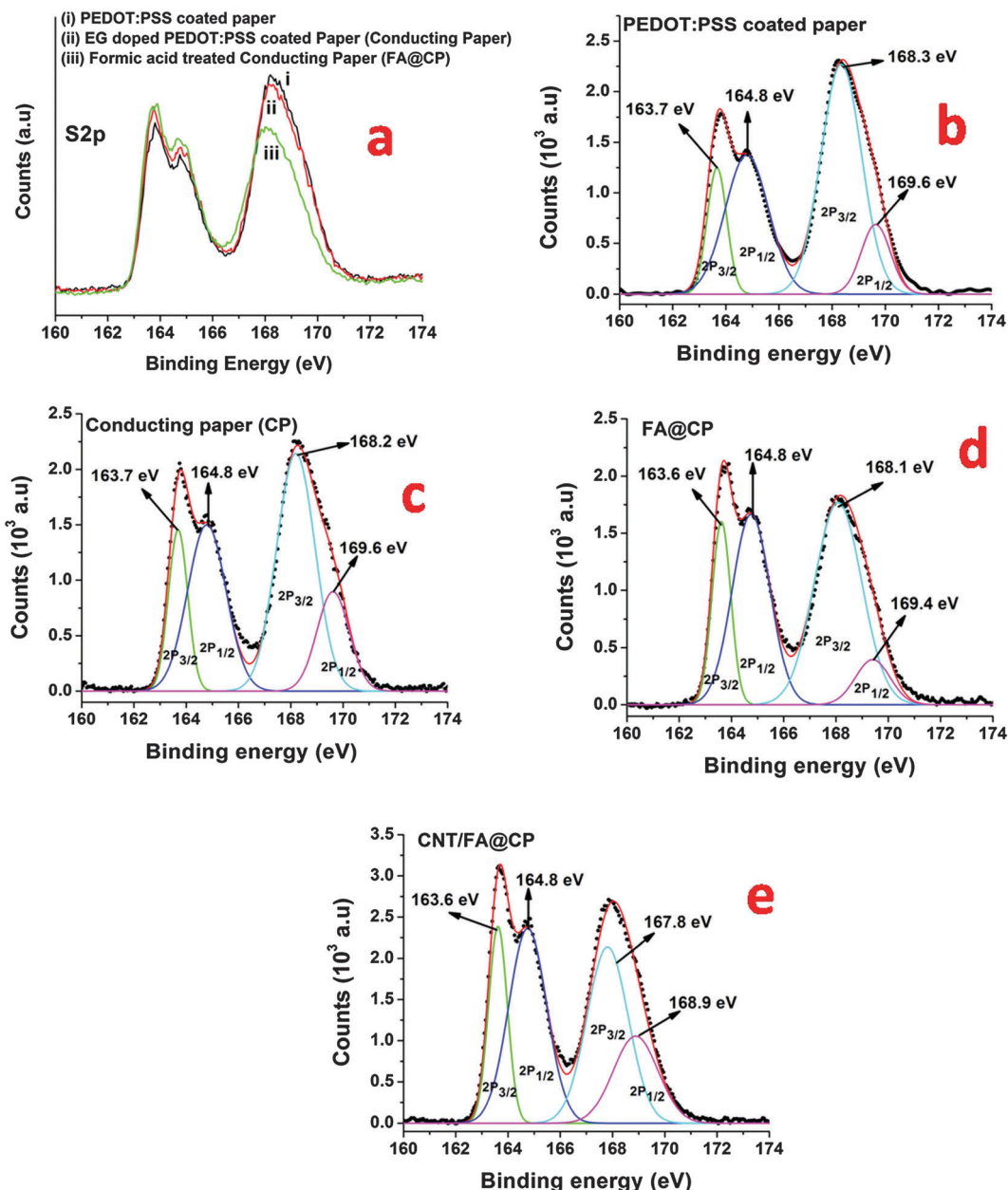


Fig. 4 S (2p) XPS spectra of (a) modified papers, XPS curve fitting of (b) PEDOT:PSS coated paper, (c) ethylene glycol doped PEDOT:PSS coated over paper i.e. conducting paper, (d) conducting paper treated with formic acid (FA@CP) and (e) CNT doped conducting paper treated with formic acid.

in enhanced charge transfer among the PEDOT chains. The ratio of PEDOT to PSS can be estimated from area under the curve. It is found that, there is no significant change in the PEDOT to PSS ratio between the PEDOT:PSS coated paper (1/1.33) and the conducting paper (1/1.30). However, the ratio of PEDOT to PSS increases from 1/1.30 to 1/1.04 after the conducting paper is treated with formic acid confirming the removal of $\sim 20\%$ PSS from the surface. It appears that exclusion of PSS due to formic acid treatment is perhaps responsible for better connectivity between the PEDOT chain that in turn results in increased conductivity.

Fig. 5a shows results of the chronoamperometric studies obtained for (i) the conducting paper [CP] (ii) the conducting

paper treated with formic acid [FA@CP], (iii) the CNT doped conducting paper treated with formic acid [CNT/FA@CP] and (iv) anti-CEA immobilized over CNT/FA@CP [anti-CEA/CNT/FA@CP] at 2 V on every 0.1 s. The increased electrochemical response current of the FA@CP electrode (~ 0.65 mA) than that of the CP electrode (~ 0.57 mA) is attributed to increased conductivity of the electrode due to the removal of PSS from the film surface. Further increase in the electrochemical current value of the CNT/FA@CP electrode (~ 0.68 mA) can be assigned to high electrochemical activity of CNTs that enhances permeability of the redox couple $[\text{Fe}(\text{CN})_6]^{3-/4-}$. Next, a decrease in the value of electrochemical current observed after immobilization of anti-CEA onto the CNT/FA@CP electrode (~ 0.60 mA) is attributed

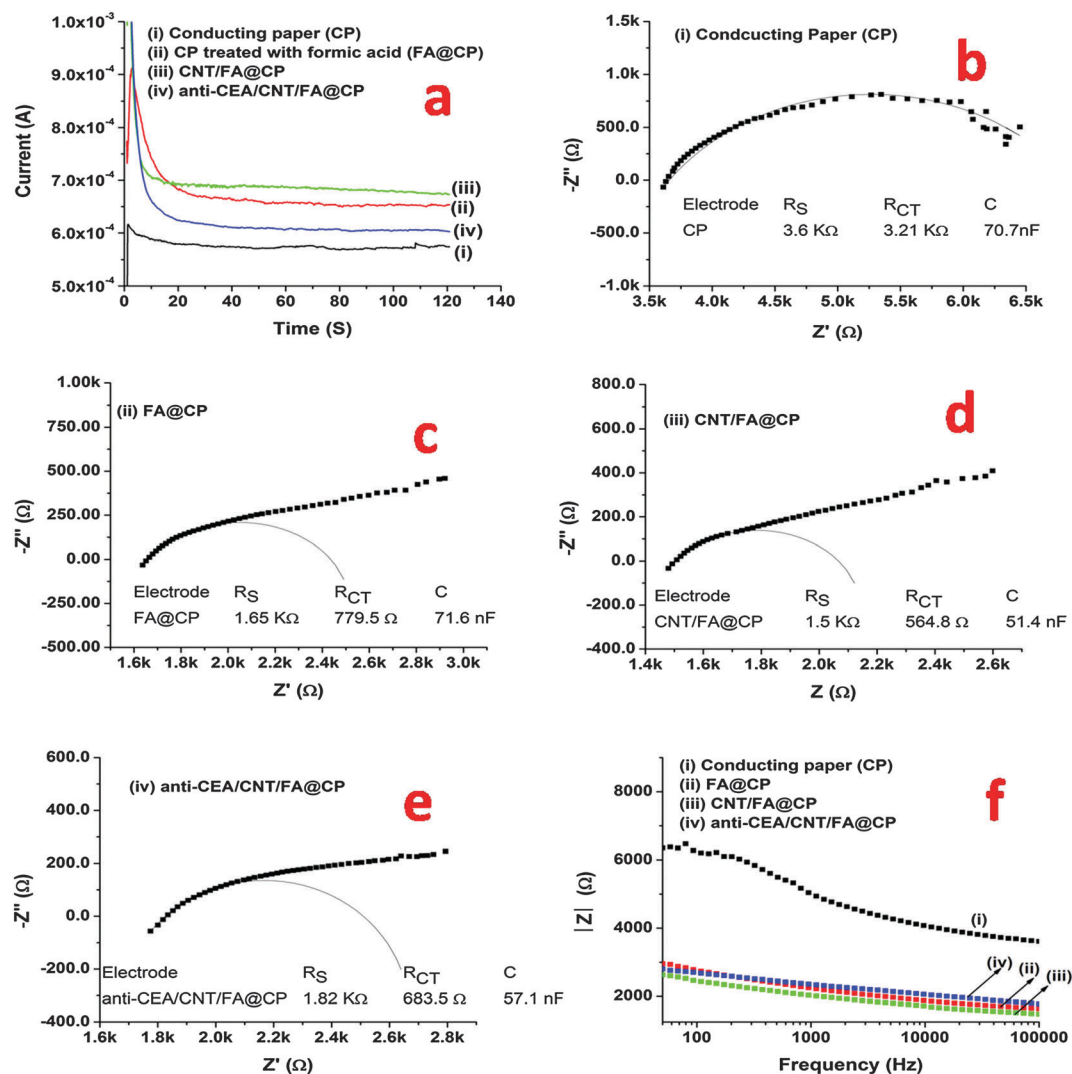


Fig. 5 Electrochemical characterization of the modified paper electrode: (a) chronoamperometric studies of the modified paper electrode. Impedance spectra of (b) conducting paper, (c) conducting paper treated with formic acid (FA@CP), (d) CNT modified conducting paper treated with formic acid (CNT/FA@CP) and (e) anti-CEA/CNT/FA@CP paper electrode and circuit were fitted with equivalent Randles circuit $R_s(R_{ct}C)$. (f) Bode plot of different modified electrodes.

to the hindrance caused by the CEA antibodies to the electron transport indicating immobilization of anti-CEA.

Electrochemical impedance spectroscopy (EIS) is an effective tool for investigating interfacial properties of the surface modified electrodes. Fig. 5 shows the Nyquist plot obtained for (b) the conducting paper [CP], (c) the conducting paper treated with formic acid [FA@CP], (d) CNT doped FA@CP [CNT/FA@CP] and (e) anti-CEA immobilized over CNT/FA@CP [anti-CEA/CNT/FA@CP] in PBS solution containing 5 mM $[\text{Fe}(\text{CN})_6]^{3-/4-}$ at 0.03 V (biasing potential) in the frequency range of 100 KHz to 50 Hz. The diameter of the semicircle in the Nyquist plot yields magnitude of the charge transfer resistance (R_{ct}) of the electrode that depends on the dielectric features of the electrode/electrolyte interface. It can be seen that the R_{ct} value of the conducting paper electrode (3.2 K Ω , Fig. 5b) decreases after formic acid treatment (779.5 Ω , Fig. 5c). This is assigned to the high dielectric constant of formic acid that facilitates

decreased coulombic interaction between PEDOT and PSS leading to the removal of the PSS molecule. The exclusion of PSS (negatively charged and non-conducting in nature) from the conducting paper provides increased exposure of the interconnected PEDOT chains (positively charged and conducting in nature) that promotes permeability of the redox probe, $[\text{Fe}(\text{CN})_6]^{3-/4-}$ to the surface of the FA@CP electrode. The value of R_{ct} (564.8 Ω , Fig. 5d) for the CNT/FA@CP electrode is smaller than that of the FA@CP electrode (779.5 Ω). This may be attributed to excellent electrochemical properties and larger surface area of CNTs that are incorporated into the PEDOT:PSS matrix resulting in increased permeability of $[\text{Fe}(\text{CN})_6]^{3-/4-}$ to the surface of the CNT/FA@CP paper electrode. Further, increase in the value of R_{ct} (683.5 Ω , Fig. 5e) of anti-CEA/CNT/FA@CP is attributed to the hindrance caused by the macromolecular structure of the antibodies that perhaps obstruct electron transfer owing to their insulating nature. These results also

confirm functionalization of the CNT/FA@CP electrode with anti-CEA. The heterogeneous electron transfer rate constant (K_{ct}) of CNT/FA@CP and FA@CP electrodes can be calculated using eqn (1).³⁸

$$K_{ct} = \frac{RT}{n^2 F^2 A R_{ct} [S]} \quad (1)$$

where R is the gas constant, T is the absolute temperature, F is the Faraday constant, A is the electrode area (cm^2), $[S]$ is the concentration of the redox probe (mol cm^{-3}) and n is the number of transferred electrons per molecule of the redox probe. The heterogeneous electron transfer rate constant (K_{ct}) value of CP, FA@CP and CNT/FA@CP has been found to be $1.66 \times 10^{-7} \text{ cm s}^{-1}$, $6.83 \times 10^{-5} \text{ cm s}^{-1}$ and $9.43 \times 10^{-5} \text{ cm s}^{-1}$, respectively. This indicates that the CNT/FA@CP electrode exhibits faster electron transfer kinetics as compared to that of the other modified paper electrodes. Thus incorporation of CNTs results in improved electrochemical activity of the paper electrode (CNT/FA@CP). Interestingly, K_{ct} of the CNT/FA@CP electrode is found to be nearly 5 times higher compared to our previous work wherein a PEDOT:PSS-RGO composite was used to fabricate the conducting paper using ethylene glycol.³⁹

The solution resistance (R_s) is found to be the highest (3.6 K Ω) for the CP electrode as compared to that of the other modified electrodes FA@CP (1.6 K Ω), CNT/FA@CP (1.5 K Ω) and anti-CEA/CNT/FA@CP (1.8 K Ω). R_s depends on the type of ions, ionic concentration, temperature and the electrode surface.⁴⁰ This suggests that after formic acid treatment, morphology of the CP electrode changes due to the removal of PSS leading to lower R_s value. Fig. 5f shows the Bode plot representing the impedance modulus ($|Z|$) vs. frequency for the modified paper electrodes. The FA@CP, CNT/FA@CP and anti-CEA/CNT/FA@CP electrodes exhibit low $|Z|$ compared to CP in the frequency range, 50 Hz to 100 KHz, confirming increased electrochemical activity due to the removal of nonconducting PSS molecules. The values of electrical conductivity and electrochemical properties of modified paper electrodes are summarized in Table 1.

The electrochemical response studies (Fig. 6a) have been conducted by varying the concentration of carcinoembryonic antigen (CEA) from 1 to 100 ng ml^{-1} in PBS (50 mM, pH 7.4, 0.9% NaCl) containing 5 mM $[\text{Fe}(\text{CN})_6]^{3-/4-}$ using chronoamperometry with an incubation time of 15 min. The magnitude of current decreases on addition of CEA due to the formation of electrically insulating antigen-antibody complexes produced due to specific interaction of the CEA and anti-CEA that may block the electron transfer *via* the redox probe, $[\text{Fe}(\text{CN})_6]^{3-/4-}$ at the paper electrode surface. Fig. 6(b) shows the calibration curve

obtained between the response current and CEA concentration (curve i). It is found that the amperometric current decreases up to 25 ng ml^{-1} after which it increases and reaches saturation up to 100 ng ml^{-1} . However, a linear relationship obtained between 2 to 15 ng ml^{-1} with a sensitivity of 7.7 $\mu\text{A ng}^{-1} \text{ ml cm}^{-2}$ follows eqn (2)

$$I(A) = 7.8 \mu\text{A ml ng}^{-1} \times [\text{CEA concentration}] + 528 \mu\text{A}; R^2 = 0.95 \quad (2)$$

A control experiment was performed to check cross reactivity of the paper sensor with CEA antigen in the absence of antibodies (curve ii). However, no significant change in current response was observed for the BSA/CNT/FA@CP in the absence of antibodies as a function of CEA concentration. The repeatability of the bio-electrode was confirmed by repeating each experiment 3 times and the error bars were included based on the RSD value.

CEA is traditionally determined by the gold standard technique for proteinaceous molecules *i.e.* ELISA to diagnose and monitor cancer. This method usually involves a complex procedure, is time-consuming and is expensive. It is thus desirable to develop techniques that are low cost, easy to use, are rapid, sensitive and do not require any laboratory infrastructure for the CEA estimation. Therefore attempts have been made to estimate CEA concentration in serum by using a BSA/anti-CEA/CNT/FA@CP bioelectrode to evaluate the feasibility of the proposed paper sensor. The blood samples were collected from patient and processed at Rajiv Gandhi Cancer Institute & Research Centre (RGCI&RC) in Rohini, Delhi, India, after ethical approval by the Institutional Review board (No. RGCIRC/IRB/61/2014). We also obtained ethical approval of Institutional Ethical and Biosafety Committee, DTU (R.NO.:BT/IEBC/2014/714). The concentration of CEA in serum of cancer patients was measured at RGCI&RC using the VITROS CEA Reagent Pack and the VITROS CEA Calibrators on the VITROS ECi/ECiQ Immunodiagnostic Systems, the VITROS 3600 Immunodiagnostic System and the VITROS 5600 Integrated System using Intellicheck[®] Technology. An immunometric immunoassay technique was used. It can be seen that a reasonable correlation exists between (a) CEA concentration in serum samples determined by immunometric immunoassay technique and (b) standard concentration of CEA (Table 2). The results exhibit reasonable relative standard deviation (%RSD) indicating high accuracy of the paper sensor.

The storage stability of this paper sensor was monitored at an interval of 3 days as shown in Fig. 6c. It was found that the paper immunoelectrode (BSA/anti-CEA/CNT/FA@CP) retained about 82% activity even after 18 days when stored at 4 °C after which the current response decreased to less than 70% in

Table 1 Conductivity and electrochemical properties of a modified paper electrode

S. no.	Material coated on Paper	Conductivity (S cm^{-1})	Charge transfer resistance (R_{ct})	Solution resistance (R_s)	Heterogeneous electron transfer rate constant (K_{ct})
1	PEDOT:PSS + EG (CP)	2.1×10^{-3}	3.21 K Ω	3.6 K Ω	$1.66 \times 10^{-7} \text{ cm s}^{-1}$
2	PEDOT:PSS + EG treated with formic acid (FA@CP)	2.4×10^{-2}	779.5 Ω	1.65 K Ω	$6.83 \times 10^{-5} \text{ cm s}^{-1}$
3	PEDOT:PSS + EG + CNT treated with formic acid (CNT/FA@CP)	2.2×10^{-2}	564.8 Ω	1.5 K Ω	$9.43 \times 10^{-5} \text{ cm s}^{-1}$

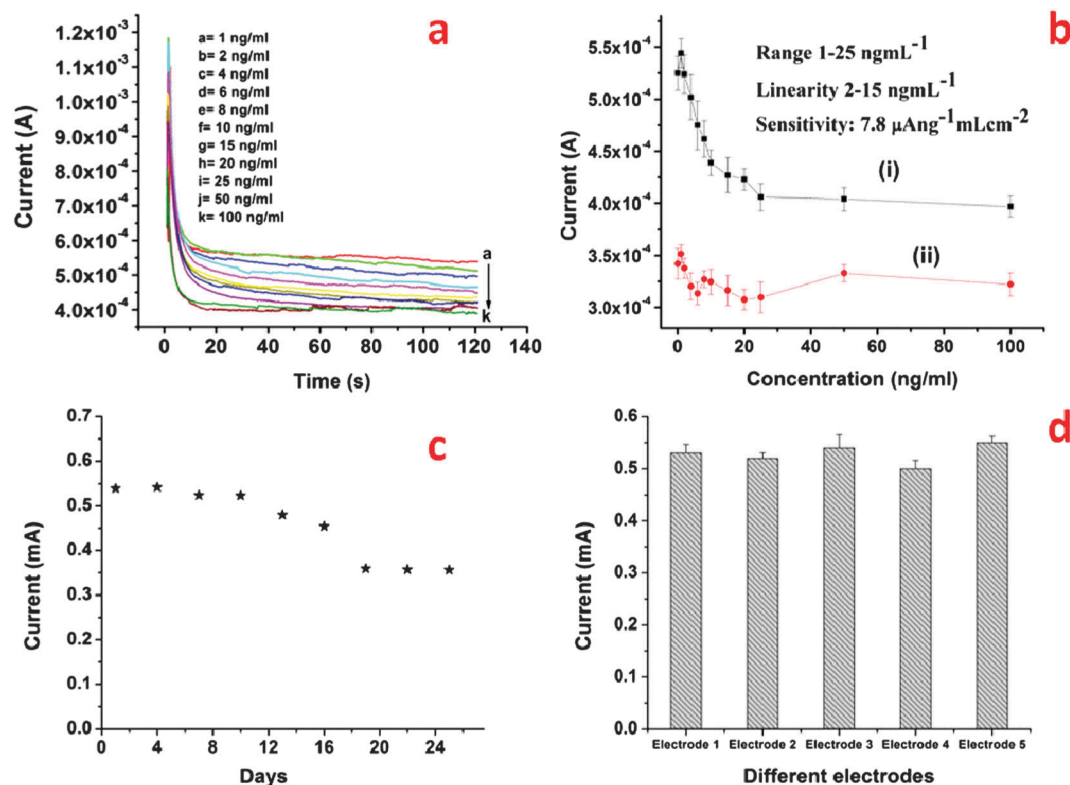


Fig. 6 (a) Electrochemical response studies of the BSA/anti-CEA/CNT/FA@CP paper electrode obtained as a function of CEA concentration (1–100 ng mL⁻¹) using chronoamperometry and (b) calibration plot between the magnitudes of current recorded and CEA concentration (curve i); control experiment in the absence of antibody (curve ii). (c) Current response time of the BSA/anti-CEA/CNT/FA@CP paper electrode as a function of time (day). (d) Current response time of five different BSA/anti-CEA/CNT/FA@CP paper electrodes fabricated using the same set of procedures in the presence of CEA concentration (2 ng mL⁻¹).

Table 2 Determination of carcinoembryonic antigen concentration in serum samples using a BSA/anti-CEA/CNT/FA@CP paper electrode

S. no.	CEA concentration (ng mL ⁻¹) determined using ELISA	Amperometric current (mA) obtained with standard CEA sample	Amperometric current (mA) obtained with serum sample	%RSD
1	2.37	0.518	0.517	0.2
2	4.03	0.501	0.507	0.8
3	5.57	0.485	0.487	0.3
4	5.96	0.474	0.493	2.81
5	10	0.439	0.482	6.5

about 25 days. This indicates that the fabricated paper immunoelectrode exhibits reasonably good stability at least for 18 days. Fig. 6d indicates electrochemical response of five different paper immunoelectrodes (BSA/anti-CEA/CNT/FA@CP) fabricated under the same set of conditions in the presence of CEA concentration (2 ng mL⁻¹). It is found that this paper immunoelectrode shows good reproducibility for five different electrodes with a constant surface area as is evident by the standard error of less than 5% (mean value = 528 μ A). Further, each measurement was repeated 3 times for each electrode and the error bars are included accordingly.

The sensing characteristics of the paper sensor are summarized in Table S1 (ESI[†]) along with those reported in the literature. It can be seen that sensitivity of the paper electrode is much

higher than that of the other reported electrodes (gold, glassy carbon and ITO electrode) and can be used to differentiate two lower values of CEA concentration. These results show that the paper based electrochemical sensor is a better candidate over conventional electrodes.

To attest the environment friendliness, these paper electrodes were decomposed by incineration. The resulting ash was investigated by the energy dispersive X-ray (EDX) technique. EDX results confirm the presence of only carbon, oxygen, sodium, phosphorous and potassium; no toxic metals were detected (Fig. S2 in the ESI[†]).

4. Conclusions

The nanocomposite of poly(3,4-ethylenedioxythiophene):poly(styrenesulfonate) (PEDOT:PSS) and carbon nanotubes (CNTs) has been used to fabricate the conducting paper (CNT/CP). It is found that the conductivity of this paper increases by 2 orders of magnitude on being treated with formic acid (CNT/FA@CP) due to the removal of the non-conducting molecule PSS from the electrode surface. This paper has been utilized to fabricate a nanomaterial modified conducting paper electrode for estimation of carcinoembryonic antigen (CEA). The fabricated BSA/anti-CEA/CNT/FA@CP bioelectrode exhibits a high sensitivity of 7.8 μ A (ng mL⁻¹)⁻¹ cm² and a linear range of 2–15 ng mL⁻¹.

The CEA concentration has been estimated in serum samples by using the BSA/anti-CEA/CNT/FA@CP bioelectrode to evaluate the feasibility of the proposed paper electrode. This simple fabrication method provides a flexible, environmentally friendly and cost effective platform that can be utilized for flexible electronics, microfluidics, energy storage devices and point of care devices. And efforts should be made to improve the stability and performance of the BSA/anti-CEA/CNT/FA@CP platform for CEA detection by selection of the suitable dopant and solvent.

Acknowledgements

We thank the Vice Chancellor, Delhi Technological University (DTU), Delhi, India, for providing the facilities. Saurabh Kumar is thankful to DTU for the award of financial assistance and Dr Saurabh Srivastava, Suveen Kumar DTU for, discussions during the preparation of the manuscript. SK is thankful to Dr LS Meena, Institute of Genomics & Integrative Biology (IGIB) for TEM facilities and Dr Birendra K. Yadav, Dr D. C. Doval, Rajiv Gandhi Cancer Institute & Research Centre for providing patient samples. The authors are also thankful to Sandeep Mishra, Central Facility Lab, Delhi Technological University for EDX studies.

References

- 1 L. Wu and X. Qu, *Chem. Soc. Rev.*, 2015, **44**, 2963–2997.
- 2 I. A. f. R. o. Cancer, World Health Organization, www.cancerresearchuk.org, 2012.
- 3 M. J. Duffy, *Clin. Chem.*, 2001, **47**, 624–630.
- 4 I. E. Tothill, *Semin. Cell Dev. Biol.*, 2009, **20**, 55–62.
- 5 S. Kumar, S. Kumar, S. Tiwari, S. Srivastava, M. Srivastava, B. K. Yadav, S. Kumar, T. T. Tran, A. K. Dewan and A. Mulchandani, *Adv. Sci.*, 2015, **2**, 1500048.
- 6 B. D. Malhotra and A. Chaudhary, *Sens. Actuators, B*, 2003, **91**, 117–127.
- 7 S. K. Arya and S. Bhansali, *Chem. Rev.*, 2011, **111**, 6783–6809.
- 8 A. W. Martinez, S. T. Phillips, G. M. Whitesides and E. Carrilho, *Anal. Chem.*, 2009, **82**, 3–10.
- 9 E. W. Nery and L. T. Kubota, *Anal. Bioanal. Chem.*, 2013, **405**, 7573–7595.
- 10 J. Hu, S. Wang, L. Wang, F. Li, B. Pingguan-Murphy, T. J. Lu and F. Xu, *Biosens. Bioelectron.*, 2014, **54**, 585–597.
- 11 L. Wang, W. Chen, D. Xu, B. S. Shim, Y. Zhu, F. Sun, L. Liu, C. Peng, Z. Jin and C. Xu, *Nano Lett.*, 2009, **9**, 4147–4152.
- 12 J. R. Windmiller, A. J. Bandodkar, G. Valdés-Ramírez, S. Parkhomovsky, A. G. Martinez and J. Wang, *Chem. Commun.*, 2012, **48**, 6794–6796.
- 13 N. Ruecha, R. Rangkipan, N. Rodthongkum and O. Chailapakul, *Biosens. Bioelectron.*, 2014, **52**, 13–19.
- 14 A. C. Glavan, D. C. Christodouleas, B. Mosadegh, H. D. Yu, B. S. Smith, J. Lessing, M. T. Fernandez-Abedul and G. M. Whitesides, *Anal. Chem.*, 2014, **86**, 11999–12007.
- 15 A. Manekthodi, M. Y. Lu, C. W. Wang and L. J. Chen, *Adv. Mater.*, 2010, **22**, 4059–4063.
- 16 A. Määttä, U. Vanamo, P. Ihalainen, P. Pulkkinen, H. Tenhu, J. Bobacka and J. Peltonen, *Sens. Actuators, B*, 2013, **177**, 153–162.
- 17 S. Kumar, K. K. Jagadeesan, A. G. Joshi and G. Sumana, *RSC Adv.*, 2013, **3**, 11846–11853.
- 18 S. Ge, L. Ge, M. Yan, X. Song, J. Yu and J. Huang, *Chem. Commun.*, 2012, **48**, 9397–9399.
- 19 M. Su, L. Ge, S. Ge, N. Li, J. Yu, M. Yan and J. Huang, *Anal. Chim. Acta*, 2014, **847**, 1–9.
- 20 V. Saxena and B. Malhotra, *Curr. Appl. Phys.*, 2003, **3**, 293–305.
- 21 U. Lang, E. Müller, N. Naujoks and J. Dual, *Adv. Funct. Mater.*, 2009, **19**, 1215–1220.
- 22 D. Tobjörk and R. Österbacka, *Adv. Mater.*, 2011, **23**, 1935–1961.
- 23 J. Kim, J. Jung, D. Lee and J. Joo, *Synth. Met.*, 2002, **126**, 311–316.
- 24 D. Alemu, H.-Y. Wei, K.-C. Ho and C.-W. Chu, *Energy Environ. Sci.*, 2012, **5**, 9662–9671.
- 25 Q. Wei, M. Mukaida, Y. Naitoh and T. Ishida, *Adv. Mater.*, 2013, **25**, 2831–2836.
- 26 D. A. Mengistie, M. A. Ibrahim, P.-C. Wang and C.-W. Chu, *ACS Appl. Mater. Interfaces*, 2014, **6**, 2292–2299.
- 27 V. V. Shumyantseva, L. V. Sigolaeva, L. E. Agafonova, T. V. Bulko, D. V. Pergushov, F. H. Schacher and A. I. Archakov, *J. Mater. Chem. B*, 2015, **3**, 5467–5477.
- 28 S. Soylemez, F. E. Kanik, S. D. Uzun, S. O. Hacioglu and L. Toppare, *J. Mater. Chem. B*, 2014, **2**, 511–521.
- 29 C. Singh, S. Srivastava, M. A. Ali, T. K. Gupta, G. Sumana, A. Srivastava, R. Mathur and B. D. Malhotra, *Sens. Actuators, B*, 2013, **185**, 258–264.
- 30 S. Razdan, P. K. Patra, S. Kar, L. Ci, R. Vajtai, A. Kukovecz, Z. Kónya, I. Kiricsi and P. M. Ajayan, *Chem. Mater.*, 2009, **21**, 3062–3071.
- 31 T. Ji, L. Tan, X. Hu, Y. Dai and Y. Chen, *Phys. Chem. Chem. Phys.*, 2015, **17**, 4137–4145.
- 32 G. Guan, Z. Yang, L. Qiu, X. Sun, Z. Zhang, J. Ren and H. Peng, *J. Mater. Chem. A*, 2013, **1**, 13268–13273.
- 33 J. Li, J.-C. Liu and C.-J. Gao, *J. Polym. Res.*, 2010, **17**, 713–718.
- 34 J. Ouyang, C. W. Chu, F. C. Chen, Q. Xu and Y. Yang, *Adv. Funct. Mater.*, 2005, **15**, 203–208.
- 35 X. Crispin, F. Jakobsson, A. Crispin, P. Grim, P. Andersson, A. Volodin, C. Van Haesendonck, M. Van der Auwerter, W. R. Salaneck and M. Berggren, *Chem. Mater.*, 2006, **18**, 4354–4360.
- 36 J. P. Thomas, L. Zhao, D. McGillivray and K. T. Leung, *J. Mater. Chem. A*, 2014, **2**, 2383–2389.
- 37 H.-S. Park, S.-J. Ko, J.-S. Park, J. Y. Kim and H.-K. Song, *Sci. Rep.*, 2013, **3**, 2454.
- 38 A. Bardea, E. Katz and I. Willner, *Electroanalysis*, 2000, **12**, 1097–1106.
- 39 S. Kumar, S. Kumar, S. Srivastava, B. K. Yadav, S. H. Lee, J. G. Sharma, D. C. Doval and B. D. Malhotra, *Biosens. Bioelectron.*, 2015, **73**, 114–122.
- 40 N. Sekar and R. P. Ramasamy, *J. Microb. Biochem. Technol.*, 2013, **S6**, 004.

PEDOT:PSS/PVA-Nanofibers-Decorated Conducting Paper for Cancer Diagnostics

Saurabh Kumar, Prabhakar Rai, Jai Gopal Sharma, Ashutosh Sharma,*
and Bansi Dhar Malhotra*

The development of a flexible, label free, low-cost, and environment friendly biosensor platform is reported for sensitive and rapid detection of cancer biomarker based on poly(3,4-ethylenedioxythiophene):poly(4-styrenesulfonate)/polyvinyl alcohol nanofiber decorated conducting paper. This conducting paper based biosensor demonstrates improved sensing performance with linear detection range of 0.2–25 ng mL⁻¹, high sensitivity of 14.2 μ A ng⁻¹ mL cm⁻², and shelf life of 22 days for a carcinoembryonic antigen (cancer biomarker) detection. This modified conducting paper electrode is a promising alternative over expensive conventional electrodes (indium tin oxide, gold, and glassy carbon) for fabrication of smart point of care devices.

1. Introduction

There is increased demand for availability of paper based devices due to their application in capacitors, batteries, displays, thin film transistors, touch pad, and biosensors.^[1,2] It has been predicted that fabrication of paper based electronic devices is highly cost effective and environment friendly. Besides this, their mass production, disposability, flexibility, and ease in processing may perhaps meet the increasing demand of desired smart electronic devices.^[2,3] For biosensing applications, a wide range of conducting substrates such as glassy carbon, indium tin oxide (ITO), and gold coated glass substrate are currently being used. These electrodes are costly, rigid and can easily break during bending, making them difficult to be used for fabrication of desired flexible electronic devices and smart point of care devices. Conducting paper (CP) has been found to play an important role in the ongoing transition to the development of paper based electrochemical biosensors due to their high flexibility, cost-effectiveness, light weight, and disposability. Moreover, coupling of paper based electrode with biological entity provides an efficient platform for conduction of both electronic

and ionic charge carriers that play a major role in efficient signal transduction.^[4,5]

Conducting polymers have been considered as promising materials for fabrication of paper based devices because of their unique combination of delocalization of π electrons, solution processability, mechanical flexibility, and low cost.^[6] These synthetic metals have been predicted to have enough potential for development of a low cost and high performance biosensor materials that offer high permeability, biocompatibility, and rapid electron transfer.^[7] One of the methods that can be used for fabrication of conducting polymer nanofiber is

electrospinning wherein high voltage is applied to the tip of the syringe which contains polymeric solution. As a result, polymer solution becomes charged at high electric field causing the solvent to evaporate and form polymeric nanofiber jets. Electrospinning is an efficient method for fabricating long ultrafine fibers of a very high surface-to-volume ratio and relatively defect free fibers at molecular level.^[8] The poly(3,4-ethylenedioxythiophene):poly(4-styrenesulfonate) (PEDOT:PSS) is a stable and commercially available material with excellent characteristics such as low band gap, electrochemical properties, thermal stability, film forming ability, and homogenous entrapment on a paper substrate.^[2,9] Electrospun nanofibers (EsNfs) of PEDOT:PSS may provide suitable matrix to improved physical contact by providing increased number of sites for biochemical interaction, improved biomolecule loading with better orientation of biomolecules resulting in enhanced capturing of a bioanalyte.^[10] These properties make PEDOT:PSS based EsNf as a promising immobilization matrix for development of paper based electrochemical biosensor.

Previously reported paper based electrochemical biosensors used costly conducting ink such as gold, silver, and graphite paste to make paper conducting. In the present work, conducting polymer (PEDOT:PSS) is used to fabricate efficient conducting platform.^[11,12] We report results of the studies relating to fabrication of PEDOT:PSS/PVA EsNf decorated conducting paper (via electrospinning technique, **Figure 1**) with improved mechanical strength and electrochemical characteristics. Here, PVA was used as a polymeric carrier material to prepare electrospun nanofiber. This low cost, flexible, and environment friendly paper electrode has been used for cancer biomarker (carcinoembryonic antigen, CEA) detection. CEA is one of the most widely used cancer biomarkers for diagnosis and routine monitoring of cancer.^[13] Therefore development of a CP based CEA biosensor is of considerable importance as it is expected to be simple, flexible, disposable, cost effective, and environment friendly.

S. Kumar, Dr. J. G. Sharma, Prof. B. D. Malhotra
Nanobioelectronics Laboratory
Department of Biotechnology
Delhi Technological University
Shahbad Daulatpur, Delhi 110042, India
E-mail: bansi.malhotra@gmail.com

Dr. P. Rai, Prof. A. Sharma
Department of Chemical Engineering
Indian Institute of Technology Kanpur
Kanpur 208016, India
E-mail: ashutos@iitk.ac.in



DOI: 10.1002/admt.201600056

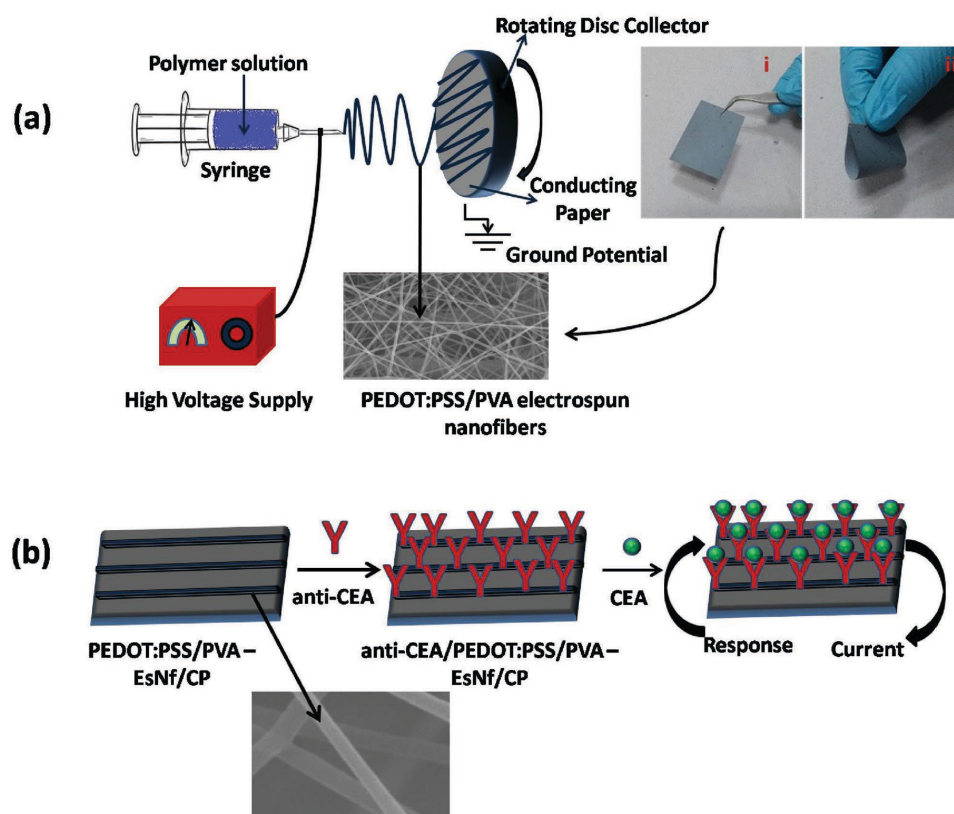


Figure 1. a) Schematic representation of the electrospinning setup for the synthesis of PEDOT:PSS/PVA nanofibers (Inset showing (i) optical image of electrospun modified paper with (ii) high degree of flexibility) and b) biofunctionalized electrospun PEDOT:PSS/PVA nanofiber for carcinoembryonic antigen (CEA) detection.

2. Results and Discussion

Figure 2 shows the Raman spectrum of the PEDOT:PSS (curve i) and PEDOT:PSS/PVA hybrid (curve ii), which is nearly identical because of resonating behavior of PEDOT:PSS that enhances the Raman scattering. No PVA peaks were observed due to the presence of dominant PEDOT:PSS intensity peak. The peaks seen at 1257, 1372, and 1440 cm^{-1} are associated with $\text{C}_\alpha\text{--C}_\alpha$ inter-ring stretching, $\text{C}_\beta\text{--C}_\beta$ stretching and $\text{C}_\alpha\text{=C}_\beta$ (--O) symmetric stretching vibration, respectively. The $\text{C}_\alpha\text{=C}_\beta$ asymmetric stretching vibration gives rise to the bands at 1502 and 1565 cm^{-1} corresponding to the thiophene rings of PEDOT:PSS chain.^[14,15] It can be seen that the Raman spectrum of the PEDOT:PSS/PVA hybrid (curve ii) shows peak shift from 1372 to 1366 cm^{-1} and 1500 to 1502 cm^{-1} due to interaction between PEDOT:PSS and PVA. Next, the surface charge of the PEDOT:PSS and PEDOT:PSS/PVA hybrid suspension was characterized by measuring the zeta potential. The observed zeta potential of PEDOT:PSS suspension in water at -24.9 mV is due to presence of sulfonyl group in the PSS molecule.^[16] However, zeta potential of PEDOT:PSS/PVA hybrid is found to be shifted toward more negative value (-28.5 mV) due to anionic behavior of PVA chain, indicating interaction between PEDOT:PSS and PVA chain.^[17]

In the PEDOT:PSS polymer, both PEDOT and PSS molecules contain one sulfur atom per monomer. In the PEDOT,

sulfur is present in thiophene ring, whereas PSS contains sulfur in the sulfonate moiety attached with styrene ring of the polymer. It appears that the changed chemical environment is perhaps responsible for the observed binding energy of sulfur in PEDOT and PSS polymer. As shown in **Figure 3**, the X-ray

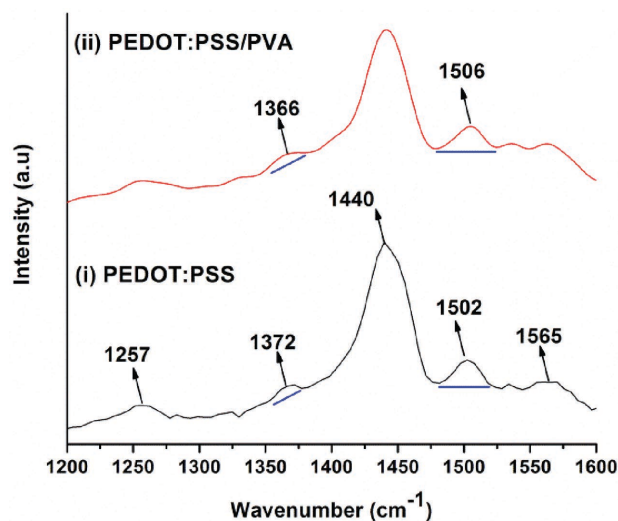


Figure 2. Raman spectrum of (i) PEDOT:PSS and PEDOT:PSS/PVA composite.

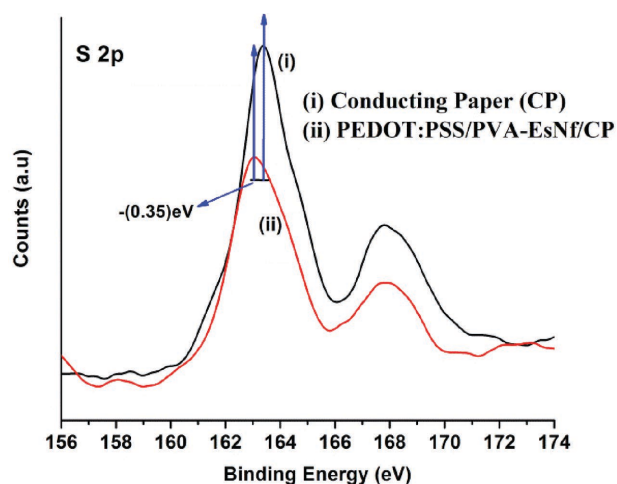


Figure 3. S 2p XPS spectra of (i) conducting paper (CP) (ii) PEDOT:PSS/PVA electrospun nanofiber coated CP.

photoelectron spectroscopy (XPS) bands seen between 166 and 172 eV are assigned to the S 2p band of the sulfur atoms present in PSS, whereas the XPS bands between 162 and 166 eV refer to the S 2p band of the sulfur atoms present in PEDOT.^[18] S 2p band of CP (curve i) and PEDOT:PSS/PVA-EsNf/CP (curve ii) is visible in Figure 3. It can be seen that the PEDOT peak of PEDOT:PSS/PVA-EsNf/CP is slightly shifted toward the lower binding energy $[-(0.35) \text{ eV}]$ suggesting the presence of interaction between positively charge PEDOT molecules and negatively charge PVA molecules which affect the electronic environment. Moreover, the atomic percentage of S 2p decreases from 2 to 1.1 after the CP is decorated with PEDOT:PSS/PVA-EsNf/CP. This result is consistent with the presence of PVA molecule.

Figure 4a shows the optical image of the conducting paper modified with PEDOT:PSS/PVA electrospun nanofiber that has high flexibility. It can be folded and cut into desired shape and size. Additionally, this platform can be easily decomposed by simple incineration.

The mechanical properties of the Whatman paper, CP, and PEDOT:PSS/PVA nanofibers deposited conducting paper (PEDOT:PSS/PVA-EsNf/CP) were evaluated through stress–strain

Table 1. Mechanical properties of modified paper.

Sample	Tensile strength [MPa]	Tensile modulus [MPa]	Extension at break [mm]
Paper	5.9	314	3.8
Conducting paper (CP)	7	198	6.0
PEDOT:PSS/PVA-EsNf/CP	8.7	232	5.5

relationship (Figure 4b). The tensile strength and the tensile modulus were found to be 5.9 and 314, 7 and 198, and 8.7 and 232 MPa, respectively. The increased tensile strength of the conducting paper may be attributed to uniform adsorption of the PEDOT:PSS molecules onto cellulose fibers of Whatman paper resulting in enhanced interfacial adherence with a high extensibility and reduced stiffness. Further, nanofiber coated conducting paper (PEDOT:PSS/PVA-EsNf/CP) exhibits high tensile strength and modulus but reduced extensibility than that of the CP. This decrease in extensibility is due to increased stiffness of the CP owing to coating of the nanofibrous network. **Table 1** summarizes the mechanical properties of the modified conducting paper.

To investigate the hydrophilic/hydrophobic properties of the modified paper electrode, contact angle (CA) measurements were carried out using the sessile drop method (**Figure 5**). There was a large decrease in the CA value of the conducting paper (108° , image i) after electrospinning it with the PEDOT:PSS/PVA polymer (68° , image ii). This decrease in the CA value may be attributed to the presence of the hydrophilic group in poly(styrenesulfonate) (PSS), hydroxyl group of PVA, and pores created due to random orientation of the PEDOT:PSS/PVA nanofiber. The CA decreases to 43° (image iii) after the immobilization of anti-CEA. The decrease in the value of contact angle is attributed to the hydrophilic nature of the surface and confirms the immobilization of antibody on the PEDOT:PSS/PVA-EsNf/CP electrode surface.

The surface morphology of the various modified paper electrodes (**Figure 6**) was investigated using scanning electron microscopy (SEM). Image a–c shows SEM of the PEDOT:PSS/PVA-EsNf deposited on CP at different magnification scale (30 μm , 5 μm , and 500 nm). It can be clearly seen that continuous, well separated, and homogenous EsNf network covers the conducting

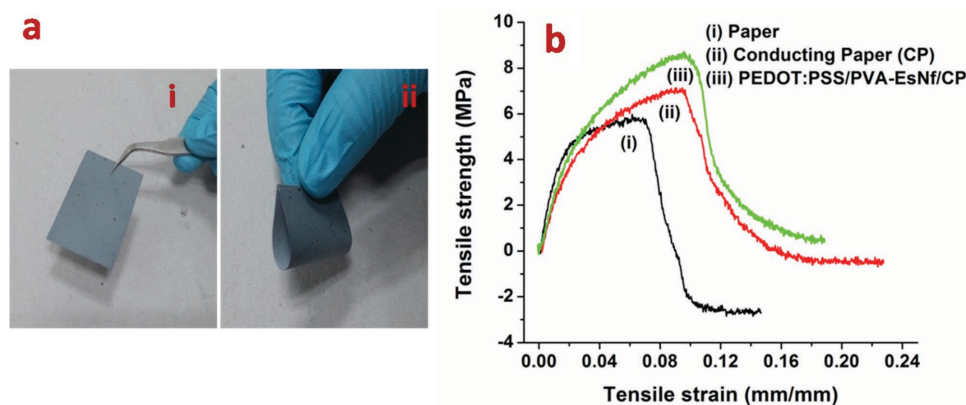


Figure 4. a) (i) Optical image of conducting paper coated with PEDOT:PSS/PVA electrospun nanofiber showing (ii) high flexibility. b) Stress–strain curve of different modified paper.

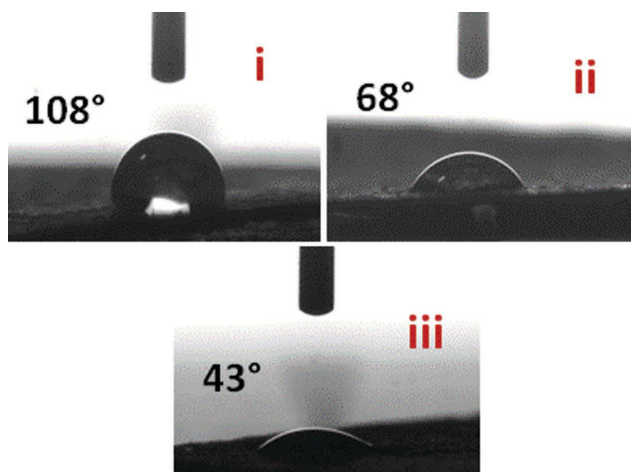


Figure 5. Contact angle measurement of (i) conducting paper (CP) (ii) PEDOT:PSS/PVA electrospun nanofibers coated over conducting paper (PEDOT:PSS/PVA-EsNf/CP) (iii) anti-CEA immobilized PEDOT:PSS/PVA-EsNf/CP.

paper. The average diameter of EsNf calculated by ImageJ software is found to be 150–200 nm. The EsNf has enhanced specific surface area of CP that perhaps plays an important role in the orientation and enhanced loading of biomolecule. However, after antibody functionalization (image d) surface morphology of the PEDOT:PSS/PVA-EsNf/CP exhibits porous and homogeneously

covered surface, indicating successful immobilization of antibody (anti-CEA). It appears that anti-CEA are entangled and covered with EsNf that may provide easier access to the analyte.

2.1. Electrochemical Studies

Figure 7a shows results of the chronoamperometric studies (current versus time) obtained for CP (a), PEDOT:PSS/PVA-EsNf/CP (b), anti-CEA/PEDOT:PSS/PVA-EsNf/CP (c), BSA/anti-CEA/PEDOT:PSS/PVA-EsNf/CP (d) at 2 V every 0.1 s. The increased value of electrochemical current (0.88 mA) of the PEDOT:PSS/PVA-EsNf/CP electrode than that of CP electrode (0.74 mA) indicates deposition of the as-spun nanofiber onto the CP. The increase in the electrochemical current value can be attributed to the conducting behavior of the PEDOT:PSS where high surface-to-volume ratio of nanofibers on CP results in enhanced permeability of the redox couple $[\text{Fe}(\text{CN})_6]^{3-/4-}$ toward CP electrode. Further increase in the value of amperometric current (1.05 mA) observed after anti-CEA immobilization onto the PEDOT:PSS/PVA-EsNf/CP electrode is attributed to well-oriented antibodies layer that facilitates electron transfer between solution and electrode. Since bovine serum albumin (BSA) was used to block non-specific sites on anti-CEA/PEDOT:PSS/PVA-EsNf/CP electrode, the observed amperometric current (0.97 mA) decreases due to macromolecular structure and insulating nature of BSA. It was found

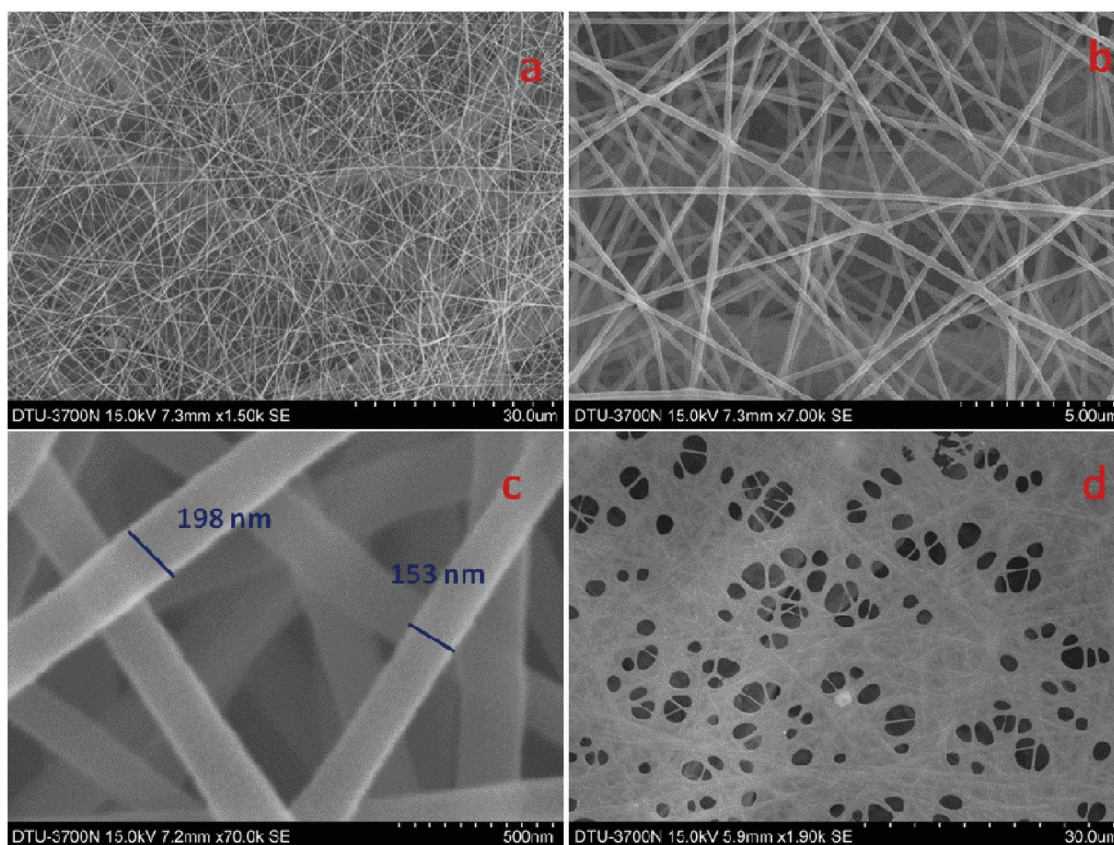


Figure 6. SEM images of a–c) PEDOT:PSS/PVA-EsNf/CP at different magnification d) anti-CEA/PEDOT:PSS/PVA-EsNf/CP.

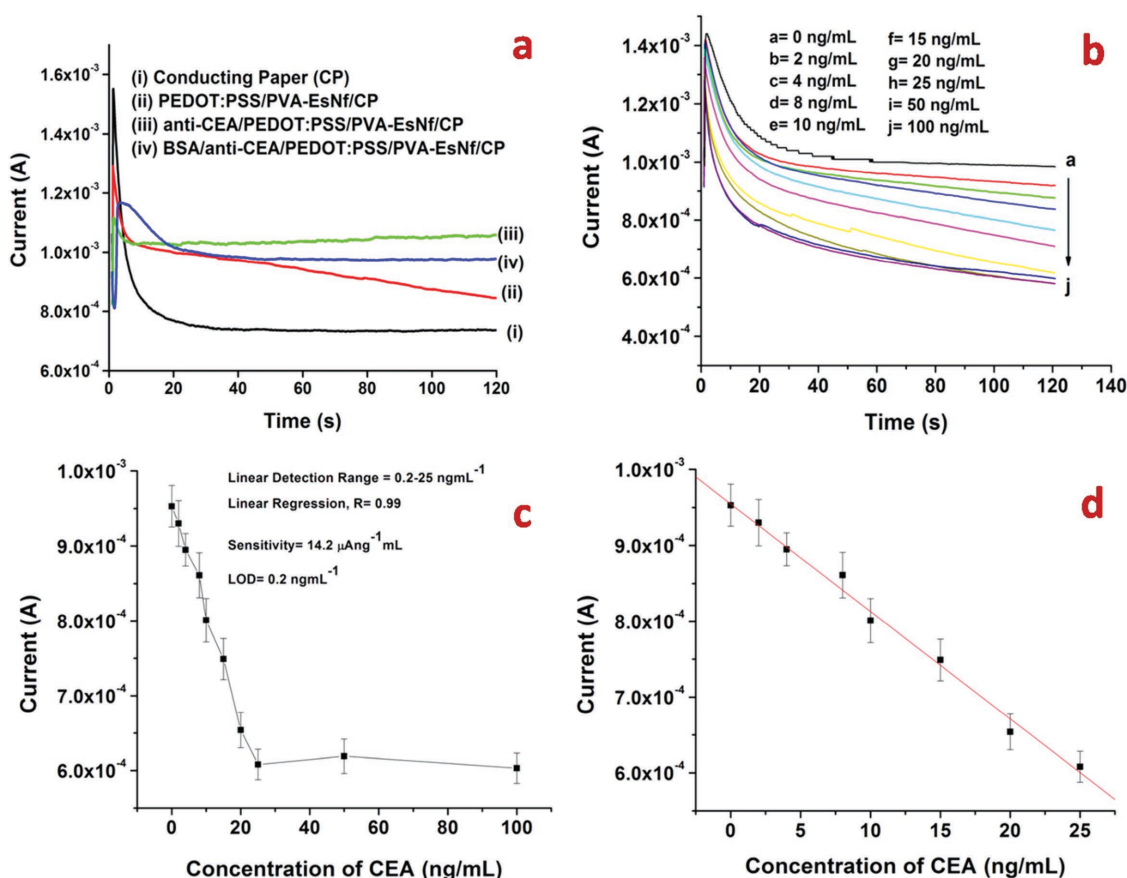


Figure 7. Electrochemical characterization of modified paper electrode a) chronoamperometry plot obtained for (i) conducting paper, CP (ii) PEDOT:PSS/PVA-EsNf/CP (iii) anti-CEA/PEDOT:PSS/PVA-EsNf/CP (iv) BSA/anti-CEA/PEDOT:PSS/PVA-EsNf/CP. b) Electrochemical response studies of BSA/anti-CEA/PEDOT:PSS/PVA-EsNf/CP electrode at different concentration (0–100 ng mL⁻¹) of CEA c) calibration plot between the magnitudes of current recorded and CEA concentration d) linearity plot of paper sensor (BSA/anti-CEA/PEDOT:PSS/PVA-EsNf/CP) with linear regression coefficient $R = 0.996$.

that amperometric current of paper sensor (BSA/anti-CEA/PEDOT:PSS/PVA-EsNf/CP) remained constant and hence could be utilized for biosensing application.

The amperometric response studies of the BSA/anti-CEA/PEDOT:PSS/PVA-EsNf/CP bioelectrode were carried out with successive addition of human carcinoembryonic antigen (CEA) concentration up to 100 ng mL⁻¹ in PBS (50 × 10⁻³ M, pH 7.0, 0.9% NaCl) containing 5 × 10⁻³ M [Fe(CN)₆]^{3-/4-} under static condition. For this, 10 μL of different antigen concentration was added into the electrochemical cell one by one and the current-time (0 to 120 s) curve was recorded after incubation of 10 min for each cycle. The variation of the amperometric response current recorded as a function of CEA (0–100 ng mL⁻¹) is shown in Figure 7b. It can be seen that (Figure 7c) at concentration up to 25 ng mL⁻¹, amperometric current decreases and saturation current is obtained at higher concentration (50, 100 ng mL⁻¹). This can be understood by immunoreactions, wherein CEA first reacts with anti-CEA on paper surface and forms the antigen-antibody complex resulting in decreased charge transfer via [Fe(CN)₆]^{3-/4-} leading to reduction in the amperometric current. This can be assigned to rearrangement of the molecules in the matrix. A linear relationship is observed between magnitude of amperometric current and CEA concentration in the range,

0–25 ng mL⁻¹ (Figure 7d) with regression coefficient of 0.996 as given in Equation (1)

$$I(A) = -14.2 \mu A \text{ mL ng}^{-1} \times [\text{CEA concentration}] + 954 \mu A; R^2 = 0.996 \quad (1)$$

The sensitivity of the BSA/anti-CEA/PEDOT:PSS/PVA-EsNf/CP bioelectrode estimated from slope of the curve has been found to be 14.2 μA ng⁻¹ mL cm⁻² and the lower detection limit (LD) has been determined to be 0.2 ng mL⁻¹ using Equation (2)

$$\text{Detection limit} = \frac{3\sigma}{m} \quad (2)$$

where σ is standard deviation and m is the slope of the curve. A control experiment was conducted using the PEDOT:PSS/PVA-EsNf/CP electrode as a function of CEA concentration (Figure S2, Supporting Information) in the absence of antibodies. It was observed that there was no significant change in the amperometric current of PEDOT:PSS/PVA-EsNf/CP electrode with increasing concentration of CEA. It appears that the PEDOT:PSS/PVA-EsNf/CP electrode does not bind the

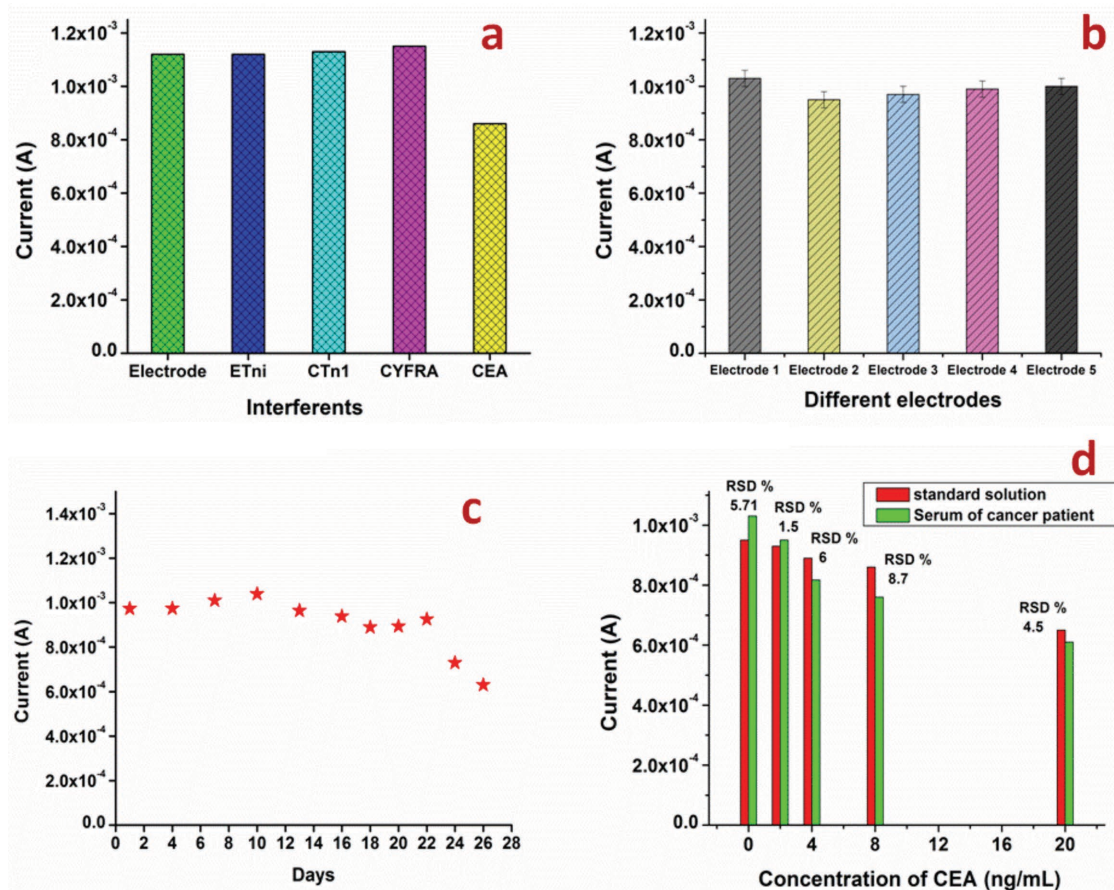


Figure 8. a) Interferents studies conducted via measurement of electrochemical current response of BSA/anti-CEA/PEDOT:PSS/PVA-EsNf/CP bioelectrode (paper sensor) in the presence of other analytes. b) Electrochemical current response of different immunoelectrode fabricated under similar condition in presence of CEA (2 ng mL^{-1}). c) Electrochemical current response of BSA/anti-CEA/PEDOT:PSS/PVA-EsNf/CP bioelectrode measured as a function of time (day) and d) CEA concentration values obtained by immunoassay and the BSA/anti-CEA/PEDOT:PSS/PVA-EsNf/CP bioelectrode.

antigen molecule and hence the amperometric current does not exhibit significant change in the PEDOT:PSS/PVA-EsNf/CP electrode surface.

2.2. Selectivity, Stability, and Reproducibility Studies

The selectivity of BSA/anti-CEA/PEDOT:PSS/PVA-EsNf/CP bioelectrode was investigated in the presence of other analytes such as endotheline-1 protein (ET-1), cardiac troponin I (cTnI), and cytokeratin-19 fragment (CYFRA-21-1), (2 ng mL^{-1}) (Figure 8a). It was found that magnitude of amperometric current decreased on addition of CEA (2 ng mL^{-1}). However, there was no significant change in amperometric current on addition of another antigen indicating high selectivity of the paper sensor toward CEA. Figure 8b shows reproducibility of the five different paper electrodes (BSA/anti-CEA/PEDOT:PSS/PVA-EsNf/CP) fabricated under similar conditions in presence of 2 ng mL^{-1} CEA concentration. It was found that BSA/anti-CEA/PEDOT:PSS/PVA-EsNf/CP bioelectrode showed good reproducibility for five different electrodes with constant surface area as is evident by low value of relative standard deviation (RSD) of 3.1% (mean value = $980 \mu\text{A}$). Further, each measurement

was repeated three times for each electrode and the error bars were included accordingly. The shelf life of BSA/anti-CEA/PEDOT:PSS/PVA-EsNf/CP bioelectrode (Figure 8c) was determined by measuring the amperometric response current at regular interval of 2–3 days. It was found that no significant change occurred in the amperometric current up to about 22 days after which the amperometric current decreased to 21%. This indicates that paper electrode (BSA/anti-CEA/PEDOT:PSS/PVA-EsNf/CP) exhibits good stability up to 22 days.

2.3. Real Sample Analysis

Quantification of CEA in serum of cancer patients was conducted at Rajiv Gandhi Cancer Institute & Research Centre (RGCI&RC) in Delhi, India using the VITROS CEA Reagent Pack and the VITROS CEA Calibrators on the VITROS ECi/ECiQ Immunodiagnostic Systems, the VITROS 3600 Immunodiagnostic System and the VITROS 5600 Integrated System using Intellicheck® Technology. The blood samples of patients were collected and processed at RGCI&RC after ethical approval by the Institutional Review board (No. RGCIRC/IRB/61/2014) and Institutional Ethical and Biosafety

Table 2. Response characteristics of the BSA/anti-CEA/PEDOT:PSS/PVA-EsNf/CP bioelectrode along with those reported in literature.

S. No.	Substrate	Material	Fabrication method	Detection method	Linear range and sensitivity	Stability [d]	Cost	References
1.	Gold electrode	AuNP, O-aminophenol	Drop cast	Electrochemical impedance spectroscopy	0.5–20 ng mL ⁻¹ and 1.08 × 10 ⁵ Ω ng ⁻¹ mL	–	High	[19]
2.	Glassy carbon electrode	AuNP, MWCNT, Chitosan	Drop cast	Differential pulse voltammetry	0.3–2.5 and 2.5–20 ng mL ⁻¹ and —	30	Moderate	[20]
3.	ITO	Au-Chitosan	Drop cast	Cyclic voltammetry	2–20 ng mL ⁻¹	14	Moderate	[21]
4.	Whatman paper 1	PEDOT:PSS/RGO, ethylene glycol	Dip coating	Amperometry	2–8 ng mL ⁻¹ and 25.8 μA (ng mL ⁻¹) ⁻¹ cm ²	21	Low	[5]
5.	Whatman paper 1	PEDOT:PSS/CNT, formic acid	Dip coating	Amperometry	2–15 ng mL ⁻¹ and 7.8 μA (ng mL ⁻¹) ⁻¹ cm ²	18	Low	[14]
6.	Whatman paper 1	PEDOT:PSS/PVA electrospun nanofiber	Electrospinning method	Amperometry	0.2–25 ng mL ⁻¹ and 14.2 μA (ng mL ⁻¹) ⁻¹ cm ²	22	Low	Present work

Committee, Delhi Technological University (DTU), Delhi, India (R.NO.:BT/IEBC/2014/714). It has been found that a reasonable correlation exists between magnitude of amperometric current response of the BSA/anti-CEA/PEDOT:PSS/PVA-EsNf/CP bioelectrode in presence of (a) standard concentration of CEA and (b) CEA concentration in serum samples obtained by RGCI&RC (Figure 8d). The observed results exhibit reasonable (less than 9%) relative standard deviation (%RSD) indicating high accuracy of paper sensor.

The sensing characteristics of this paper sensor are summarized in **Table 2** and the results have been compared with those obtained using conventional electrode such as gold, glassy carbon and ITO reported in literature for CEA detection. It can be seen that fabricated paper electrode (BSA/anti-CEA/PEDOT:PSS/PVA-EsNf/CP) covers broad detection range and display improved sensing parameters compared to conventional electrodes (gold, glassy carbon, and ITO electrode).

The fabricated paper sensor (BSA/anti-CEA/PEDOT:PSS/PVA-EsNf/CP) can be easily decomposed by incineration (Movie S1, Supporting Information), which is a major drawback in disposal of expensive conventional electrodes such as gold, glassy carbon and ITO electrodes. The resulting ash was investigated by energy dispersive X-ray (EDX) technique. EDX results confirm the presence of carbon, oxygen, sulfur, potassium, calcium, and iron. No traces of toxic metals were detected (Figure S3, Supporting Information). It shows that the proposed paper sensor is disposable, environment friendly, and a promising platform for point of care diagnostics.

3. Conclusions

We have demonstrated the fabrication of a flexible, cost-effective, lightweight, label free, and environment friendly electrochemical sensor. For this, nanofiber of PEDOT:PSS/PVA have been grown on CP platform using electrospinning technique. The deposition of EsNf results in improved mechanical strength and electrochemical properties. In addition high aspect ratio of PEDOT:PSS/PVA-EsNf results in improved charge transfer between electrode and solution resulting in

higher sensitivity toward the electrochemical detection of cancer biomarker (CEA). The PEDOT:PSS/PVA-EsNf functionalized with anti-CEA biomolecule has been found to have good precision and reproducibility for CEA detection. The results of the amperometric response studies indicate that the paper electrode (BSA/anti-CEA/PEDOT:PSS/PVA-EsNf/CP) can be used to estimate the CEA from 0.2 to 25 ng mL⁻¹, has high sensitivity (14.2 μA ng⁻¹ mL cm⁻²) and shelf life of 22 days. This EsNf decorated CP shows excellent electrochemical behavior and has the potential use in the development of electrochemical biosensors for detection of other analytes including cholesterol, urea, environment pollutant chemical, etc. Efforts should be made to investigate the effect of film thickness on the characteristics of this sensor. This paper based environment friendly electrode can be easily disposed off by simple incineration.

4. Experimental Section

Materials and Reagents: PEDOT:PSS aqueous solution (1.3 wt% dispersion in H₂O), PEDOT content: 0.5 wt%, PSS content (0.8 wt%), polyvinyl alcohol (PVA), carcinoembryonic antibody monoclonal (anti-CEA), CEA, and BSA were procured from Sigma-Aldrich, India. Whatman filter paper #1 was purchased from GE healthcare, UK. Deionized water from Millipore water purification systems (resistivity 18.2 MΩ cm) was used in all experiments.

Fabrication of Conducting Paper (CP): Conducting paper was fabricated as reported earlier.^[5] In brief, the Whatman paper (1cm×3cm) was dipped in PEDOT:PSS aqueous suspension (1.3 wt%, 3%EG) for 1 h and was then dried at 100 °C in a hot air oven. Thereafter it was treated with EG by dipping in the EG solution for 20 min. The EG treated conducting paper was finally dried at 100 °C for about 1 h.

Fabrication of PEDOT:PSS/PVA Electrospun Nanofiber (EsNf) Decorated Conducting Paper (PEDOT:PSS/PVA-EsNf/CP): The PEDOT:PSS/PVA nanofibers were synthesized using electrospinning (Figure 1a).^[22] Briefly, 0.3 g of PVA powder was added to 5 mL of PEDOT:PSS in a vial and magnetically stirred and heat at 60 °C for 1–2 h to ensure that the solution was homogenous. The PVA was used as a polymeric carrier material to prepare PEDOT:PSS based electrospun nanofiber. Besides this, PVA is a nontoxic, environment friendly polymer that can be helpful to attest the environmental concern of paper sensor.^[23] The black viscous solution was kept overnight to remove the air bubbles. Thereafter, the as-prepared viscous solution was transferred into syringe for electrospinning. During the electrospinning process, a direct current voltage of 20 KV was applied to the syringe needle and a feed rate of 1.4 mL h⁻¹ was used. The distance between the needle tip and the conducting paper (collector) was kept at 10 cm.

Biofunctionalization of PEDOT:PSS/PVA Electrospun Nanofiber Decorated Conducting Paper (anti-CEA/PEDOT:PSS/PVA-EsNf/CP): For biofunctionalization, the monoclonal carcinoembryonic antibodies (anti-CEA) solution of 100 $\mu\text{g mL}^{-1}$ was uniformly spread over the PEDOT:PSS/PVA-EsNf/CP electrode (anti-CEA/PEDOT:PSS/PVA-EsNf/CP). The anti-CEA is physically absorbed onto the PEDOT:PSS/PVA-EsNf/CP electrode. The efficiency of binding between antibodies and PEDOT:PSS/PVA-EsNf/CP electrodes was investigated. In this approach we washed the fabricated anti-CEA/PEDOT:PSS/PVA-EsNf/CP electrodes with phosphate buffer saline (PBS, pH 7.0) upto ten times and it was found that no significant changes in current occurred (as shown in Figure S1, Supporting Information). This may be due to the strong interaction between negatively charged PEDOT:PSS/PVA hybrid (-28.5 mV) and positively charged end ($-\text{NH}_3^+$) of the anti-CEA molecules, indicating that highly stable films were formed and the immobilized antibodies did not get easily washed by buffer solution. Further, to block unspecific sites 0.1% of BSA was added to the anti-CEA functionalized PEDOT:PSS/PVA-EsNf/CP electrode. After rinsing again with PBS, the fabricated paper electrodes (BSA/anti-CEA/PEDOT:PSS/PVA-EsNf/CP) were stored at 4 °C before carrying out the sensing studies. A schematic of the experiment is shown in Figure 1.

Measurements and Characterization: The PEDOT:PSS/PVA composite was characterized using Raman spectroscopy (Varian 7000 FT-Raman) and zeta potential (Zetasizer Nano-ZS90, Malvern Instruments Ltd., U.K.) using dynamic light scattering technique. Fourier transform infrared (FTIR) and XPS studies of modified paper electrodes were recorded using Bruker Optics, Vertex 70V in transmission mode, and PHI 5000 Versa Prob II, FEI Inc, respectively. Tensile strength properties of the modified paper were measured using a universal testing machine (UTM, Instron 3369) according to ASTM D 882-02. The preconditioned test samples ($50 \times 10 \times 0.18$ mm) were mounted between grips of the machine with span length 27 mm and pulled at cross head speed of 5 mm min^{-1} . The average tensile properties of five specimens were measured. Contact angle measurements (Data Physics OCA15EC) were done using sessile drop method. The morphology of the deposited electrospun nanofiber and energy dispersive X-ray (EDX) analysis was determined with scanning electron microscopy (Hitachi S-3700N). The electrochemical behavior of the electrode was studied via chronoamperometry measurement on an Autolab Potentiostat/Galvanostat (Metrohm, The Netherlands) using a three-electrodes cell with the modified conducting paper electrode as a working electrode, platinum as auxiliary electrode, and a Ag/AgCl as the reference electrode in phosphate buffer saline (PBS, 50×10^{-3} M, pH 7.0, 0.9% NaCl) containing 5×10^{-3} M $[\text{Fe}(\text{CN})_6]^{3-/4-}$.

Supporting Information

Supporting Information is available from the Wiley Online Library or from the author.

Acknowledgements

The authors thank Prof. Yogesh Singh, Vice Chancellor, Delhi Technological University (DTU), Delhi, India for providing the facilities. Saurabh Kumar is thankful to DTU for the award of financial assistance and Chandra Mohan Srivastava, DTU for scientific discussions during electrospinning. S.K. is thankful to Dr. Birendra K. Yadav, Dr. D. C. Doval, Rajiv Gandhi Cancer Institute & Research Centre for providing the clinical samples.

Received: April 1, 2016

Revised: April 22, 2016

Published online:

- [1] a) S. Hu, R. Rajamani, X. Yu, *Appl. Phys. Lett.* **2012**, *100*, 104103; b) L. Hu, J. W. Choi, Y. Yang, S. Jeong, F. La Mantia, L.-F. Cui, Y. Cui, *Proc. Natl. Acad. Sci. USA* **2009**, *106*, 21490; c) Q. Cheng, Z. Song, T. Ma, B. B. Smith, R. Tang, H. Yu, H. Jiang, C. K. Chan, *Nano Lett.* **2013**, *13*, 4969; d) T. H. Nguyen, A. Fraiwan, S. Choi, *Biosens. Bioelectron.* **2014**, *54*, 640; e) W. J. Hyun, O. O. Park, B. D. Chin, *Adv. Mater.* **2013**, *25*, 4729; f) R. Martins, P. Barquinha, L. Pereira, N. Correia, G. Gonçalves, I. Ferreira, E. Fortunato, *Appl. Phys. Lett.* **2008**, *93*, 203501; g) A. D. Mazzeo, W. B. Kalb, L. Chan, M. G. Killian, J. F. Bloch, B. A. Mazzeo, G. M. Whitesides, *Adv. Mater.* **2012**, *24*, 2850; h) C. Desmet, C. A. Marquette, L. J. Blum, B. Doumèche, *Biosens. Bioelectron.* **2015**, *76*, 145; i) S. Kumar, K. K. Jagadeesan, A. G. Joshi, G. Sumana, *RSC Adv.* **2013**, *3*, 11846.
- [2] D. Töbjörk, R. Österbacka, *Adv. Mater.* **2011**, *23*, 1935.
- [3] E. W. Nery, L. T. Kubota, *Anal. Bioanal. Chem.* **2013**, *405*, 7573.
- [4] a) L. Wang, W. Chen, D. Xu, B. S. Shim, Y. Zhu, F. Sun, L. Liu, C. Peng, Z. Jin, C. Xu, *Nano Lett.* **2009**, *9*, 4147; b) K. K. Jagadeesan, S. Kumar, G. Sumana, *Electrochem. Commun.* **2012**, *20*, 71.
- [5] S. Kumar, S. Kumar, S. Srivastava, B. K. Yadav, S. H. Lee, J. G. Sharma, D. C. Doval, B. D. Malhotra, *Biosens. Bioelectron.* **2015**, *73*, 114.
- [6] V. Saxena, B. Malhotra, *Curr. Appl. Phys.* **2003**, *3*, 293.
- [7] a) C. Liao, C. Mak, M. Zhang, H. L. Chan, F. Yan, *Adv. Mater.* **2015**, *27*, 676; b) L. Li, Y. Wang, L. Pan, Y. Shi, W. Cheng, Y. Shi, G. Yu, *Nano Lett.* **2015**, *15*, 1146.
- [8] a) A. Frenot, I. S. Chronakis, *Curr. Opin. Colloid Interface Sci.* **2003**, *8*, 64; b) H. Park, S. J. Lee, S. Kim, H. W. Ryu, S. H. Lee, H. H. Choi, I. W. Cheong, J.-H. Kim, *Polymer* **2013**, *54*, 4155.
- [9] a) U. Lang, E. Müller, N. Naujoks, J. Dual, *Adv. Funct. Mater.* **2009**, *19*, 1215; b) S. Kirchmeyer, K. Reuter, *J. Mater. Chem.* **2005**, *15*, 2077.
- [10] a) A. Laforgue, L. Robitaille, *Macromolecules* **2010**, *43*, 4194; b) J. A. Arter, D. K. Taggart, T. M. McIntire, R. M. Penner, G. A. Weiss, *Nano Lett.* **2010**, *10*, 4858.
- [11] A. Maattanen, U. Vanamo, P. Ihalainen, P. Pulkkinen, H. Tenhu, J. Bobacka, J. Peltonen, *Sensors and Actuators B: Chemical* **2013**, *177*, 153.
- [12] B. D. Malhotra, S. Kumar, C. M. Pandey, *J. Phys. Conf. Ser.* **2016**, *704*, 012011.
- [13] H. J. Hansen, J. J. Snyder, E. Miller, J. Vandevoorde, O. N. Miller, L. Hines, J. Burns, *Hum. Pathol.* **1974**, *5*, 139.
- [14] S. Kumar, M. Willander, J. G. Sharma, B. D. Malhotra, *J. Mater. Chem. B* **2015**, *3*, 9305.
- [15] J. S. Hwang, T. H. Oh, S. H. Kim, S. S. Han, S. J. Lee, S. G. Lee, Y. J. Lee, S. S. Jang, *J. Appl. Polym. Sci.* **2015**, *132*, 42628.
- [16] M. Horikawa, T. Fujiki, T. Shirosaki, N. Ryu, H. Sakurai, S. Nagaoka, H. Ihara, *J. Mater. Chem. C* **2015**, *3*, 8881.
- [17] H. Moayedi, A. Asadi, F. Moayedi, B. B. Huat, *Int. J. Electrochem. Sci.* **2011**, *6*, 1294.
- [18] Y. Xia, K. Sun, J. Ouyang, *Adv. Mater.* **2012**, *24*, 2436.
- [19] H. Tang, J. Chen, L. Nie, Y. Kuang, S. Yao, *Biosens. Bioelectron.* **2007**, *22*, 1061.
- [20] K.-J. Huang, D.-J. Niu, W.-Z. Xie, W. Wang, *Anal. Chim. Acta* **2010**, *659*, 102.
- [21] J. Lin, W. Qu, S. Zhang, *Anal. Sci.* **2007**, *23*, 1059.
- [22] N. Liu, G. Fang, J. Wan, H. Zhou, H. Long, X. Zhao, *J. Mater. Chem.* **2011**, *21*, 18962.
- [23] Y.-T. Jia, J. Gong, X.-H. Gu, H.-Y. Kim, J. Dong, X.-Y. Shen, *Carbohydr. Polym.* **2007**, *67*, 403.

BIODATA

Name: Saurabh Kumar
Father's Name: Jagdish Prasad
Date of Birth: 22 January 1987
Permanent Address: Village: Tulsipur
P.O + P.S: Hulasganj
District: Jhanabad,
Bihar: 804407
Mobile No.: 9015841169
E mail: sau2203@gmail.com



ACADEMIC QUALIFICATIONS

Degree	Year	Subject	Division	University/Board
Ph. D.	2012-Present	Biotechnology	First (Course Work)	Delhi Technological University, Delhi
M. Sc.	2008-2010	Bioelectronics & Instrumentation	First	Jamia Hamdard, Delhi
B. Sc. (H)	2005-2008	Biotechnology	First	CCS University, Meerut, U.P
Intermediate	2001-2003	Science	First	B.I.E.C, Patna
High School	2001	Science, Social science, Maths, English, Hindi, Sanskrit.	First	B.S.E.B, Patna

RESEARCH EXPERIENCE

1. Setup a Nanobioelectronics Laboratory at Department of Biotechnology, Delhi Technological University, Delhi under supervision of Prof B. D. Malhotra.
2. Worked as Project assistant, in the area of fabrication of paper based immunosensor for detection of infectious disease, at Biomedical Instrumentation Section, National Physical Laboratory (CSIR), New Delhi (From Jan 2011 to July 2012).
3. Worked on Self-assembled monolayer based cholesterol biosensor as a last semester project work during Masters (Jan 2010 to June 2010) in Centre on Biomolecular Electronics, National Physical Laboratory, New Delhi.

PUBLICATIONS

1. **S. Kumar[#]**, A. Sen[#], S. Kumar, S. Augustine, B.K. Yadav, S. Mishra and B.D. Malhotra, Polyaniline modified flexible conducting paper for cancer detection, **Applied Physics Letters**, 2016, 108(20), 203702. (#Authors with equal contribution, Impact factor 3.1)
2. S. Kumar, **S. Kumar**, S. Tiwari, S. Augustine, S. Srivastava, B.K. Yadav and B.D. Malhotra, Highly sensitive protein functionalized nanostructured hafnium oxide based biosensing platform for non-invasive oral cancer detection, **Sensors and Actuators B: Chemical**, 2016, 235, 1-10. (Impact factor 4.7)
3. **S. Kumar**, P. Rai, J.G. Sharma, A. Sharma and B.D. Malhotra, PEDOT:PSS/PVA-nanofibers-decorated conducting paper for cancer diagnostics, **Advanced Materials Technologies**, 2016. (doi: 10.1002/admt.201600056).
4. **S. Kumar**, M. Willander, J.G. Sharma and B.D. Malhotra, A solution processed carbon nanotube modified conducting paper sensor for cancer detection, **Journal of Material Chemistry B**, 2015, 3, 9305–9314. (Impact factor 4.9)
5. **S. Kumar**, S. Kumar, S. Srivastava, B.K. Yadav, S.H. Lee, J.G. Sharma, D.C. Doval and B.D. Malhotra, Reduced graphene oxide modified smart conducting paper for Cancer biosensor, **Biosensors and Bioelectronics**, 2015, 73, 114-122. (Impact factor 7.5)
6. S. Kumar, **S. Kumar**, S. Tiwari, S. Srivastava, M. Srivastava, B.K. Yadav, S. Kumar, T.T. Tran, A.K. Dewan, A. Mulchandani and B.D. Malhotra, Biofunctionalized nanostructured zirconia for biomedical application: A smart approach for oral cancer detection, **Advanced Science**, 2015, 2, 1-9. (Impact factor 6.0)
7. S. Kumar[#], **S. Kumar[#]**, Md. A. Ali[#], P. Anand, V.V. Agrawal, R. John, S. Maji and B.D. Malhotra, Microfluidic-integrated biosensors: Prospects for point-of-care diagnostics, **Biotechnology Journal**, 2013, 8, 1267-1279. (#Author with equal contribution, Impact factor 3.5)
8. **S. Kumar[#]**, K.K. Jagadeesan[#], A.G. Joshi and G. Sumana, Immuno-CoPS (conducting paper strips) for futuristic cost-effective cancer diagnostics, **RSC Advance**, 2013, 3, 11846-11853. (#Author with equal contribution, Impact factor 3.3)
9. K.K. Jagadeesan[#], **S. Kumar[#]** and G. Sumana, Application of conducting paper for selective detection of troponin, **Electrochemistry Communications**, 2012, 20, 71-74. (#Author with equal contribution, Impact factor 4.6)

10. **S. Kumar**, J. Singh, V.V. Agrawal, M. Ahamad and B.D. Malhotra, Biocompatible self-assembled monolayer platform based on (3-glycidoxypopyl)trimethoxysilane for total cholesterol estimation, **Analytical Methods**, 2011, 3, 2237-2245. (Impact factor 1.9)

CONFERENCE PAPERS

1. **S. Kumar**, S. Kumar, C.M. Pandey and B.D. Malhotra, Conducting paper based sensor for cancer biomarker detection, **Journal of Physics: Conference Series**, IOP Publishing: 2016; pp 12010-12018.
2. B.D. Malhotra, **S. Kumar** and C.M. Pandey, Nanomaterials based biosensors for cancer biomarker detection, **Journal of Physics: Conference Series**, IOP Publishing: 2016; pp 012011.

AWARDS AND ACHIEVEMENTS

1. Research paper entitled “Reduced graphene oxide modified smart conducting paper for cancer biosensor” by **S. Kumar**, S. Kumar, S. Srivastava, B.K. Yadav, S.H Lee, J.G. Sharma, D.C. Doval and B.D. Malhotra has been selected as research news entitled “Graphene-modified paper sensor detect cancer” on **Nature India** Published online 16 June 2015. (<http://www.natureasia.com/en/nindia/article/10.1038/nindia.2015.80>)
doi:10.1038/nindia.2015.80
2. Research paper entitled “Application of conducting paper for selective detection of troponin” by K.K Jagadeesan, **S. Kumar**, and G. Sumana has been selected as research news entitled “Polymer Paper to Detect heart Disease” on **Nature India** Published online 22 June 2012. (<http://www.nature.com/nindia/2012/120622/full/nindia.2012.90.html>)
doi:10.1038/nindia.2012.90
3. **Best poster award** for the paper entitled “Solution-Processed PEDOT:PSS/Graphene Composites as the electroactive paper for biosensor application” by **S. Kumar**, S. Kumar, S. Augustine, B.K. Yadav, J.G. Sharma, D.C. Doval, and B.D. Malhotra is selected at the 6th World Congress on Biotechnology” held on October 05-07, 2015 in New Delhi, India (Organized by OMICS International).
4. **Best poster award** for the paper entitled “Low Cost Conducting paper based impedimetric biosensor for cancer detection” by **S. Kumar**, S. Kumar, A. Sen, S. Srivastava, B.K. Yadav, J.G. Sharma, D.C. Doval and B.D. Malhotra is selected in the 14th Annual International Conference **RGCON 2015**, Changing Landscape in Head & Neck oncology Future & Beyond held from 27th February to 01st March 2015 (Organized by Rajiv Gandhi Cancer Institute & Research Centre Delhi).